



UNIVERSIDAD MIGUEL HERNÁNDEZ
DEPARTAMENTO DE CIENCIA DE MATERIALES, ÓPTICA
Y TECNOLOGÍA ELECTRÓNICA

**Symbolic-Numeric Tools for the Analysis of
Motorcycle Dynamics. Development of a Virtual
Rider for Motorcycles based on Model Predictive
Control.**

PhD. Dissertation
October 2016

Ph.D. Candidate: David Moreno Giner
Advisor: Professor Miguel Sánchez Lozano

Universidad Miguel Hernández de Elche. Departamento de Ciencia de Materiales, Óptica y Tecnología Electrónica. Avda. de la Universidad, s/n. Edificio Torrevaillo, 03202 Elche (Spain).

All rights reserved. No part of the publication may be reproduced in any form by print, photoprint, microfilm or any other means without written permission from the author.

AUTORIZACIÓN DEL DIRECTOR DE LA TESIS

D. Miguel Sánchez Lozano, Profesor Doctor del Área de Ingeniería Mecánica en el Departamento de Ingeniería Mecánica y Energía de la Universidad Miguel Hernández de Elche,

Autoriza:

La presentación de la Tesis Doctoral titulada “Symbolic-Numeric Tools for the Analysis of Motorcycle Dynamics. Development of a Virtual Rider for Motorcycles based on Model Predictive Control”, realizada por D. David Moreno Giner, bajo mi dirección y supervisión, en el Departamento de Ciencia de Materiales, Óptica y Tecnología Electrónica de la Universidad Miguel Hernández de Elche, y que presenta para la obtención del grado de Doctor por la Universidad Miguel Hernández de Elche.

En Elche, a 23 de septiembre de 2016.

Fdo: Miguel Sánchez Lozano

Director de la Tesis Doctoral

**DEPARTAMENTO DE CIENCIA DE MATERIALES,
ÓPTICA Y TECNOLOGÍA ELECTRÓNICA**

Dña. Piedad de Aza Moya, Catedrática de Universidad y Directora del Departamento de Ciencia de Materiales, Óptica y Tecnología Electrónica de la Universidad Miguel Hernández de Elche,

Certifica:

Que el trabajo realizado por D. David Moreno Giner, titulado “Symbolic-Numeric Tools for the Analysis of Motorcycle Dynamics. Development of a Virtual Rider for Motorcycles based on Model Predictive Control”, ha sido dirigido por el Dr. Miguel Sánchez Lozano, realizado en el Departamento de Ciencia de Materiales, Óptica y Tecnología Electrónica y se encuentra en condiciones de ser leído y defendido como Tesis Doctoral ante el correspondiente tribunal en la Universidad Miguel Hernández.

Y para que así conste y surta los efectos oportunos, firmo la presente en Elche, a 23 de septiembre de 2016.

Fdo: Dña. Piedad de Aza Moya
Directora del Departamento de Ciencia de
Materiales, Óptica y Tecnología Electrónica



Elche, 23 de septiembre de 2016

Referencia: Doctorado

Asunto: Certificado Doctorado

D. JOSÉ ÁNGEL PÉREZ ÁLVAREZ, SECRETARIO DE LA COMISIÓN DE ESTUDIOS DE DOCTORADO DE LA UNIVERSIDAD MIGUEL HERNÁNDEZ DE ELCHE,

CERTIFICA

En la reunión del día 19 de septiembre de 2016 de la Comisión de Estudios de Doctorado de esta Universidad se acordó por UNANIMIDAD, la PROTECCIÓN, dada la posible patentabilidad de los resultados obtenidos en la Tesis Doctoral "Symbolic-Numeric Tools for the Analysis of Motorcycle Dynamics. Development of a Virtual Rider for Motorcycles based on Model Predictive Control", de los siguientes apartados:

-5.1.1, 5.1.2 y 5.1.3,

-5.2 (excepto 5.2.1 y 5.2.2) y 5.2.3,

- 6.2.4 y 6.2.5,

- 6.3, 6.3.1, 6.3.2 y 6.3.3,

tal y como solicitó el Doctorando D. David Moreno Giner, con el visto bueno del Director de la Tesis el Dr. D. Miguel Sánchez Lozano, mediante escrito remitido al Vicerrectorado de Investigación e Innovación con fecha 20/07/2016 y número de registro RG/MH001/12576.

Y para que así conste, firmo el presente certificado en Elche a veintitrés de septiembre de dos mil dieciséis.

Fdo. José Ángel Pérez Álvarez

Secretario de la Comisión de Estudios de Doctorado

Servicio de Gestión de Estudios

Edificio de Rectorado y Consejo Social

To Jim and Luna.

Acknowledgements

I would like to express below my gratitude to everybody who has given me guidance and inspiration, making this thesis possible.

First and foremost I wish to express my gratitude to my PhD advisor, Prof. Miguel Sánchez Lozano, for his support during all these years. Thank you for sparking my interest in the field of vehicle dynamics, which began during your undergraduate lessons and has grown throughout the years to become one of my greatest passions.

I would also like to thank the European Commission for supporting my research through the Marie Curie grant MRTN-CT-2006-035965 as part of the MYMOSA project. Thanks to it, I had the opportunity to spend three years working for the simulation division of LMS International in Belgium. Those three years left a huge mark on me both from a professional and personal point of view. I feel that being awarded a Marie Curie grant has been one of the most privileged events of my career.

A special thanks to my former colleagues from LMS International for sharing with me their knowledge and for many unforgettable moments. In particular, I am especially grateful to Joris De Cuyper and Jian Kang for guiding my research. My gratitude goes out to Herman Van der Auweraer for his support, especially during difficult times in the Czech Republic. And I cannot forget to mention my officemates and friends, Leonard Ciubotaru, Nicola Cofelice, Marco Gubitosa, Michal Manka and Alessandro Toso. It was an exceptional experience to work with such an outstanding group of researchers.

I will never forget the wonderful experiences I had during the MYMOSA project, in particular during my stay at the University of Florence. I would like to thank Prof. Pierini, Prof. Baldazini, Claudio Brenna, Giovanni Savino and Avinash Prabhakar for a great time in Tuscany.

I have developed most of this thesis in my spare time, combining it with my everyday job as a simulation engineer in the automotive and motorcycle industries. I would like to thank next all the people that, not being directly related to this PhD thesis, contributed in one way or another to broaden my knowledge in the area of vehicle dynamics.

Thanks to all the colleagues that I had the pleasure to meet at the Red Bull F1

team. I doubt I will ever forget the two years I spent working there. In particular I would like to mention Chris, Emiliano and Matteo from whom I learned a great deal about vehicle simulation and performance analysis. I am also grateful to my current colleagues and friends from the Yamaha MotoGP team, Fabio, Fabrizio, Federico, Jun, Michele, Shirou and Yasuhiro for sharing your experience with me. I would like to especially thank Koen for your support and flexibility. Guys, I have learned a lot in the last three years working by your side.

On a personal level several people whose friendship I value greatly have helped me along the way. Thanks to Fran, you were the first to challenge me during our years at the university and you have been a continuous source of inspiration. David, your friendship has been a constant presence all these years. I know I can always count on you. Tommaso, I love our discussions, especially those in front of a good bottle of Belgian beer. I truly appreciate your help with the revision of this manuscript. Thanks to my flatmates Alessia, Laura, Nicola and Simone, the year we spent together in Ferrara has been one of the most beautiful of my life. I am looking forward to sharing more wonderful moments with you all.

Finally, I would like to thank my family for their love and support. You have always encouraged me to pursue my dreams, inspiring me to continue growing regardless the path I decided to follow. You gave me strong wings.

Last but not least, I would like to thank Jimena to whom this dissertation is dedicated. You only know how much effort and time there has been behind this project. Your love and patience have been of invaluable support during these years. It is difficult to describe in a few words how much you mean to me. *In yaakumech.*

May 2015



Some of the MYMOSA researchers during a riding course in Eindhoven (The Netherlands).

Abstract

Over the years, the design of modern vehicles is becoming an extremely complex task. This trend is caused by the increasing functional requirements of new designs and by the vast amount of mechatronic systems within the vehicle. Motorcycle technology has reached a point where, to make further improvements, a global and multidisciplinary understanding of the vehicle is essential. In this respect, it has become indispensable to consider the interaction of such diverse elements as road, suspensions, chassis, engine, rider, sensors and electronics in the design process of new devices.

It is in this challenging framework where simulation takes a crucial role in the evolution and development of new ideas. Virtual models offer a faster and cost-effective alternative to physical testing, they decrease the development time, limit the number of prototypes needed to validate a new design and, most importantly, they permit conducting experiments with no risk for the human operator. This last feature, for instance, results especially attractive for the development of new active safety systems.

In order to achieve realistic results, it is essential to properly replicate the behavior of the human operator within the simulation environment. This is the main scope of the present thesis, which focuses on the application of control techniques to drive a virtual motorcycle model along a predefined path. This implies generating appropriate control actions to govern the throttle, the brakes and the steering system during the simulation.

Two-wheeled vehicles are complex dynamic systems; they are highly nonlinear, non-minimum phase, unstable and underactuated. This makes motorcycle control a rather challenging task. Building upon Model Predictive Control theory, we have developed a novel control strategy capable of riding a nonlinear motorcycle model in a wide range of conditions, including extremely demanding manoeuvres such as those performed by racing riders.

The lack of appropriate simulation packages for vehicle control motivated the in-house development of all necessary tools for the realization of this project. These include, in addition to the virtual rider, a detailed multibody model of the motorcycle and a new methodology for the quasi-steady state analysis of motorcycles.

The research performed in this PhD project yields new insights into the simulation of motorcycle dynamics and extends the working range of existing controllers. Although a sports motorcycle has been used throughout this document, both the modeling approach and the results can be extended to other vehicle typologies. This research has also paved the way for improvements and further developments that are suggested as future research lines.

Resumen

Con el paso de los años, el desarrollo de vehículos se está convirtiendo progresivamente en una tarea cada vez más compleja. Esto es debido, en parte, a los requisitos funcionales de los nuevos diseños y a la gran cantidad de sistemas mecatrónicos que incorporan los vehículos modernos. Se ha llegado a un punto en que, para mejorar el comportamiento de las motocicletas actuales, es esencial una comprensión global y multidisciplinar del vehículo. En este sentido, es indispensable considerar la interacción entre elementos tan diversos como el terreno, las suspensiones, el chasis, el motor, el piloto y la electrónica en el proceso de diseño de nuevos dispositivos.

Es en este difícil contexto donde la simulación juega un papel crucial en la evolución y el desarrollo de nuevas ideas. Los modelos virtuales ofrecen una alternativa más rápida y rentable que los ensayos físicos, disminuyen el tiempo de desarrollo, limitan el número de prototipos necesarios para validar un nuevo diseño y, lo que es más importante, permiten llevar a cabo experimentos sin ningún riesgo para el ser humano. Esta última característica, por ejemplo, resulta especialmente atractiva para el desarrollo de nuevos sistemas de seguridad activa.

Con el fin de lograr resultados realistas, es esencial replicar adecuadamente el comportamiento del piloto en el entorno de simulación. Este es el objetivo principal de la presente tesis, en la que se aplican técnicas de control al modelado del piloto.

Los vehículos de dos ruedas son sistemas dinámicos complejos; son altamente no lineales, de fase no mínima, inestables y subactuados. Esto hace del control de la motocicleta una tarea particularmente difícil. Tomando la teoría de control predictivo como punto de partida, se ha desarrollado una estrategia de control capaz de estabilizar un modelo no lineal de motocicleta en un amplio rango de condiciones, incluyendo maniobras agresivas, como por ejemplo, las realizadas por los pilotos de carreras. Para ello el sistema de control actúa sobre el acelerador, los frenos y la dirección tal y como lo haría un piloto real.

La carencia de herramientas de simulación adecuadas para el control de vehículos motivó el desarrollo interno de todos los elementos necesarios para la realización de

este proyecto. Éstos incluyen, además del piloto virtual, un modelo multicuerpo de la motocicleta y una nueva metodología para el análisis quasi-estático del vehículo.

La investigación realizada en este proyecto de doctorado aporta nuevos conocimientos sobre la simulación de la dinámica de la motocicleta y amplía el rango de trabajo de los controladores existentes. Aunque se ha utilizado una motocicleta deportiva a lo largo de este documento, tanto la metodología como los resultados pueden ser extendidos fácilmente a otras tipologías de vehículos. Al final de la investigación se proponen futuras líneas de trabajo para continuar el desarrollo del piloto virtual.

Contents

Contents	xvii
List of figures	xx
List of tables	xxiii
Nomenclature	xxiv
1 Introduction and objectives	1
1.1 Motivation	1
1.2 Context of the research: the MYMOSA project	4
1.3 Objectives of the thesis	6
1.4 Outline of the thesis	9
2 Review of motorcycle dynamics and rider modelling	13
2.1 Dynamics of single track vehicles and its modelling	13
2.1.1 The early stages	13
2.1.2 The multibody era	20
2.2 Motorcycle tyre modelling for dynamic simulations	27
2.3 Rider modelling	30
2.3.1 Rider models based on classical control theory	32
2.3.2 Rider models based on modern control theory	41
2.4 Concluding remarks	49
3 A motorcycle model for virtual rider design and simulation	53
3.1 Introduction	53
3.2 A brief review of multibody dynamics	55
3.2.1 Reference frames and coordinate systems	56
3.2.2 Kinematics	59
3.2.3 Dynamics	62

3.2.4	Numerical vs. symbolic formalisms	68
3.3	The symbolic motorcycle model	70
3.3.1	Model kinematics	71
3.3.2	Force and control elements	87
3.3.3	Equations of Motion	100
3.4	Model verification	107
3.4.1	Longitudinal dynamics	107
3.4.2	Lateral dynamics	109
3.5	Concluding remarks	111
4	A new methodology for the quasi-steady state analysis of motorcycles	113
4.1	Introduction	113
4.2	The quasi-steady state method	116
4.2.1	Reference frames and kinematic constraints	116
4.2.2	Steady state equations	119
4.2.3	Quasi-steady state equations	122
4.3	Solution of the equilibrium equations	125
4.4	Steady state motion: sensitivity study	127
4.4.1	Power balance check	127
4.4.2	Effect of speed and curvature	132
4.4.3	Directional behaviour	143
4.5	Quasi-steady state motion: sensitivity study	146
4.5.1	Effect of longitudinal acceleration	146
4.5.2	Effect of roll motion	153
4.6	Concluding remarks	160
5	Quasi-steady state analysis of continuous manoeuvres	163
5.1	Roll dynamics estimation	164
5.1.1	Problem formulation	164
5.1.2	Results: effect of trajectory	168
5.1.3	Results: effect of speed	172
5.2	Quasi-steady state solution of continuous manoeuvres	173
5.2.1	Results: slalom test	177
5.2.2	Results: chicane	182
5.3	Concluding remarks	186

6	A rider model for the dynamic simulation of motorcycles	189
6.1	Introduction	189
6.2	The rider model as a control problem	191
6.2.1	General structure of the controller	191
6.2.2	The internal model	193
6.2.3	Stability analysis	195
6.2.4	Formulation of the prediction model	202
6.2.5	Derivation of the control gains	204
6.3	Path tracking simulations	212
6.3.1	Motorcycle-rider coupling	213
6.3.2	Strategy comparison: feedforward vs predictive	215
6.3.3	Combined strategy	217
6.3.4	Results: slalom test	222
6.3.5	Results: chicane	225
6.3.6	Results: corner exit	228
6.3.7	Results: corner entry on uneven road	232
6.4	Concluding remarks	237
7	Conclusions and future work	241
7.1	Conclusions	241
7.2	Summary of the main contributions	247
7.3	Practical application of the results	248
7.4	Future research lines	249
A	Reduced model	253
A.1	Newton-Euler equations	253
A.2	Tyre longitudinal forces	256
A.3	Tyre lateral forces	256
A.4	Tyre vertical forces	257
A.5	Roll dynamics	257
B	Model parameters	259
C	Extended literature	263
	References	267
	Curriculum Vitae	283

List of figures

2.1	Motorcycle model developed by Koenen (1983)	18
2.2	Evolution of Sharp's model throughout the years	24
2.3	Input/output quantities of the Magic Formula model	28
2.4	Shape of the sine version of the Magic Formula	29
2.5	General scheme of a SISO closed-loop system	33
2.6	Driver model proposed by Yoshimoto (1968)	34
2.7	Multi-loop rider model proposed by Weir and Zellner	35
2.8	Multi-loop rider model proposed by Prem and Good (1983)	36
2.9	Rider model proposed by Lot and Cossalter (2006)	39
2.10	Rider model proposed by Lot and Massaro (2007)	40
2.11	Sharp Preview Model (2001)	45
2.12	Motorcycle model proposed by Getz (1995)	46
3.1	Coordinate systems available for multibody systems	57
3.2	Newton-Euler vs. Lagrange methods	67
3.3	Structure of numerical and symbolic formalisms	69
3.4	Multibody model of the motorcycle	72
3.5	Set of generalized coordinates	74
3.6	Topology of the multibody model	76
3.7	Tyre model kinematics	79
3.8	Front tyre orientation parameters	82
3.9	Tyre-road tangency condition	85
3.10	Front fork properties	89
3.11	Suspension forces	91
3.12	Rear shock properties	92
3.13	Tyre forces, Pacejka model	95
3.14	Sign conventions for tyre forces and moments	96
3.15	Schematic of the chain model	99

3.16	Scheme of the lateral relaxation model of the tyre	102
3.17	Definition of curvilinear coordinates	104
3.18	Reference multibody model - Virtual.Lab Motion	107
3.19	Model validation: acceleration	108
3.20	Model validation: corner entry	109
3.21	Model validation: slalom	110
4.1	Definition of the quasi-steady state problem: top view	117
4.2	Definition of the quasi-steady state problem: rear view	119
4.3	Power balance check: engine and aerodynamics	128
4.4	Power balance check: tyres	130
4.5	Power balance check: output/input percentages	132
4.6	Effect of speed and curvature: steering torque and kinematics	134
4.7	Effect of speed and curvature: roll angle decomposition	136
4.8	Effect of speed and curvature: tyre vertical loads	136
4.9	Effect of speed and curvature: tyre forces	138
4.10	Effect of speed and curvature: tyre moments and grip coefficients	141
4.11	Effect of speed and curvature: grip analysis	143
4.12	Effect of speed and curvature: steering ratio	145
4.13	Effect of speed and curvature: kinematic steering angle comparison	145
4.14	Effect of longitudinal acceleration: longitudinal tyre forces	148
4.15	Effect of longitudinal acceleration: lateral and vertical tyre forces	149
4.16	Effect of longitudinal acceleration: steering torque and main kinematics	151
4.17	Effect of longitudinal acceleration: wheel acceleration	152
4.18	Effect of roll rate: tyre forces	154
4.19	Effect of roll rate: steering torque and main kinematics	157
4.20	Effect of roll acceleration: roll angle	158
4.21	Effect of roll acceleration: tyre forces	159
5.1	Roll dynamics estimation: pendulum model	165
5.2	Roll dynamics estimation: reference trajectories	169
5.3	Roll dynamics estimation: steady-state vs dynamic solutions	170
5.4	Roll dynamics estimation: speed sensitivity	171
5.5	Discretization of the desired trajectory	176
5.6	Quasi-steady state results: slalom test (1)	179
5.7	Quasi-steady state results: slalom test (2)	180
5.8	Quasi-steady state results: chicane (1)	183
5.9	Quasi-steady state results: chicane (2)	184

6.1	Rider model control scheme	192
6.2	Root locus: straight line conditions	197
6.3	Root locus: vibration modes	198
6.4	Root locus: cornering conditions	200
6.5	Family of internal models	201
6.6	Preview gains in straight running conditions	208
6.7	Effect of weighting factors	211
6.8	Preview gains in cornering conditions	212
6.9	Mapping from time to distance domain.	215
6.10	Control strategy comparison: feedforward vs predictive	216
6.11	Control strategy comparison: results	218
6.12	Combined strategy: iterative procedure	219
6.13	Combined strategy: applied results	221
6.14	Combined strategy: maximum path error	221
6.15	Slalom results (i)	223
6.16	Slalom results (ii)	224
6.17	Chicane results (i)	226
6.18	Chicane results (ii)	227
6.19	Corner exit results (i)	229
6.20	Corner exit results (ii)	230
6.21	Road profile and statistical properties	233
6.22	Corner entry results (i)	235
6.23	Corner entry results (ii)	236
7.1	Future research lines: laptime optimization	251
A.1	Reduced model	254
A.2	Reduced model: roll dynamics	258

List of tables

1.1	Japanese motorcycle production by engine displacement	2
1.2	Members of the MYMOSA consortium	5
2.1	The early stages: main contributions	14
2.2	The multibody era: main contributions	21
3.1	List of bodies included in the model	72
3.2	List of generalized coordinates	73
3.3	Cost of one call to the state equation	106
4.1	Steady state equations: list of degrees of freedom	120
4.2	Steady state equations: list of tyre states	121
4.3	Steady state equations: list of model inputs	121
4.4	Quasi-steady state equations: list of degrees of freedom	123
4.5	Quasi-steady state equations: list of tyre states	123
4.6	Quasi-steady state equations: list of model inputs	124
5.1	Simulation of continuous manoeuvres: list of degrees of freedom	174
5.2	Simulation of continuous manoeuvres: list of tyre states	174
5.3	Simulation of continuous manoeuvres: list of model inputs	175
A.1	Gyroscopic and inertial torques generated by the main body.	255
A.2	Gyroscopic and inertial torques generated by the wheels.	255
B.1	Inertial properties of the motorcycle	259
B.2	Motorcycle model parameters	260
B.3	Tyre model parameters	261

Nomenclature

Vectors and matrices

\mathbf{a}	acceleration vector
$\mathbf{A}, \mathbf{B}, \mathbf{C}, \mathbf{D}$	discrete-time linear state space matrices
$\mathcal{A}, \mathcal{B}, \mathcal{C}$	state space matrices of the rider's prediction model
$\mathbf{A}_c, \mathbf{B}_c, \mathbf{C}_c, \mathbf{D}_c$	continuous-time linear state space matrices
\mathbf{A}_p	velocity projection matrix
\mathbf{C}_0, \mathbf{C}	theoretical and actual contact points of the tyre model
\mathbf{f}^e	vector of external forces
\mathbf{f}^r	vector of reaction forces
g_j^x, g_j^y, g_j^z	coordinates of the j^{th} CoG expressed in the body frame
\mathbf{h}	angular momentum vector
$\hat{\mathbf{i}}, \hat{\mathbf{j}}, \hat{\mathbf{k}}$	unitary vectors along the x , y and z axes respectively
\mathbf{I}	inertia matrix
\mathbf{J}_T	Jacobian matrix of the translation coordinates
\mathbf{J}_R	Jacobian matrix of the rotation coordinates
\mathbf{K}	rider gain matrix (reduced)
\mathcal{K}	rider gain matrix (full)
\mathbf{K}_x	rider feedback matrix
\mathbf{K}_y	rider preview matrix
\mathbf{l}^e	vector of external torques
\mathbf{l}^r	vector of reaction torques
\mathbf{M}	mass matrix
$\hat{\mathbf{M}}$	mass matrix in minimal coordinates
\mathcal{M}	projection of $\hat{\mathbf{M}}$ on the vehicle frame \mathbf{T}_ψ
\mathbf{p}	linear momentum vector

\mathbf{p}_j	origin of the j^{th} reference frame \mathbf{T}_j
\mathbf{p}_λ	vector of tyre states
\mathbf{p}_t	vector of track states
\mathbf{P}	motorcycle reference point
\mathbf{q}	vector of generalized coordinates
\mathbf{q}_p	vector of generalized positions excluding cyclic coordinates
\mathbf{q}_v	vector of generalized velocities
\mathbf{Q}, \mathbf{R}	weighting matrices of the rider cost function
\mathbf{Q}^e	vector of generalized external forces
\mathbf{Q}^r	vector of generalized reaction forces
$\hat{\mathbf{Q}}$	vector of generalized forces in minimal coordinates
$\hat{\mathbf{Q}}$	projection of $\hat{\mathbf{Q}}$ on the vehicle frame \mathbf{T}_ψ
\mathbf{r}	position vector
\mathbf{S}	orientation matrix
\mathbf{T}	reference frame (homogeneous transformation matrix)
\mathbf{u}	input vector
\mathbf{u}^*	nominal value of the input vector \mathbf{u}
$\bar{\mathbf{u}}$	variation of vector \mathbf{u} with respect to its nominal value \mathbf{u}^*
\mathbf{U}	vector of current and future inputs up to the preview horizon
\mathbf{v}	velocity vector
\mathbf{x}	state vector
\mathbf{x}^*	nominal value of the state vector \mathbf{x}
$\bar{\mathbf{x}}$	variation of vector \mathbf{x} with respect to its nominal value \mathbf{x}^*
\mathbf{X}	vector of estimated states up to the preview horizon
\mathbf{y}	output vector
\mathbf{y}^*	nominal value of the output vector \mathbf{y}
$\bar{\mathbf{y}}$	variation of vector \mathbf{y} with respect to its nominal value \mathbf{y}^*
\mathbf{y}_d	desired output vector
$\bar{\mathbf{y}}_d$	variation of vector \mathbf{y}_d with respect to the nominal value \mathbf{y}^*
\mathbf{Y}	vector of estimated outputs up to the preview horizon
\mathbf{Y}_d	vector of desired outputs up to the preview horizon
\mathbf{z}	vector of unknowns in quasi-steady state problems/vector of independent coordinates in the multibody review of Ch. 3

α	angular acceleration vector
ε	vector of predicted errors up to the preview horizon
Γ	world-to-vehicle projection matrix
λ	vector of Lagrange multipliers
ω	angular velocity vector
Φ	vector of constraint equations
Φ_q	Jacobian of constraint equations
Φ_t	derivative of constraint equations with respect to time
Ψ	projects the current state vector $\bar{\mathbf{x}}$ on the future outputs \mathbf{Y}
Θ	projects the input vector \mathbf{U} on the future outputs \mathbf{Y}
Υ	vector of wheel acceleration constraints
ξ	vector of imposed derivatives

Scalars

a	distance from the vehicle CoG to the front contact point
$a_{x\beta}, a_{y\beta}$	acceleration of point \mathbf{P} resolved in the trajectory frame \mathbf{T}_β
$a_{x\psi}, a_{y\psi}$	acceleration of point \mathbf{P} resolved in the vehicle frame \mathbf{T}_ψ
b	distance from the vehicle CoG to the rear contact point
d_f, d_r	displacement of the front and rear suspensions
F_{ax}, F_{az}, M_{ay}	aerodynamic forces
F_{ch}	chain force
F_{frk}, F_{shock}	fork and shock forces
F_x, F_y, F_z	tyre forces
h	height of the vehicle CoG in upright conditions
l_f	front assembly offset
l_{frk}	length of the fork at full extension
l_m	frame length
l_r	swingarm length
l_{shock}	length of the shock at full extension
L	Lagrangian
m	mass
M_{ch}	chain torque
M_{fw}, M_{rw}	braking torques
M_{swg}	equivalent swingarm moment

M_x, M_y, M_z	tyre moments
n	path error
n_x, n_u, n_y	number of states, inputs and outputs
N	preview horizon
r, R	radii of the front and rear sprockets
s	curvilinear abscissa (distance travelled along the track)
s_f, s_r	front and rear suspension strokes
T	kinetic energy, sampling time of the rider model
u, v	velocity of point \mathbf{P} resolved in the vehicle frame \mathbf{T}_ψ
U	potential energy
v_t	absolute velocity of point \mathbf{P}
V	rider cost function
V_{sx}, V_{sy}	slip velocities of the tyre contact path
V_x	longitudinal velocity of the tyre contact path
x, y	position of the point \mathbf{P} resolved in the inertial frame
z	height of the main assembly CoG measured on the bike plane
β	vehicle sideslip angle
β_{fw}, β_{rw}	pitch angle of the front and rear assemblies
χ	angle of the vehicle with respect to the track
δ	steering angle
Δ	kinematic steering angle
η	motion ratio of the rear suspension $\partial s_r / \partial \gamma$
γ	angle of the swingarm with respect to the frame
\mathcal{I}	moment of inertia
κ	track curvature
κ_f, κ_r	longitudinal slip of the front and rear tyres
λ_f, λ_r	sideslip angle of the front and rear tyres
μ	pitch angle of the main assembly
μ_r	pitch angle of the rear assembly
Ω_{fw}, Ω_{rw}	absolute angular speed of the front and rear wheels
ϕ	roll angle
ϕ_{fw}, ϕ_{rw}	camber angle of the front and rear wheels
ψ	yaw angle

ρ	distance between the contact patch and the wheel axis
σ_y	tyre relaxation length in the lateral direction
τ	steering torque
θ_{fw}, θ_{rw}	angle of the front and rear wheels (relative)
ξ	steering ratio
ξ_f, ξ_r	carcass deflection of the front and rear tyres
ζ_y, ζ_z	local coordinates of the tyre profile

Reference frames

\mathbf{T}_0	ground-fixed reference frame
\mathbf{T}_{fw}	front wheel reference frame
\mathbf{T}_{fwp}	front wheel reference frame (x -axis parallel to the ground)
\mathbf{T}_{fwg}	front wheel reference frame (xy -plane parallel to the ground)
\mathbf{T}_i	auxiliary reference frame
\mathbf{T}_{lf}	lower fork reference frame
\mathbf{T}_m	main assembly reference frame
\mathbf{T}_r	rear assembly reference frame
\mathbf{T}_{rw}	rear wheel reference frame
\mathbf{T}_{rwp}	rear wheel reference frame (x -axis parallel to the ground)
\mathbf{T}_{rwg}	rear wheel reference frame (xy -plane parallel to the ground)
\mathbf{T}_{uf}	upper fork reference frame
\mathbf{T}_β	reference frame tangent to the trajectory
\mathbf{T}_ψ	reference frame aligned with the vehicle

Miscellaneous

c_α, s_α	abbreviation for $\cos(\alpha)$ and $\sin(\alpha)$
CoG	centre of gravity
DOF	degree of freedom
$\hat{\mathbf{i}}^{(\mathbf{T})}$	vector $\hat{\mathbf{i}}$ projected on frame \mathbf{T}
$\mathbf{M}(:, j)$	j^{th} column of matrix \mathbf{M}
$\mathbf{M}(j, :)$	j^{th} row of matrix \mathbf{M}
$\mathbf{Rot}_\xi(\alpha)$	transformation matrix - rotation of angle α around axis ξ
$\mathbf{Tra}(x, y, z)$	transformation matrix - translation along three axes
$\mathbf{0}^{m \times n}$	$m \times n$ null matrix

Because riding is good for my soul...
Anonymous answer to the question
“Why do you ride your motorcycle?”

From SAFERIDER public survey.

Chapter 1

Introduction and objectives

1.1 Motivation

The first motorcycle ever built was actually an engine attached to a wooden bicycle; it was designed and built by the German Engineers Gottlieb Daimler (who later teamed up with Karl Benz to form the Daimler-Benz Corporation) and Wilhelm Maybach in Bad Cannstatt (Stuttgart) in 1885. That marked the moment in history when the development of the petrol-powered engine and the modern bicycle collided. This new vehicle was powered by a single-cylinder Otto-cycle engine, and may have already had a spray-type carburettor since at that time Maybach was working on the development of the first prototype. It is worth noting the first motorcycles did not fit pneumatic tyres as they were introduced for the first time in 1888 by John Boyd Dunlop.

There is a previous invention that could have the honour of being the first motorcycle if the steam propulsion is considered. The American inventor Sylvester Howard Roper built a two-wheeled vehicle powered by a two-cylinder steam-engine in 1867. His steam-powered bike was demonstrated at fairs in the eastern US and anticipated many modern motorbike features, including the twisting-handgrip throttle control.

The first production two-wheeler was the Hildebrand & Wolfmüller, patented in Munich in 1894. Only a few hundred examples of this model were ever built. Apart from the high purchase price, technical problems such as the absence of a clutch prevented

the motorbike from becoming a commercial success. In the early period of motorcycle history, many producers of bicycles adapted their designs to accommodate the new internal combustion engine. As the engines became more powerful and designs outgrew the bicycle origins, the number of motorcycle producers increased.

Until the First World War, the largest motorcycle manufacturer in the world was Indian, producing over 20.000 bikes per year. By 1920, this honour went to Harley-Davidson, with their motorcycles being sold by dealers in 67 countries. In 1928, the German DKW took it over as the largest manufacturer. After the Second World War, the British BSA Group became the largest producer of motorcycles in the world, producing up to 75.000 bikes per year in the 1950s. By that time, streamlining began to play an increasing role in the development of racing motorcycles and held out the possibility of radical changes to motorcycle design. The German company NSU Motorenwerke AG, which held the position of largest manufacturer from 1955 until the 1970s, and the Italian Moto-Guzzi were in the vanguard of this development, both producing very innovative designs well ahead of their time. Many other factories have appeared throughout the twentieth century, among them: Triumph (1902), Harley-Davidson (1903), Moto-Guzzi (1921), Honda (1946), Ducati (1952), Suzuki (1952), KTM (1954), Kawasaki (1954), Yamaha (1955)...

Maker	<50cc	50-125cc	126-250cc	>250cc	>50cc	Total
Suzuki	21.703	2.865	10.832	51.265	64.962	86.665
Yamaha	1.804	6.445	14.321	55.720	76.486	78.290
Honda	10.013	619	6.568	53.678	60.865	70.878
Kawasaki	-	965	5.516	20.698	27.179	27.179
Total	34.170	10.894	37.245	181.361	229.500	263.670

Table 1.1: Japanese motorcycle production by engine displacement and manufacturer. January to June 2013 (source: JAMA).

Today, the Japanese manufacturers Honda, Kawasaki, Suzuki, and Yamaha dominate the motorcycle market, although Harley-Davidson still maintains a high degree of popularity in the United States. Aside from these high-powered motorcycles, there is a very large market for low capacity motorcycles and mopeds. In this latter reference market, the Italian manufacturer Piaggio is currently leader in Europe and one of the four world's largest producers of two-wheeled vehicles.

The motorcycle has evolved since its early days and so has the concept that people have about this vehicle. Nowadays two-wheeled vehicles are more and more used not only for pleasure as in the past, but also because of the increasing mobility needs in

the crowded urban and sub-urban roads of many European towns. In the *developing world* there is an increasingly large demand for mopeds due to the lack of common forms of mass public transport and to the fact that mopeds are much more affordable compared to other motor vehicles. In general, space efficiency and low consumption make two-wheeled vehicles very attractive for urban transport.

Many innovations have been introduced since the Daimler-Maybach motorcycle was built in 1885. For instance, hydraulic shock absorbers were introduced in the 1930s with the aim of improving vehicle handling and comfort as speeds increased. Even though the early design of hydraulic dampers was rudimentary, its concept is still used today: current dampers are based on a moving piston, placed inside a canister, and on the use of oil to control the relative movement of both elements.

The braking performance of motorcycles took a significant step forward with the introduction of disc brakes in the early 1960s. By that time they were only available on racing machines although it did not take long before they were mounted on mass-production motorcycles. The first road motorcycle to fit a front disc brake was the Honda CB750 in 1969. Since then the disc brake has evolved to become the most used braking device nowadays. Compared to drum brakes, disc brakes are lighter, perform better in wet weather and are less prone to fade under severe usage as they dissipate heat better.

The first progressive monoshock rear suspension was introduced in the 1970s. Previous systems used two shock absorbers, one on each side of the vehicle, fitted directly between the arm and the frame. The single shock absorber allowed the use of a linkage to make the suspension progressive, which implied several advantages over traditional systems such as better riding comfort and easier setup.

Above all, improvements in the manufacturing techniques allowed two-wheeled vehicles to be produced at decreasing costs causing thus an extraordinary increment in the number of users. An example of this is the aluminium perimeter frames, which debuted on street bikes in the mid 1980s.

The introduction of computers and electronics in the automotive market during the last decades of the twentieth century initiated a revolution which rapidly gained in importance and has not yet reached its peak. Lately terms such as ABS (Antilock Braking System), TCS (Traction Control System), CBS (combined braking system) are becoming more and more common in the motorcycle jargon. These acronyms designate mechatronic devices aimed at improving the stability, maneuverability and comfort of motorcycles, helping thus the rider and ultimately enhancing safety.

Despite the huge effort put forward by motorcycle manufacturers to improve the road safety and riding comfort of motorcycle riders, the current technology available for

single track vehicles still lags behind the automotive industry. In general, the knowhow acquired for cars cannot be simply reused in motorcycles as two and four-wheeled vehicles differ in many aspects: motorcycles are intrinsically unstable; they reach large roll angles; there is less space for sensors/actuators and less power available; and what is most important, motorcyclists are less prone than car drivers to accept a system that interferes with motorcycle dynamics and personal driving style.

In addition, most of the current devices involve the enhancement of an individual component at a time, regardless of the vehicle as a whole. Current technology has reached the point where, to further improve the performance of the motorcycle, a global and multidisciplinary understanding of the vehicle is essential; it is indispensable to consider the interaction of such diverse elements as road, suspensions, chassis, engine, driver, sensors, electronics, etc. in the design process of new devices.

It is in this challenging framework where simulation takes a crucial role in the evolution and development of new ideas and concepts. The use of virtual models allows to reduce costs, decreases the development time and limits the number of prototypes needed to validate a new design. Furthermore, computer simulations also permit conducting experiments in conditions that would not be feasible in the real world. A key element in this process is the mathematical algorithm employed to mimic the behaviour of the human rider within the simulation environment, also known as rider model. Existing virtual riders have not reached its maturity yet. This fact has motivated the development of this thesis, which final target is the design of a novel rider model based on Model Predictive Control (MPC).

1.2 Context of the research: the MYMOSA project

The number of fatalities in road accidents has decreased in Europe during the last years. This happens in global terms where not only motorcyclists but all types of vehicles are considered. However, the total number of dead motorcyclists in road accidents has remained almost unchanged [1]. Motorcyclists and moped drivers are road users with a particularly high damage risk since motorcycle accidents are severe in nature due to the relative lack of protection of motorcyclists. Furthermore, given the young age of many victims, these accidents often result in a high loss of life expectancy for fatalities and high social-economic costs for severely injured motorcyclists.

Within this context, the European project MYMOSA was born with the ambition to provide a significant contribution to the reduction of motorcycle fatalities and injuries on European roads. The acronym MYMOSA stands for MotorcYcle and MOrtocyclist SAfety. This project was funded by 6th Framework Programme of the European Union

Universities	Companies	Research centres
Imperial College (UK), University of West Bohemia (CZ), L.M. University Munich (D), University of Florence (IT) and University Louis Pasteur (FR).	TRL (UK), IBEO (D), Altair (FR), Dainese SpA (IT), Cellbond Ltd (UK), LMS International (BE), DEKRA (D) and Uniresearch (NL).	TNO (NL).

Table 1.2: Members of the MYMOSA consortium.

(MRTN-CT-2006-035965) and included multiple universities, research institutes and companies as listed in Table. 1.2.

The main outcomes of the MYMOSA project were the collaborative generation of multidisciplinary knowhow in accident dynamics, vehicle dynamics and biomechanics, the development of simulation tools, predictive models, new protective equipment concepts and a new safety vision through the implementation of novel integrated safety devices. For further info the reader is referred to [2].

This PhD thesis was mostly developed within the MYMOSA project and the support of the company LMS International (Belgium), where the author worked for three years in the development of a novel virtual rider for motorcycles as a simulation tool to assess new safety devices. A brief description of the company and its interests is introduced next with the aim of establishing the context in which this research project was carried out.

LMS (Leuven Measurement and Systems) was born as a spin-off of the Catholic University of Leuven in 1980. In its early stages it became widely known in the modal analysis sector for being one of the first companies in the world to make a unified modal data acquisition and analysis system. In addition to this, in the last decade the company has expanded its business into simulation software. Nowadays LMS offers a combination of virtual simulation software, testing systems and engineering services to key manufacturing industries, including structural integrity, system dynamics, handling, safety, reliability, comfort and sound quality. It has more than 400 employees in Belgium and more than 1200 distributed in 40 offices worldwide. As far as the economic aspect is concerned, it produces an annual turnover of more than 140 million euro (2012). From November 2012 LMS is part of the German multinational company Siemens.

LMS took a very active part in the development of this PhD thesis by providing full access to their knowhow and by supporting, both from a technical and a theoretical point of view, the use of their multibody software Virtual.Lab Motion, formerly known as DADS (Dynamic Analysis and Design System).

DADS was born in the 80's based on the research done at the University of Iowa under Prof. Ed Haug [3,4] and financed from the US Army project TACOM (Tank Automotive COMmand). The aim was to develop a more numerically stable and accurate solver since their experience with ADAMS showed poor reliability. Progressively DADS incorporated several technical features based on advanced research successes: superior DAE solver, flexible bodies based on finite element methods, coupled controls and hydraulics, cosimulation with Matlab/Simulink, etc. In 1999 LMS acquired CADSI, the company that had developed DADS since 1983, and incorporated the motion solver to its simulation suite Virtual.Lab, thus giving rise to Virtual.Lab Motion. LMS software was used as a validation tool for the symbolic motorcycle model presented in this thesis.

1.3 Objectives of the thesis

Given the context depicted in the previous sections, the aim of this research project is the development of a novel rider model for the dynamic simulation of motorcycles.

Dynamic simulation is applied nowadays within the motorcycle industry for a great variety of purposes. Typical applications go, for example, from comfort analysis to the design of advanced riding assistance systems. However, most of these simulations are limited to basic manoeuvres, generally straight line and slow cornering (low roll rates). Although significant progress has been made in the last decade in the field of rider modelling, a satisfactory solution for the dynamic simulation of motorcycles is yet to be found.

Two-wheeled vehicles are complex dynamic systems; they are highly nonlinear, non-minimum phase, unstable and underactuated. This makes motorcycle control a rather challenging task. As a matter of fact, existing rider models work well only in a limited set of conditions. In general, they are not able to cope with severe manoeuvres, showing poor performance when simulating aggressive acceleration profiles, quick direction changes, etc. Most of them also require a great deal of interaction from the user to adjust the controller parameters. In addition to that, many of these rider models are based on highly simplified motorcycle models that do not take into account the main vibration modes of the vehicle (e.g. capsize, wobble and weave), which results in a loss of accuracy.

The rider model presented in this thesis is expected to increase the range of application of the current simulation tools. In particular, we intend to develop a control strategy capable of riding a multibody motorcycle model in a wide range of conditions, including extremely demanding manoeuvres such as those performed by racing riders. For that purpose, the following points are deemed necessary:

- Development of a symbolic multibody model of the motorcycle. Such model must describe the nonlinear dynamics of a generic road motorcycle, thus providing a suitable framework for the development of the thesis. The model will be employed at two different levels throughout the project. In the first place, it will be used as the *nonlinear plant* to be controlled, i.e. it will represent the real vehicle within the simulation environment. In the second place, and more importantly, the motorcycle model will be used to develop the *internal model* associated to the rider control strategy. This last application imposes several requirements on the model that are described next.
- Characteristics of the multibody model. In order to facilitate the design of the rider control strategy, it is desirable to formulate the multibody model as a system of Ordinary Differential Equations (ODE) in state space form. In addition to this, we will augment the model equations in order to include the curvilinear coordinates of the vehicle with respect to the target path. Such coordinates will allow us to define the rider model in a direct and intuitive way. Finally, we will improve the efficiency of the multibody code by using Computer Algebra Software (CAS).
- Quasi-steady state solution of the target manoeuvre. As part of the process to build the rider model, it is considered essential to obtain the quasi-steady state solution of the motorcycle equations along the desired manoeuvre. Given the manoeuvre specifications, defined in terms of the target trajectory and the desired speed profile, the solution of the quasi-steady state problem will provide a suitable estimation of the model states and control inputs along the target trajectory.
- Characteristics of the quasi-steady state solution. The study of the stationary motion of vehicles is widespread in the automotive literature, especially as far as four-wheeled vehicles are concerned. Unlike previous works, the quasi-steady solution introduced in this thesis will not be limited to the constant speed case. In order to get a suitable estimation of the vehicle's states and control inputs, it is intended to include the effect of the longitudinal acceleration in the problem formulation. We will also consider the effect of the most relevant derivatives such as the roll rate and the roll acceleration. The quasi-steady state solution will be obtained by solving the nonlinear algebraic equation system that arises from the dynamic model when the desired quasi-steady state conditions are imposed.
- Sensitivity study. An extensive parametric study will be conducted in steady and quasi-steady state conditions in order to gain insight into the behavior of the motorcycle. The steady state motion of the motorcycle will allow us to explore

how the most relevant variables (e.g. steering torque, tyre forces, attitude, etc) vary as a function of the corner radius and the vehicle speed. On the other hand, the quasi-steady state analysis will assess the effect of the longitudinal acceleration and the roll derivatives. Basically, we will determine to what extent these terms modify the solutions obtained assuming pure stationary conditions. The information obtained from this analysis will allow us to sketch the design requirements of the virtual rider.

- Definition of the internal model and stability analysis. The internal model of the rider's control strategy will be defined as the linearization of the motion equations along the quasi-steady state solution of the manoeuvre. In addition to that, we will use the results of the linearization to perform a stability analysis of the motorcycle in straight line and cornering conditions. Results will provide valuable information on how the vibration modes of the vehicle (frequency, damping and modal shape) vary in function of the running conditions.
- Development of the prediction model and related control strategy. The internal model symbolizes the rider's mental image of the motorcycle, i.e. a representation of the inverse dynamics of the vehicle that the human mind constantly tunes based on experience. Humans use this stored knowledge while riding to estimate the future behavior of the vehicle and then act accordingly to achieve the desired goal, e.g. to follow a predefined path. The rider model introduced in this thesis will behave in a similar way. We will employ the internal model to formulate a prediction model, which will be subsequently optimized in order to minimize the error between the system's output and the desired control targets. The development of the control strategy will be based on Model Predictive Control theory.
- Representative simulations and analysis of results. We will conclude this thesis by applying the developed methodology to four severe manoeuvres. In the first place, we will perform a slalom test, which typically consists of multiple line-up cones that must be avoided by the rider. Such manoeuvre will allow us to investigate the response of the rider against fast variations in the lateral acceleration target. In the second place, we will use a chicane to assess the behaviour of the rider model under severe combined conditions. In this case the motorcycle will be ridden along an s-shaped trajectory typical of race tracks. The combination of high longitudinal and lateral accelerations, together with the abrupt transition from acceleration to braking, make this manoeuvre a challenging test for the rider model. The third example will be a corner exit manoeuvre. Similarly to racing riders, the rider model will accelerate along the corner until the front tyre is lifted.

Finally, we will simulate a corner entry maneuver where the rider will decelerate aggressively as the vehicle rolls into the corner. We will use this last manoeuvre to test the robustness of the rider model against road perturbations. For that purpose, we will use an uneven road profile.

1.4 Outline of the thesis

This thesis consists of seven main chapters, not counting annex and references. It presents a comprehensive collection of mathematical tools for the analysis and control of motorcycles. The document is organized as follows:

- Chapter 1. **Introduction and objectives.** The present chapter describes the motivation that led to the development of this thesis, introduces the context of the MYMOSA research project and presents an overview of the different chapters that compose this dissertation along with its objectives.
- Chapter 2. **Review of motorcycle dynamics and rider modelling.** This chapter presents a literature review on motorcycle dynamics and rider control. In first place, the most relevant motorcycle models presented to date are studied and their characteristics are comprehensively analyzed. The second part of the chapter introduces the topic of tyre modelling and emphasizes its importance in the field of computational vehicle dynamics. The chapter continues with a detailed description of the existing rider models, paying special attention to the most relevant approaches used in their development, namely classical and modern control theories. A thorough analysis of the existing rider models reveals that the problem is still open. Finally, a critical summary of the results is presented together with some concluding remarks.
- Chapter 3. **A symbolic motorcycle model for virtual rider design and simulation.** An analytical motorcycle model based on the symbolic multibody approach is presented in this chapter. The chapter starts with a brief review of the multibody formulations currently available in literature, including a comparison between symbolic and numeric formalisms. The multibody model of the motorcycle model is presented in the second part of the chapter along with a detailed description of its implementation. The tyre model and the underlying assumptions of its formulation complete this section. In the third part, an additional multibody model developed in LMS Virtual.Lab Motion is introduced and then used as a validation tool. To conclude, some considerations regarding the advantages of the symbolic model are presented and discussed.

- Chapter 4. **A new methodology for the quasi-steady-state analysis of motorcycles.** This chapter, together with Chapter 5, introduces a new methodology for the quasi-steady state analysis of motorcycles. The approach presented here is based on the reduction of the dynamic model to a set of nonlinear algebraic equations. The first part of the chapter describes the quasi-steady state assumptions and how they are applied to the multibody model. This section also includes the development of a continuation strategy to efficiently explore the effect that the input parameters (curvature, speed, etc) have on the motorcycle behaviour (tyre forces, sideslip angle, etc). Such strategy is applied in the second part of the chapter to perform an extensive parametric study. A thorough analysis of the results completes the chapter.
- Chapter 5. **Quasi-steady state analysis of continuous manoeuvres.** This chapter extends the methodology introduced in Chapter 4 to simulate continuous manoeuvres. Fundamentally, this means that, instead of finding the solution for a predefined set of input parameters, in this chapter we solve the states and control inputs needed to drive the vehicle along a given path. As the name of the chapter indicates, this is done in a quasi-steady state fashion. The chapter is structured in two parts. In the first part we use a dynamic inversion approach to estimate the roll rate and its derivative along the target trajectory. The results of the estimation problem are then used in the second part of the chapter to develop a novel procedure for the quasi-steady state analysis of motorcycles. The resulting strategy is applied to two different manoeuvres, a slalom test and a chicane. Finally, the advantages and drawbacks of the proposed methodology are discussed.
- Chapter 6. **A rider model based on MPC.** This chapter introduces a new approach for the dynamic simulation of motorcycles based on Model Predictive Control. In particular, we develop an algorithm to drive a nonlinear motorcycle model along a control target, defined by a reference path and a given speed profile. The first part of this chapter deals with the linearization of the motion equations along the quasi-steady state solution of the problem. The outcome is a family of state space models that represent the rider's mental model of the vehicle at every point of the reference path. The underlying equations of the rider model are described in the second part of the chapter together with the details of its implementation. In the third part, a series of maneuvers are simulated and their results are thoroughly discussed. The robustness of the rider model is ultimately demonstrated by including the road unevenness in one additional simulation. The

chapter ends with some remarks and conclusions on the performance of the rider model.

- Chapter 7. **Conclusions and future work.** This chapter summarizes the main findings of the present work and their practical applications. A series of recommendations for future research lines are also presented at the end of the chapter.

Steering a motorcycle or bicycle is counterintuitive; to turn right, you must steer left initially, and vice versa. You can execute this initially counter-directed turn by turning the handlebars explicitly (called counter-steering) or by throwing your hips to the side. Contrary to common belief, gyroscopic forces play only a limited role in balancing and steering.

D. E. H. Jones, Phys. Today (1970)

Chapter 2

Review of motorcycle dynamics and rider modelling: the state of the art

2.1 Dynamics of single track vehicles and its modelling

2.1.1 The early stages

Since the first single track vehicles were built in the early 19th century, many vehicle dynamicists have investigated their dynamic behaviour attracted by the fascinating stability characteristics of bicycles, motorcycles and similar vehicles. One of the first publications on this field dates back to 1869, when Rankine [5] presented semi-quantitative observations on the stability and steering behaviour of velocipedes. He was probably the first to provide a basic description of the countersteering¹ phenomenon, noticing that centrifugal forces were sufficient to balance the gravitational overturning moment caused by the roll angle of the vehicle.

Another early investigation worth mentioning was developed in the late nineteen century by Whipple [6] and Carvallo [7] who derived, independently of each other, the nonlinear differential equations that describe the dynamic behaviour of a bicycle.

¹‘Riders briefly turn to the left to generate the rightward lean necessary for a steady rightward turn’. Rankine, 1869.

Year	Author	Main contribution
1869	Rankine	Presented semi-quantitative observations on the steering behaviour of velocipedes. First description of countersteering.
1899	Whipple Carvallo	Derived the motion equations of the bicycle and studied its linear motion in straight-running conditions.
1971	Sharp	Investigated the straight line stability of large motorcycles. Sharp was one of the first to consider the effects of tyre relaxation.
1974	Sharp	Studied the influence of frame flexibility on the lateral stability of motorcycles.
1974	Jenninngs	First to observe the coupling between pitch and weave modes.
1976	Sharp	Demonstrated the interaction of pitch and weave at high speeds.
1978	Kane	Studied the effect of frame flexibility on high speed weave of motorcycles.
1979	Weir & Zellner	Investigated experimentally the steering behavior of motorcycles in transient conditions.
1983	Koenen	Presented a pioneering study of the motorcycle vibration modes in steady-state cornering conditions.
1985	Nishimi	Developed a 12-dof motorcycle model including the rider's body. Studied the effect of body properties in the straight running stability of motorcycles.
1988	Katayama	Modelled the human rider as a 2-dof inverted pendulum. Studied the control behaviour of motorcycle riders.
1994	Sharp	Put together the state-of-the-art features into one simulation model: flexibilities, rider's torso lean, tyre model, etc.

Table 2.1: The early stages: summary of the most relevant contributions to the study of single track vehicles before the introduction of multibody codes.

Whipple's equations were derived using a Lagrangian approach and already included the possibility of the rider applying a control action modelled as a torsional steering stiffness. His model consisted essentially of two bodies, frame and fork, connected through a revolute joint along the steering head. The wheels were assumed to be infinitely thin, and were included in the model as nonholonomic constraints, meaning that no tyre slipping was possible. In total the model had only two degrees of freedom, roll and steering, as the speed was imposed through a kinematic constraint applied to

the frame. Whipple's model did not include any aerodynamic effects, suspensions or flexibility. Carvallo's model, on the other hand, was slightly simpler as it neglected the mass and moments of inertia of the front assembly in comparison to those of the front wheel.

By that time no computational tools were available to integrate such a set of differential equations, and in consequence Whipple's equations were never used directly. Instead, they were simplified into a linear set of differential equations and then used to study the small motions of the vehicle about a straight-running trim condition. Whipple used the Routh criterion to assess the stability of the system at constant speed, concluding that the bicycle was self-stable without rider control in the small speed range between 16 and 20 kph. However, at higher speeds the rider was concluded to be essential for bicycle stability. Carvallo, on the other hand, identified the eigenmodes of the bicycle and derived the equations that predict its critical speeds during hands-free straight running. Despite of the solid foundations laid by Whipple and Carvallo, research on the dynamics of single track vehicles evolved slowly in the subsequent years. A detailed description of early mathematical models can be found in [8], [9] and [10].

In fact, it wasn't until 1971 that the first relevant analysis of motorcycle dynamics was published. Robin Sharp [11] used a linear model to carry out a theoretical analysis of the straight line stability properties of a large motorcycle, including discussions about rider control and its implications on vehicle design. He used a Lagrangian approach to derive the equations of motion of his model, which was composed of two rigid bodies joined at an inclined steering axis; suspensions were not included, and the rider was assumed to be rigidly attached to the rear frame. In total, the model had four degrees of freedom, namely lateral motion, roll, yaw and steer. No aerodynamic forces were included. Probably the most interesting feature of this work was inside the tyre model as Sharp, unlike previous authors, did not assume that the lateral force builds up instantaneously in response to sideslip. Instead he used a first order filter to model the so called relaxation behaviour of the tyre [12]. The aim of this filter was to limit the bandwidth of the tyre response, hence making the model behaviour more realistic.

Sharp used the model described above to investigate the main motorcycle modes in steady-state straight line conditions. To that end he wrote the system equations in state-space form and obtained the model eigenvalues and eigenvectors from the state matrix. His results and, in particular, the variation of the modal damping and frequency with speed, contributed significantly to the current understanding of motorcycle dynamics. During his research, Sharp explored two possible rider control strategies: fixed and free control. In order to investigate the so-called fixed control approach, Sharp removed the steering dynamics from his model, thus assuming that the rider was able to control the

steering angle regardless of the required torque. On the other hand, in free-control mode steering dynamics were necessary as the rider was assumed to control the handlebar by means of the steering torque. After multiple studies, fixed-control was found to be unattractive for motorcycle simulations, as opposed to double track vehicles (cars, trucks, etc) where the low forces required to steer the vehicle make this assumption more realistic. Therefore, Sharp concluded that motorcycle dynamics should be regarded as involving free-control.

Sharp predicted the presence of three important vibration modes by using a free-control model, which were denominated *capsize*, *wobble* and *weave*. Capsize is a divergent instability where the whole vehicle behaves as an inverted pendulum, falling onto its side. This mode evolves very slowly, on the order of seconds, being easy for the rider to control it. For this reason, capsizing stabilization is normally done subconsciously. Furthermore, this mode can be intentionally excited by the rider to initiate a turn [13, 14]. Instead, weave is a low frequency oscillation of the whole motorcycle (2-3 Hz) involving roll, yaw and steer motions. This mode is stable at low and medium speeds, becomes progressively less damped at higher speeds and may become unstable at very high speeds. The third mode, wobble, is a high frequency mode (7-9 Hz) involving primarily the steering system rotating with respect to the main frame. Sharp's model predicted this mode to be stable at low speeds, becoming less damped as the speed increases. Wobble is qualitatively similar to the well-known wheel shimmy on aircrafts and cars [12]. Sharp performed a series of experiments with his model to assess the effect of the tyre relaxation on motorcycle modes, coming to the conclusion that it was an essential feature of the model as its absence unrealistically stabilized the wobble mode. In contrast, capsizing and weave were almost unaffected by the tyre relaxation. Sharp also demonstrated that the steering damper improves wobble stability while is detrimental for the weave mode.

Sharp's groundbreaking work can be considered the starting point of modern motorcycle dynamics. As a matter of fact, his research has inspired a great number of papers on this subject. Models have become more and more complex, including new features and making use of the latest computational advances. However, the influence of his findings is still relevant to this day.

Following Sharp's 1971 publication, and acknowledging the great utility of his new approach as a potential design tool, several research groups developed advanced models to explore further aspects of motorcycle behaviour. By the middle of the seventies, Sharp [15] and Kane [16] investigated the influence of frame flexibility on the lateral stability of motorcycles. To that end, Sharp extended his original model by adding a new degree of freedom, the roll motion of the rear wheel with respect to the frame, and introduced a

(lumped) torsional spring-damper between these two bodies that represented the frame compliance. Low frame flexibility was found to be detrimental to the stability of the weave mode at medium and high speeds, while its influence on the capsize and wobble modes proved to be irrelevant. It was also demonstrated that increasing the frame stiffness above a certain level does not produce significant changes in stability. It is worth noting that the structures of modern motorcycles, especially in motorsports, are quite stiff and the reported effects have limited value nowadays. Other aspects that Kane studied were the influence of mass distribution and fork trail.

Parallel to this research, Jennings [17] and Sharp [18] studied the most compliant structural element of the motorcycle: the suspensions. Jennings was the first to observe an unprecedented weave oscillation in cornering with significant suspension movement, suggesting that pitch and weave modes could be interacting. A few years later, following a Dunlop film showing this phenomenon, Sharp demonstrated by a simple analysis [18] that the natural frequency of the weave mode gets closer to that of the pitch as the speed increases, which could lead to the interaction of both modes at high speeds. At that time it was clear that the mode coupling between in-plane and out-of-plane modes was weak in straight running conditions; on the contrary, these new findings suggested that the coupling would become stronger at higher roll angles. Hence, a full analysis of the motorcycle vibration modes in cornering conditions was needed to shed light on this question.

Koenen PhD thesis in 1983 [19], along with his previous work with Pacejka [20, 21], represented a big step forward in motorcycle theoretical analysis. His most significant contribution was a pioneering study of the motorcycle vibration modes in steady-state cornering conditions. To that end, Koenen's model comprised two sets of equations: a set of nonlinear algebraic equations, needed to describe the stationary cornering equilibrium, and a system of linear differential equations with constant coefficients that described the dynamic response of the system. Koenen was aware that including the suspension degrees of freedom in the model was crucial for the accurate modelling of the cornering motorcycle, as suggested by [18]. Consequently, he used a total of eleven generalized coordinates, including both suspension strokes as well as the torsion of the frame and the lean angle of the rider's torso. The tyres were treated as radially flexible, taking into account their cross-sectional shape in a simple geometrical fashion similar to that employed by Eaton [22], except that the overturning moments were neglected. The outputs of the tyre model, i.e. side forces and aligning moments, were applied at the contact patch as functions of the slip angle, the camber angle, the turn-slip and the normal load. The tyre relaxation behaviour was also taken into account, assuming the same relaxation length for all tyre inputs. The model featured also in-plane

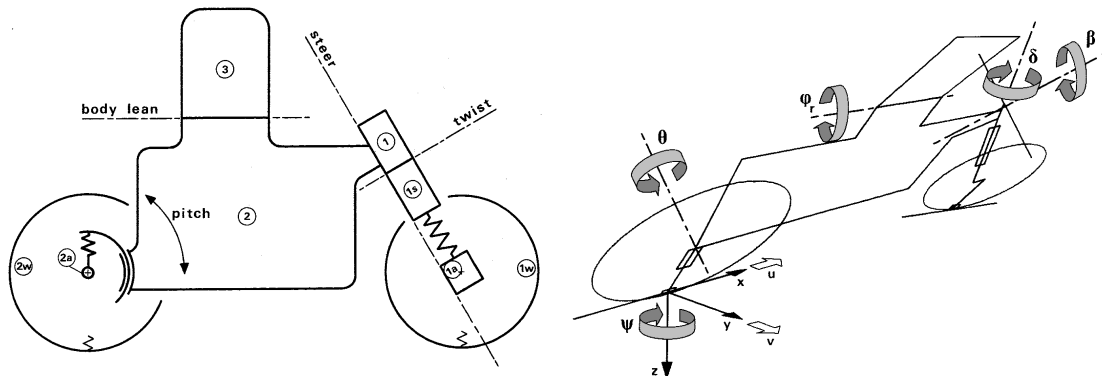


Figure 2.1: Motorcycle model developed by Koenen (1983). This model comprised a total of eleven generalized coordinates, including suspension strokes, frame torsion and rider's lean. Note the simplified rear suspension, modelled as a vertical stiffness applied at the wheel center. Images from [19].

aerodynamic forces.

Koenen used the set of linear equations described above to study the stability of the cornering motorcycle. Nowadays it is a well known fact that lightly damped modes can lead to catastrophic consequences if they are excited. When this happens, the steering torques and frequencies involved make it very difficult for the rider to control the vehicle. In cornering conditions the risk is even higher as the vehicle is usually more difficult to control. In this context, Koenen's results were very useful. He was the first to prove what Sharp suggested in [18], i.e. the coupling between in-plane and out-of-plane modes increases with increased roll angle, the suspensions playing an important role in this phenomenon. Koenen showed that a significant energy transfer between in-plane and out-of-plane modes is possible in cornering conditions; modes with similar frequencies tend to interact, thus giving rise to new modal shapes. He introduced for the first time the cornering weave and other cornering modes such as those arising from the coupling between wheel-hops and wobble modes. His results included multiple root-loci in an attempt to study the sensitivity of the vehicle response to parameter variations. Unexpectedly, and in contrast with the experimental results of Jennings [17] and Weir & Zellner [23], Koenen's model predicted that the suspension damping had a very little effect on cornering stability. Many years later, in 2000, Sharp suggested in [24,25] that these discrepancies could be due to an error in Koenen's calculations. Despite this, Koenen's research settled the basis for the study of motorcycle dynamics in cornering conditions. It is important to note that the computational resources available at that time were very limited, what makes his contribution even more impressive. We could mention, as a curiosity, that he recorded on film the computer graphic output in order to

animate the mode shapes, which would otherwise have been very difficult to interpret.

By the middle of the eighties rider modelling started to receive more and more attention as body motions were suspected to have a big impact on the motorcycle response. Early studies had simplified the analysis by rigidly connecting the rider to the rear frame or, in the most detailed models, by modelling the lean of the rider's torso with respect to the main frame as in [19, 26]. In the subsequent years to Koenen's work, several authors focused their research on the rider model, proposing different alternatives to model the human body motion on the motorcycle. We can divide them into two groups: passive models, which used simple springs and dampers to keep the rider position, and active models, which included additional control elements to dynamically control the rider position during the simulation. In this section we will only focus on the structural part of the rider model as the control algorithms deserve special attention in this thesis, and thus they will be discussed later in a dedicated section.

A noteworthy example of rider structural modelling was presented in 1985 by Nishimi [27], who used an elaborated model to study the straight running stability of motorcycles. His mathematical model consisted of twelve degrees of freedom, divided as follows: two degrees of freedom were used to represent the rider motions, including the leaning movement of the upper body and the lateral displacement of the lower body with respect to the frame, while the remaining ten degrees of freedom were used to model the vehicle, including four rigid motions (lateral displacement, yaw, roll and steer) along with the torsional and bending deformations of the fork, frame and swing arm. A passive combination of linear springs and dampers were used to keep the rider upright.

The parameters of the rider model were obtained experimentally; Nishimi identified the vibration response of the rider's body to vehicle roll by means of an excitation bench and an innovative device to measure the rider's position and attitude with respect to the motorcycle. He then used his model to obtain the frequency and damping ratios of the weave and wobble modes for the straight running case at several speeds. Experimental tests were conducted with four motorcycles of different sizes and the outcome was compared with numerical results, obtaining a good correlation. Measured damping factors were observed to be slightly greater than those predicted by the model. Nishimi also used a second model, without the rider's degrees of freedom, which showed worse correlation. Additionally he also investigated numerically the effect of several body parameters (mass, inertia and CG position) on motorcycle stability, concluding that upper body parameters influence mainly the weave mode while those regarding the lower body influence primarily the wobble mode.

Following Nishimi's trend of using two degrees of freedom to model the rider's body, Katayama [28] presented in 1988 a new rider model with two rotational degrees of

freedom, allowing the lower body to lean relative to the frame instead of moving laterally as in [27]. Basically, the rider was treated as a double inverted pendulum connected to the main frame. The motorcycle model used by Katayama was much simpler than Nishimi's as no compliances were included; it was essentially the same as Sharp's 1971 model [11], described by a linear system with four degrees of freedom. Katayama's tyre model included lateral forces, aligning moments and overturning moments due to sideslip and camber angle. He also included the tyre relaxation behaviour as a first order system. The main objective of his research was to study the control behaviour of motorcycle riders. For this purpose a lane change manoeuvre was simulated and results were compared with experimental tests carried out by several riders, showing a good correlation. Katayama's control algorithm is described in detail in section 2.3.1.

Returning to the general motorcycle modelling overview, in 1994 Sharp presented an update of his model [29] that put together most of the state-of-the-art features available at that time, such as lateral and twist frame flexibilities (lumped at the steering head), flexibility of the rear wheel assembly (around an axis attached to the main frame), rider's torso lean, in-plane aerodynamic effects and a detailed tyre model. Sharp's tyre model included lagged and instantaneous outputs in response to sideslip and camber angles respectively: side forces and aligning moments were produced by both mechanisms, while the overturning moment depended only on the camber angle. The tyre model was basically linear, with the only exception that its coefficients were defined as functions of the tyre load. The tyre was considered infinitely thin, and an overturning moment was used to account for the lateral shift of the tyre contact patch in camber conditions. Other details of the tyre modelling, e.g. turn slip and tread band mass effects, were known to be negligible from [30] and therefore were not included. The parameters of the model were obtained from laboratory experiments. Sharp used his new model to conduct a sensitivity study on several design parameters that affect the straight running stability of motorcycles. Hence, no suspensions were included in the model due to the low coupling between in-plane out-of-plane modes in these conditions. He also studied the effect of the rider impedance on motorcycle dynamics in what he called "hands on" and "hands off" case studies. The main difference between both cases was the amount of stiffness, damping, and inertia applied to the handlebar in order to model the rider's arms. Sharp's results showed a good correlation with experimental data [31]. It is worth noting that this was one of the last Sharp's models derived using a manual method.

2.1.2 The multibody era

By the middle of the nineties, the ever-increasing model requirements were so high that the manual derivation of the equations of motion was not practical anymore. It was

Year	Author	Main contribution
1994	Sharp	Presented a review on the existing multibody codes and their application to the mathematical modelling of road vehicles.
1996	Ghani	Successfully reproduced Sharp's results with the multibody modelling package AutoSim.
1996	Imaizumi	Developed a multibody model of the rider's body composed of twelve rigid bodies, thus allowing naturalistic movements.
1998	De Vries & Pacejka	Adapted the Magic Formula to motorcycles.
1999	Cossalter	Presented a comprehensive analysis of the steady turning of two-wheeled vehicles based on an algebraic symbolic model.
2001	Sharp	Presented a new version of his model based on AutoSim and confirmed the cornering results established by Koenen.
2001	Limebeer	First stability analysis of the motorcycle under acceleration and braking in straight running conditions.
2002	Cossalter	Presented a motorcycle model for real time applications. Introduced a new tyre model with a detailed description of the elastic deformation of the carcass.
2002	Cossalter	Published the first book entirely dedicated to motorcycle dynamics.
2004	Sharp & Evangelou	Latest version of Sharp's model. Included an improved tyre geometry, an analytic treatment of the rear suspension and a new tyre model fully based on Pacejka's Magic Formula.
2004	Evangelou	Introduced the first steering compensator for sport motorcycles motivated by the poor stability of these vehicles at high speeds.
2008	Cossalter	Presented the first riding simulator based on a detailed multibody model.

Table 2.2: The multibody era: summary of the most relevant contributions to the study of motorcycle dynamics after the introduction of multibody codes.

during that period when the need of automated tools for model generation converged with the emerging computer codes for mechanical modelling such as multibody packages, thus opening a new era in the field of vehicle dynamics. A review on the application of multibody codes to the mathematical modelling of road vehicles was presented by Sharp in 1994 [32]. In this publication the existing multibody codes were classified in two categories, numeric and symbolic, and their main characteristics were discussed. In general,

numeric codes prepare and solve the equations numerically, and then post-process the results to produce outputs provided to the user as tables, graphs or animations. These codes are oriented to the product's final design, and model equations are not available for the user to explore or manipulate them. Symbolic codes, as opposed to numerical, derive the equations of motion in a fashion similar to hand derivation; obtaining first the model equations which are then converted into a C or FORTRAN source code in order to produce highly specialized, problem-oriented, simulation programs. This approach allows a low-level control of the model. Furthermore, some of these symbolic codes exploit algebraic manipulation to simplify the equations of motion with the aim of producing extremely efficient simulation codes. In a second stage the code is compiled and numerical results are obtained via numerical integration (time histories), perturbation (linear analysis), etc.

A significant example of this new era can be found in [33], where Gani (1996) revisited Sharp's latest model [29] with the aim of reproducing his results with the multibody modelling package AutoSim [34]. He successfully verified that both approaches yielded the same results, and highlighted in the conclusions the advantages of using an automated approach for model development with respect to manual procedures: reduced building time, less probability of error, and effortless parametric studies and topology changes.

Contemporary to Gani's research, Imaizumi [35] took the rider structural modelling a step forward by introducing a very complex multibody model composed of twelve rigid bodies, representing the rider's arms, legs, trunk, etc. Imaizumi used a combination of spring, dampers, and proportional control elements to stabilize the rider's joints, allowing naturalistic movements such as steering, body leaning, body pitching, weight shift and knee grip. The motorcycle model used in this work was based on Nishimi's [27]. Several simulations corresponding to a corner entry manoeuvre were presented with small roll angles of up to twenty degrees. Imaizumi developed his model in a series of later papers [36–38].

The application of multibody codes to motorcycle dynamics spread very fast during the last years of the nineties, giving rise to an unprecedented boost in this field. For instance, Cossalter used an algebraic² symbolic model in 1999 [39] to study the steady turning of two-wheeled vehicles, giving special emphasis to the influence of speed and curvature on the steering torque. His model included detailed steering kinematics and a comprehensive tyre model with circular cross-section, thus automatically accounting for the lateral migration of the contact point. Tyre forces and moments were applied at the

²Cossalter's equations were derived specifically for a steady-state cornering analysis. In these conditions the vehicle differential equations become algebraic as the states and its derivatives are constant.

contact patch in response to longitudinal slip, sideslip and camber angle. In particular, the tyre model included longitudinal and lateral forces as well as rolling resistance and aligning/twisting moments. Suspensions were not considered. The resulting system of nonlinear algebraic equations was solved by means of a fixed-point iteration method for several combinations of roll and steering angles. Cossalter showed that the steering torque is the result of the simultaneous action of several forces and moments with either aligning or twisting effects. In the range of velocities and curvatures considered, sideslip and roll stiffness showed little effect on the steering torque while the twisting torque was found to be the most important contribution at high roll angles. It was also shown that the design of the front fork has a significant effect on the steering torque; over a wide range of speed and curvature values, increasing the trail reduces the steering torque, whereas increasing the castor angle has the opposite effect.

In 2001 Sharp developed a new dynamic model [41] for the stability and control analysis of motorcycles based on Gani's work [33]. Sharp's new model became more general and powerful than any other model in the literature of that time [41] due to the use of state-of-the-art multibody tools; the model was implemented in the commercial multibody code AutoSim [34] and comprised thirteen degrees of freedom. Rider's lean and frame twist degrees of freedom were included, as well as a detailed description of the steering kinematics and front tyre contact point. The most relevant differences with respect to Sharp's 1994 model [29] were the possibility to simulate the motorcycle in corner conditions and the presence of suspensions. Furthermore, unlike Koenen [19] who used a simplified suspension, Sharp's new model included a detailed modelling of the swinging arm and its associated suspension system. A historical review of Sharp's models is shown in Fig. 2.2. Currently, the commercial multibody package BikeSim [42], developed by the same company of AutoSim, is largely based on Sharp's 2001 model.

This new model confirmed the fundamental patterns of behaviour of the cornering motorcycle established by Koenen [19]. In particular, the in-plane and out-of-plane modes were shown to become increasingly coupled as the roll angle increases. Sharp's root loci were similar to those of Koenen. However, detailed results did not match and it was suggested that the reason might be an error in Koenen's calculations. Sharp acknowledged Koenen's monumental dedication in deriving the equations of motion by hand, and was not surprised that exact results could not be reproduced. With respect to the major prediction problem of Koenen's model, which predicted that the suspension damping had a very little effect on cornering stability, Sharp's results were in line with experimental evidence [17,23] and conflicted with Koenen's, thus showing his predictions were not correct.

Limebeer used Sharp's 2001 model to investigate the straight running stability of

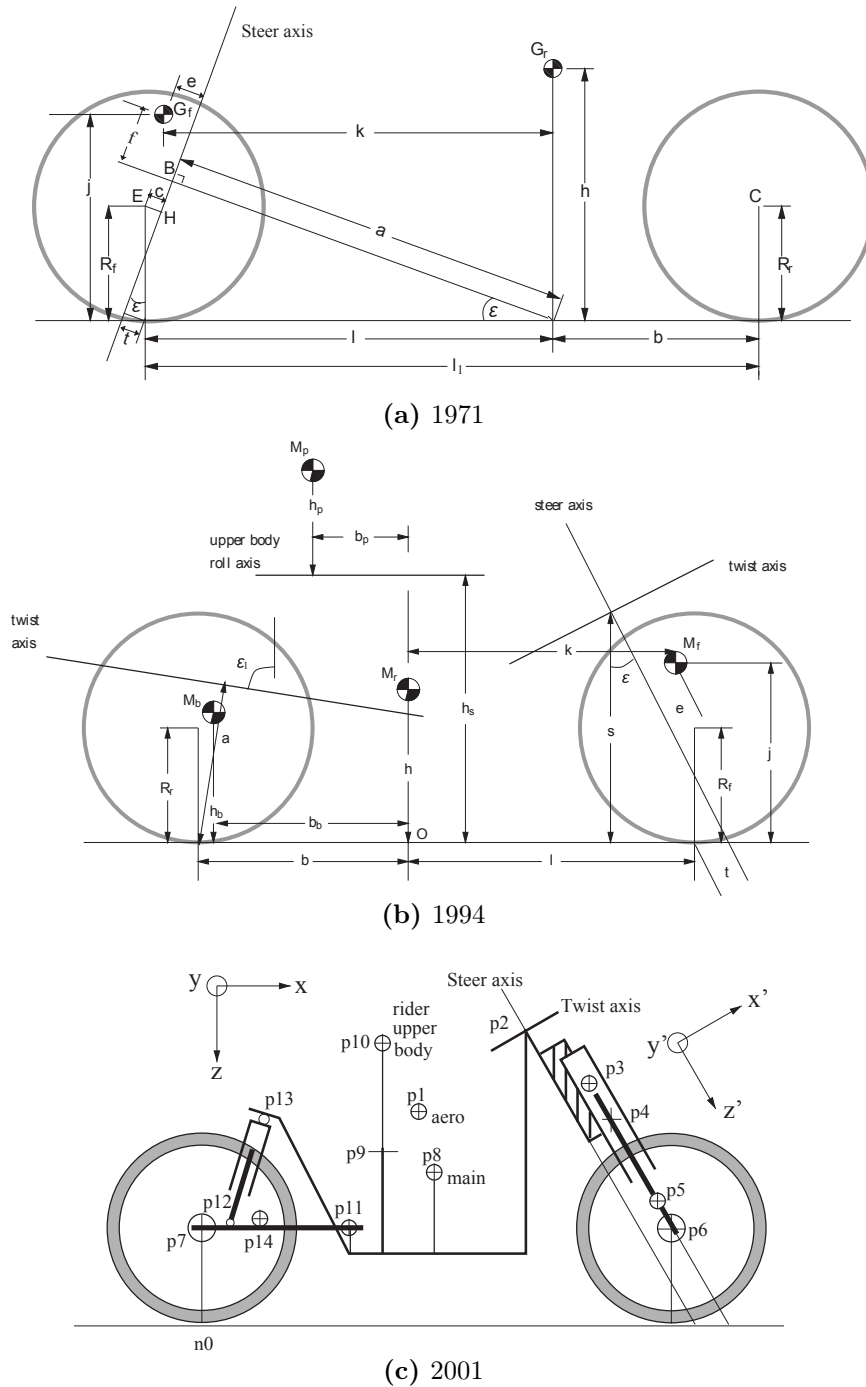


Figure 2.2: Evolution of Sharp's model topology throughout the years. (a) 1971, Sharp's first model was composed of two rigid bodies joined at an inclined steering axis: rear and front frames. (b) 1994, new degrees of freedom were added to model the flexibility of the fork and frame as lumped parameters. (c) 2001, multibody tools were used for the first time to derive the equations of motion (AutoSim). The model comprised thirteen degrees of freedom. Images from [40].

motorcycles under mild acceleration and braking conditions [25]. His work can be considered the first successful analysis of the accelerated motion of two-wheeled vehicles. Twenty five years earlier, in 1976, Sharp had made an early attempt but his results were proved incorrect by Limebeer, who suggested that Sharp's model was too simple to explore this phenomenon. Limebeer simulated the motorcycle in two different scenarios, accelerating/decelerating on a flat surface and ascending/descending an inclined surface at constant speed. He showed that both conditions have similar effects on vehicle stability. In particular, he concluded that the wobble mode is significantly destabilized when the machine descends an incline or brakes on a horizontal surface. And conversely, he showed that the damping of the wobble mode is substantially increased when the machine ascends an incline at constant speed or accelerates on a horizontal surface. Inclines, acceleration and deceleration appeared to have very little effect on the damping or frequency of the weave mode, except at very low speeds.

Another nonlinear dynamic model worth mentioning was introduced in 2002 by Cossalter and Lot [43]. Their model had eleven degrees of freedom and included an original dynamic tyre model, which featured a detailed geometric description of the cross-section along with the elastic deformation of the carcass. Cossalter and Lot's tyre model explained the physical behaviour of the tyre in more detail than previous relaxation models, making unnecessary the use of specific equations to simulate the tyre relaxation behaviour. However, this was at the cost of adding a number of implicit differential equations to the model, which required special treatment. Lot further elaborated this approach in [44], where more details on this innovative tyre model can be found. Unlike Sharp's model, neither frame compliance nor rider's leaning were modelled. The equations of motion of the motorcycle model were derived symbolically using Maple [45,46] according to the natural coordinates approach [47] with the aim of making the model real-time capable. This approach produces very simple equations of motion and kinematic relationships. However, the downside is that the number of variables required to describe the system is much larger than the number of degrees of freedom and consequently algebraic equations (constraints) must be introduced, yielding a set of differential-algebraic equations (DAE). This kind of equations is not convenient if the system is to be utilized as the internal model of a control algorithm, as it will be the case in this PhD thesis.

Cossalter's code, named FastBike, was validated against experimental data obtained with an Aprilia RSV 1000. The geometrical and inertial properties of the vehicle were measured at the University of Padua along with the non-linear elastic and damping characteristics of the suspensions and the tyre parameters [48–50]. The motorcycle was equipped with a measurement system to log the roll and yaw rates, the steering angle,

the spin velocity of both wheels and the steering torque. Two different manoeuvres were compared, a lane change and a slalom manoeuvre, showing a very good agreement between numerical simulations and experimental data. Furthermore, the performance of FastBike was compared against several commercial codes, namely DADS and Visual Nastran, with FastBike being 10 and 100 times faster respectively.

The first book entirely dedicated to motorcycle dynamics was published by Cossalter in 2002 [13]. It was written from an engineering perspective, unlike other books published earlier oriented to riders and general public, and summarized Cossalter's decades of experience in the field, including multiple topics such as kinematics, tyre modelling, steady-state straight running and cornering analysis, in-plane dynamics, vibration modes and stability, manoeuvrability and handling, etc.

One of the latest models available in literature was presented by Sharp and Evangelou in 2004 [51], which featured the latest advances in the modelling of motorcycle dynamics at that time, including the outcomes of Evangelou's PhD thesis [40]. This model was developed with the commercial multibody code AutoSim [34], and presented substantial improvements with respect to previous models developed by Sharp [11, 29, 41], namely: an improved tyre/road contact geometry, a new analytic treatment of the monoshock rear suspension mechanism, speed-dependent relaxation lengths and an accurate description of the tyre shear forces and moments based on Pacejka's "Magic Formula" [52–54]. All these improvements represented an important progress towards a complete parametric description of modern high performance motorcycles. Additionally, the calculation of steady-turning equilibrium states and steer torque requirements was refined and verified. The use of this model for the stability analysis in cornering conditions was demonstrated by means of multiple root-loci. Furthermore, their publication included the derivation of all "Magic Formula" coefficients for a series of high performance motorcycle tyres, which constitute the only tyre dataset publicly available in literature.

The model described above was used by Evangelou [55] to develop a mechanical steering compensator³ for high-performance motorcycles, motivated by the reported poor stability of this type of vehicles at high speed. The compensator was seen as a possible replacement for the conventional steering damper, commonly used in high-powered sports motorcycles to increase the damping of the wobble mode at the expense of destabilizing the weave. In this context, a new device able to improve both modes at the same time was desirable. The compensator designed by Evangelou comprised a spring, a damper and a less familiar component called inerter. All components were

³A steering compensator is a passive mechanical device aimed at improving the stability of motorcycles. It is usually fitted between the fork and the chassis, in replacement of the steering damper.

tuned so that the system behaved as a damper in the wobble frequency band, and as an inerter at lower frequencies. Evangelou showed that his device could provide significant improvements to the dynamics of both wobble and weave modes compared to the conventional steering damper. This approach was further elaborated in 2006 [56], including the presentation of physical prototypes.

Recently other minor contributions to the field of motorcycle modelling have been presented, however none of them introduced unprecedented features with respect to their predecessors. Among these works, it is worth mentioning, for instance: the Modelica motorcycle modelling package (2006) [57–59], an open library developed by the Politecnico di Milano to prototype and test active control systems in the field of motorcycle dynamics; an analysis of alternative suspension models developed by Mavroudakos (2006) [60]; a flexible model presented by the University of Padua to study the impact that rider’s mobility and frame compliance have on scooter stability [61]; a real time motorcycle model integrated within an innovative riding simulator [62] developed by the same university, etc.

2.2 Motorcycle tyre modelling for dynamic simulations

A precise description of the tyre behaviour is essential for the dynamic analysis of road vehicles. For this reason, tyre modelling has been extensively studied over the past decades. The most relevant results for the development of this thesis are briefly reviewed in this section, where special emphasis has been put on those works focused on tyre modelling for full vehicle simulations. For a complete description of tyre mechanics and modelling techniques the reader is referred to [12].

We can classify existing works according to the amount of theoretical/experimental effort needed to develop the tyre model. At one extreme of this classification we find pure theoretical models, which describe the physical behaviour of the tyre through complex mathematical equations representing the tyre structure and the tread-ground interaction. For instance, the multi-radial-spoke model developed by Sharp in [63] and all finite element models belong to this category. At the other extreme there are pure empirical models that describe measured tyre characteristics through lookup tables and fitted formulae. The best known example of this group is the so-called Magic Formula [52–54]. In between these two groups there are simple physical models based on empirical knowledge. These models, although being less accurate, allow to obtain an analytical solution, thus providing a better understanding of tyre behaviour. The brush model presented by Fujioka in [64,65] belongs to this group as it lies between the pure physical and pure empirical models.

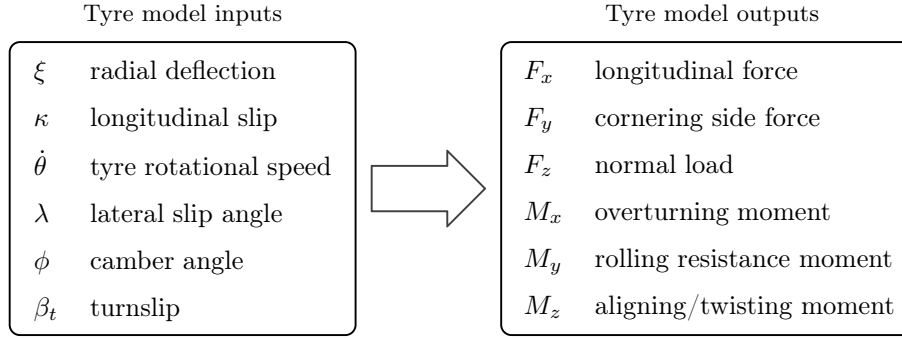


Figure 2.3: Input/output quantities of the Magic Formula model.

Pure theoretical models can be very accurate and cover a wide range of working conditions. However, they are computationally expensive and therefore not suitable for full vehicle simulations. This kind of models is often used for component performance analysis, e.g. to assess the tyre construction. On the other hand, the accuracy of intermediate models is generally not very high, especially for motorcycle simulations where the camber thrust plays an important role. Currently the most widely used model in the field of computational vehicle dynamics is the Magic Formula, which belongs to the pure empirical group. This is the approach that will be used throughout this thesis and consequently the other two groups will not be further discussed.

The Magic Formula model was originally developed in 1987 for car tyres in a joint project between TU-Delft and Volvo [66]. More than one decade later, in 1998, De Vries and Pacejka [52] improved the model to make it suitable for motorcycles, where the camber angles can reach much higher values. For this purpose, they performed steady state measurements on public roads and then modified the Magic Formula so that it fitted all experimental data, including a wide range of camber angles. Special attention was paid to ensure a consistent behaviour outside the measured domain. This tyre model was further improved by several authors [12, 54, 67].

The Magic Formula is composed of a set of parametric equations that express the steady-state longitudinal forces, side forces, aligning moments and overturning moments as a function of the longitudinal slip, side-slip, camber angle and normal load. All model inputs and outputs are summarized in Fig. 2.3; it is worth noting that all inputs are kinematic quantities whereas all outputs represent tyre forces and moments. The general form of the Magic Formula is reproduced in Eq. 2.1, while Fig. 2.4 illustrates its shape and the meaning of its parameters by means of the classic side force characteristic curve.

$$y = D \sin [C \arctan \{Bx - E (Bx - \arctan Bx)\}] \quad (2.1)$$

The Magic Formula equations include a great number of parameters which, depending on the model version, can be over two hundred. Therefore, extensive experimental tests are needed to fit all required data. In the last decades several tyre suppliers, automotive companies and a number of universities have developed test facilities for full-scale tyre measurements in order to identify the tyre force and moment generation capabilities. Two examples of these facilities are the test truck developed by the Dutch company TNO for outdoor testing [12] and the machine designed at the University of Padua for indoor testing [68]. In spite of this, the amount of motorcycle tyre data available in literature is still very limited. Sharp [51] published in 2004 a comprehensive collection of Magic Formula parameters for modern high-performance motorcycle tyres, which is probably the only dataset publicly available nowadays. Sharp's parameters will be used in this PhD thesis to populate the Magic formula model.

In the last decade, in addition to the advances described above, one of the most active groups on motorcycle tyre modelling has been the one coordinated by Professors Cossalter and Lot out at the University of Padua. In 1999 they presented a motorcycle model for steady state analysis with circular cross-section [39] which considered the lateral migration of the contact point with camber. In contrast to previous thin-disc models, their results led to a more faithful description of the tyre contact kinematics

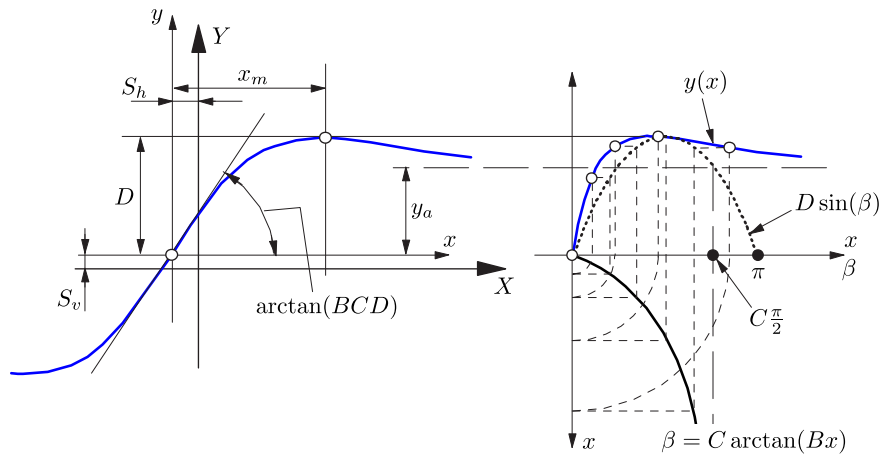


Figure 2.4: Shape of the sine version of the Magic Formula. The curve $y(x)$ passes through the point (S_h, S_v) , reaches a maximum peak value D and subsequently tends to a horizontal asymptote y_a . S_h and S_v are the offsets with respect to the origin in the horizontal and vertical directions respectively. The slope at the origin is given by the product of the coefficients BCD . The coefficient B is called the stiffness factor and is used to set the slope at the origin. The coefficient C is a shape factor used to control the range of the sine function, which in turn modifies the shape of the curve. The remaining coefficient E is introduced to control both the curvature at the peak and its horizontal position.

for large camber angles and, consequently, of all related forces and torques generated by the tyre-ground interaction. This concept was later extended in [43, 44, 69] for dynamic simulations. Unlike other authors, Cossalter and Lot did not use a first order relaxation equation to model the lag between sideslip angle and lateral force. Instead, they included the compliance of the tyre carcass in their model, thus leading to a more physical model which better explained the dynamic tyre behaviour.

2.3 Rider modelling

In the previous section an overview of motorcycle dynamics and existing models was presented. A comprehensive understanding of the system is essential in order to develop a representative rider model. The following section introduces the concept of virtual rider and reviews the most relevant literature in this field.

It should first be noted that the topic of rider modelling can be quite broad in scope as it may involve multiple fields of research in addition to vehicle dynamics. This thesis will focus on the lateral and longitudinal control behaviour of human riders, not considering other behavioural activities of motorcycle riding such as rider distraction, traffic-derived effects, side-tasking, rider impairments, etc.

While riding, a human rider applies certain actions to the motorcycle in order to follow a desired trajectory. During this process, the rider must also prevent the vehicle from falling by stabilising the capsized mode. In this respect, the rider behaves as a control system, continuously sensing the environment and generating precise control actions that stabilize the system and allow it to follow a given reference. Lateral and longitudinal control tasks such as path-following, obstacle avoidance, and headway control are examples of typical activities carried out by human riders. Interestingly, Rashevsky [70] observed in 1966 the following regarding the interaction between car and driver:

“The car and driver constitute a complex feedback system. The behaviour of the car results in certain reactions by the driver. Inversely, the behaviour of the driver affects the behaviour of the car. This man-machine system cannot, in many instances, be separated into the purely mechanical and the purely human components. The system must be treated as a whole.”

Rashevsky’s statement applies not only to cars, but also to motorcycles, where the interaction man-machine is even stronger. This idea of treating the vehicle and driver together as a combined system has been adopted by researchers since the early stages of rider/driver modelling.

A human rider can employ various forms of control to guide the motorcycle such as *feedback*, i.e. reacting to perceived errors between the actual and desired motorcycle response, and *preview*, where the rider's experience and the environment information are used to anticipate the behaviour of the vehicle. The ability of humans to look ahead on the road and preview information compensates part of their intrinsic reaction time, thus significantly reducing the control effort needed to guide the vehicle. Preview is a fundamental feature of riders, and feedback control can work in parallel to it with the aim of rejecting external disturbances. These two terms, feedback and preview, are widely used in control theory. In the present thesis the human rider will be modelled as a control system; henceforward the control algorithm that models the rider behaviour will be referred to as rider model or virtual rider. On the other hand, the term rider structural model, introduced in the previous section, will be used to describe the rider's topology (e.g. bodies, joints, etc) as far as mathematical modelling is concerned. Three important characteristics of virtual riders are explained next.

The main distinctive feature of rider models is the control target, which is directly related to the concepts discussed above. Authors generally distinguish two main control targets: stabilizing control and path following control. Stabilizing control is normally used to study the motorcycle in steady state conditions, e.g. to assess the effort required to keep the vehicle from capsizing in straight running or during steady state cornering. In contrast, path following control is used when the target is to follow a given trajectory with a predefined speed profile. Feedback control theory, also called compensatory control, and preview control are commonly used in literature to achieve these two targets.

A second important feature of rider modelling is the type of steering control used to guide the vehicle, which can be classified into two categories: position control and force control. In the first case the steering angle is directly imposed by the control algorithm and therefore no steering dynamics are included in the motorcycle model. By contrast, the second approach applies a steering torque to control the vehicle, and in consequence steering dynamics cannot be excluded from the model. Car drivers perform large rotational motions of the steering wheel during normal driving with minimal effort thanks to assisted steering systems. In this context it has been widely accepted to model drivers through angle control [71]. On the contrary, motorcycle riders turn the handlebar only a few degrees and steering torques may reach high values, thus requiring a significant effort. Furthermore, steering dynamics must be included in the model as they are essential to properly simulate weave and wobble modes [11]. Consequently, nowadays most authors use torque control in order to model the rider steering action. However, several exceptions can be found in literature, e.g. in [72–76] the authors used

angle control in order to simplify the complexity of the control problem.

The third characteristic aspect of rider modelling is the structural model of the rider. The number of additional degrees of freedom used to model the rider's body depends on the scope of the model and its application. For stability analysis, handling and control design, most authors consider the rider rigidly attached to the main frame [43] or include the rider's torso lean as an additional degree of freedom [51]. More elaborated models including two [27] or more degrees of freedom [35] are often developed to carry out detailed rider analyses such as, for instance, vibration and comfort assessment [77].

In the following sections the most relevant rider models in the existing literature will be reviewed. They have been classified in two groups according to the underlying theory used to design the control system: classical control methods and modern control methods.

2.3.1 Rider models based on classical control theory

Classical control theory was developed between 1940 and 1950, and mainly relies on the root locus technique and the various frequency response representations of linear time invariant systems (LTI) in order to set the parameters of the controller transfer function. The tuning of these parameters is typically performed via an educated (heuristic) trial-and-error approach, and therefore the creativity and experience of the designer play an important role in the design process. Classical techniques are characterized by the use of transfer functions in the complex frequency domain, the use of feedback, emphasis on the use of graphical techniques, and the use of simplifying assumptions to approximate the time response. Methods such as root locus, Bode and Nyquist plots, and Routh-Hurwitz stability criteria are widely used in the classical design approach, which is usually restricted to single-input-single-output systems (SISO). Multiple-input-multiple-output systems (MIMO) can be analyzed and designed but only one loop can be considered at a time.

Proportional-integral-derivative controllers (PID) and lead-lag compensators are some examples of classical tools that have been applied to rider modelling. A PID is a generic control loop feedback system widely used in industrial applications. Historically it is considered the best controller when no knowledge is available about the underlying process [78]. The target of the PID controller is to minimize the error between the process output and a desired reference. It comprises three terms, the error itself (P) and its integral (I) and derivative values (D), which are linearly combined to produce the control action:

$$u(t) = k_p e(t) + k_i \int_0^t e(\tau) d\tau + k_d \frac{d}{dt} e(t) \quad (2.2)$$

These terms can be heuristically interpreted as follows: the term P reacts to the present error, I to the accumulation of past errors, and D reacts to a prediction of future errors based on current rate of change. On the other hand, lead-lag compensators improve/stabilize the response of a dynamic system by introducing pole-zero pairs into the open loop transfer function, and are normally designed in the frequency domain. A comprehensive description of PID controllers, lead-lag compensators and other classical tools for control design can be found in [79].

Most of the early works on human operator modelling (e.g. drivers, riders, pilots, etc) were focused on aircraft control [80,81]. One of the first attempts to model human car drivers as a control system dates back to 1959, when Iguchi [82, 83] presented a PID compensation model based on the block diagram of Fig. 2.5. In this figure the plant

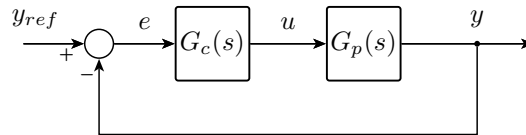


Figure 2.5: General scheme of a SISO closed-loop system, where G_c is the transfer function of the controller and G_p represents the transfer function of the plant.

G_p represents the vehicle while the controller G_c was introduced to model the driver's response. Iguchi used the angle of the steering wheel as the control action (u) with the aim to reduce the error (e) between the reference signal (y_{ref}) and the output of the vehicle (y). Some of the controlled outputs were, for instance, the speed of the vehicle and its lateral deviation with respect to the reference path. Tuning the coefficients k_p , k_i , and k_d proved to be very difficult, this being one of the reasons why this approach has not been used extensively.

Shortly after Iguchi, in 1962, McRuer published a driver model [84] based on the following lead-lag network,

$$G_c(s) = \frac{K e^{-t_d s} (1 + T_l s)}{(1 + t_h s) (1 + T_i s)} \quad (2.3)$$

where K is a static gain, T_l is the lead time constant, T_i is the lag time constant, t_d is a pure time delay and t_h is an additional time constant. Experiments showed that t_d and t_h were vehicle independent and had typical values of 0.2s and 0.1s respectively. In fact, these values characterized the driver's response delay induced by muscle dynamics and neural transport. On the other hand, K , T_l and T_i depended on the controlled vehicle and on the driver's experience. Later, in 1967, McRuer [80] proposed a method to determine K , T_l and T_i based on the well-known crossover law, according to which the driver adapts his response so that the open loop transfer function $G_c(s)G_p(s)$, i.e. the

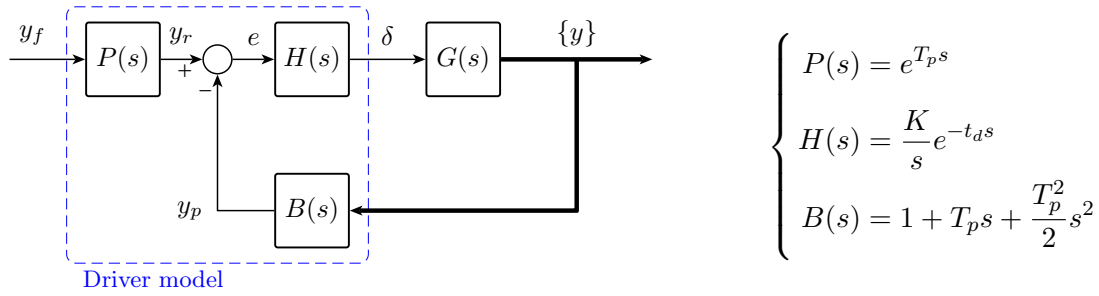


Figure 2.6: Driver model proposed by Yoshimoto (1968).

combined system vehicle-driver, has the following form for disturbances in the vicinity of the crossover frequency ω_c ⁴,

$$G_c(s)G_p(s) = \frac{\omega_c e^{-t_d s}}{s} \quad (2.4)$$

which emphasizes the driver adaptation to changing plant dynamics. This capability of human drivers was also recognized in many early laboratory experiments [85, 86].

However, an important observation was surprisingly ignored in the first driver models. Today it is a well known fact that human drivers look ahead along the road while driving. This allows them not only to anticipate the control response for upcoming manoeuvres, but also to conduct planning activities in reaction to developing scenarios. One of the first authors to include future path information in the control scheme was Kondo in 1968 [87], who focused on measuring the driver's look-ahead point⁵ and developed a driver model based on the error between this point and the planned trajectory.

Yoshimoto [88], also in 1968, presented the driver model shown in Fig. 2.6. Where $P(s)$ characterizes the preview delay, $H(s)$ represents the main control function, $G(s)$ is the vehicle model, and $B(s)$ is a prediction function used to estimate the response of the vehicle. The parameter T_p is the time required to reach the look-ahead point, while K and t_d represent the driver's gain and delay respectively. The main novelty of this model was the use of the second order prediction function $B(s)$, which allowed to estimate the position of the vehicle at the look-ahead point by simply integrating the velocity and acceleration terms. In addition to this, an integrator was added to $H(s)$ in order to model the correction ability of drivers. All the single-loop controllers introduced so far, including Yoshimoto's, were focused on path following control of automobiles. Single track vehicles (i.e. bicycles and motorcycles) require, in addition to the path following loop, an inner loop to stabilize roll dynamics.

⁴The crossover frequency is defined as the frequency at which the open loop gain is unity.

⁵Term used to define the point along the road where the driver/rider is looking at.

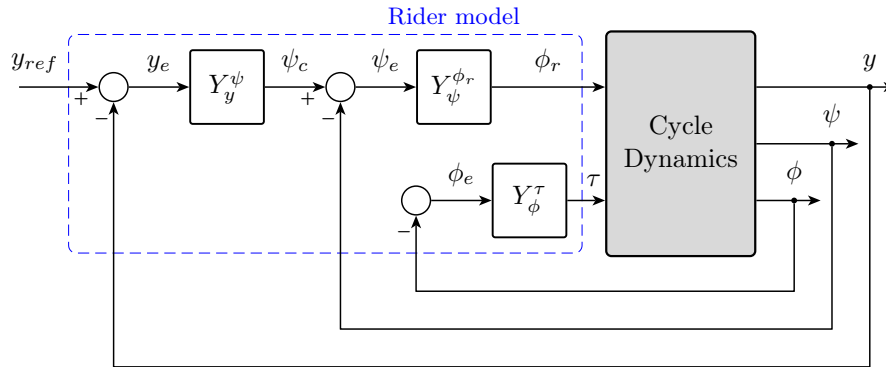


Figure 2.7: Multi-loop rider model proposed by Weir and Zellner. The control scheme is composed of three loops: an inner loop for roll angle stabilization (ϕ), an intermediate loop for heading control (ψ), and an outer loop for the lateral position control (y).

Weir and Zellner were probably the first authors to study in detail the interaction between rider and motorcycle. They carried out an exhaustive theoretical investigation on the rider control process, published in a series of papers between 1972 and 1979 [23, 26, 89–91]. One of their main conclusions was that the primary objective of human riders is to stabilize the roll angle, showing that this behaviour could be easily simulated by using the transfer function between roll angle and steer torque Y_ϕ^τ . Their finding emphasized the importance of this transfer function, which plays a key role in motorcycle control, and is usually characterized by a high cross over frequency (1 rad/s) and large gain and phase margins. Other transfer functions that Weir and Zellner found relevant were those between roll angle and rider's lean angle, and between yaw rate and rider's lean angle.

To achieve both good stabilization and tracking performance they proposed the multi-loop rider model shown in Fig. 2.7, composed of three loops: an inner loop for roll angle stabilization (ϕ) around the upright condition, an intermediate loop for heading control (ψ), and an outer loop for lateral position control (y). The inner loop includes the transfer function Y_ϕ^τ , which generates the steering torque τ from the roll angle ϕ . It is worth noting that this loop is decoupled from the other two as it has no reference signal. This clearly shows that the target of this control scheme was to stabilize the vehicle assuming small perturbations with respect to the straight running condition, i.e. $\phi = 0$. On the other hand, the intermediate and outer loops work together in order to control the rider's lean ϕ_r as follows: first the transfer function Y_y^ψ transforms the lateral position error y_e into the required yaw angle ψ_c , from which the actual yaw angle ψ is subtracted to obtain the yaw angle error ψ_e ; subsequently the transfer function $Y_\psi^{\phi_r}$ transforms ψ_e into the rider's lean ϕ_r that is required to follow the target path.

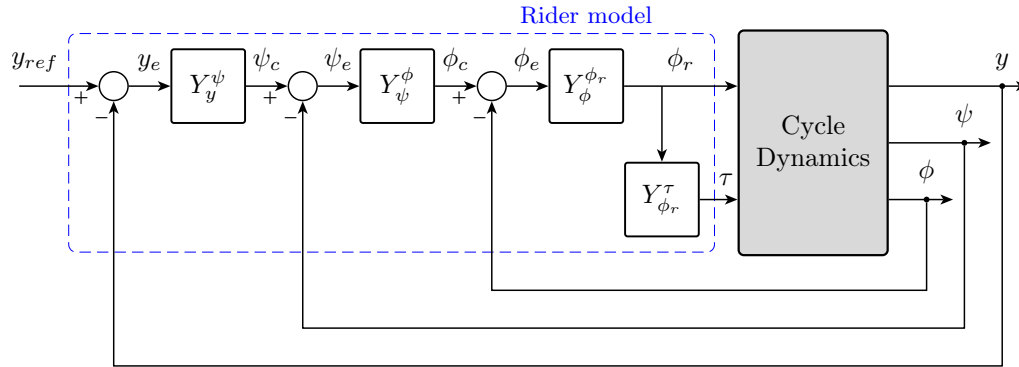


Figure 2.8: Multi-loop rider model proposed by Prem and Good (1983). Note that the steering torque τ is coupled to the rider's lean angle ϕ_r through the transfer function $Y_{\phi_r}^{\tau}$. Prem and Good found that this kind of coupling was typical of novice riders.

Weir and Zellner's algorithm was coupled to a vehicle model with four degrees of freedom, namely the lateral velocity, the roll angle, the yaw rate and the steering angle. The full model was then used to assess the control actions exerted by the rider in different conditions of forward speed, front wheel trail and tyre response. Additionally, Weir and Zellner investigated how to adjust the design parameters of a given motorcycle to achieve the desired handling properties and system performance.

Another significant example of multi-loop control was published by Prem and Good [92] in 1983. These authors suggested, based on experimental evidence, that skilled motorcycle riders are able to independently control the upper body lean and the steer torque, which is consistent with the above model proposed by Weir and Zellner. However, they found that there was a strong coupling between lean and steering inputs when it comes down to less skilled riders. Following Weir and Zellner's line of work, Prem and Good proposed the block diagram of Fig. 2.8 to model novice riders.

The main control method proposed by Prem and Good was the upper body lean ϕ_r , while the steer torque was considered a consequence of the rider's motion, i.e. when the rider leans laterally, his arms apply a steering torque to the handlebar which is not generated deliberately but as a reaction in order to keep the rider's body in the desired position. This coupling between steer torque and rider's lean is shown in Fig. 2.8, where the steering torque τ is generated from the rider's lean angle ϕ_r through the transfer function $Y_{\phi_r}^{\tau}$.

Prem and Good showed that a comparable tracking performance could be achieved with their novice and expert rider models. However, differences were found in the amplitude of the control actions and in the stability margins. They observed that unskilled riders may have lower stability margins but require physically less extreme upper body

motions to control the motorcycle. Similar results were observed in experimental tests conducted with multiple riders of varying experience performing an avoidance manoeuvre.

A more elaborated structural model of the rider was used by Nishimi [27] in 1985 to study the influence of the rider's movements on the straight running stability of motorcycles. His model comprised two passive degrees of freedom: the leaning of the torso and the lateral movement of the lower body with respect to the chassis. Nishimi's numerical results correlated well with full scale experiments, showing that upper body parameters influence mainly the weave mode while those regarding the lower body influence primarily the wobble mode. Some years later, in 1988, Katayama [28] extended Nishimi's work with the aim to investigate what control inputs had a bigger effect on the response of the motorcycle. To that end, he modelled the rider as a double inverted pendulum and included three control actions to stabilize the vehicle: the steering torque applied to the handlebars, and two torques applied to the lower and upper parts of the rider's body. The rider model designed by Katayama was a straightforward linear controller; all three control torques were written as linear functions of the roll angle and the heading error of the vehicle with respect to the reference path.

The rider model described above was coupled with a four degree-of-freedom motorcycle model, which included the lateral velocity, and the yaw, roll and steer angles. Katayama performed numerous lane change simulations with his model and compared the results with the responses of twelve real riders, concluding that the major source of control is the steer torque whereas rider's movements are of secondary importance. The relative importance of the rider's actions was quantified as follows: the lower body effect was found to be 1/12 of the steer torque, with the upper body contribution being 1/80. According to Katayama's results, the lower part of the body helps in generating the steering torque (i.e. as the reaction body), while the upper part is usually positioned to keep the rider in a comfortable position.

Classical control theory did not receive much attention in the years following the work of Katayama. During the nineties, alternative and newly-developed control theories captured the attention of most researchers. As a matter of fact, we have to move forward to the year 2000 in order to find again relevant works based on the classical approach. One of them was presented by Berrita in [93]. During his research, Berrita used two parallel PD controllers to model the steering torque generated by the rider τ . He proposed the following control law,

$$\tau = k_\phi \phi + c_\phi \frac{\partial \phi}{\partial t} + k_n n^* + c_n \frac{\partial n^*}{\partial t} \quad (2.5)$$

where the first two terms were designed to stabilize the roll angle ϕ and the last two

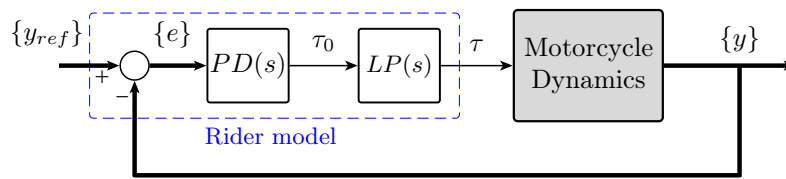
were introduced to reduce the error with respect to the reference path n . Unlike most of previous works, which used the actual position of the motorcycle to compute the trajectory error, the path-following control proposed by Berrita was based on a future estimation of n , indicated by the asterisk in Eq. 2.5. This technique allowed not only to anticipate the response of the vehicle, but also to reduce the control effort needed to follow the target path. Berrita coupled his virtual rider with the commercial multibody code MSC Working Model, showing that a single look-ahead point was sufficient to successfully simulate simple manoeuvres such as constant radius turns and slaloms.

Berrita's controller was extended by his colleagues Lot and Cossalter in 2006 [94]. They introduced three new ideas: a new architecture of the virtual rider (Fig. 2.9a), an algorithm for vehicle tracking and look-ahead (Fig. 2.9b), and a procedure to optimize the control gains. The vehicle tracking algorithm was based on the curvilinear coordinates approach, i.e. the distance travelled along the road s_v , the lateral deviation from the road center n_v , and the angle of the vehicle with respect to the track centerline χ_v were included as additional model states in order to track the position of the vehicle (v). This technique was also applied to track the position of the look-ahead point (f), defined by the look-ahead distance L_{ahead} in Fig. 2.9b.

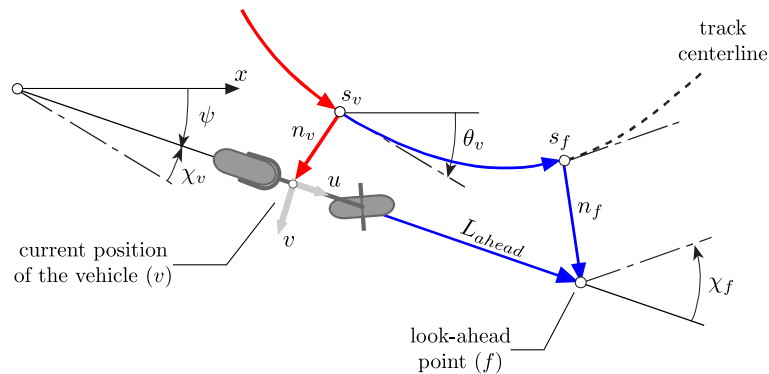
Lot and Cossalter wrote the rider's control law as a function of the curvilinear coordinates defined above. The resulting controller, represented by Eq.2.6, comprised two PDs and several damping terms. The first two rows of the equation constitute the PDs, which stabilize the capsize mode, preventing the motorcycle from falling over, and reduce the error with respect to the target trajectory. Note that the target values, denoted by the subscript t , are evaluated at the look-ahead point. In addition to the PDs, the damping terms of the third row complete the rider model. These terms are proportional to the yaw and steering rates respectively and were introduced to stabilize the weave and wobble modes. Moreover, a low-pass filter was added in order to limit the rider's bandwidth, thus replicating human neuromuscular limitations during fast manoeuvres.

$$\begin{aligned} \tau = & k_\phi [\phi_t(s_f) - \phi_v] - c_\phi \frac{\partial \phi_v}{\partial t} \\ & + k_n [n_t(s_f) - n_v] - c_n \frac{\partial n_v}{\partial t} \\ & + c_\psi \left[\frac{\partial \psi_v}{\partial t} - u_v \Theta_v \right] + c_\delta \frac{\partial \delta_v}{\partial t} \end{aligned} \quad (2.6)$$

Lot and Cossalter developed an optimization procedure based on Laplace's transform to find the controller gains $(k_\phi, k_n, c_\phi, c_n, c_\psi, c_\delta)$ for different conditions of speed and roll angle. Their method was based on the minimization of a cost function, namely the trajectory error with respect to the target path, subject to three inequality constraints.



(a)



(b)

Figure 2.9: Rider model proposed by Lot and Cossalter (2006). (a) Structure of the closed-loop simulation model. It comprises three main blocks: the steering controller $PD(s)$, a low pass filter $LP(s)$ to limit the bandwidth of the virtual rider, and the non-linear motorcycle model. (b) Tracking algorithm based on the curvilinear coordinates approach. The current position and orientation of the vehicle (v) and the look-ahead point (f) are expressed in track coordinates by six additional states (s_v, n_v, χ_v) and (s_f, n_f, χ_f).

These constraints were added to keep the vehicle within the track boundaries and to limit the maximum values of the roll angle and the steering torque.

The rider model described above was coupled to a complex non-linear multibody model of the motorcycle [43] and used to simulate typical handling tests, e.g. lane change, slalom and cornering manoeuvres. A good correlation against experimental data was achieved for constant speed manoeuvres. As part of the conclusions, Lot and Cossalter highlighted the main difficulties in extending this method to more general manoeuvres: the linearization of the model for control optimization and the necessity to update the control gains during the simulation to account for changes in vehicle speed and roll angle.

Lot and Massaro presented an improved version of their rider model in 2007 [95], where an integral term was added to remove the steady-state error of the roll angle. One year later they proposed a new methodology with speed dependent gains and two nested control loops [96], shown in Fig. 2.10. The inner loop included a PI controller, $H_2(s)$,

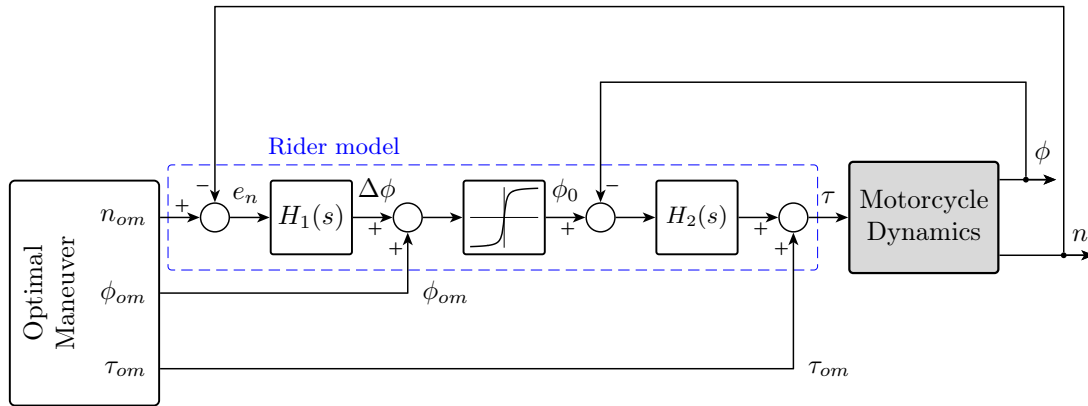


Figure 2.10: Rider model proposed by Lot and Massaro (2007). Their control scheme included two control loops: an inner loop designed to stabilize the roll angle ϕ , and an outer loop to make the motorcycle follow the target path n_{om} . The references n_{om} , ϕ_{om} and τ_{om} were computed offline by the Optimal Maneuver method.

designed to stabilize the roll angle, whereas the outer featured a PD, $H_1(s)$, designed to make the motorcycle follow the desired path. Between these two loops, a saturation block was included to prevent the motorcycle from leaning above a given threshold. A third loop, not shown in the figure, was used for speed control. Unlike their previous rider models [94, 95], this version did not include any preview information.

The nominal solution of the problem was computed with the Optimal Maneuver method [97]. Given the track boundaries, the vehicle model and the rider physiological limits, this approach allows finding the optimal trajectory and control inputs that minimize the time needed to complete a certain manoeuvre. However, this nonlinear control method can only be used with simple models due computational limitations, which precludes its practical application to detailed multibody models such as that used by Lot and Massaro.

In order to overcome such limitation, they proposed to split the problem into two subtasks: trajectory planning and vehicle control. They solved the first by applying the Optimal Maneuver to a simple motorcycle model, and then the second by using the rider model described above in combination with a detailed motorcycle model. Note in Fig. 2.10 that the results of the Optimal Manoeuvre provide a feedforward action to the control blocks. The feedforward action includes the desired path n_{om} , expressed in curvilinear coordinates, the roll angle ϕ_{om} and the steering torque τ_{om} .

Lot and Massaro computed the gains of the roll controller by applying the Nyquist theorem to the open loop transfer function between the steering torque and the roll angle. This process was repeated for different conditions, covering the typical speed, roll and acceleration ranges of the motorcycle. As a matter of fact, these two authors

were probably the first to successfully simulate the motorcycle-rider system at both high roll angles and variable speed.

They presented promising results corresponding to the simulation of three corners of the Mugello track. Nonetheless, significant trajectory errors can be observed in their results. The error between the desired and the actual trajectories of the motorcycle ranges between two and three meters, meaning that there is still possibility for further improvements in the development of virtual riders. Moreover, no information is provided on how close the motorcycle is to its performance limits during the manoeuvre, e.g. acceleration, tyre loads, etc.

In any case, we can state that Lot and Massaro's algorithm is the most advanced rider model based on classical control theory that has been presented to this day.

2.3.2 Rider models based on modern control theory

In contrast to the classical approach, modern control theory employs a more formal methodology for the design of control systems. Modern controllers are based on the state-space representation of dynamic systems [79], and are modelled in time-domain as a set of inputs \mathbf{u} , outputs \mathbf{y} and states \mathbf{x} (internal variables) related by first-order differential equations,

$$\begin{cases} \dot{\mathbf{x}}(t) = \mathbf{f}(t, \mathbf{x}(t), \mathbf{u}(t)) \\ \mathbf{y}(t) = \mathbf{g}(t, \mathbf{x}(t), \mathbf{u}(t)) \end{cases} \quad (2.7)$$

where \mathbf{f} is called the state equation and \mathbf{g} is the output equation. The application of matrix methods provides a convenient and compact way to represent dynamic systems, and makes possible the treatment of multiple-input-multiple-output (MIMO) problems. Inputs, outputs and states are expressed as vectors and, when the system is linear, the differential equations can also be written in matrix form. A general state-space representation of a linear system with n_u inputs, n_y outputs and n_x state variables can be written as follows:

$$\begin{cases} \dot{\mathbf{x}}(t) = \mathbf{A}(t)\mathbf{x}(t) + \mathbf{B}(t)\mathbf{u}(t) \\ \mathbf{y}(t) = \mathbf{C}(t)\mathbf{x}(t) + \mathbf{D}(t)\mathbf{u}(t) \end{cases} \quad \text{where} \quad \begin{matrix} \mathbf{A} = \left. \frac{\partial \mathbf{f}}{\partial \mathbf{x}} \right|_{\hat{\mathbf{x}}} & \mathbf{B} = \left. \frac{\partial \mathbf{f}}{\partial \mathbf{u}} \right|_{\hat{\mathbf{x}}} \\ \mathbf{C} = \left. \frac{\partial \mathbf{g}}{\partial \mathbf{x}} \right|_{\hat{\mathbf{x}}} & \mathbf{D} = \left. \frac{\partial \mathbf{g}}{\partial \mathbf{u}} \right|_{\hat{\mathbf{x}}} \end{matrix} \quad (2.8)$$

where $\hat{\mathbf{x}}$ represents the nominal trajectory around which the system is linearized. When matrices $A(t)$, $B(t)$, $C(t)$ and $D(t)$ depend on time, Eq. 2.8 is known as a Linear Time-Varying (LTV) system. On the other hand, if those matrices are constant, the above equation is referred to as a Linear Time-Invariant (LTI) system.

The trial-and-error aspect of the classical design method is significantly reduced in modern control theory as the design target can be quantified by means of a cost function or performance index: the main objective of the controller is to determine the control signals that will cause the system to move from one state to another and, at the same time, extremize (maximize or minimize) a given performance criterion. Several examples of cost functions are described below:

- a) Cost function for time-optimal problems. The index below can be used to minimize the time required to transfer the system from an arbitrary initial state $x(t_0)$ to a specified final state $x(t_f)$. This type of formulation is widely used in the motorsports industry for laptime simulations. For further information, see [97,98].

$$J = \int_{t_0}^{t_f} dt = t_f - t_0 \quad (2.9)$$

- b) Cost function for minimum-energy problems. If $u(t)^2$ is proportional to the power required to drive the system, then Eq. 2.10 represents a measure of the energy required to perform a certain manoeuvre, where R is a positive definite matrix that allows the user to specify different weights for each control input. This index can be also used to reduce the rider/driver effort as it penalizes large control actions.

$$J = \int_{t_0}^{t_f} \sum_{i=1}^m u_i^2(t) r_i dt = \int_{t_0}^{t_f} \mathbf{u}^T(t) \mathbf{R} \mathbf{u}(t) dt \quad (2.10)$$

- c) Cost function for regulation problems. If a system is required to work in the neighbourhood of a given setpoint, then the index below can be used to minimize the deviation of the states with respect to the equilibrium point x_0 , where $x(t)$ is defined as the difference between the current states and x_0 . This index is widely used in the design of driver models for steady state cornering.

$$J = \int_{t_0}^{t_f} \sum_{i=1}^m x_i^2(t) q_i dt = \int_{t_0}^{t_f} \mathbf{x}^T(t) \mathbf{Q} \mathbf{x}(t) dt \quad (2.11)$$

- d) Combined cost function. By merging the last two formulations, and using the system outputs $y(t)$ instead of the states $x(t)$, we have a performance index suited for modelling human operators. This cost function tends to reduce the error with respect to the desired trajectory $y_d(t)$ while keeping control actions low.

$$J = \int_{t_0}^{t_f} \left[(\mathbf{y}(t) - \mathbf{y}_d(t))^T \mathbf{Q} (\mathbf{y}(t) - \mathbf{y}_d(t)) + \mathbf{u}^T(t) \mathbf{R} \mathbf{u}(t) \right] dt \quad (2.12)$$

Examples of this type of cost function applied to rider and driver modelling can be found in [99–101].

A great number of techniques are available in literature to solve the control problem formed by Eqs. 2.7, 2.8 and the above cost functions. For linear plants the control inputs $u(t)$ can be computed as a linear combination of the states $x(t)$ as follows,

$$\mathbf{u}(t) = -\mathbf{K}(t)\mathbf{x}(t) \quad (2.13)$$

where $K(t)$ is known as the feedback matrix. One of the most extended methods to design this matrix is the Linear Quadratic Regulator (LQR) approach [102], which can be applied when the system is described by a set of linear differential equations and the cost index is a quadratic function of the states and the inputs, e.g. 2.12. In the nonlinear case, however, more advanced approaches are required. Techniques such as nonlinear optimal control [103] and manoeuvre regulation [76] have been successfully applied to the control of vehicles. For a detailed description of modern control techniques, the reader is referred to [76, 79, 102, 103].

The Eqs. 2.7 and 2.8 constitute the so called *internal model* of the controller in its non-linear and linear versions respectively. This concept is widely used in literature to denote the rider’s mental model of the vehicle, i.e. a representation of the inverse dynamics of the vehicle that the human mind develops and tunes to anticipate its behaviour. The term *simulation model*, on the other hand, will be used throughout this dissertation to denote the model to which the rider model will be coupled. It is important to note the differences between these two models: the internal model behaves as the ‘brain’ of the rider, while the simulation model represents the real vehicle within a computer program. Although it is not strictly necessary for the simulation and the internal models to be the same, significant differences between them would lead to a poor performance of the rider model. To illustrate this, imagine a scooter rider trying for the first time a powerful machine; his mental model of the motorcycle would be far from the actual vehicle, which in turn would result in inadequate control actions.

Next, the most relevant controllers based on modern control theory are reviewed. Kleinman, Baron and Levison were among the first to apply optimal control techniques to simulate human control tasks. In 1970 they presented a quantitative model of the human operator [104, 105] based on the assumption that humans always behave optimally in some sense when carrying out control tasks, e.g. to achieve a given target in minimum time, with a minimum effort, etc. In order to render the model more realistic, human psychophysical limitations were also accounted for. Kleinman, Baron and Levison used their model, along with a linear feedback controller, to validate experimen-

tally measured data for three simple tracking tasks, and to study a complex hovering manoeuvre of a VTOL (Vertical Take-Off and Landing) aircraft.

In the following years several authors developed car driver models based on modern control theory. In 1980 MacAdam [106, 107] presented a linear time-invariant (LTI) steering controller based on preview control theory. This novel approach was based on the minimization of a cost function involving the future lateral error of the vehicle with respect to a target trajectory. To simplify the problem, MacAdam obtained the gains of the controller on the basis that the driver keeps the steer angle constant over the preview distance. His driver model proved especially useful in the study of straight-line driving tasks and transient lane-change manoeuvres. MacAdam's findings were successfully validated against experimental measurements. Later on, in 2002, Peng [108] would extend Macadam's work to include yaw displacement errors in the cost function and non-constant steer angle preview.

It was not until the end of the nineties that the first rider models based on modern control theory appeared. One of the first examples was presented in 1998 by Cossalter [98], who developed an innovative technique to assess motorcycle handling and manoeuvrability denominated the *Optimal Manoeuvre* method. Unlike previous works, his purpose was not to reproduce measured experimental data but to create a control algorithm able to guide the motorcycle in the most efficient manner. The aim was to measure the best motorcycle performance regardless of the rider's ability. Cossalter included handling and manoeuvrability indexes in the cost function, where handling was defined as the "easy to drive" (control effort) and manoeuvrability as the ability to perform complex manoeuvres fast (minimum time). The former involves the judgement of the rider, as he may find one vehicle easier to drive than another, while the latter is regarded as an intrinsic property of the motorcycle, independent of the rider's skills.

The Optimal Manoeuvre was posed as a nonlinear optimal control problem and then solved by an indirect method [103], i.e. by transforming it into a two-point boundary value problem (TPBV) derived from the necessary condition of optimality. It is worth noting that the motorcycle used by Cossalter was rather simple as it was focused on the gross motion of the vehicle. It comprised only one body and did not consider realistic control inputs. As a matter of fact, the front lateral force was directly used as the steering input in order to reduce the complexity of the problem. Later works from Cossalter's group at the University of Padua improved the method by using more complex models and more advanced solution procedures [109, 110].

The above approach was applied in [98] to simulate three different manoeuvres that are commonly used to evaluate motorcycle manoeuvrability: slalom, lane change and U-turn. Four different setups were compared to assess the effect of a number of mod-

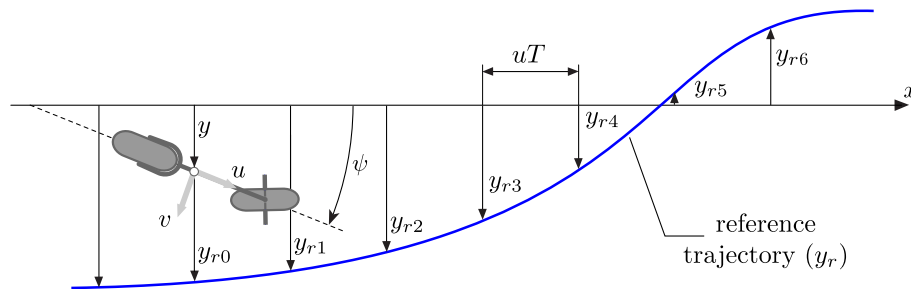


Figure 2.11: Sharp Preview Model (2001). At the current simulation instant (k), the road preview data observed by the driver comprises $h + 1$ equally spaced references y_{r_i} at and ahead of the car. E.g. $h = 6$ in the above figure. The distance between points is uT , where u is the car speed, considered constant by Sharp. At the next instant, $(k + 1)$, the car moves forward and the first sample y_{r_0} disappears from the preview. The index of all the other samples i becomes $i - 1$, and a new value, previously outside the preview, is added at position h . This road preview updating process is continuously repeated throughout the simulation.

ifications regarding wheelbase, centre of mass position, rotating inertias (gyroscopic effect) and tyre grip. The increase of the wheelbase showed significant favourable effects, whereas moving the centre of mass forward was found to be detrimental to bike performance. The results of the U-turn manoeuvre showed that the tyre grip has a big impact on motorcycle trajectory. On the other hand, the increase of the gyroscopic effect did not show significant results. In [97] Cossalter validated his numerical results against experimental data with good results. For that purpose data from a racing motorcycle logged at the Mugello track was used. Professional riders are able to take the motorcycle close to its limits, producing thus results that are in line with the *Optimal Manoeuvre* method. This method was later modified in [111] to simulate average riders with the aim to integrate it in the design process of advanced driving assistance systems (ADAS).

In 2001 Sharp applied a methodology originally elaborated for active suspension control to develop the first path-following driver model with multiple preview points [112,113]. One of the most interesting features of this work was the approach adopted to model the driver's preview, which is briefly explained in Fig. 2.11. Sharp approached the design of the virtual driver as an optimal linear discrete time preview control problem, and showed that the linear quadratic regulator theory (LQR) could be applied to solve it⁶. The result was a LTI controller that minimized a cost function involving future path and yaw errors along with the control action, i.e. the steer angle, which was assumed to vary over an infinite horizon. Sharp found that the gains of the feedback controller

⁶Standard Matlab tools were used to solve the problem, namely DLQR.

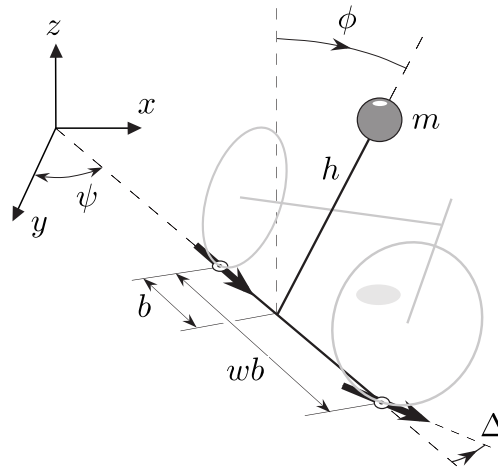


Figure 2.12: Motorcycle model proposed by Getz (1995). This is probably the most simple representation of a single track vehicle that takes into account the countersteering effect. It comprises one body with two degrees of freedom: the displacement of the vehicle in its longitudinal direction and the roll angle. The tyres were modelled as nonholonomic constraints. Image from [72].

depended significantly on the weights of the cost function. Based on his results, he came to the conclusion that preview gains reflect the dynamics of the vehicle under analysis. This finding was further exploited in [114] to propose a new handling index.

Frezza and Beghi applied model predictive control techniques to model the rider's steering action in a series of papers published between 2003 and 2006 [73–75]. Their control algorithm was based on a simple motorcycle model with two degrees of freedom, namely longitudinal displacement and roll angle, similar to that presented by Getz in [72] (Fig. 2.12). The most distinctive feature of their work was the inversion of the cause-effect relationship. Frezza and Beghi used the motorcycle roll angle as the control action instead of the steering angle, thus avoiding to directly deal with the non-minimum phase behavior of the motorcycle (countersteering). Their controller computed, for each time step, the roll angle trajectory necessary to bring the motorcycle back to the target path in T seconds, with T being the preview time. Once the roll trajectory was known, the steering angle was obtained by a simple geometric calculation based on Getz's model. This rider model showed very good performance results when applied to the same motorcycle model used to derive the controller. However, a significant loss of performance was observed for more complex motorcycle models, especially those including pitch dynamics and sliding tyres, as these features were neglected by the internal model. In fact, Frezza and Beghi's virtual rider is not considered suitable for controlling multibody motorcycle models of similar complexity to [43] or [51].

Based on an earlier publication from Antos and Ambrosio on car driver modelling

[115], in 2005 Huyge investigated the use of a bilinear motorcycle model to design a new virtual rider [116]. The target of Huyge's control algorithm was to follow a given roll trajectory, and not a reference path as had been previously done by other authors. The linear quadratic regulator theory (LQR) was used to obtain the feedback gains but, as opposed to Sharp [112], Huyge did not include any preview information. His motorcycle model included two control inputs, the steering torque and the throttle, while the rider lean was included only as a passive degree of freedom. Two manoeuvres were successfully simulated, a constant radius turn with a roll angle of 29° and a S-shaped manoeuvre where the roll angle was smoothly swept from -29° to 29° . Huyge's results were not fully conclusive due to the limited number of cases studied. Furthermore, it is unlikely that the performance of this approach could be competitive against models with road preview.

In 2006 Sharp extended his previous work [112] and developed an optimal preview steering controller for motorcycles [99, 100] with multiple preview points. The road preview model described in Fig. 2.11 was combined with a linear version of Sharp's motorcycle model, giving rise to the following discrete LTI system:

$$\begin{Bmatrix} x_v(k+1) \\ y_r(k+1) \end{Bmatrix} = \begin{bmatrix} A_v & 0 \\ 0 & A_r \end{bmatrix} \begin{Bmatrix} x_v(k) \\ y_r(k) \end{Bmatrix} + \begin{bmatrix} B_v \\ 0 \end{bmatrix} T(k) + \begin{bmatrix} 0 \\ B_r \end{bmatrix} y_{ri}(k) \quad (2.14)$$

where $x_v(k)$ is the state vector of the vehicle, A_v and B_v are the corresponding state space matrices, and $T(k)$ contains the motorcycle inputs (e.g. steering torque, thrust, brakes, etc). Sharp modelled the dynamics of the driver's preview as a shift register, represented in Eq. 2.14 by the road state vector $y_r(k)$ and by matrices A_r and B_r , which have the following structure:

$$A_r = \begin{bmatrix} 0 & 1 & 0 & 0 & \cdots & 0 \\ 0 & 0 & 1 & 0 & \cdots & 0 \\ 0 & 0 & 0 & 1 & \cdots & 0 \\ \vdots & \vdots & \vdots & \vdots & \ddots & \vdots \\ 0 & 0 & 0 & 0 & \cdots & 0 \end{bmatrix} \quad B_r = \begin{bmatrix} 0 \\ 0 \\ 0 \\ \vdots \\ 1 \end{bmatrix}$$

Each element of $y_r(k)$ stores a past observation of the road ahead of the vehicle and hence the register includes as many states as preview points. At every time step (k), the register captures the farthest point of the preview through the input $y_{ri}(k)$. Subsequently, as the system moves forwards in time, a new input is considered $y_{ri}(k+1)$, and the previous input $y_{ri}(k)$ is shifted through the states, one per time step. This process is continuously done to populate the road states with the preview information. Once

the vehicle has already passed a certain point on the road, its preview information is shifted out (discarded) from the shift register.

As in [112], the controller gains were calculated by solving a LQR problem. The cost function to be minimized included a weighted sum of trajectory errors and the rider control actions, i.e. the torque applied to the handlebars and the torque applied to balance the leaning of the rider's torso with respect to the frame. Sharp used this methodology to simulate two manoeuvres at constant speed, a lane change and an S-shape trajectory, both with good results. His results reinforced what Katayama anticipated in [28] regarding motorcycle control: the main control action applied by the rider is the steering torque, whereas the movement of the torso is an order of magnitude less important.

Sharp made very interesting observations about the preview gain vector. He noticed that, for optimal path tracking at high speeds, i.e. when wobble and weave become lightly damped, his rider model required an oscillatory preview gain vector which exhibited the same frequency content as the less damped modes of the vehicle. He also observed that the components of the preview gain vector tended to zero as the preview length was increased, meaning that seeing further than a certain distance does not improve the rider's performance. Another interesting conclusion, which agrees with riding experience, is that the ideal preview length increases with the speed. In 2007, Sharp [117] applied the same methodology to control motorcycle speed, however only straight line results were presented. In 2009 Sharp published two new papers on the application of the linear preview theory to car driver modelling [118, 119].

Another interesting contribution was made by Saccon during his PhD thesis [76] (2006). Following Hauser's research on nonlinear *manoeuvre regulation*⁷, he developed an innovative virtual rider based on an extension of Getz's model [72]. Saccon improved Getz's model by including a linear tyre model and by increasing the number of degrees of freedom from two to four, these being the planar coordinates (x, y) of the rear contact point and the roll and yaw angles. He made several simplifications to derive the dynamic equations of the motorcycle: the kinematic structure did not include the castor angle of the steering system; tyres were modelled as having no thickness, thereby simplifying the calculation of the front contact point; and neither the suspensions nor the chain were considered. Unlike other authors [99, 100, 116] who used the steering torque as the main control input, Saccon decided to control the vehicle through the steering angle (position control) following the trend of his research group at the University

⁷Maneuver regulation is a technique for the control of nonlinear systems when the target output trajectory is known in advance. It relies on a state feedback to make the system output follow the desired reference while satisfying a given speed profile. It is based on an appropriate change of coordinates that allows to rewrite the system equations, replacing the time with the longitudinal abscissa along the desired trajectory. See [120–123] for more details.

of Padua [73–75, 124]. Despite the simplifications described above, the rider model presented by Saccon succeeded in controlling a more complex model developed in the commercial code ADAMS. Two manoeuvres were simulated at variable speed, a chicane and a slalom, with good results. However, it is noteworthy that the simplifications introduced by the internal model, along with the position control approach, greatly limit the application of this methodology. As a matter of fact, position control locks the steering dynamics and therefore it does not allow to properly simulate some of the characteristic vibration modes of the motorcycle such as wobble or weave.

Cole presented in [101] one of the first applications of Model Predictive Control (MPC) theory to driver modelling. His work was based on a simple linear car model with two degrees of freedom, namely the lateral velocity of vehicle measured on the moving frame and the yaw velocity with respect to the ground. Cole used the control theory developed by Maciejowski in [125] to derive a novel virtual driver able to guide his vehicle model along a desired target trajectory at constant speed. Several methods to transform the controller gains from global to vehicle-fixed axes were comprehensively discussed following [112], where it was stated by Sharp that the driver views the road relative to the longitudinal axis of the vehicle instead of relative to the ground-fixed axes. Despite the simplicity of the model and the limitation imposed by the constant speed assumption, the results obtained by using MPC were very promising and showed a great potential for developing more advanced vehicle controllers.

2.4 Concluding remarks

A thorough review of current literature on motorcycle dynamics and rider modelling has been presented in this chapter. The analysis reveals that current motorcycle models have reached a high level of applicability, which has not been matched by the existing virtual riders. Although significant progress has been made in the last decade in the field of rider modelling, based on both classical and modern control theories, a fully satisfactory solution to the problem has not yet been found.

Existing algorithms work well only under certain conditions such as moderate longitudinal acceleration, low roll angles, etc. Most of them also require a great deal of interaction from the user to adjust the controller parameters for each condition. In addition, many of these rider models are based on highly simplified models that do not take into account the main modes of vibration of the motorcycle (capsize, wobble and weave), which compromises their accuracy.

In 2009 the author of this dissertation published a motorcycle model specifically focused on control system design [126] with the purpose of using it as the internal model

of his virtual rider. On the other hand, models published previously, such as Cossalter's and Sharp's, were mainly created for simulation purposes and presented some limitations as far as the design of the virtual rider is concerned. The author's mathematical multibody model was born with the aim of solving these limitations. It was developed symbolically in Maple⁸ using relative coordinates, thus obtaining a set of ordinary differential equations (ODE) suited for control system design. Cossalter's model, on the contrary, had been formulated as a system of differential algebraic equations (DAE) due to the great number of constraints introduced by the natural coordinates approach [47]. Although Cossalter's model showed very good computational performance, the presence of algebraic equations made it less suitable for control purposes.

Sharp, on the other hand, developed his model in the commercial multibody code AUTOSIM [34]. Commercial multibody tools simplify the modelling task considerably as the user does not have to focus on writing the equations of motion; complex mechanisms can be defined by specifying the spatial layout of the components and their interconnections. These codes, however, do not allow direct access/manipulation of the underlying equations, which greatly limits the development of more advanced tools. Furthermore, the user is generally constrained to use a limited set of numerical tools integrated in the multibody package, usually static equilibrium solvers and integrators. The development of the rider model proposed in this thesis requires special tools not available in any commercial code. An example of the realization of such tools was presented by the author in [127], where the motorcycle equations of [126] were rearranged to solve the quasi-steady-state equilibrium problem by means of a nonlinear equation solver. The solution of the quasi-steady-state problem in straight line and in cornering conditions is an essential step in the development of the virtual rider as will be shown throughout this dissertation.

Sharp, in contrast, used a time-integration procedure to find the equilibrium states [99, 100]. Basically, his method consisted in running a controlled dynamic simulation until the vehicle reached the desired trim condition. This approach presents several disadvantages compared to using a nonlinear solver. In the first place, the motorcycle is unstable and consequently a steering controller is needed to stabilize the vehicle as described by Sharp in [51]. This procedure is obviously not ideal when the final target is to design the controller itself, i.e. it means that one needs to first design a simple virtual rider to find the equilibrium conditions which will be then used to obtain the gains of the final rider model. Additionally, this process is slow, requires many simulations, and does not guarantee that all desired conditions (e.g. position along the track, curvature, velocity and acceleration) are met at the same time, especially in presence of longitudinal

⁸Maple is a commercial software for the symbolic manipulation of equations.

acceleration. As a matter of fact, Sharp did not include any longitudinal acceleration in his equilibrium solutions.

As far as the control theory is concerned, it is expected that the application of Model Predictive Control (MPC) to the field of rider modelling can improve the results presented to date. In fact, the author of this dissertation introduced in [128] the first successful application of MPC to control both the speed and the trajectory of a motorcycle. In this work, the methodology suggested by Cole to steer a two degree-of-freedom car model [101, 125] was extended to control a twenty-two-state multibody model of a sports motorcycle [126]. Several manoeuvres were successfully simulated at constant and varying speeds by controlling the steering torque and the braking/throttle commands. Later, in [129, 130] some of the tools developed during the course of this PhD project were integrated into the commercial code LMS Virtual.Lab Motion.

An improved version of the motorcycle model developed by the author of this thesis in [126] is comprehensively described in Chapter 3, while the tools introduced in [127] for the quasi-static analysis of motorcycles are described and extended in Chapters 4 and 5. Finally, in Chapter 6 a novel virtual rider based on MPC is presented, which concludes the research first published in 2010 [128].

Even now, after we've been building them for 100 years, it's very difficult to understand just why a bicycle works - it's even difficult to formulate it as a mathematical problem.

Freeman Dyson in Wired News
(February 1998)

Chapter 3

A symbolic motorcycle model for virtual rider design and simulation

The present chapter introduces a motorcycle model based on the symbolic multibody approach. The chapter can be divided in four sections. In the first part, a brief review of the most relevant multibody formulations available in literature is provided. The differences between symbolic and numeric codes are then discussed. In the second part of the chapter, the motorcycle model is presented together with a detailed description of its implementation. The tyre model and the underlying assumptions of its formulation are also discussed. In the third part, a model developed in LMS Virtual.Lab Motion is introduced and then used as a validation tool. Finally, some considerations regarding the development of the model and its application to the development of the virtual rider are presented and discussed.

3.1 Introduction

One of the most relevant innovations that has taken place in the field of automotive engineering during the last decades is the integration of computer simulation techniques into the vehicle design process. These techniques, which are usually grouped under the

name of *virtual product design*, are nowadays present in all stages of vehicle development, from the design of all its parts up to the dynamic simulation of the full vehicle including complex control systems like ABS, ESP, ADAS, etc.

The development of a new vehicle is usually an iterative process. Before reaching the market, a vehicle must pass numerous tests that assess their safety, performance and durability. If the test results are not satisfactory a new iteration is performed, i.e. the design is modified and the tests are repeated. This iterative process represents a considerable investment for the manufacturer and, what is more important, increases significantly the time-to-market of the product. In this context, the use of virtual models allows to reduce costs, decreases the development time and limits the number of functional prototypes needed to validate a new design. Furthermore, computer simulations permit conducting experiments in conditions that would not be feasible in the real world.

Over the years, numerical simulation has become a key part of the design and development of new vehicles, to the point that today it is possible to accurately predict the mechanical behaviour of new components in a completely virtual environment. However, not all simulation techniques have spread equally in the automotive and motorcycle industries. Unlike computer design software (CAD) and structural analysis (FEA), which are nowadays considered standard tools in both industries, multibody simulation tools are still far from reaching in the motorcycle industry the same level of penetration found in the automotive sector. In this respect, there is an obvious lag between both industries.

One of the major reasons of this discrepancy lies in the intrinsic instability of single track vehicles, which makes their dynamic simulation a complex task. As a matter of fact, it is not even possible to simulate basic manoeuvres, e.g. steady-state cornering, without a suitable rider model that keeps the vehicle on the desired path and prevents the motorcycle from falling over. Although several rider models are available in literature, none of them has been wholly accepted in the industry yet. The main drawback of current models is the lack of robustness and versatility as has been previously discussed in Chapter 2. In this context, the low performance observed in the existing virtual riders has been one of the main motivations to develop this PhD thesis, where a novel rider model based on model predictive control theory is introduced.

There are two key elements in the development of model-based controllers: the dynamic model of the plant (internal model) and the simulation model. The first is used in the control design process, while the second represents the real vehicle within a simulation environment and is generally used to validate the resulting control strategy. The quality of the virtual rider highly depends on the underlying models. Surprisingly,

some of the existing algorithms are based on extremely simplified models [73–75, 124] that do not take into account the main modes of vibration of the vehicle (wobble and weave). In general, mathematical models must be as detailed as possible to accurately represent the real system and, at the same time, they must be as simple as possible to allow efficient and fast calculations. These conflicting requirements were highlighted by Sharp in [131]:

“Models do not possess intrinsic value. They are for solving problems. They should be thought of in relation to the problem or range of problems which they are intended to solve. The ideal model is that with minimum complexity which is capable of solving the problems of concern with an acceptable risk of the solution being wrong. This acceptable risk is not quantifiable and it must remain a matter of judgement. However, it is clear that diminishing returns are obtained for model elaboration.”

In the market there are many commercial codes for the modelling and simulation of mechanical systems which greatly simplify the generation of the model as the user does not have to focus on writing the equations of motion. Complex mechanisms can be defined by simply specifying its components and their interconnections. Furthermore, most of these codes come with specific libraries for vehicle modelling, including predefined components such as suspensions, tyres, transmission, aerodynamics, etc. However, commercial multibody codes offer a limited set of numerical tools, usually static equilibrium solvers and integrators, which are usually not sufficient to develop suitable internal models for control purposes.

The development of the rider model proposed in this thesis requires special tools not available in any commercial or research code. Because of this reason, the elaboration of a motorcycle model tailored to the needs of this project is considered an essential step towards improving the performance of existing virtual riders.

3.2 A brief review of multibody dynamics

Wheeled vehicles are usually composed by a main body to which the powertrain, steering and suspension subsystems are connected. All these elements interact dynamically with each other, with the tyres playing a key role in this process as they constitute the interface between the vehicle and the road. The analysis of this interplay of forces and motions requires a unified treatment of all components. Interestingly, Milliken had already identified the need of an integrated approach for handling analysis in 1956 [132] when simulation tools were yet to appear:

“The major effort in handling research to date has been in the recognition of individual effects, their isolation, and examination as separate entities. [...] All the individual effects now known need quantitative analytical expression. More significant, however, is the need for comprehensive, integrated analysis methods, for such overall theories will enable the prediction of the actual motion by rationally and simultaneously taking into account all the separate effects.”

Nowadays multibody dynamics provide powerful solutions to approach this scenario: starting from the set of bodies, joints and forces defined by the user, multibody tools are capable of generating the equations of motion of the vehicle. This section presents a brief review of some contemporary methods to model and simulate mechanical systems, putting special emphasis on wheeled vehicles. Some definitions and remarks regarding the nomenclature used throughout this thesis are also introduced next.

3.2.1 Reference frames and coordinate systems

The definition of appropriate frames of reference is the first step in modelling a mechanical system. Frames are mainly employed to describe the position and orientation of the different bodies that compose the model and to define the attachment points of joints and external forces. Mathematically, frames are unequivocally parameterized by a set of variables called coordinates.

There are multiple ways to parameterize the motion of a mechanical system which, if properly chosen, may lead to remarkable improvements in the performance and efficiency of the resulting model. The most relevant types of coordinates used currently in multibody dynamics are relative coordinates, reference point coordinates (Cartesian), and natural coordinates. They are briefly introduced next, more details can be found in the book by Jalon and Bayo [47] and in the works of Nikravesh [133] and Haugh [3].

Relative coordinates

Relative coordinates define the position and orientation of each body with respect to the previous one in the kinematic chain, see Fig. 3.1b. In particular, every coordinate is chosen so that it represents one of the degrees of freedom allowed by the joint that connects two consecutive bodies. As a result, this approach builds up a system where the number of degrees of freedom is equal to the number of coordinates and hence no constraint equations are required.

The main features of this formulation [47] are: a minimal number of coordinates, good numerical efficiency for open-loop configurations, and the possibility to directly

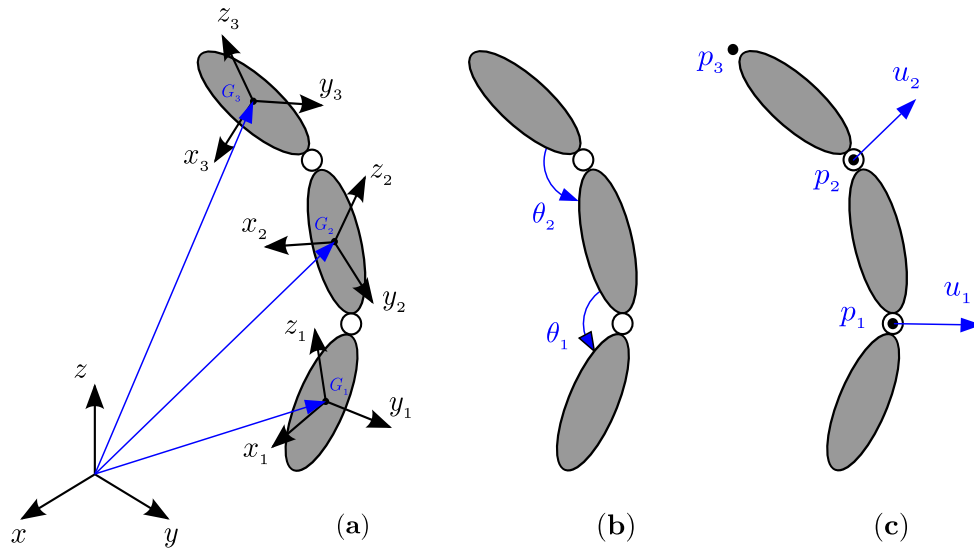


Figure 3.1: Coordinate systems available for multibody systems. (a) Reference point coordinates. (b) Relative coordinates. (c) Natural coordinates.

control the motion of each joint due to a one-to-one correspondence between the coordinates and the degrees of freedom of the joints. Furthermore, as no constraint equations are included, relative coordinates provide a straightforward state space representation of the model (ODE) which is perfectly suited for control system design and analysis. For instance, relative coordinates have been shown to be particularly advantageous and effective in robotics [134] where multibody models are essential to develop advanced control strategies.

The negative aspect of this approach is the high level of coupling found in the resulting equations of motion due to the fact that the absolute position of each body depends on the positions of all preceding bodies in the kinematic chain. Moreover, relative coordinates are not suited for closed-loop systems, where the computational effort required by this technique often makes its application prohibitive.

Reference point coordinates

Reference point coordinates (Cartesian coordinates) define the absolute position of each body by means of the Cartesian coordinates of one of its points along with the angular orientation of a reference frame rigidly attached to the body, see Fig. 3.1a. Thus, at least six parameters are needed for each single body: three for the position and three for the angular orientation. The centre of gravity of the body is usually chosen as the reference point, whereas the parameterization of the angular orientation is a well known problem of mechanics that allows different solutions.

Probably the most general way of defining the angular orientation of a rigid body is by means of the rotation matrix \mathbf{S} , composed of nine elements: three direction cosines for each one of the moving axes. These elements are not independent, but are related by six constraint equations given that the rotation matrix must be orthonormal, i.e. the three column vectors must be orthogonal to each other and each vector must have unit modulus. It is worth noting that no subset of three elements of the matrix \mathbf{S} can unequivocally represent the orientation of the moving frame at any possible position. Therefore, several alternatives to direction cosines have been developed as it is usually inconvenient to work with nine coordinates and six constraint equations.

We can classify these alternatives in two groups [3, 133], one based on three coordinates without constraint equations and another based on four coordinates with one constraint equation. The first group represents the spatial orientation of any reference frame as a composition of three elemental rotations (about x , y or z) starting from the inertial frame. The most widespread sequences are the Euler angles and the Tait-Bryan angles, also known as roll-pitch-yaw. The problem is that all the existing three-parameter systems have singular configurations where the rotation sequence can not be defined unequivocally. In order to avoid this problem, a set of four parameters known as Euler parameters can be used at the expense of adding one constraint equation and increasing the number of coordinates, which become seven instead of six for each body.

One of the main advantages of reference point coordinates is their simplicity as the position of each body is directly included in the equations, thus making the formulation of the problem simple with low pre-processing requirements. Furthermore, joints are defined at a local level, i.e. the constraint equation associated to any joint only includes the coordinates of those bodies connected by the joint in question.

The above two features of reference point coordinates make straightforward the automatic generation of the equations of motion for arbitrarily complex models. Therefore it is not surprising that these coordinates have become the preferred solution of many commercial codes [135]. In addition, reference point coordinates can be easily integrated with multiple formalisms: NEWEUL and DADS are based on the Newton-Euler equations, MESA VERDE on Jourdain's principle, SIMPACK uses D'Alembert's principle, and ADAMS obtains its equations of motion directly from Lagrange's approach. All of them are based on reference point coordinates.

Although reference point coordinates are probably the best choice to automatically build efficient simulation models, the fact that they do not directly reflect the degrees of freedom of the mechanism, the need to include one constraint equation for each kinematic joint and the large number of required parameters (six per body) make these

coordinates less appealing to design internal models for control system design.

Natural coordinates

Natural coordinates are characterized by the absence of angular variables in its formulation. They were originally introduced by Jalón in 1981 for planar cases, and then extended to spatial systems in 1986 by the same author [136]. In the case of planar multibody systems, natural coordinates can be seen as an evolution of the reference point coordinates where the reference points have been moved to the joints, see Fig. 3.1c. In this case, the Cartesian coordinates (x, y) of the *basic points* constitute the natural coordinates. For three dimensional systems, on the other hand, the Cartesian coordinates of the basic points are augmented with a set of unit vectors associated with the joints of the system. Non-commercial codes COMPAMM and MBSNAT, both based on Jourdain's principle, use this type of coordinates.

The number of natural coordinates necessary to describe a system is usually an average between the number of relative coordinates and the number of reference point coordinates. This is due to the elimination of the angular coordinates and to the sharing of the basic points by two or more bodies.

According to Jalón [47], the most significant advantage of natural coordinates over relative and reference point coordinates is their easy formulation and implementation from a programming point of view. As a matter of fact, the resulting mass matrix is constant and therefore no Coriolis or centrifugal forces appear explicitly in the model equations. Furthermore, the nonlinearity of the constraints is generally low; the constraint equations are linear for the most common joints encountered in practice, and at most quadratic. This makes the constraint equations and their Jacobian matrix very easy to evaluate

Natural coordinates have similar disadvantages to reference point coordinates as far the development of internal models for control design is concerned: these coordinates do not directly reflect the degrees of freedom of the mechanism, they need to be completed with constraint equations, and the number of required coordinates is high.

3.2.2 Kinematics

In general, the position and orientation of a rigid body can be unequivocally described with respect to the inertial frame by means of the position vector \mathbf{r}_i and the rotation matrix \mathbf{S}_i .

$$\mathbf{r}_i = [r_{i1}, r_{i2}, r_{i3}]^T \quad (3.1)$$

$$\mathbf{S}_i = \mathbf{S}_i(\alpha_i, \beta_i, \gamma_i) \quad (3.2)$$

This means that we need six coordinates to define each body, three for the position and three for the orientation, which may be collected in the column vector \mathbf{q}_i .

$$\mathbf{q}_i(t) = [r_{i1}, r_{i2}, r_{i3}, \alpha_i, \beta_i, \gamma_i]^\top \quad (3.3)$$

As a result, a multibody system composed of n rigid bodies will include $6n$ position coordinates, resulting in a $6n \times 1$ global position vector.

$$\mathbf{q}(t) = [\mathbf{q}_1^\top, \dots, \mathbf{q}_n^\top]^\top \quad (3.4)$$

Generally these coordinates are not independent as their number is bigger than the number of degrees of freedom of the system. Consequently, m constraint equations must be added to the system.

$$\Phi(\mathbf{q}, t) = 0 \quad (3.5)$$

In realistic vehicle models only *holonomic* constraints are found; they define the relative translation or rotation between two bodies through geometric or integrable equations. However, in very specific applications it can be useful to constrain the relative velocity between two bodies. For example, to model non-slipping tyres, where the relative velocity of the contact point with respect to the ground must be zero. In this particular case the velocity constraint cannot be integrated and requires special treatment. These constraints receive the name of *non-holonomic* constraints, and will not be further mentioned in this dissertation. For more details, see Chapter 3 of [47].

Due to the introduction of the constraints, there remain only $f=6n-m$ linearly independent position coordinates, which characterize the f degrees of freedom of the mechanism. This set of independent coordinates may be collected in a $f \times 1$ column vector as follows:

$$\mathbf{z}(t) = [z_1 \dots z_f]^\top \quad (3.6)$$

By combining Eqs. 3.5 and 3.6, the vector of dependent coordinates \mathbf{q} can be expressed as a function of the independent coordinates \mathbf{z} .

$$\mathbf{q} = \mathbf{q}(\mathbf{z}, t) \quad (3.7)$$

It is worth noting that the choice of independent coordinates is not unique as has been discussed in Section 3.2.1, and therefore multiple parameterizations of the same mechanical system are possible. Once the set of independent coordinates has been

chosen, the position and orientation of each body can be expressed as a function of this new set of coordinates \mathbf{z} .

$$\mathbf{r}_i = \mathbf{r}_i(\mathbf{z}, t) \quad (3.8)$$

$$\mathbf{S}_i = \mathbf{S}_i(\mathbf{z}, t) \quad (3.9)$$

The velocity variables associated to \mathbf{r}_i and \mathbf{S}_i , i.e. \mathbf{v}_i and $\boldsymbol{\omega}_i$ respectively, can be obtained by differentiating the above equations as follows,

$$\mathbf{v}_i(t) = \dot{\mathbf{r}}_i(t) = \frac{\partial \mathbf{r}_i}{\partial \mathbf{z}^\top} \dot{\mathbf{z}} + \frac{\partial \mathbf{r}_i}{\partial t} = \mathbf{J}_{T_i}(\mathbf{z}, t) \dot{\mathbf{z}} + \bar{\mathbf{v}}_i(\mathbf{z}, t) \quad (3.10)$$

$$\boldsymbol{\omega}_i(t) = \dot{\mathbf{s}}_i(t) = \frac{\partial \mathbf{s}_i}{\partial \mathbf{z}^\top} \dot{\mathbf{z}} + \frac{\partial \mathbf{s}_i}{\partial t} = \mathbf{J}_{R_i}(\mathbf{z}, t) \dot{\mathbf{z}} + \bar{\boldsymbol{\omega}}_i(\mathbf{z}, t) \quad (3.11)$$

where ∂s_i represents the infinitesimal rotation vector 3×1 associated to the rotation matrix S , in a similar fashion to the rotational velocity vector¹.

$$\partial \tilde{\mathbf{s}}_i = \partial \mathbf{S}_i \mathbf{S}_i^\top := \begin{bmatrix} 0 & -\partial s_{i3} & \partial s_{i2} \\ \partial s_{i3} & 0 & -\partial s_{i1} \\ -\partial s_{i2} & \partial s_{i1} & 0 \end{bmatrix}, \quad \partial \mathbf{s}_i = \begin{bmatrix} \partial s_{i1} \\ \partial s_{i2} \\ \partial s_{i3} \end{bmatrix} \quad (3.12)$$

The $3 \times f$ Jacobian matrices \mathbf{J}_{T_i} and \mathbf{J}_{R_i} directly relate the dependent $\dot{\mathbf{q}}$ and independent $\dot{\mathbf{z}}$ velocities when there are no rheonomous constraints. The structure of these matrices may be defined using the chain rule of differentiation. E.g. for the translation coordinates it yields:

$$\mathbf{J}_{T_i} = \frac{\partial \mathbf{r}_i}{\partial \mathbf{z}^\top} = \begin{bmatrix} \frac{\partial r_{i1}}{\partial z_1} & \frac{\partial r_{i1}}{\partial z_2} & \dots & \frac{\partial r_{i1}}{\partial z_f} \\ \frac{\partial r_{i2}}{\partial z_1} & \frac{\partial r_{i2}}{\partial z_2} & \dots & \frac{\partial r_{i2}}{\partial z_f} \\ \frac{\partial r_{i3}}{\partial z_1} & \frac{\partial r_{i3}}{\partial z_2} & \dots & \frac{\partial r_{i3}}{\partial z_f} \end{bmatrix} = \frac{\partial \mathbf{r}_i}{\partial \mathbf{q}^\top} \frac{\partial \mathbf{q}}{\partial \mathbf{z}^\top} \quad (3.13)$$

The acceleration variables \mathbf{a}_i and $\boldsymbol{\alpha}_i$ are obtained by differentiating Eqs. 3.10 and 3.11, obtaining:

$$\mathbf{a}_i(t) = \dot{\mathbf{v}}_i(t) = \mathbf{J}_{T_i}(\mathbf{z}, t) \ddot{\mathbf{z}} + \frac{\partial \mathbf{v}_i}{\partial \mathbf{z}^\top} \dot{\mathbf{z}} + \frac{\partial \mathbf{v}_i}{\partial t} \quad (3.14)$$

$$\boldsymbol{\alpha}_i(t) = \dot{\boldsymbol{\omega}}_i(t) = \mathbf{J}_{R_i}(\mathbf{z}, t) \ddot{\mathbf{z}} + \frac{\partial \boldsymbol{\omega}_i}{\partial \mathbf{z}^\top} \dot{\mathbf{z}} + \frac{\partial \boldsymbol{\omega}_i}{\partial t} \quad (3.15)$$

It is interesting to observe that for scleronomic joints, which do not depend explicitly

¹The rotational velocity vector $\boldsymbol{\omega}_i(t)$ can be represented by the skew symmetric tensor $\dot{\boldsymbol{\omega}}_i(t) = \dot{\mathbf{S}}_i \mathbf{S}_i^\top$.

on time, the partial time derivatives in Eqs. 3.10, 3.11, 3.14 and 3.15 vanish.

3.2.3 Dynamics

In this section two basic formulations to derive the equations of motion of a multibody system are briefly introduced, namely the Newton-Euler approach and the Lagrangian approach. The first method describes the behaviour of the system by means of vector and tensor quantities with clear mechanical and geometrical meaning such as mass centre, inertia tensor, angular velocity, linear and angular momentums, etc. The main drawback of this method is that reaction forces have to be included in the motion equations and then eliminated, which often turns out to be a complicated problem. On the other hand, the Lagrange approach uses only scalar quantities based on energy considerations, which usually do not reflect directly the geometry and the dynamics of the system considered. Furthermore, this second method does not provide any information about the reaction forces.

The Newton-Euler approach

The fundamental laws of Newton (1687) and Euler (1758) relate respectively the translational motion of a body, represented by the momentum \mathbf{p} , to the sum of applied external forces \mathbf{f} and its rotational motion, represented by the angular momentum \mathbf{h}_0 , to the sum of external torques \mathbf{l}_0 .

$$\frac{d\mathbf{p}}{dt} = \mathbf{f}, \quad \frac{d\mathbf{h}_0}{dt} = \mathbf{l}_0 \quad (3.16)$$

The time derivatives in the above equations must be evaluated in the inertial frame. On the other hand, the reference point 0 in the second equation may be either a fixed point attached to the inertial frame or a moving point. Then, if the centre of mass is chosen as the reference point for all bodies, we get for the i^{th} body,

$$\mathbf{p}_i = m_i \mathbf{v}_i, \quad \mathbf{h}_i = \mathbf{I}_i \boldsymbol{\omega}_i \quad (3.17)$$

where m_i is the mass of the body, \mathbf{I}_i is the inertia tensor with respect to centre of mass, and vectors \mathbf{v}_i and $\boldsymbol{\omega}_i$ represent the absolute linear and angular velocities respectively. By introducing Eq. 3.17 into 3.16 we get the Newton-Euler equations expressed in the inertial reference frame.

$$m \dot{\mathbf{v}}_i = \mathbf{f}_i^e + \mathbf{f}_i^r \quad (3.18)$$

$$\mathbf{I}_i \dot{\boldsymbol{\omega}}_i + \tilde{\boldsymbol{\omega}}_i \mathbf{I}_i \boldsymbol{\omega}_i = \mathbf{l}_i^e + \mathbf{l}_i^r \quad (3.19)$$

In order to apply the previous equations to a multibody system, it must be first disassembled as a set of single bodies and all constraints must be replaced by external reaction forces \mathbf{f}^r and torques \mathbf{l}^r acting on the involved bodies. For instance, a joint connecting two bodies would be replaced by two forces, one on each body, with the same magnitude and opposite sign, according to the action-reaction principle. Vectors \mathbf{f}^e and \mathbf{l}^e represent the external forces and torques applied to the i^{th} body respectively.

Subsequently, a set of six Newton-Euler equations is obtained for each one of the n bodies composing the system. This results in a total of $6n$ scalar equations, which may be expressed in terms of the dependent coordinates \mathbf{q} as,

$$\mathbf{M}(\mathbf{q})\ddot{\mathbf{q}} + \mathbf{k}(\mathbf{q}, \dot{\mathbf{q}}, t) = \mathbf{Q}^e(\mathbf{q}, \dot{\mathbf{q}}, t) + \mathbf{Q}^r \quad (3.20)$$

where \mathbf{M} is the inertia matrix of the system, \mathbf{Q}^r includes the reaction forces, \mathbf{Q}^e includes the external forces applied to the system and \mathbf{k} includes the centrifugal, Coriolis and gyroscopic terms. Furthermore, the reaction forces can be rewritten as a function of the m generalized constraint forces $\boldsymbol{\lambda}$ [137], which yields:

$$\mathbf{M}(\mathbf{q})\ddot{\mathbf{q}} + \mathbf{k}(\mathbf{q}, \dot{\mathbf{q}}, t) + \Phi_{\mathbf{q}}^T \boldsymbol{\lambda} = \mathbf{Q}^e(\mathbf{q}, \dot{\mathbf{q}}, t) \quad (3.21)$$

In general Eq. 3.21 is not well defined as the number of unknowns $6n+m$ is bigger than the number of equations $6n$; the unknowns comprise the $6n$ elements of vector $\ddot{\mathbf{q}}$ and the m elements of vector $\boldsymbol{\lambda}$. Therefore, it is necessary to include m more equations in order to obtain a determined system. The constraints from Eq. 3.5 can be used for this purpose, which, along with Eq. 3.21, constitute a set of differential algebraic equations (DAE) of index three. This form of the equations of motion receives the name of *descriptor form* [135],

$$\begin{cases} \mathbf{M}(\mathbf{q})\ddot{\mathbf{q}} + \Phi_{\mathbf{q}}(\mathbf{q})^T \boldsymbol{\lambda} = \mathbf{Q}(\mathbf{q}, \dot{\mathbf{q}}, t) \\ \Phi(\mathbf{q}, t) = 0 \end{cases} \quad (3.22)$$

where now \mathbf{Q} includes the applied forces as well as the centrifugal, Coriolis and gyroscopic terms.

The index of a DAE represents the number of times that the system must be differentiated with respect to time in order to convert it into an explicit ordinary differential system, known as the underlying ODE [138]. The index of a DAE can also be understood as a perturbation index, i.e. a measure of the sensitivity of the solution to numerical perturbations. For instance, the solution of an index-3 problem like Eq. 3.22 is affected by the second derivative of any error introduced during the solution procedure. As a

consequence, both index three and index two formulations are in general not suitable for direct integration.

Several techniques exist in literature to deal with index three DAEs, which are usually classified into index and coordinate reduction techniques. Index reduction techniques transform the original system into a lower index DAE, keeping the same coordinates as the original problem. On the other hand, coordinate reduction techniques transform the original DAE into an ODE containing a smaller set of independent coordinates. A brief overview of these two methods is presented next. For an extensive review of reduction techniques, the reader is referred to [139,140].

- a) **Index reduction.** A DAE of index one can be obtained by differentiating twice with respect to time the constraint equations in Eq. 3.5:

$$\Phi_{\mathbf{q}}\ddot{\mathbf{q}} = -\dot{\Phi}_{\mathbf{q}}\dot{\mathbf{q}} - \dot{\Phi}_t \quad (3.23)$$

which can be combined with Eq. 3.21 to yield the well known index one expression of the multibody equations:

$$\begin{bmatrix} \mathbf{M} & \Phi_{\mathbf{q}}^T \\ \Phi_{\mathbf{q}} & 0 \end{bmatrix} \begin{Bmatrix} \ddot{\mathbf{q}} \\ \lambda \end{Bmatrix} = \begin{bmatrix} \mathbf{Q} \\ -\dot{\Phi}_{\mathbf{q}}\dot{\mathbf{q}} - \dot{\Phi}_t \end{bmatrix} \quad (3.24)$$

The above equations are numerically unstable due to the double zero eigenvalues originating from the differentiation of the constraints. This problem is known as drift-off phenomenon, and makes necessary the use of additional stabilisation techniques to enforce the constraints. During the last decades great progress has been achieved in the stabilization of the solutions of Eq. 3.24; among the most relevant, we can highlight Baumgarte's approach and the penalty formulation proposed by Bayo [140–142].

- b) **Coordinate reduction.** The coordinate reduction approach converts the original descriptor form (Eq. 3.22) into a minimal formulation of the problem [137,143]. For that purpose, the constraint forces are eliminated by means of D'Alembert's principle, which exploits the orthogonality of generalized motions and constraints in order to obtain a set of ODEs containing the minimal number of equations,

$$\hat{\mathbf{M}}(\mathbf{z})\ddot{\mathbf{z}} = \hat{\mathbf{Q}}(\mathbf{z}, \dot{\mathbf{z}}, t) \quad (3.25)$$

where \mathbf{z} is the vector of independent coordinates, $\hat{\mathbf{M}}$ is the symmetric inertia matrix of the system and $\hat{\mathbf{Q}}$ includes the gyroscopic, Coriolis and centrifugal forces along with the generalized applied forces.

The main characteristic of Eq.3.25 is that the number of coordinates used to describe the system \mathbf{z} is equal to its number of degrees of freedom, and therefore no (algebraic) constraint equations are needed.

The Lagrangian approach

Unlike the Newton-Euler approach, where the reaction forces have to be included in the motion equations to subsequently eliminate them, the Lagrangian approach allows to directly obtain the minimal representation of open loop systems without having to deal with the constraint equations.

The key element of this approach is the Lagrangian function, which summarizes the dynamics of the entire system in one expression,

$$L = T - U \quad (3.26)$$

where T and U are the total kinetic and potential energy of the system respectively. For a system composed of n bodies, the kinetic energy can be computed as,

$$T = \frac{1}{2} \sum_{i=1}^n \left[\mathbf{v}_i^T m_i \mathbf{v}_i + \boldsymbol{\omega}_i^T \mathbf{I}_i \boldsymbol{\omega}_i \right] \quad (3.27)$$

which can be expressed as a function of the independent coordinates \mathbf{z} and its derivatives $\dot{\mathbf{z}}$,

$$T = T(\mathbf{z}, \dot{\mathbf{z}}) \quad (3.28)$$

On the other hand, the potential energy U depends only on the independent coordinates \mathbf{z} and can be used to derive the contribution of the conservative forces.

$$Q_k = -\frac{\partial U(\mathbf{z})}{\partial z_k} \quad (k=1 \dots f) \quad (3.29)$$

In order to introduce general forces into the system, the concept of virtual displacement must be first introduced: a virtual displacement is defined as an arbitrary, infinitesimally small variation of the system position which is compatible with the constraints at any time. It is called virtual rather than real since no actual displacement can occur if the time stays constant. The symbol δ is usually employed to represent the virtual motion operator, which behaves mathematically as the regular differential operator, i.e.

$$\delta(c\mathbf{r}) = c\delta\mathbf{r}, \quad \delta(\mathbf{r}_1 + \mathbf{r}_2) = \delta\mathbf{r}_1 + \delta\mathbf{r}_2, \quad \delta\mathbf{r}(\mathbf{z}) = \frac{\partial \mathbf{r}}{\partial \mathbf{z}^T} \delta\mathbf{z} \quad (3.30)$$

Hence, the virtual motion of a multibody system can be expressed by means of the

Jacobian matrices introduced in Eqs. 3.10 and 3.11 as follows:

$$\delta \mathbf{r}_i = J_{T_i} \delta \mathbf{z}, \quad \delta \mathbf{s}_i = J_{R_i} \delta \mathbf{z} \quad (i=1 \dots n) \quad (3.31)$$

The principle of virtual work [144] allows to project the external forces f_i^e and torques l_i^e on the direction of the generalized coordinates,

$$\delta W^e = \sum_{i=1}^n \left[(\mathbf{f}_i^e)^\top \delta \mathbf{r}_i + (\mathbf{l}_i^e)^\top \delta \mathbf{s}_i \right] = \sum_{k=1}^f Q_k^e \delta z_k \quad (3.32)$$

where Q_k^e is the projection of all external forces on the k^{th} generalized coordinate. The above equation may be rewritten as follows:

$$Q_k^e = \sum_{i=1}^n \left[\left(\frac{\partial \mathbf{r}_i}{\partial z_k} \right)^\top \mathbf{f}_i^e + \left(\frac{\partial \mathbf{s}_i}{\partial z_k} \right)^\top \mathbf{l}_i^e \right] = \sum_{i=1}^n \left[\mathbf{J}_{T_i}(:, k)^\top \mathbf{f}_i^e + \mathbf{J}_{R_i}(:, k)^\top \mathbf{l}_i^e \right] \quad (3.33)$$

where the Matlab notation $(:, k)$ has been used to denote the k^{th} column of the Jacobians. It is worth noting that only those forces that perform work are included, and therefore the reaction forces do not appear in the equations. Once the expression of the Lagrangian is known and the generalized forces have been obtained, the equations of the multibody system can be obtained by means of the Lagrange equations [144],

$$\frac{d}{dt} \left(\frac{\partial L}{\partial \dot{z}_k} \right) - \frac{\partial L}{\partial z_k} = Q_k^e, \quad (k=1 \dots f) \quad (3.34)$$

where the conservative forces are implicitly included in the term $\partial L / \partial z_k$. The above equations are known as Lagrange equations of the second kind and constitute a system of ODEs which can be rewritten in matrix form as in Eq. 3.25.

$$\hat{\mathbf{M}}(\mathbf{z}) \ddot{\mathbf{z}} = \hat{\mathbf{Q}}(\mathbf{z}, \dot{\mathbf{z}}, t) \quad (3.35)$$

In fact, both Newton-Euler and Lagrange's approaches yield identical results if the same set of independent coordinates is used. For systems with a closed kinematic structure, Eq. 3.34 can be augmented to include the corresponding m Lagrange multipliers arising from Eq. 3.5.

$$\frac{d}{dt} \left(\frac{\partial L}{\partial \dot{q}_j} \right) - \frac{\partial L}{\partial q_j} + \Phi_{q_j}^\top \boldsymbol{\lambda} = Q_j^e, \quad (j=1 \dots f+m) \quad (3.36)$$

In this case, reduction techniques like those presented for the Newton-Euler approach would be needed to integrate the system of DAEs. However, the motorcycle model

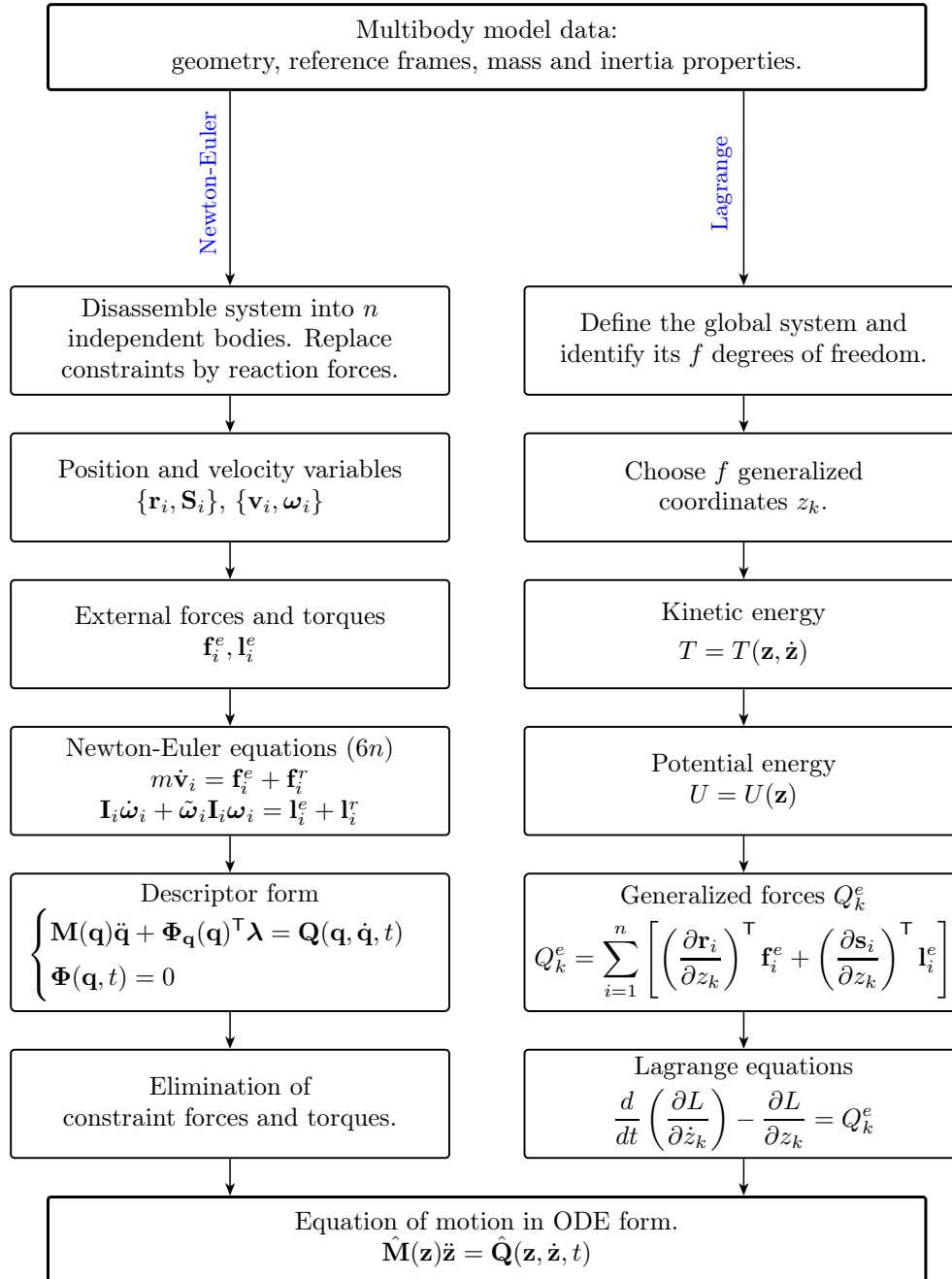


Figure 3.2: Summary of the different steps required to generate of the equations of motion by the Newton-Euler and Lagrange methods.

that is presented in the next sections does not have any closed loop and therefore this formulation will not be further discussed here. For more details regarding multibody dynamics, see [3, 47, 133].

Comparison of the Newton and Lagrange approaches

The main steps to derive the equation of motion of a multibody system by the methods of Newton-Euler and Lagrange are depicted in Fig. 3.2. As shown in the figure, both approaches share the same starting point, the mechanical model of the system, and produce the same equations of motion if the same generalized coordinates are chosen. Furthermore, in both cases the resulting equations of motion can be reduced to a set of ODEs. However, the effort required to obtain those equations is different.

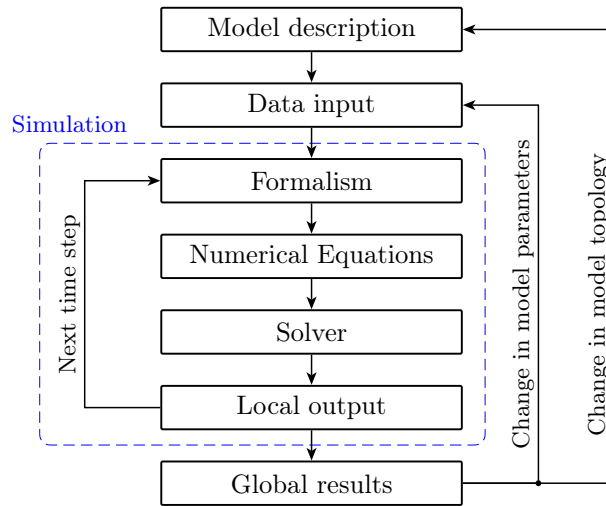
The most important advantage of the Lagrange's approach is that it allows to directly write the equations of motion in a minimal form. However, there appear terms in $d/dt(\partial L/\partial \dot{z}_k)$ which are then eliminated by $\partial L/\partial z_k$ according to Eq. 3.34. This implies a useless computational effort which is not present in the Newton-Euler approach. On the other hand, if the Newton-Euler approach is chosen, additional steps need to be carried out in order to remove the reaction forces from the equations.

In this thesis, the Lagrange approach is preferred over the Newton-Euler equations as its implementation in a symbolic tool such as Maple[®] [45] is simpler due to the minimal form of the problem. Furthermore, the use of computer algebra software (CAS) allows to overcome the main drawback of Lagrange's approach by simplifying the equations of motion symbolically. This means that the duplicated terms described above will be cancelled during the symbolic manipulation stage and therefore will not appear in the final equations.

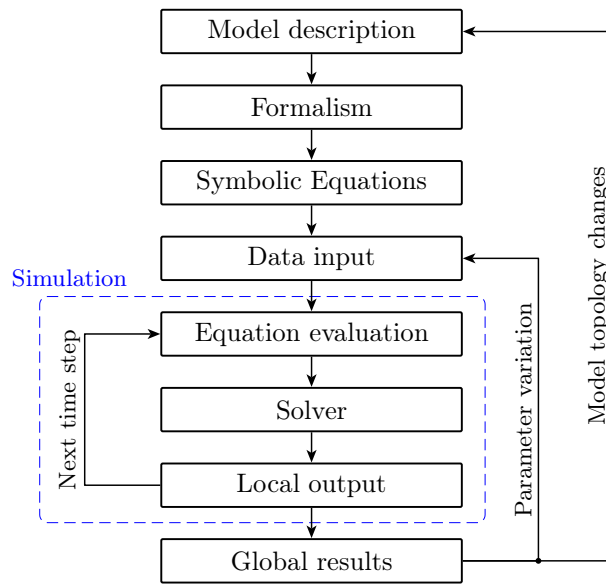
3.2.4 Numerical vs. symbolic formalisms

Two formalisms to generate the mathematical equations representing a multibody model are found in literature, namely numerical and symbolic formalisms.

Generally, numerical codes generate and solve the equations numerically at each timestep of the integration procedure. Symbolic codes, on the other hand, derive the equations of motion only once, in a fashion similar to hand derivation; obtaining first the model equations which are then converted into a C or FORTRAN source code. In a second stage the symbolic code is compiled and numerical results are obtained via numerical integration. The symbolic derivation of the equations of motion is usually more complex than the numeric one; however, there is no need to regenerate the equations every time a new simulation is run or during parametric studies. Both formalisms are summarized in Fig.3.3



(a)



(b)

Figure 3.3: Structure of numerical and symbolic formalisms. (a) Numeric formalism. (b) Symbolic formalism.

Numerical codes are oriented to the product's final design, and model equations are not available for the user to explore or manipulate them. Symbolic codes, on the other hand, allow a low-level control of the model in order to produce specialized, problem-oriented, simulation programs. For example, the symbolic manipulation of the equations of motion allows the user to neglect insignificant details that are not relevant to the problem bandwidth, to treat small displacements in an efficient manner or to neglect them. Furthermore, some of these symbolic codes exploit algebraic manipulation to simplify the equations of motion and thus produce extremely efficient simulation codes.

Multibody codes are nowadays the most widespread tool for the dynamic analysis of complex mechanisms. Most of the commercially available codes for modelling and simulating multibody systems are based on a numerical approach. However, it has been proven that symbolic codes are more suited to analyse fundamental problems and/or when high computational efficiency is required [32,46]. Furthermore, they allow a deeper understanding of the system by providing access to the underlying equations.

Lastly, it can be concluded from literature that the symbolic generation of the equations of motion is especially suited for control design and optimization [46,137]. Symbolic models may be obtained by Computer Algebra Software like Maple[®] [45] or Mathematica[®] [145], or with special software like NEWEUL [146], ROBOTRAN [147] or MBSymba [46]. Most of the symbolic routines developed in this thesis are based on the latter. MBSymba is a Maple library developed at the University of Padova for the symbolic modelling of multibody systems that contains a variety of routines for defining the elements of the multibody systems and for the derivation and manipulation of the equations of motion. A comprehensive review of numerical and symbolic formalisms is found in [143].

3.3 The symbolic motorcycle model

In this section, a motorcycle model comprising eleven degrees of freedom is presented and its equations of motion are derived in a symbolic fashion using the computer algebra software Maple[®]. The scope of this model is not to improve the level of detail or the computing performance of existing models but to provide a suitable framework for the development of a novel virtual rider and a set of symbolic-numeric tools aimed at the study and optimization of motorcycle dynamics. These tools, which are not available in any commercial multibody software, play a key role in the development of the rider algorithm presented in this thesis and will be introduced in subsequent chapters.

Models published previously, such as Cossalter's [43] and Sharp's [51], were mainly developed for simulation purposes and present some drawbacks as far as the design

of control algorithms is concerned. Cossalter's model is symbolically formulated as a system of DAEs due to the great number of constraints introduced by the natural coordinates approach [47]. Although it shows very good computational performance, the algebraic equations make it unsuitable for control purposes, in particular for state-space based approaches, where a system of ODEs is required. Sharp, conversely, created his model with the commercial multibody code AUTOSIM [34]. Commercial multibody tools simplify the modelling task significantly by numerically deriving and solving the equations of motion of complex mechanical systems. This process is however transparent to the user, who does not have access to the underlying equations and is often constrained by the limited set of numerical tools integrated in the multibody package, basically static equilibrium solvers and integrators. These tools are insufficient to develop the rider model proposed in this thesis and hence a more suitable model will be derived here.

In the first part of this section the kinematics of the model are described, including the bodies that compose the system and the generalized coordinates employed to describe their configuration. The position of the tyre contact points is also derived in this section for a generic cross section. In the second part, the force elements (tyres, suspensions, control inputs, etc) are introduced along with their kinematic inputs. Then these forces are projected on the generalized coordinates by means of the virtual work principle. In the third part, the equations of motion are derived and the resulting code is optimized in order to improve the computing performance of the model. Finally, the code is translated into C and then compiled in Matlab[®] as an `S-function` for time-domain simulations and as a `.mex` file for optimization and other purposes.

3.3.1 Model kinematics

The motorcycle model proposed here is composed of six bodies as depicted in Fig. 3.4 and Table 3.1: the front and rear wheels, the main assembly (including the frame, the engine and the fuel tank), the rear assembly (including the swingarm and the rear brake calipers), the upper part of the front assembly (including the sprung part of the forks, both triple clamps, the steering column, and the handlebar), and the lower part of the front assembly (including the unsprung part of the forks and the front brake calipers). Based on the conclusions of [28, 99], where the rider movements were found to be an order of magnitude less important than the steering torque as far as the control of the motorcycle is concerned, it has been decided to model the rider as a rigid body attached to the main assembly. No rider motions are therefore considered.

The geometry of the standard motorcycle chassis can be characterized by means of three main parameters as shown in Fig. 3.4: the length of the swinging arm l_r , measured

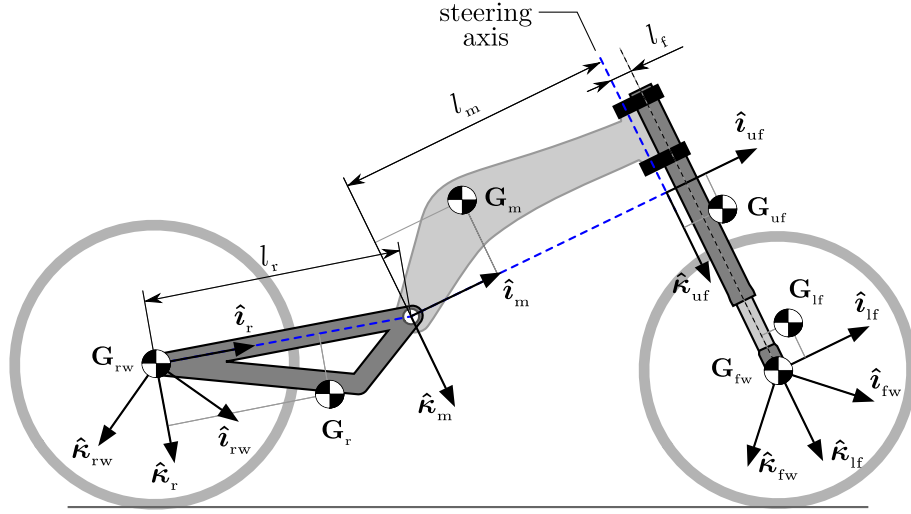


Figure 3.4: Multibody model of the motorcycle. Note that each body is represented by its center of gravity \mathbf{G}_i . The drawing includes also the main reference frames used to define the model and the main geometric parameters of the chassis: l_r , l_m , and l_f .

Body	Subscript	Reference frame	Unit vectors
front wheel	fw	\mathbf{T}_{fw}	$(\hat{\mathbf{i}}_{fw}, \hat{\mathbf{j}}_{fw}, \hat{\mathbf{k}}_{fw})$
rear wheel	rw	\mathbf{T}_{rw}	$(\hat{\mathbf{i}}_{rw}, \hat{\mathbf{j}}_{rw}, \hat{\mathbf{k}}_{rw})$
main assembly	m	\mathbf{T}_m	$(\hat{\mathbf{i}}_m, \hat{\mathbf{j}}_m, \hat{\mathbf{k}}_m)$
rear assembly	r	\mathbf{T}_r	$(\hat{\mathbf{i}}_r, \hat{\mathbf{j}}_r, \hat{\mathbf{k}}_r)$
front assembly (upper fork)	uf	\mathbf{T}_{uf}	$(\hat{\mathbf{i}}_{uf}, \hat{\mathbf{j}}_{uf}, \hat{\mathbf{k}}_{uf})$
front assembly (lower fork)	lf	\mathbf{T}_{lf}	$(\hat{\mathbf{i}}_{lf}, \hat{\mathbf{j}}_{lf}, \hat{\mathbf{k}}_{lf})$

Table 3.1: List of bodies included in the model.

from the rear wheel centre to the pivot²; the length of the frame l_m , measured along the line connecting the pivot and the fork at right angles; and the offset between the front wheel and the steering axis l_f . The geometry of the tyres and their cross section, which will be elaborated later in this section, complete the geometric description of the vehicle.

Generalized coordinates and reference frames

In addition to the geometric parameters, a suitable set of generalized coordinates and reference frames is needed in order to properly describe the position and orientation of the different bodies that compose the model. The motorcycle system presents an

²In motorcycle terminology, the term pivot is usually employed to describe the joint where the swingarm connects to the frame.

open-loop topology and possesses eleven degrees of freedom, from which six correspond to the rigid motion of the vehicle, one to the steering system, two to the suspensions and the last two correspond to the rotation of the wheels. In view of the above, eleven independent coordinates are sufficient to unequivocally describe the motion of the system. We can collect them in the 11×1 vector \mathbf{q} :

$$\mathbf{q}(t) = [x, y, z, \psi, \phi, \mu, \delta, d_f, \mu_r, \theta_{rw}, \theta_{fw}]^T \quad (3.37)$$

Note that the letter \mathbf{q} has been used to denote the vector of generalized coordinates instead of the usual letter \mathbf{z} introduced in Section 3.2.2. This avoids confusion with the coordinate z and does not imply any further changes in the nomenclature as the model presented here does not include any dependent coordinates. The set of chosen coordinates is described in Table 3.2 and illustrated in Fig. 3.5.

Coordinate	Definition
x, y, z	Coordinates of the centre of gravity of the main assembly \mathbf{G}_m . The pair (x, y) represents the Cartesian position of the reference point \mathbf{P} with respect to the inertial frame. The coordinate z , on the other hand, measures the distance from \mathbf{P} to \mathbf{G}_m .
ψ	Yaw angle. Angle between the x -axis of the inertial frame and the intersection of the mid-plane of the vehicle with the road plane.
ϕ	Roll angle, also called lean or camber. Angle between the road normal vector and the mid-plane of the vehicle.
μ	Pitch angle. Angle between the x -axis of the main assembly $\hat{\mathbf{i}}_m$ and the road plane measured on the mid-plane of the vehicle.
δ	Steering angle.
d_f	Front suspension travel.
μ_r	Pitch angle of the rear assembly. Angle between the x -axis of the swingarm $\hat{\mathbf{i}}_r$ and the road plane measured on the mid-plane of the vehicle.
θ_{fw}, θ_{rw}	Rotation angle of the front and rear wheels measured with respect to the lower fork and the rear assembly respectively.

Table 3.2: List of generalized coordinates.

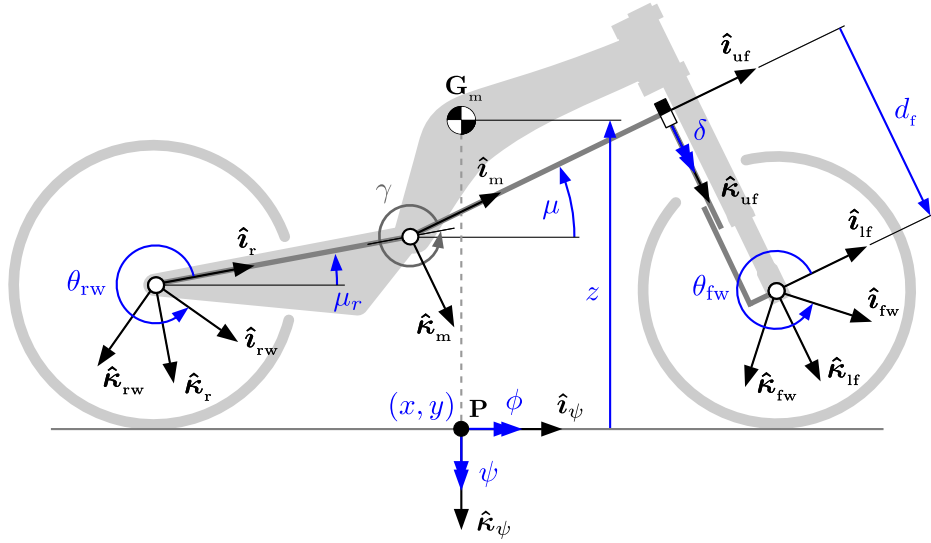


Figure 3.5: Set of generalized coordinates. The model possesses eleven degrees of freedom, which are depicted in blue in the above figure: six correspond to the rigid motion of the main assembly $(x, y, z, \psi, \phi, \mu)$, one to the steering system (δ) , two to the suspensions (d_f, μ_r) and the last two represent to the angular rotation of the wheels $(\theta_{fw}, \theta_{rw})$.

It is important to point out that, contrary to what seems intuitive, the relative angle between the swingarm and the main assembly is not present among the generalized coordinates. Instead, we included the pitch angle of the swingarm with respect to the road μ_r . Note that due to the particular parameterization of the motorcycle orientation defined in Table 3.2, the absolute pitch angle of the main assembly μ and the relative rotation of the swingarm with respect to it γ can be directly added as their rotation axes remain always parallel, i.e.

$$\mu_r = \mu + \gamma \quad (3.38)$$

A preliminary version of the model created using γ as a generalized coordinate revealed that the two terms in the right hand side of Eq. 3.38 could be always collected together in the kinematic equations. However, this symbolic procedure was not straightforward and resulted even more complex for the dynamic equations. For this reason, and in order to obtain a more compact set of equations, the absolute pitch angle of the swingarm has been selected as a generalized coordinate.

Usually it is more convenient to express the vehicle motion in a moving frame attached to the vehicle. If we project the derivative of \mathbf{q} on the vehicle frame, i.e. a non-inertial reference frame that moves with the motorcycle but does not include the roll and pitch rotations, we get a new set of generalized velocities in body coordinates \mathbf{q}_v . As shown in Eq. 3.39, such projection only involves the first two generalized veloc-

ities \dot{x} and \dot{y} . We will use \mathbf{q} to describe the model kinematics at position level and \mathbf{q}_v for the velocities.

$$\mathbf{q}_v = \begin{bmatrix} c_\psi & s_\psi & 0 & 0 & \cdots & 0 \\ -s_\psi & c_\psi & 0 & 0 & \cdots & 0 \\ 0 & 0 & 1 & 0 & \cdots & 0 \\ 0 & 0 & 0 & 1 & \cdots & 0 \\ \vdots & \vdots & \vdots & \vdots & \ddots & \vdots \\ 0 & 0 & 0 & 0 & \cdots & 1 \end{bmatrix} \dot{\mathbf{q}} = \mathbf{\Gamma} \dot{\mathbf{q}} \quad (3.39)$$

The vector of generalized coordinates \mathbf{q} has been used to parameterize the reference frames attached to the bodies of the model and to other relevant points such as the application points of external forces and additional measurement points. One way of defining these frames is by means of 4×4 homogeneous transformation matrices \mathbf{T}_j [144],

$$\mathbf{T}_j = \begin{bmatrix} \mathbf{S}_j^{3 \times 3} & \mathbf{p}_j^{3 \times 1} \\ \mathbf{0}^{1 \times 3} & 1 \end{bmatrix} \quad (3.40)$$

where \mathbf{p}_j is a position vector defining the origin of the j^{th} frame and \mathbf{S}_j is a 3×3 rotation matrix representing its orientation. The columns of the rotation matrix contain the unit vectors $(\hat{\mathbf{i}}_j, \hat{\mathbf{j}}_j, \hat{\mathbf{k}}_j)$ of the frame expressed in the inertial reference system. The advantage of this notation is that the frame position and orientation can be described by one single matrix. It is however important to note that, unlike rotation matrices, homogeneous transformations are not orthogonal, i.e.

$$\mathbf{T}_j^{-1} \neq \mathbf{T}_j^T \quad (3.41)$$

The sequence of transformations followed to derive all the reference frames contained in the model is shown in the tree diagram of Fig. 3.6. A combination of basic transformation matrices has been used to obtain them starting from the inertial reference frame, where $\mathbf{Rot}_\xi(\alpha)$ applies a relative rotation α around the ξ -axis of the preceding frame and $\mathbf{Tra}(x, y, z)$ applies a relative translation (x, y, z) also with respect to the preceding frame. These matrices are detailed in Eq. 3.42.

The first element of the kinematic chain is the ground-fixed frame \mathbf{T}_0 , which has been defined according to the SAE convention so that its x and y axes lie on the road plane and its z -axis points downwards. If we continue down the tree diagram we find the auxiliary³ frame \mathbf{T}_ψ . This reference system is usually known as the vehicle frame or moving frame. Its origin is coincident with the point \mathbf{P} while its x -axis $\hat{\mathbf{i}}_\psi$ is aligned

³We call auxiliary frames those frames that are not directly used to define the bodies of the system.

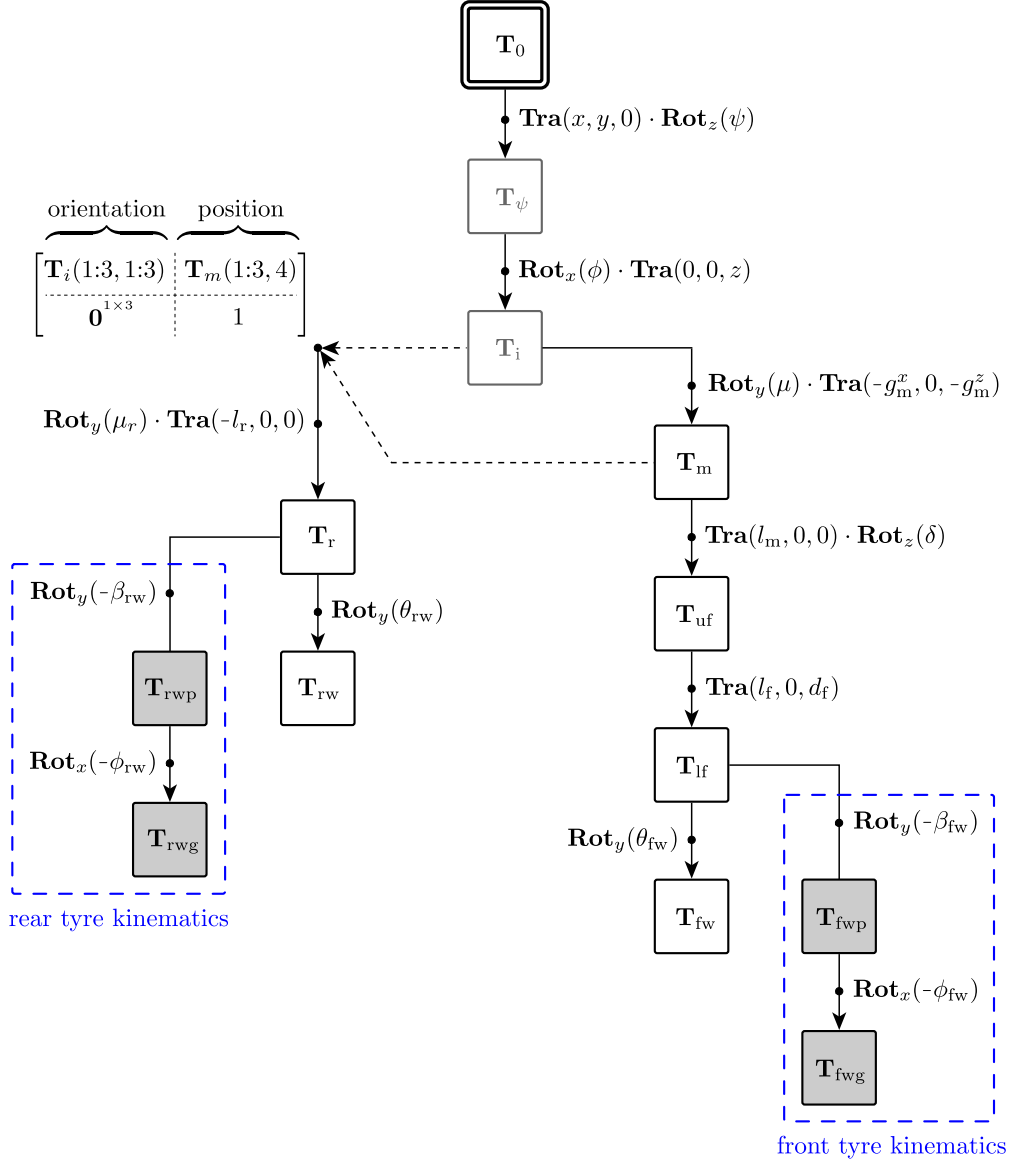


Figure 3.6: Topology of the multibody model. The figure shows the sequence of transformations needed to derive all the reference frames included in the model. A combination of 4×4 transformation matrices has been used to derive them starting from the inertial reference frame \mathbf{T}_0 , where $\mathbf{Rot}_\xi(\alpha)$ represents a relative rotation α around the ξ -axis while $\mathbf{Tra}(x, y, z)$ represents a relative translation (x, y, z) , both with respect to the preceding frame. Auxiliary frames are depicted in grey.

$$\begin{aligned}
\mathbf{Rot}_x(\alpha) &= \begin{bmatrix} 1 & 0 & 0 & 0 \\ 0 & c_\alpha & -s_\alpha & 0 \\ 0 & s_\alpha & c_\alpha & 0 \\ 0 & 0 & 0 & 1 \end{bmatrix} & \mathbf{Rot}_y(\alpha) &= \begin{bmatrix} c_\alpha & 0 & s_\alpha & 0 \\ 0 & 1 & 0 & 0 \\ -s_\alpha & 0 & c_\alpha & 0 \\ 0 & 0 & 0 & 1 \end{bmatrix} \\
\mathbf{Rot}_z(\alpha) &= \begin{bmatrix} c_\alpha & -s_\alpha & 0 & 0 \\ s_\alpha & c_\alpha & 0 & 0 \\ 0 & 0 & 1 & 0 \\ 0 & 0 & 0 & 1 \end{bmatrix} & \mathbf{Tra}(x, y, z) &= \begin{bmatrix} 1 & 0 & 0 & x \\ 0 & 1 & 0 & y \\ 0 & 0 & 1 & z \\ 0 & 0 & 0 & 1 \end{bmatrix}
\end{aligned} \tag{3.42}$$

with the longitudinal direction of the vehicle, see Fig. 3.5. This is the same frame on which the vector of generalized velocities $\dot{\mathbf{q}}$ was projected in Eq. 3.39 in order to obtain \mathbf{q}_v .

The next element of the kinematic chain is the auxiliary frame \mathbf{T}_i , where the subscript i stands for intermediate. This frame is located at the center of gravity of the main assembly \mathbf{G}_m with its xz -plane being parallel to the mid-plane of the motorcycle, i.e. the angle between the z -axis of \mathbf{T}_i and the z -axis of the inertial frame \mathbf{T}_0 is equal to the roll angle ϕ . The intermediate frame is not depicted in Fig. 3.5 as it has no particular interest. It is required however in the tree diagram of Fig.3.6 to represent the point where the kinematic chain bifurcates. After \mathbf{T}_i the diagram splits into two branches: the first includes the main and front assemblies (right) while the second contains only the rear assembly (left).

The first frame in the right branch is the body-fixed reference system of the main assembly \mathbf{T}_m . The origin of such frame is located at the pivot while its x -axis $\hat{\mathbf{i}}_m$ is rotated with respect to the road by the pitch angle μ as shown in Fig. 3.5. The position vector of the centre of gravity of the main assembly \mathbf{G}_m is defined in this reference frame as

$$\mathbf{r}_m(\mathbf{q}) = \mathbf{T}_m [g_m^x, 0, g_m^z, 1]^\top \tag{3.43}$$

where g_m^x and g_m^z are local coordinates (constant).

It is worth noting that the attitude of the main frame is expressed by a non-standard rotation sequence z - x - y or yaw-roll-pitch. This sequence however is convenient to model single-track vehicles where the roll and pitch angles have special definitions as described in Table 3.2. In particular, the rotation order is chosen so that the roll angle represents the camber of the chassis and the pitch is measured in the bike plane, both with respect to the road.

The next frame is the body-fixed reference system of the upper fork \mathbf{T}_{uf} . This frame is located at the headpipe and is rotated around the steering axis $\hat{\mathbf{r}}_{uf}$ by the steering

angle δ . Hence, the position vector of \mathbf{G}_{uf} may be defined as follows:

$$\mathbf{r}_{\text{uf}}(\mathbf{q}) = \mathbf{T}_{\text{uf}}[g_{\text{uf}}^x, 0, g_{\text{uf}}^z, 1]^\top \quad (3.44)$$

After that, the translation $(l_f, 0, d_f)$ places the body-fixed reference system of the lower fork \mathbf{T}_{lf} at the centre of the front wheel. Note that l_f is a constant offset while d_f is the generalized coordinate representing the fork travel. Therefore, we can write the position vector of the centre of gravity \mathbf{G}_{lf} as:

$$\mathbf{r}_{\text{lf}}(\mathbf{q}) = \mathbf{T}_{\text{lf}}[g_{\text{lf}}^x, 0, g_{\text{lf}}^z, 1]^\top \quad (3.45)$$

Finally, the front wheel frame \mathbf{T}_{fw} is defined by a rotation θ_{fw} around the y -axis of \mathbf{T}_{lf} . The centre of gravity of the wheel \mathbf{G}_{fw} is located at the wheel hub, i.e.

$$\mathbf{r}_{\text{fw}}(\mathbf{q}) = \mathbf{T}_{\text{fw}}[0, 0, 0, 1]^\top \quad (3.46)$$

The remaining two blocks, depicted in grey, are auxiliary frames included to model the tyre kinematics. The frame \mathbf{T}_{fwp} is defined so that its y -axis is parallel to the rotation axis of the wheel and its x -axis is parallel to the road. The frame \mathbf{T}_{fwg} , on the other hand, shares the same x -axis as \mathbf{T}_{fwp} but has its xy -plane parallel to the road. The pitch and roll angles of the front assembly, i.e. β_{fw} and ϕ_{fw} , are derived in the next section dedicated to tyre kinematics. Fig. 3.7 illustrates the tyre frames.

The first frame of the left branch is the body-fixed reference system of the rear assembly \mathbf{T}_r . This frame is not defined as the previous ones since, as discussed earlier in this section, we want to use the absolute angle μ_r to parameterize the motion of the rear assembly instead of the relative coordinate γ . To do so, we first build a new frame that has the same position vector of \mathbf{T}_m and the same orientation matrix of \mathbf{T}_i . This may be expressed by using Matlab notation as,

$$\begin{bmatrix} \mathbf{S}_i & \mathbf{p}_m \\ \mathbf{0} & 1 \end{bmatrix} = \begin{bmatrix} \mathbf{T}_i(1:3, 1:3) & \mathbf{T}_m(1:3, 4) \\ \mathbf{0} & 1 \end{bmatrix} \quad (3.47)$$

which represents a frame located at the pivot and oriented with its x -axis parallel to the ground. Then, \mathbf{T}_r can be obtained by rotating the frame introduced above around its y -axis by the angle μ_r followed by a translation from the pivot to the rear wheel. The resulting frame \mathbf{T}_r is the body-fixed reference system of the rear assembly and may be used to define its centre of gravity \mathbf{G}_r as follows:

$$\mathbf{r}_r(\mathbf{q}) = \mathbf{T}_r[g_r^x, 0, g_r^z, 1]^\top \quad (3.48)$$

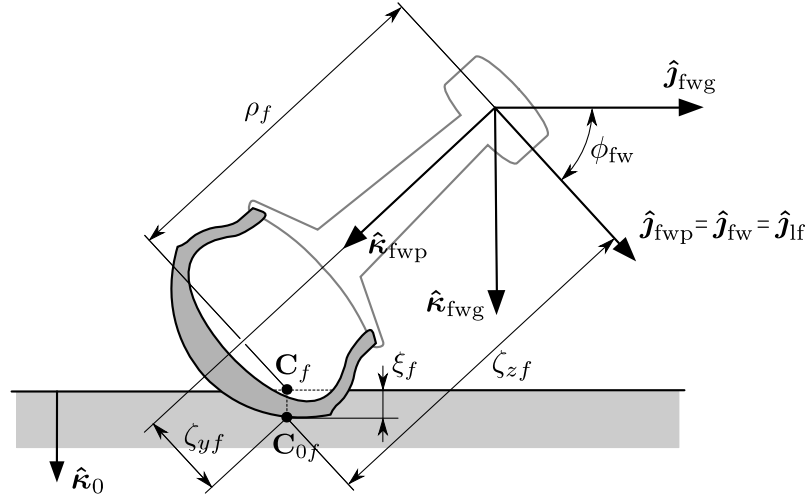


Figure 3.7: Front tyre kinematics. Two reference frames are involved in the kinematic definition the tyre model: \mathbf{T}_{fwp} and \mathbf{T}_{fwg} . The coordinates ζ_y and ζ_z define the position of the geometric contact point. Note that the road normal vector points downwards.

A rotation θ_{rw} around the y -axis of the swingarm defines the rear wheel frame \mathbf{T}_{rw} , which is located at the centre of the rear wheel, i.e.

$$\mathbf{r}_{rw}(\mathbf{q}) = \mathbf{T}_{rw} [0, 0, 0, 1]^T \quad (3.49)$$

The remaining two frames, depicted in grey, are homologous to those described for the front assembly. The frame \mathbf{T}_{rwp} is defined so that its y -axis is parallel to the rotation axis of the wheel and its x -axis parallel to the road. The frame \mathbf{T}_{rwg} , on the other hand, shares the same x -axis as \mathbf{T}_{rwp} but has its xy -plane parallel to the road.

Tyre kinematics

A proper modelling of the tyre forces is essential for the dynamic simulation of any ground vehicle; this becomes especially important when it comes down to motorcycles due to the high camber angles achieved and the curvature of the tyre cross section. When a tyre cambers, the contact patch shifts laterally with respect to the mid-plane of the tyre, thus modifying the projection of the tyre forces on the vehicle. In the past, motorcycle tyres were inaccurately represented as thin discs; Sharp [51] and Lot [44] were the first to introduce advanced models with a detailed description of the tyre cross section and of the contact point migration. These approaches have the advantage that the longitudinal and vertical forces automatically produce realistic yawing and overturning moments without the need of introducing artificial terms in the tyre equations. The concept proposed by Sharp regarding the contact point migration has been adopted

here to develop the tyre model of this thesis.

In order to evaluate the tyre forces during the simulation, a series of kinematic inputs are needed (see Fig.2.3). These inputs can be usually expressed as functions of the position and velocity of the contact patch and the spatial orientation of the tyre. The purpose of this section is to derive symbolic expressions for the tyre kinematics considering the real shape of the tyre cross section.

We will start with the kinematic description of the front tyre. In the tree diagram of Fig.3.6 we introduced two frames to describe the position and orientation of the front wheel, namely \mathbf{T}_{fwp} and \mathbf{T}_{fwg} . Both of them share the same origin, located at the front wheel center, and the same x -axis, which is parallel to the road, is contained on the mid-plane of the front assembly and points forwards. The main difference between these reference systems is the camber angle ϕ_{fw} as shown in Fig.3.7. Note that the y -axis of \mathbf{T}_{fwp} is parallel to the rotation axis of the wheel while the respective y -axis of \mathbf{T}_{fwg} is parallel to the ground.

The first frame \mathbf{T}_{fwp} is very useful to define the position of the undeformed or geometrical contact point of the front wheel \mathbf{C}_{0f} , which can be written as

$$\mathbf{C}_{0f} = \mathbf{T}_{\text{fwp}} \begin{bmatrix} 0 \\ \zeta_{yf} \\ \zeta_{zf} \\ 1 \end{bmatrix} \quad (3.50)$$

where ζ_y and ζ_z constitute a local parametric representation of the tyre profile. The second frame \mathbf{T}_{fwg} , on the other hand, is the reference frame where the tyre forces will be defined on since it has its xy -plane parallel to the road. Additionally, the angle between the x -axis of this frame $\hat{\mathbf{i}}_{\text{fwg}}$ and the longitudinal axis of the vehicle $\hat{\mathbf{i}}_{\psi}$ determines the kinematic steering angle Δ .

The orientation of \mathbf{T}_{fwp} and \mathbf{T}_{fwg} is characterized by two angles, the pitch angle of the front assembly β_{fw} and the camber angle of the front tyre ϕ_{fw} , which in turn depend on the generalized coordinates \mathbf{q} . Both angles can be derived from the unit vector that represents the rotation axis of the wheel $\hat{\mathbf{j}}_{\text{lf}}$, i.e. from the second column of the orientation matrix \mathbf{S}_{lf} . According to Fig. 3.6, such matrix may be obtained by applying four successive rotations as follows:

$$\begin{bmatrix} \mathbf{S}_{\text{lf}} & \mathbf{0} \\ \mathbf{0} & 1 \end{bmatrix} = \mathbf{Rot}_z(\psi) \cdot \mathbf{Rot}_x(\phi) \cdot \mathbf{Rot}_y(\mu) \cdot \mathbf{Rot}_z(\delta) \quad (3.51)$$

No translations need to be considered in the above expression given that we are only

interested in the frame orientation. It then follows that,

$$\mathbf{S}_{\text{lf}} = \mathbf{S}_{\psi} \begin{bmatrix} c_{\delta}c_{\mu} & -c_{\mu}s_{\delta} & s_{\mu} \\ c_{\delta}s_{\phi}s_{\mu} + c_{\phi}s_{\delta} & -s_{\delta}s_{\phi}s_{\mu} + c_{\phi}c_{\delta} & -s_{\phi}c_{\mu} \\ -c_{\phi}s_{\mu}c_{\delta} + s_{\phi}s_{\delta} & c_{\phi}s_{\mu}s_{\delta} + s_{\phi}c_{\delta} & c_{\phi}c_{\mu} \end{bmatrix} \quad (3.52)$$

where the expanded matrix of the right hand side is expressed in the vehicle frame. Based on the above, the camber angle can be obtained from the dot product between $\hat{\mathbf{j}}_{\text{lf}}$ and the unit vector perpendicular to the road plane $\hat{\mathbf{k}}_0$ as:

$$\begin{aligned} \hat{\mathbf{j}}_{\text{lf}} \cdot \hat{\mathbf{k}}_0 &= \cos(\pi/2 - \phi_{\text{fw}}) \\ \phi_{\text{fw}} &= \arcsin(c_{\phi}s_{\mu}s_{\delta} + s_{\phi}c_{\delta}) \end{aligned} \quad (3.53)$$

Note that the camber angle of the front wheel ϕ_{fw} is in general different from the roll angle of the main assembly ϕ ; they only match when the steering angle δ is zero. According to Eq. 3.53, ϕ_{fw} depends solely on the roll ϕ and pitch μ angles of the chassis and on the steering angle δ . The effect of these parameters on the front camber angle is depicted in Figs. 3.8a and 3.8c. We show that, for a given roll angle of the chassis, the steering angle tends to increase the camber of the front wheel when the handlebar is turned in the same direction of the vehicle roll (same sign) and viceversa, the steering angle tends to decrease the camber of the front wheel when the handlebar is turned in the opposite direction (opposite sign). In normal riding conditions roll and steering have the same sign, and therefore the front wheel is usually more inclined than the chassis. This has an important implication in the lateral forces generated by the tyres as they strongly depend on the camber angle.

The pitch angle of the front assembly β_{fw} is slightly more complicated to obtain than the camber. First, the cross product between $\hat{\mathbf{j}}_{\text{lf}}$ and $\hat{\mathbf{k}}_0$ is used to get $\hat{\mathbf{i}}_{\text{fwp}}$

$$\hat{\mathbf{i}}_{\text{fwp}} = \frac{\hat{\mathbf{j}}_{\text{lf}} \times \hat{\mathbf{k}}_0}{c_{\phi_{\text{fw}}}} \quad (3.54)$$

which is parallel to the ground and is contained in the mid-plane of the front assembly (xz -plane). The projection of $\hat{\mathbf{i}}_{\text{fwp}}$ on the body-fixed frame of the lower fork \mathbf{T}_{lf} yields

$$\hat{\mathbf{i}}_{\text{fwp}}^{(\mathbf{T}_{\text{lf}})} = \begin{bmatrix} \frac{c_{\phi}c_{\mu}}{c_{\phi_{\text{fw}}}} \\ 0 \\ \frac{c_{\phi}s_{\mu}c_{\delta} - s_{\phi}s_{\delta}}{c_{\phi_{\text{fw}}}} \end{bmatrix} \quad (3.55)$$

which can be also obtained, according to Fig. 3.6, by rotating $\hat{\mathbf{i}}_{\text{lf}}$ around the y -axis of

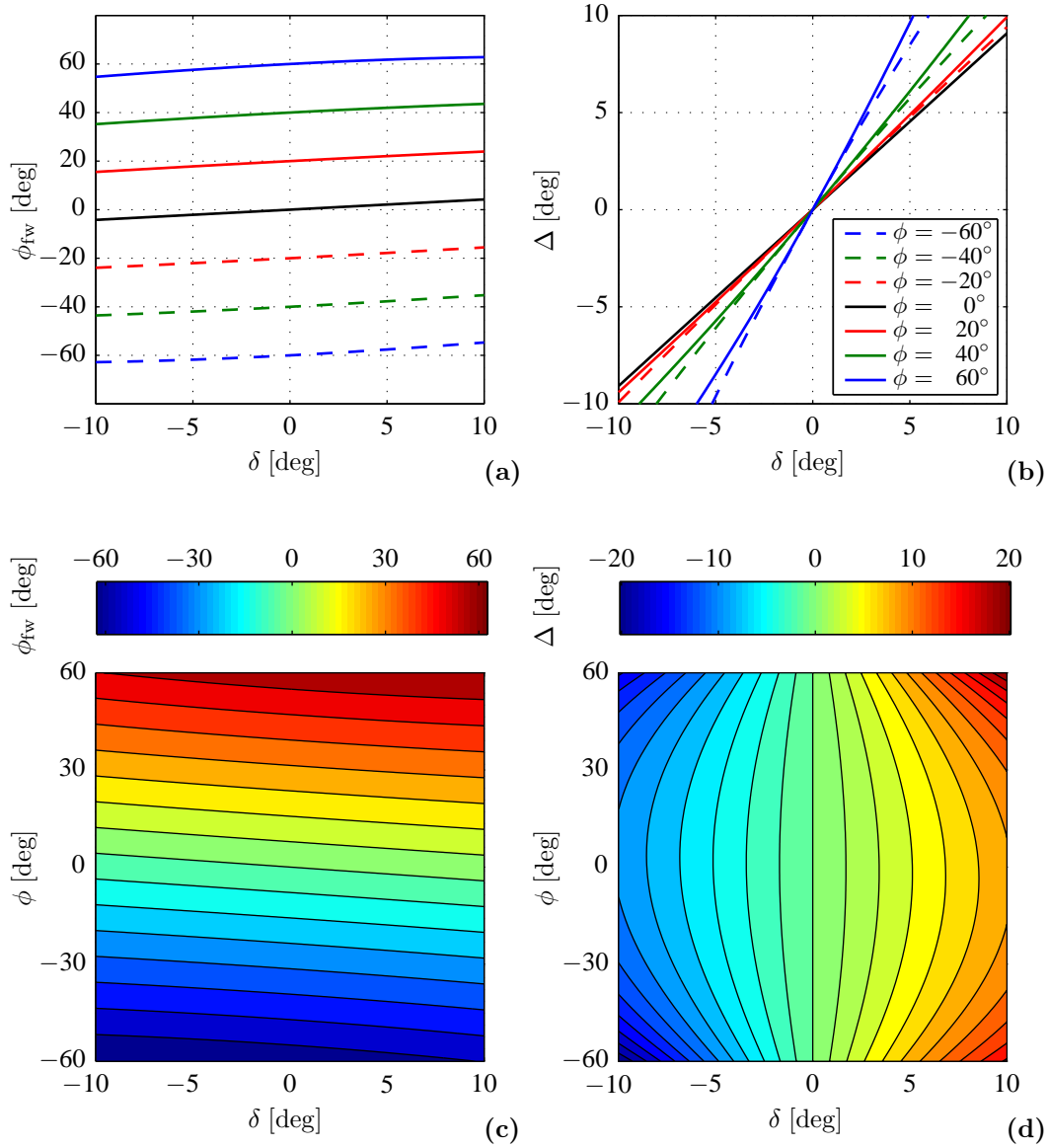


Figure 3.8: Front tyre orientation parameters. The front tyre orientation is characterized by its camber angle ϕ_{fw} and by the kinematic steering angle Δ . The first parameter measures the angle between the road normal vector and the symmetry plane of the wheel, while the second represents the projection of the steering angle on the road plane. Both parameters depend solely on the chassis roll ϕ and pitch μ angles and on the steering angle δ . The effect of the pitch angle is usually small and therefore is not included in the above figure for the sake of clarity. (a) Front camber as a function of the steering angle for several roll angles of the chassis. (b) Kinematic steering angle as a function of the steering angle for several roll angles of the chassis. (c) Contour plot, front camber angle as a function of the steering and chassis roll angles. (d) Contour plot, kinematic steering angle as a function of the steering and chassis roll angles.

\mathbf{T}_{lf} by the angle $-\beta_{fw}$. Therefore we can write

$$\hat{\mathbf{i}}_{fwp}^{(\mathbf{T}_{lf})} = \left([1 \ 0 \ 0 \ 0] \cdot \mathbf{Rot}_y(-\beta_{fw}) \right)^T = \begin{bmatrix} c\beta_{fw} \\ 0 \\ s\beta_{fw} \end{bmatrix} \quad (3.56)$$

where the fourth element of the resulting vector is always null and has been omitted. Finally, by combining Eq. 3.55 and Eq. 3.56, we can put β_{fw} as:

$$\beta_{fw} = \tan^{-1} \left(\frac{c_\phi s_\mu c_\delta - s_\phi s_\delta}{c_\phi c_\mu} \right) \quad (3.57)$$

It is important to note that the terms in the denominator cannot become zero during the simulation as both the roll and the pitch angles are always below ninety degrees. This condition has been ensured for all the expressions appearing in the model in order to avoid singularities.

One additional angle that can be computed regarding the front tyre is the kinematic steering angle Δ , which is basically the projection of the handlebar angle δ on the road plane. Although it is not strictly required for the simulation of the model, the kinematic steering angle can be helpful to simplify some of the expressions appearing in the model equations as well as to gain insight on the steering system of the motorcycle. We may use the unit vector $\hat{\mathbf{j}}_{lf}$ to derive it. By projecting $\hat{\mathbf{j}}_{lf}$ on the vehicle reference system \mathbf{T}_ψ we get the second column of Eq. 3.52, i.e.

$$\hat{\mathbf{j}}_{lf}^{(\mathbf{T}_\psi)} = \begin{bmatrix} -c_\mu s_\delta \\ -s_\delta s_\phi s_\mu + c_\phi c_\delta \\ c_\phi s_\mu s_\delta + s_\phi c_\delta \end{bmatrix} \quad (3.58)$$

We can also obtain $\hat{\mathbf{j}}_{lf}$ through a sequence of rotations different to that shown in Fig. 3.6. Instead of following the kinematic chain of the motorcycle, we can start from the unitary vector $\hat{\mathbf{j}}_\psi$ and apply directly the rotations associated to the kinematic steering angle Δ and to the camber angle of the front assembly ϕ_{fw} as follows,

$$\hat{\mathbf{j}}_{lf}^{(\mathbf{T}_\psi)} = \left([0 \ 1 \ 0 \ 0] \cdot \mathbf{Rot}_z(\Delta) \cdot \mathbf{Rot}_z(\phi_{fw}) \right)^T = \begin{bmatrix} -s_\Delta c\phi_{fw} \\ c_\Delta c\phi_{fw} \\ s\phi_{fw} \end{bmatrix} \quad (3.59)$$

which can be combined with Eq. 3.58 to obtain the kinematic steering angle.

$$\Delta = \tan^{-1} \left(\frac{c_\mu s_\delta}{-s_\delta s_\phi s_\mu + c_\phi c_\delta} \right) \quad (3.60)$$

As with the front camber angle, the kinematic steering angle is a function of the roll, pitch and handlebar angles. Fig. 3.8b shows how the kinematic steering angle varies in function of the handlebar position for several roll angles. It is interesting to note here that there is a roll angle above which the kinematic steering angle Δ becomes bigger than the handlebar angle δ . In this specific case, such threshold is found at $\phi = 22^\circ$, i.e. those curves representing roll angles above that value have slopes greater than unity and viceversa. Below that threshold, the kinematic steering angle is lower than the handlebar angle. This has an important implication in motorcycle control. For low values of the roll angle, the steering mechanism of the motorcycle attenuates the handlebar angle imposed by the rider ($\Delta < \delta$), thus making it easier to steer the motorcycle. On the contrary, for high roll angles, the steering mechanism amplifies the rider's input ($\Delta > \delta$), which in turn makes the vehicle more sensitive to steering inputs. Fig. 3.8d, on the other hand, shows how the roll angle modifies the kinematic steering angle for a given handlebar position. With this we finish the kinematic description of the reference frames that characterize the front wheel. Next we derive the position and velocity of the front contact patch together with other related expressions such as the tyre deflection, the effective rolling radius and the tyre slips.

The position of the geometric contact point, denoted by \mathbf{C}_{0f} , can be obtained from the tangency condition between the road and the tyre profile as shown in Fig.3.9. In order for the tyre and the road to have a common tangent plane, the parametric coordinates ζ_y and ζ_z must fulfil the following equation [43],

$$\tan \phi_{fw} = -\frac{d\zeta_{zf}}{d\phi_{fw}} \bigg/ \frac{d\zeta_{yf}}{d\phi_{fw}} \quad (3.61)$$

which allows to express the position of \mathbf{C}_{0f} as a function of the wheel camber, i.e.

$$\begin{aligned} \zeta_{yf} &= \zeta_{yf}(\phi_{fw}) \\ \zeta_{zf} &= \zeta_{zf}(\phi_{fw}) \end{aligned} \quad (3.62)$$

As a consequence, the position of \mathbf{C}_{0f} can be determined from the vector of generalized coordinates \mathbf{q} and Eq. 3.53. Subsequently, the position of the actual contact point \mathbf{C}_f is obtained by projecting \mathbf{C}_{0f} on the road plane. This allows to compute the deflection of the tyre carcass ξ as the distance between the undeformed and the actual contact points,

$$\xi_f = (\mathbf{C}_{0f} - \mathbf{C}_f) \cdot \hat{\mathbf{r}}_0 \quad (3.63)$$

with the result being positive when the tyre is compressed. Its derivative represents the

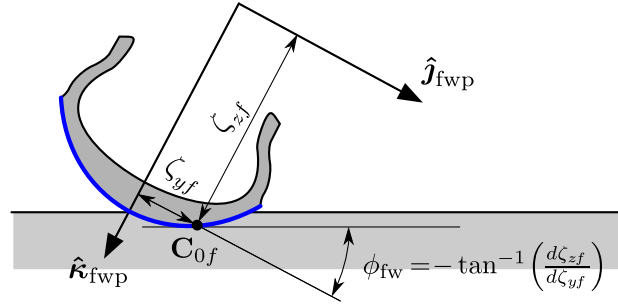


Figure 3.9: Tangency condition between the tyre and the road plane.

deformation velocity of the carcass measured perpendicular to the road plane.

$$\dot{\xi}_f = \dot{\mathbf{C}}_{0f} \cdot \hat{\mathbf{k}}_0 \quad (3.64)$$

In order to derive the remaining kinematic parameters, it results convenient to use the wheel frame \mathbf{T}_{fwp} to parameterize the position of the actual contact point \mathbf{C}_f . From Fig. 3.7 we can write

$$\mathbf{C}_f = \mathbf{T}_{fwp} \begin{bmatrix} 0 \\ \zeta_{yf}^* \\ \zeta_{zf}^* \\ 1 \end{bmatrix} \quad (3.65)$$

where

$$\begin{aligned} \zeta_{yf}^* &= \zeta_{yf} - s_{\phi_{fw}} \xi_f \\ \zeta_{zf}^* &= \zeta_{zf} - c_{\phi_{fw}} \xi_f \end{aligned} \quad (3.66)$$

are the local coordinates of \mathbf{C}_f on the wheel frame. As a result, the last coordinate coincides with the effective radius of the tyre ρ_f , defined as the distance between the actual contact point \mathbf{C}_f and the wheel axis, i.e.

$$\rho_f = \zeta_{zf}^* \quad (3.67)$$

The absolute velocity of the contact point with respect to the inertial frame can be obtained by differentiating Eq.3.65 with respect to time,

$$\dot{\mathbf{C}}_f = \dot{\mathbf{T}}_{fwp} \begin{bmatrix} 0 \\ \zeta_{yf}^* \\ \zeta_{zf}^* \\ 1 \end{bmatrix} + \mathbf{T}_{fwp} \begin{bmatrix} 0 \\ \dot{\zeta}_{yf}^* \\ \dot{\zeta}_{zf}^* \\ 1 \end{bmatrix} = \dot{\mathbf{C}}'_f + \dot{\mathbf{C}}_{rel} \quad (3.68)$$

where the first term on the right hand side corresponds to the velocity of a point \mathbf{C}'_f

that belongs to the tyre, i.e. that is attached to \mathbf{T}_{fwp} , and is instantaneously coincident with \mathbf{C}_f . The second term, on the other hand, corresponds to the relative velocity between \mathbf{C}_f and \mathbf{C}'_f .

We can use Eq. 3.68 to obtain the longitudinal slip of the tyre κ , defined as the ratio between the longitudinal slip velocity of the contact point V_{sx} and its absolute forward velocity V_x .

$$\kappa_f = -\frac{V_{sxf}}{V_{xf}} \quad (3.69)$$

The forward velocity V_{xf} is easily obtained by projecting the velocity of the contact point $\dot{\mathbf{C}}_f$ onto the x -direction of the front frame \mathbf{T}_{fwg} , i.e.

$$V_{xf} = \dot{\mathbf{C}}_f \cdot \hat{\mathbf{i}}_{fwg} \quad (3.70)$$

whereas the slip velocity V_{sx} may be derived by adding the rolling velocity of the wheel $\rho_f \Omega_{fw}$ to the previous expression, which yields

$$V_{sxf} = V_{xf} + \rho_f \Omega_{fw} \quad (3.71)$$

Note that Ω_{fw} is the absolute angular speed of the wheel, which is different from the derivative of the generalized coordinate θ_{fw} . The first represents the wheel speed with respect to the ground, whereas the second is the relative speed between the wheel and the front assembly. Both are related by the following equation:

$$\Omega_{fw} = \dot{\theta}_{fw} + \dot{\beta}_{fw} \quad (3.72)$$

Hence, due to the adopted SAE reference system, Ω_{fw} will be always negative while the longitudinal slip will be positive in traction and negative in braking.

Finally, the sideslip angle λ is defined as the angle between the velocity of the contact point and the intersection of the wheel plane with the road. It can be computed as follows,

$$\lambda_f = -\arctan\left(\frac{V_{syf}}{V_{xf}}\right) \quad (3.73)$$

where V_{syf} is known as the sideslip velocity of the front contact point. It is obtained by projecting the velocity of the material point of the tyre that is in contact with the road, i.e. the point denoted as \mathbf{C}'_f , onto the y -axis of the front frame \mathbf{T}_{fwg} .

$$V_{syf} = \dot{\mathbf{C}}'_f \cdot \hat{\mathbf{j}}_{fwg} \quad (3.74)$$

The sideslip angle is therefore defined as positive when the tyre slides to the left side,

e.g. on a right corner.

The kinematic description of the rear tyre may be obtained from the orientation matrix of the rear assembly S_r ,

$$\begin{bmatrix} \mathbf{S}_r & \mathbf{0} \\ \mathbf{0} & 1 \end{bmatrix} = \mathbf{Rot}_z(\psi) \cdot \mathbf{Rot}_x(\phi) \cdot \mathbf{Rot}_y(\mu_r) \quad (3.75)$$

by using the same procedure that has been applied to the front tyre. In fact, Eqs. 3.61 to 3.74 apply also to the rear wheel. Furthermore, the absence of steering at the rear tyre makes its kinematics straightforward: the rear camber angle is equal to the roll angle of the main assembly and the angle β_{rw} is equal to the pitch angle of the rear assembly, i.e.

$$\begin{aligned} \phi_{rw} &= \phi \\ \beta_{rw} &= \mu_r \end{aligned} \quad (3.76)$$

This concludes the section dedicated to tyre kinematics; the expressions derived here constitute the inputs of the tyre model.

3.3.2 Force and control elements

The last step before we can generate the motorcycle equations is to characterize the external actions applied to the vehicle. These actions are represented in the model by forces and torques that are usually grouped under the names of *force* and *control elements* depending on their purpose. In general, force elements are evaluated within the model code whereas control elements interface the model with external applications. The motorcycle model introduced in this thesis comprises the following force elements: the fork, the rear shock absorber, the aerodynamic map and the tyre-ground interaction. It also includes four control elements that interface the motorcycle with the virtual rider: the steering torque, the wheel braking torques and the chain force.

The principle of virtual work introduced in Eq. 3.33 may be used to project the external forces along the direction of the generalized coordinates. If a force element j applies a force \mathbf{f}_j and a torque \mathbf{l}_j to the body i , its contribution to the k^{th} generalized force is given by the following expression

$$Q_{k,j}^e = \left(\frac{\partial \mathbf{r}_j}{\partial q_k} \right)^\top \mathbf{f}_j^e + \left(\frac{\partial \mathbf{s}_i}{\partial q_k} \right)^\top \mathbf{l}_j^e \quad (3.77)$$

where \mathbf{r}_j is the point of application of the force. The partial derivatives involved in the previous equation can be obtained from the transformation matrices used to describe

the position of each body \mathbf{T}_i and the corresponding rotation submatrices \mathbf{S}_i .

$$\frac{\partial \mathbf{r}_j}{\partial q_k} = \frac{\partial \mathbf{T}_i}{\partial q_k} \mathbf{r}_{ij} \quad (3.78)$$

$$\partial \tilde{\mathbf{s}}_i = \partial \mathbf{S}_i \mathbf{S}_i^\top = \begin{bmatrix} 0 & -\partial s_{i3} & \partial s_{i2} \\ \partial s_{i3} & 0 & -\partial s_{i1} \\ -\partial s_{i2} & \partial s_{i1} & 0 \end{bmatrix} \rightarrow \frac{\partial \mathbf{s}_i}{\partial q_k} = \begin{bmatrix} \frac{\partial s_{i1}}{\partial q_k} \\ \frac{\partial s_{i2}}{\partial q_k} \\ \frac{\partial s_{i3}}{\partial q_k} \end{bmatrix} \quad (3.79)$$

In this case \mathbf{r}_{ij} is the vector that connects the origin of body i with the application point of the force \mathbf{f}_j . The above equations may be combined with the kinematic description of the model introduced in the preceding section in order to derive the vector of generalized forces \mathbf{Q}^e . With the purpose of minimizing the size of the resulting equations, it has been found convenient to project the generalize forces onto the vehicle frame. This new set of forces, referred to as \mathbf{Q}^e , can be computed by multiplying the projection matrix $\mathbf{\Gamma}$ introduced in Eq. 3.39 by the vector \mathbf{Q}^e .

$$\mathbf{Q}^e = \mathbf{\Gamma} \mathbf{Q}^e \quad (3.80)$$

Next, the mathematical representation of the force elements included in the model is elaborated together with their contribution to the vector of generalized forces.

Front suspension

The present model includes the most widespread front suspension system for motorcycles, the fork. Such system consists of two telescopic sliders which move along the interior of two cylindrical tubes. If the sliders are connected to the triple clamp, the fork is referred to as *conventional*; on the other hand, the constructive solution with the outer tubes fastened to the steering head is called *upside-down*. The main advantage of the fork resides in the simplicity of its design. As a matter of fact, the kinematics of the fork are rather simple and may be modelled as a relative translation between the upper (sprung) and lower (unsprung) parts of the front assembly (Fig. 3.6). The main drawbacks of telescopic forks are the high value of the unsprung mass and the friction forces that appear under braking and during cornering.

The nonlinear force introduced by the fork can be modeled as the contribution of four different terms. The first is the elastic force due to the helicoidal springs,

$$F_{\text{frk},1} = \Delta F_f - k(1 + \alpha s_f) s_f \quad (3.81)$$

where s_f is the stroke of the suspension, k is the stiffness of the springs, ΔF_f is the

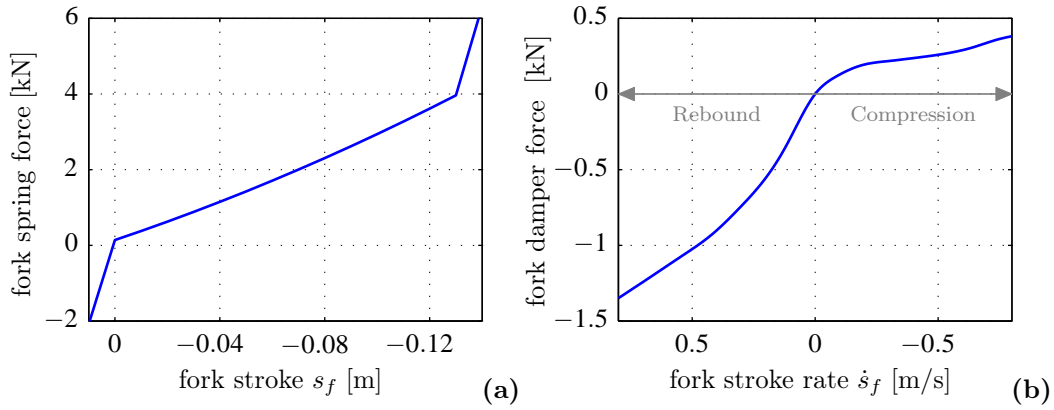


Figure 3.10: Front fork properties. (a) Elastic force. The curve includes the contribution of the linear spring together with the nonlinear effect of the air contained in the sleeves. Bump and rebound stops limit the course of the suspension. (b) Damping force. The damping force in rebound is in general higher than in compression so that the wheel follows road bumps without opposing an excessive force.

preload and α represents the nonlinear stiffening of the springs. The stroke is measured with respect to the fully extended position as

$$s_f(t) = d_f(t) - l_{\text{frk}} \quad (3.82)$$

where l_{frk} is a positive constant equal to the maximum length of the fork. As a result, the stroke will be always negative in the working range of the suspension.

The second term represents the effect of the air contained in the fork tubes; this small volume of air acts as a pneumatic spring in parallel with the main springs when the suspension is compressed. The force exerted by the air can be computed by means of a polytropic transformation law.

$$F_{\text{frk},2} = p_0 A \left(\frac{V_0}{V_0 + A s_f} \right)^{\gamma_p} \quad (3.83)$$

In this case p_0 is the initial pressure in the fork sleeves, A is the cross section area of the chamber containing the air, γ_p is the polytropic coefficient of the transformation and V_0 is the initial volume, which depends on the amount of oil in the chamber. If required, the initial volume may be decreased by adding oil so as to increase the elastic effect of the air.

The third term that contributes to build up the total fork force is the end-stroke spring, which represents the physical limit of the fork travel. This element is usually disabled and engages only when the suspension is compressed below the bump limit or extended above the rebound limit. Such a discontinuity is modelled by an if-then

clause,

$$F_{\text{frk},3} = \begin{cases} -k_{\text{stop}}(s_f - s_{\text{min},f}) & \text{if } s_f < s_{\text{min},f} & \text{(bump stop)} \\ 0 & \text{if } 0 \geq s_f \geq s_{\text{min},f} \\ -k_{\text{stop}}s_f & \text{if } s_f > 0 & \text{(rebound stop)} \end{cases} \quad (3.84)$$

where k_{stop} is the stiffness of the end-stroke springs and $s_{\text{min},f}$ is the suspension stroke at which the bump stop engages. The first three terms constitute the elastic component of the fork force, depicted in Fig. 3.10a.

The fourth term is the damping force, which is usually quite complex to be described by an algebraic expression and hence a spline has been used to accurately represent it as a function of the stroke derivative, see Fig. 3.10b.

$$F_{\text{frk},4a} = f(\dot{s}_f) \quad (3.85)$$

However, in order to perform parametric studies a simpler expression may be useful. If we define c_c and c_e as the compression and rebound damping coefficients respectively, we may represent the damping as a piecewise function of the stroke derivative as follows:

$$F_{\text{frk},4b} = \begin{cases} -c_c \dot{s}_f & \text{if } \dot{s}_f < 0 \\ -c_e \dot{s}_f & \text{if } \dot{s}_f \geq 0 \end{cases} \quad (3.86)$$

Finally, the total force applied by the fork is computed as the sum of all components,

$$F_{\text{frk}} = F_{\text{frk},1} + F_{\text{frk},2} + F_{\text{frk},3} + F_{\text{frk},4a} + F_{\text{frk},4b} \quad (3.87)$$

with the result being positive if the suspension force tends to extend the fork and negative if it tends to compress it. The fork force is applied between the lower and upper parts of the front assembly as an action-reaction pair, see Fig. 3.11. Its projection on the generalized coordinates according to Eq. 3.77 is straightforward as the force is applied in the same direction of d_f .

$$\mathbf{Q}_{\text{frk}}^e = \begin{bmatrix} \mathbf{0}^{7 \times 1} \\ 1 \\ \mathbf{0}^{3 \times 1} \end{bmatrix} F_{\text{frk}} \quad (3.88)$$

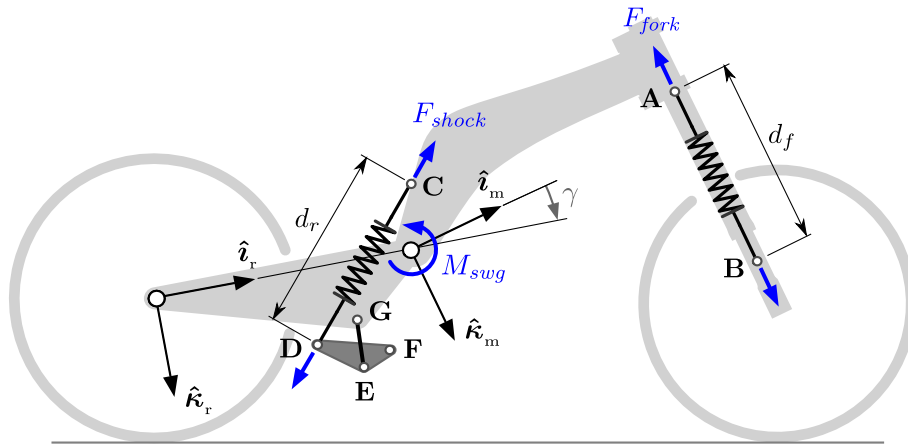


Figure 3.11: Suspension forces. The fork force is directly applied between the upper and lower parts of the front assembly. The rear suspension, on the other hand, is more complex due to the geometry of the monoshock arrangement. This system is characterized by having only one shock absorber, generally mounted between the frame and the swingarm through a four-bar linkage. The link point **F** is usually connected to the frame or to the engine, not depicted in the figure for the sake of clarity.

Rear suspension

A monoshock arrangement is employed for the rear suspension as shown in Fig. 3.11. This system is characterized by having only one shock absorber, generally mounted between the frame and the swingarm through a four-bar linkage. The linkage is designed to make the suspension progressive, which has two advantages over direct systems [13]: first, it improves the riding comfort as the suspension responds softly to the small disturbances of the road and, in second place, it allows to keep the frequencies of the in-plane modes approximately constant when the load is increased by the second passenger or by the luggage.

It is important to note that the linkage introduces a closed kinematic loop in the model. Such mechanism may be modelled online, by considering all the bodies and joints, or offline, by a map that projects the force of the shock absorber onto an equivalent moment applied to the swingarm. The second solution is computationally faster as the kinematic loop does not need to be solved at each time step. Furthermore, it allows to keep the model equations as a system of ODEs, which is an important requirement for the development of the rider control system. The main drawback of this approach is that the bodies composing the linkage and the shock cannot be included in the model and hence their mass must be distributed between the frame and swingarm. This however does not represent a very restrictive limitation as the neglected elements are very light compared to the frame and the swingarm-wheel assemblies. The derivation of the

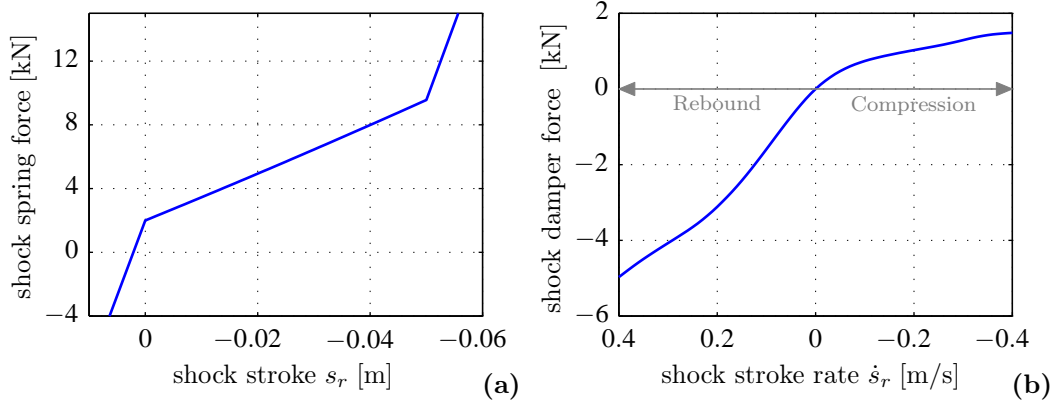


Figure 3.12: Rear shock properties. (a) Elastic force. The spring of the shock absorber is usually linear; it is the linkage that makes the rear suspension progressive. Bump and rebound stops limit the course of the suspension. (b) Damping force. As with the fork, the damping force in rebound is in general higher than in compression.

geometric equations for a pro-link suspension can be found in [51], where an analytical expression g is defined to compute the stroke of the shock absorber s_r as a function of the swingarm angle γ .

$$s_r(t) = d_r(t) - l_{\text{shock}} = g(\gamma(t)) \quad (3.89)$$

As with Eq. 3.82, the term l_{shock} is simply a positive constant equal to the maximum length of the shock. The above equation may be used to find the stroke velocity as a function of the arm angular speed. By differentiating it with respect to time we obtain,

$$\dot{s}_r = \frac{\partial g}{\partial \gamma} \frac{d\gamma}{dt} = \eta \dot{\gamma} \quad (3.90)$$

where η represents the motion ratio of the rear suspension and is defined, for a given position of the system, as the ratio between an infinitesimal stroke variation and the resulting infinitesimal rotation of the swingarm. Once the stroke and its derivative are known, the force generated by the shock may be computed in the same way of the fork, i.e. by the addition of the elastic force of the spring, the air effect, the end-stroke stops and the damping curve.

The elastic and damping forces of the rear shock are depicted in Fig. 3.12. The total shock force is obtained by adding the elastic and damping components and is then transformed into an equivalent moment around the pivot by means of the virtual work principle. Let F_{shock} be the shock force and M_{swg} the equivalent torque applied to the swingarm, then by means of the principle of virtual work we can write

$$M_{\text{swg}} = \frac{\partial g}{\partial \gamma} F_{\text{shock}} = \eta F_{\text{shock}} \quad (3.91)$$

which allows to express the arm torque as a function of the shock force. Finally, the moment applied to the swingarm is projected on the generalized coordinates.

$$\mathbf{Q}_{\text{swg}}^e = \begin{bmatrix} \mathbf{0}^{5 \times 1} \\ -1 \\ \mathbf{0}^{2 \times 1} \\ 1 \\ \mathbf{0}^{2 \times 1} \end{bmatrix} M_{\text{swg}} \quad (3.92)$$

This way of modelling the suspension has one additional advantage compared to the online approach as parametric studies can be performed in an intuitive way by simply modifying the motion ratio map instead of the hard-points of the mechanism.

Aerodynamic forces and moments

The aerodynamic effect is included in the model as a set of two forces (drag and lift) and one moment⁴ (pitch) applied at the centre of gravity of the main assembly \mathbf{G}_m and oriented according to the reference frame \mathbf{T}_1 . The x -axis of this frame lies on the mid-plane of the vehicle and is always parallel to the ground; its z -axis points downwards when the motorcycle is upright and forms an angle with the road normal equal to the roll angle ϕ in cornering conditions; finally, the y -axis is perpendicular to the other two axes and to the mid-plane of the vehicle. All forces have been assumed to be proportional to the square of the motorcycle velocity u ,

$$\begin{aligned} F_{ax} &= -1/2\rho c_x A u^2 \\ F_{az} &= -1/2\rho c_z A u^2 \\ M_{ay} &= -1/2\rho c_\mu A u^2 \end{aligned} \quad (3.93)$$

where ρ represents the density of the air, A is the area of the motorcycle cross section and c_x , c_z and c_μ are the drag, lift and pitch coefficients respectively. The drag force F_{ax} is strongly influenced by the shape of the motorcycle, especially by the presence or lack of fairings, and affects both the maximum attainable speed and the performance in acceleration. The lift force F_{az} , on the other hand, reduces the tyre loads and may become dangerous at high speeds. As a matter of fact, modern fairings are designed to reduce lift force to a minimum. Both effects produce a load variation at the tyres, which can modify significantly the dynamic response of the vehicle.

⁴This moment arises from the fact that the pressure centre is not coincident with \mathbf{G}_m .

The aerodynamic forces introduced in Eq. 3.93 may be projected along the generalized coordinates by using Eq. 3.77.

$$\mathbf{Q}_a^e = \begin{bmatrix} 1 & 0 & 0 \\ 0 & -s_\phi & 0 \\ 0 & 1 & 0 \\ zs_\phi & 0 & s_\phi \\ 0 & 0 & 0 \\ 0 & 0 & 1 \\ \mathbf{0}^{5 \times 1} & \mathbf{0}^{5 \times 1} & \mathbf{0}^{5 \times 1} \end{bmatrix} \begin{bmatrix} F_{ax} \\ F_{az} \\ M_{ay} \end{bmatrix} \quad (3.94)$$

Tyre forces and moments

The tyre model presented by Sharp in [51] is used in the present work to evaluate the forces and moments that characterize motorcycle tyres⁵. The underlying equations, which are based on Pacejka's Magic Formula [12], have been implemented symbolically in a Maple routine and the resulting code has been coupled with the motorcycle model. The accuracy of Pacejka's approach is considered appropriate for the handling simulations needed to assess the behaviour of the virtual rider.

The inputs of the tyre model are the normal load F_z , the camber angle ϕ , the longitudinal slip κ and the sideslip angle λ . All of them may be calculated from the tyre kinematics and expressed as functions of the generalized coordinates as discussed in Section 3.3.1.

The outputs of the tyre model, on the other hand, comprise three forces and three moments. The most relevant components are depicted in Fig. 3.13 for a reference tyre. They are expressed according to the modified SAE convention, which is explained in Fig. 3.14. Note that the tyre forces and moments are applied at the centre of the contact patch. All of them are computed from Pacejka's Magic Formula except the normal load, the value of which is proportional to the carcass deformation ξ and its derivative $\dot{\xi}$,

$$F_z = -k_z \xi - c_z \dot{\xi} \quad (3.95)$$

where k_z is the vertical stiffness of the tyre and c_z represents its damping coefficient.

Figs. a) to c) depict the pure slip case, defined as the situation when either longitudinal slip or lateral sideslip occur in isolation. The remaining graphs, d) to f), depict the combined slip case, where the tyre is simultaneously subject to both longitudinal and sideslip inputs.

⁵To increase the oversteering character of the vehicle, the front cornering stiffness has been increased by +15% with respect to Sharp's data, whereas the rear has been decreased by the same amount.

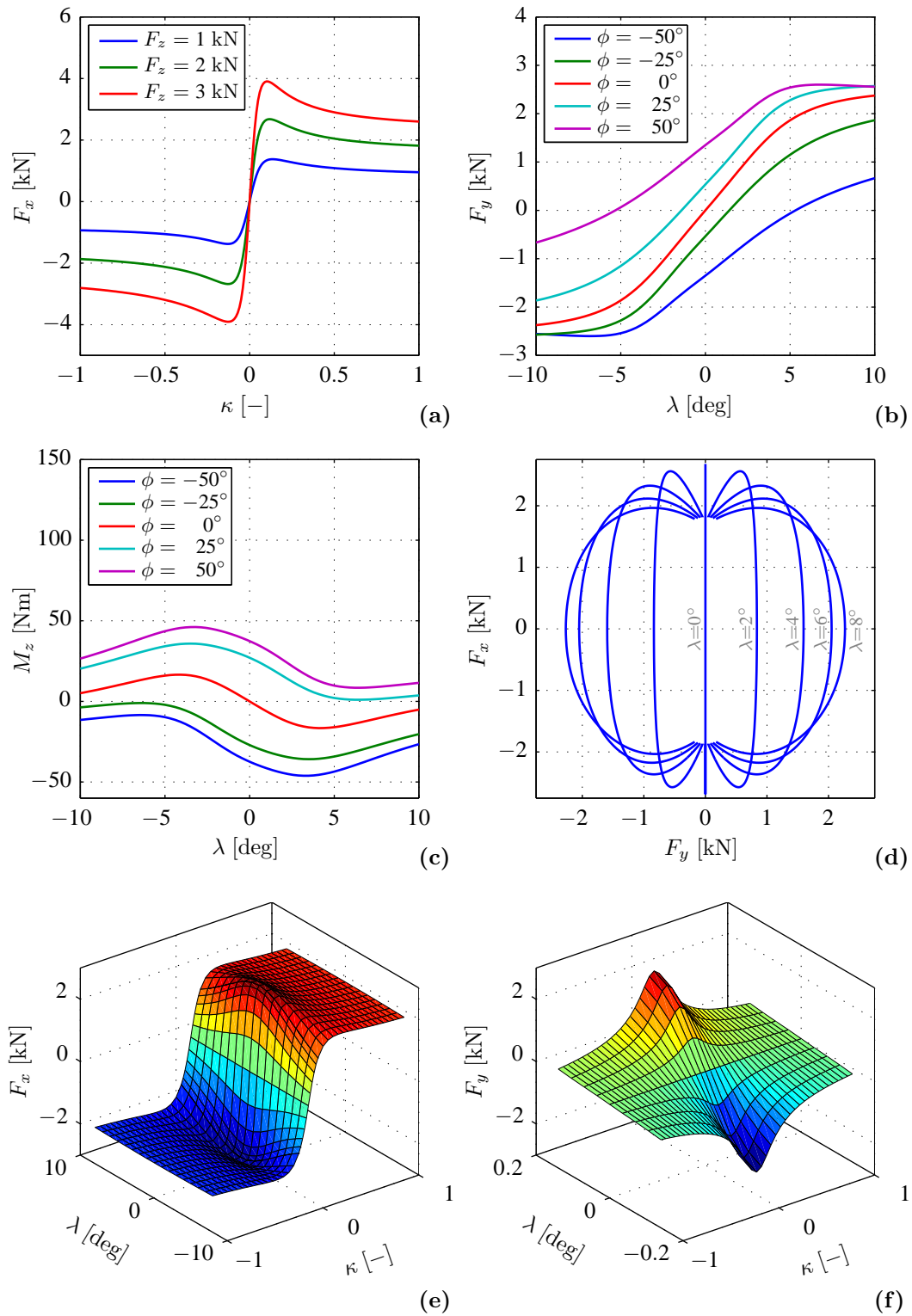


Figure 3.13: Pacejka forces for a 180/55ZR17 rear tyre. (a) Pure longitudinal force. (b) Pure lateral force. (c) Aligning/twisting moment. (d) Friction ellipse. (e) Combined longitudinal force. (f) Combined lateral force. A vertical load of 2000N has been used in all figures with the exception of (a).

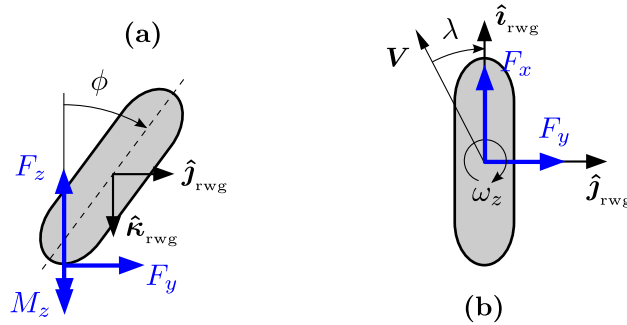


Figure 3.14: Sign conventions for tyre forces and moments based on the modified SAE frame [12]. In this reference frame the x and y axes lie on the road plane whereas the z-axis points downwards. (a) Rear view. (b) Top view.

The longitudinal force F_x is depicted in Fig. 3.13a as a function of the slip ratio for several values of the vertical load. We can divide the curve in three different regions; for small slip values the force is linear with respect to the slip, then the curve presents a peak where the maximum force occurs and finally the longitudinal force saturates as the slip increases. Average riders usually work within the first region.

The lateral force F_y is represented in Fig. 3.13b as a function of the sideslip angle for five different values of the camber angle. We can observe how the response of the tyre is linear at the origin and then progressively saturates, only showing a peak at very high camber angles. Motorcycle tyres can generate lateral force by two different mechanisms, namely sideslip and camber thrust [13]. The red curve shows the effect of pure sideslip variations ($\phi=0$), while the effect of pure camber variations can be observed by comparing the origin of all five curves ($\lambda=0$). Unlike car tyres, which build up lateral force mainly through sideslip, in motorcycle tyres the dominant mechanism is the camber thrust.

Fig. 3.13c shows the aligning/twisting moment M_z . This torque results from the addition of two different effects, one that tends to align the tyre with the direction of travel (self-aligning) and another that has the opposite effect (twisting). The aligning moment has its origin in the asymmetric distribution of the shear stress along the longitudinal direction of the contact patch. Such bias in the stress distribution shifts the lateral force rearwards with respect to the centre of the contact patch, which in turn translates into an aligning moment. The twisting moment, on the other hand, arises when the motorcycle is cambered due to an asymmetrical distribution of the shear stress in the lateral direction of the contact patch. In the most external area of the patch, the peripheral velocity of the tyre is greater than the forward velocity, thus leading to positive longitudinal slip. The opposite happens in the interior area, which undergoes negative slip. As a result, the shear stress pushes the tyre forward in the external area

and backward in the interior, thus generating a torque that tends to rotate the tyre towards the centre of the corner.

The aligning effect dominates at low roll angles while the twisting effect becomes more important as the roll angle increases. Let's use a right corner to explain Fig. 3.13c. According to the SAE reference system, a right corner implies positive values of the sideslip and roll angles. In this situation M_z is negative (aligning) for small roll angles and increases rapidly with the roll angle, becoming positive (twisting).

Figs. d) to f) depict the combined slip case. This condition is characterized by the reduction of lateral force due to longitudinal slip and vice versa, i.e. by the reduction of longitudinal force due to sideslipping. Pacejka's tyre model includes a series of *loss functions* to account for this phenomenon, which shape the friction ellipse shown in Fig. 3.13d. Each line in the graph is obtained by varying the longitudinal slip for a given value of the sideslip. It can be observed that all lines converge towards two points with null lateral force and a constant value of longitudinal force. As the longitudinal slip increases, the longitudinal force saturates and the capability of the tyre to generate lateral force tends to zero.

The saturation of the tyres is also appreciated in Fig. 3.13e, where the maximum longitudinal force F_x is obtained with no sideslip, and especially in Fig. 3.13f, where the lateral force F_y tends to zero for high values of the longitudinal slip κ .

The last step in the definition the tyre element is to project the resulting forces on the generalized coordinates. This is done in two steps. First the tyre forces and moments at the contact patch are transformed into an equivalent set of forces applied at the wheel hub. To simplify the projection, this new set of forces and moments is expressed in the body reference frames \mathbf{T}_f and \mathbf{T}_r for the front and rear tyres respectively. The resulting forces and moments are then projected on the generalized coordinates by using Eq. 3.77. The result is not shown here due to its size. We can express it in compact form as

$$\mathbf{Q}_{fw}^e = \mathbf{J}_{fw} [F_{xf} \ F_{yf} \ F_{zf} \ M_{xf} \ M_{yf} \ M_{zf}]^T \quad (3.96)$$

$$\mathbf{Q}_{rw}^e = \mathbf{J}_{rw} [F_{xr} \ F_{yr} \ F_{zr} \ M_{xr} \ M_{yr} \ M_{zr}]^T \quad (3.97)$$

where \mathbf{J}_{fw} and \mathbf{J}_{rw} are the Jacobian matrices that project the tyre forces of the front and rear tyres onto the vector of generalized forces.

Control inputs

The forces and torques used by the rider to control the motorcycle are described in this section. Average human riders generally use the brakes and the throttle for the longitudinal control of the bike, while the lateral dynamics are mainly controlled through

the steering system. Racing riders, on the other hand, take advantage of the coupling between longitudinal and lateral dynamics to fully exploit the performance of the vehicle. In order to simulate the control actions that human riders exert on the motorcycle, the model presented in this thesis comprises four independent control elements: the braking torques applied to the front and rear wheels, denoted as M_{fw} and M_{rw} , the chain force F_{ch} and the steering torque τ .

In the virtual world, this set of forces and torques represents the interface between the motorcycle equations and the rider model, i.e. the outputs of the rider constitute the inputs of the motorcycle and vice versa. This means that, unlike the force elements introduced so far, the generalized forces associated to the rider are not entirely evaluated within the motorcycle equations. Their values are actually determined, at every integration step, by the rider model, which then feeds them back to the motorcycle in order to close the control loop.

Both the braking and the steering torques are directly applied to the corresponding degrees of freedom of the model, and therefore their projection on the generalized coordinates is straightforward. This direct projection is represented by the unit values in the first three columns of Eq. 3.98, which correspond to the front, rear and steering torques respectively. The term $b_\delta \dot{\delta}$ in the third column models the rotational steering damper.

$$\mathbf{Q}_u^e = \begin{bmatrix} \mathbf{0}^{5 \times 1} & \mathbf{0}^{5 \times 1} & \mathbf{0}^{5 \times 1} & \mathbf{0}^{5 \times 1} \\ 0 & 0 & 0 & l_r s_\alpha + R \\ 0 & 0 & 1 - b_\delta \dot{\delta} & 0 \\ 0 & 0 & 0 & 0 \\ 0 & 0 & 0 & -l_r s_\alpha - R \\ 0 & 1 & 0 & -R \\ 1 & 0 & 0 & 0 \end{bmatrix} \begin{bmatrix} M_{fw} \\ M_{rw} \\ \tau \\ F_{ch} \end{bmatrix} \quad (3.98)$$

On the other hand, the projection of the chain force on the generalized coordinates requires some additional steps. The chain transmits the engine power from the drive sprocket to the rear wheel and influences considerably the load distribution during acceleration and braking, thus reducing or increasing the rear force available for traction. It is therefore important to consider its effect on the vehicle model. As a matter of fact, it would not be realistic to represent the engine as a simple torque applied on the rear wheel as doing so would introduce significant errors, especially under high acceleration.

The projection of the chain force on the generalized coordinates comes down to finding the angle α between the chain and the swinging arm. This geometric problem, depicted schematically in Fig. 3.15, presents a closed solution that can be easily derived from the auxiliary angles α_1 and α_2 . The first of them is defined as the angle between

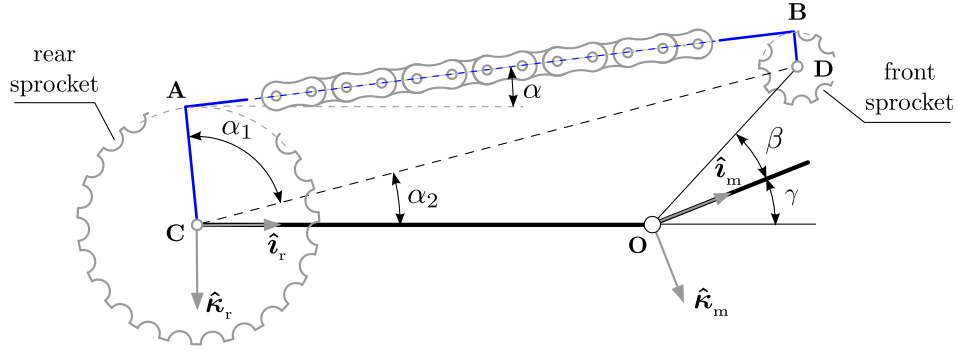


Figure 3.15: Schematic of the chain model. The chain transmits the engine power from the drive sprocket to the rear wheel. The geometry of the system formed by the arm, the chain and both sprockets have a big impact on the load distribution during acceleration and braking.

the vector normal to the chain and the line that connects the sprocket centres, i.e. the angle enclosed between the lines AC and CD ,

$$\alpha_1 = \widehat{ACD} = \arccos\left(\frac{R-r}{CD}\right) \quad (3.99)$$

where r and R are the radii of the front and rear sprockets respectively. The second angle, on the contrary, measures the orientation of the line CD with respect to the swingarm, depicted in the Figure by the line CO .

$$\alpha_2 = \widehat{DCO} = \arctan\left(\frac{\overline{OD} \sin(\beta - \gamma)}{\overline{CO} + \overline{OD} \cos(\beta - \gamma)}\right) \quad (3.100)$$

Finally, the expression of the chain angle may be computed as follows:

$$\alpha = \alpha_1 + \alpha_2 - \frac{\pi}{2} \quad (3.101)$$

The projection of the chain force along the direction of the generalized coordinates depends solely on α and is represented by the fourth column of Eq. 3.98. The non-zero terms correspond to the following generalized coordinates: the chassis pitch, the swingarm pitch and the rear wheel rotation respectively.

To conclude this section regarding the force and control elements, we derive the global vector of generalized forces \mathbf{Q}^e by adding the contribution of all the external forces applied to the model, i.e. front and rear suspensions, aerodynamics, tyre forces and control inputs.

$$\mathbf{Q}^e = \sum_j \mathbf{Q}_j^e = \mathbf{Q}_{\text{frk}}^e + \mathbf{Q}_{\text{swg}}^e + \mathbf{Q}_a^e + \mathbf{Q}_{\text{fw}}^e + \mathbf{Q}_{\text{rw}}^e + \mathbf{Q}_u^e \quad (3.102)$$

3.3.3 Equations of Motion

The dynamic equations of the motorcycle model are derived in this section, which is structured in four parts. The first three introduce the multibody dynamic equations of the vehicle, the tyre relaxation model and the track equations respectively. In the fourth, the precedent elements are coupled to build the full model in state space form.

Motorcycle equations

We now derive the dynamic equations of the motorcycle model by using the Lagrange approach. In consequence, the equations of motion will be obtained from Eq. 3.34, which is repeated below for convenience.

$$\frac{d}{dt} \left(\frac{\partial L}{\partial \dot{q}_k} \right) - \frac{\partial L}{\partial q_k} = Q_k, \quad (k=1 \dots f)$$

In the above expression the Lagrangian L is defined as $L = T - U$, where T is the kinetic energy of the motorcycle and U is its potential energy. All the steps described in section 3.2.3 to derive the equations of motion for multibody systems have been implemented in the computer algebra software Maple[®] [45]. Symbolic software allows to derive the equations of motion for large systems in a fashion similar to hand derivation; obtaining first the model equations which are then compiled in order to produce highly efficient simulation programs. The details of the resulting motorcycle equations are not shown here due to their size; it is possible however to include them in their compact form,

$$\hat{\mathbf{M}}(\mathbf{q})\ddot{\mathbf{q}} = \hat{\mathbf{Q}}(\mathbf{q}, \dot{\mathbf{q}}, \mathbf{p}_\lambda, \mathbf{u}) \quad (3.103)$$

where \mathbf{q} is the vector of generalized coordinates, \mathbf{u} is the vector of control inputs, $\hat{\mathbf{M}}$ is the inertia matrix of the system and $\hat{\mathbf{Q}}$ includes the gyroscopic, Coriolis and centrifugal forces along with the vector of generalized applied forces defined in Eq. 3.102. The vector \mathbf{p}_λ , on the other hand, comprises the tyre states, which are described in the next section dedicated to tyre dynamics. We can project these equations on the vehicle frame \mathbf{T}_ψ through the transformation matrix $\mathbf{\Gamma}$ introduced in Eq. 3.39.

$$\mathbf{\Gamma}\hat{\mathbf{M}}(\mathbf{q})\ddot{\mathbf{q}} = \mathbf{\Gamma}\hat{\mathbf{Q}}(\mathbf{q}, \dot{\mathbf{q}}, \mathbf{p}_\lambda, \mathbf{u}) \quad (3.104)$$

In order to fully convert the dynamic equations to the vehicle frame, we also need to transform the velocity of the vehicle from Cartesian coordinates (\dot{x}, \dot{y}) to body coordinates (u, v) , i.e.

$$\begin{bmatrix} \dot{x} \\ \dot{y} \end{bmatrix} = \mathbf{S}_\psi \begin{bmatrix} u \\ v \end{bmatrix} \quad (3.105)$$

which can be written in function of the transformation matrix $\mathbf{\Gamma}$ and the vector of generalized velocities \mathbf{q}_v .

$$\dot{\mathbf{q}} = \mathbf{\Gamma}^{-1} \mathbf{q}_v \quad (3.106)$$

The same needs to be done with the accelerations (\ddot{x}, \ddot{y}) , i.e.

$$\begin{bmatrix} \ddot{x} \\ \ddot{y} \end{bmatrix} = \mathbf{S}_\psi \begin{bmatrix} \dot{u} \\ \dot{v} \end{bmatrix} + \dot{\mathbf{S}}_\psi \begin{bmatrix} u \\ v \end{bmatrix} = \mathbf{S}_\psi \begin{bmatrix} \dot{u} - \dot{\psi}v \\ \dot{v} + \dot{\psi}u \end{bmatrix} \quad (3.107)$$

which can also be expressed in function of $\mathbf{\Gamma}$ and \mathbf{q}_v .

$$\ddot{\mathbf{q}} = \dot{\mathbf{\Gamma}}^{-1} \mathbf{q}_v + \mathbf{\Gamma}^{-1} \dot{\mathbf{q}}_v \quad (3.108)$$

By substituting Eqs. 3.106 and 3.108 into Eq. 3.104, we obtain the desired system of first-order differential equations expressed in the vehicle frame \mathbf{T}_ψ ,

$$\frac{d}{dt} \begin{bmatrix} \mathbf{q}_v \\ \mathbf{q}_p \end{bmatrix} = \begin{bmatrix} \mathcal{M}^{-1}(\mathbf{q}_p) \mathbf{Q}(\mathbf{q}_v, \mathbf{q}_p, \mathbf{p}_\lambda, \mathbf{u}) \\ \mathbf{A}_p \mathbf{q}_v \end{bmatrix} \quad (3.109)$$

with $\mathcal{M} = \mathbf{\Gamma} \hat{\mathbf{M}} \mathbf{\Gamma}^{-1}$ and $\mathbf{Q} = \mathbf{\Gamma} \hat{\mathbf{Q}} - \mathbf{\Gamma} \hat{\mathbf{M}} \dot{\mathbf{\Gamma}}^{-1} \mathbf{q}_v$. Not all the generalized coordinates appear in the Lagrangian. In particular, the Cartesian coordinates (x, y) , the yaw angle ψ , and the tyre rotation angles θ_{fw} and θ_{rw} are not present at position level. These coordinates are known as *cyclic* or *ignorable* coordinates [144] and their presence is associated with the existence of symmetries in the system; e.g. wheel angles are cyclic because the wheels are axially symmetric and their center of mass lies along their rotation axis. The matrix \mathbf{A}_p projects the generalized velocities \mathbf{q}_v onto a new set of velocities $\dot{\mathbf{q}}_p$, with

$$\mathbf{q}_p = [z, \phi, \mu, \delta, d_f, \mu_r]^T \quad (3.110)$$

not including any cyclic coordinates. This projection reduces the number of system states and also avoids the integration of the vehicle speeds u and v , which would lack of physical meaning as they are expressed in the body frame.

Tyre Dynamics

It is a well known fact that tyre forces do not originate instantaneously [12], they need a certain time to build up, which depends on the carcass stiffness and damping characteristics of the tyre. To illustrate the dynamic response of the tyres, let's suppose that the motorcycle is initially running in straight line. In these conditions the roll and sideslip angles are zero and, in consequence, so are the lateral forces at the contact patch. If we

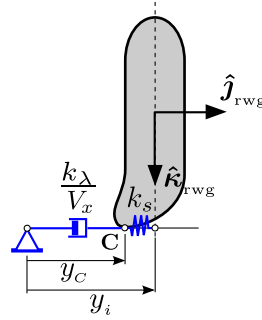


Figure 3.16: Scheme of the lateral relaxation model of the tyre.

instantaneously change the attitude of the tyre, the lateral force will increase gradually from zero to the steady state value corresponding to the assigned sideslip and roll angles. In other words, the contact forces will follow, with a delay, the variation of the angles on which they depend. Measurements also show that the component due to camber has a smaller lag than that due to sideslip.

This transient behaviour of the tyre in the lateral direction can be represented by the first order model of Figure. 3.16, which is composed of a contact point **C** that is suspended with respect to the wheel by a lateral spring and a damper connected in series. The contact point may move (slip) with respect to the tyre in the lateral direction, thus exciting the spring and damper elements. The spring represents the lateral compliance of the tyre and depends mainly on the characteristics of the carcass while the damper models the response of the tyre to lateral slip.

As the spring and the damper are in series, the cornering force due to sideslip must be equal to the elastic force generated by the elastic deformation of the tyre if the carcass inertia is neglected, i.e.

$$\frac{k_\lambda}{V_x} \dot{y}_C = -k_s (y_C - y_i) \quad (3.111)$$

where y_C represents the lateral displacement of the contact point, y_i is the displacement imposed on the tyre and V_x is the longitudinal component of the contact patch velocity. If we introduce the definition of the (linear) sideslip angle in the above expression, after some manipulation we can write

$$\frac{\sigma_y}{V_x} \frac{d\lambda}{dt} = \lambda_{ss} - \lambda \quad (3.112)$$

which defines the tyre dynamics in terms of the transient sideslip λ and its steady-state counterpart λ_{ss} previously defined in Eq. 3.73, where the subscript ss was omitted for simplicity. The term $\sigma_y = k_\lambda/k_s$ is known as the relaxation length and determines

transient behaviour of the tyre as it represents the space that the wheel has to travel in order for the lateral force to reach a 63% of the steady-state value. This follows from the fact that Eq. 3.112 corresponds to a first order filter with time constant $\tau = \sigma_y/V_x$.

The transient sideslip angles of the front and rear tyres constitute two first order states that must be integrated along with the motorcycle equations. At each simulation step, the current value of the transient sideslips, λ_f and λ_r , will be passed to the tyre model in order to calculate the tyre forces. We can collect these two states in the following vector equation:

$$\frac{d}{dt} \begin{bmatrix} \lambda_f \\ \lambda_r \end{bmatrix} = \begin{bmatrix} f_{\lambda_f}(\lambda_f, \mathbf{q}_v, \mathbf{q}_p) \\ f_{\lambda_r}(\lambda_r, \mathbf{q}_v, \mathbf{q}_p) \end{bmatrix} \quad (3.113)$$

Note that the vehicle states, \mathbf{q}_v and \mathbf{q}_p , are present in the right hand side of the equation as they appear in the definition of the steady-state sideslip λ_{ss} . It is more convenient to express this equation in compact form,

$$\dot{\mathbf{p}}_\lambda = \mathbf{f}_\lambda(\mathbf{p}_\lambda, \mathbf{q}_v, \mathbf{q}_p) \quad (3.114)$$

with \mathbf{p}_λ being the vector of tyre states.

The effect of the relaxation length on the camber thrust is almost negligible [13] and therefore is not included in the present model. This assumption implies that forces and moments arising from wheel camber occur without delay, while those arising from sideslip are lagged. The same considerations are made by Sharp in [51], who considers it the most physically accurate approach since camber builds up the lateral forces geometrically whereas sideslip leads to forces through a distortion of the tyre carcass, which requires time to develop. As in Sharp's model, the longitudinal slip is also assumed to be instantaneous. A detailed relaxation model in the longitudinal direction would become necessary, for instance, to capture high-frequency phenomena like the so-called chatter [148], typical of the racing machines, which is out of the scope of this thesis.

Track Coordinates

Road vehicles typically travel along a path (e.g. a road, a track, etc), which makes it convenient to describe their motion by means of curvilinear coordinates rather than the usual Cartesian parameterization employed to derive the equations of motion. The shape of the path, slender along its main dimension and narrow across it, makes the curvilinear coordinates a natural choice for the simulation of road vehicles [94, 97].

This new set of coordinates comprises three elements as shown in Fig. 3.17: the longitudinal coordinate s , which defines the position of the vehicle along the track; the

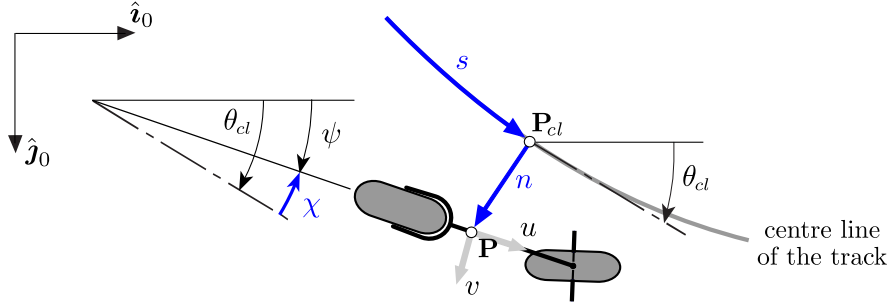


Figure 3.17: Definition of curvilinear coordinates.

lateral coordinate n , which represents the transverse displacement of the vehicle with respect to the track centre line; and the angle χ , that represents the orientation of the vehicle, also with respect to the track centre line. In order to fully exploit these coordinates, it is convenient to parameterize the road by its arc-length s and its local curvature κ .

Thus, the coordinates of the reference point of the motorcycle \mathbf{P} can be defined with respect to the track by taking the nearest point of the centre line \mathbf{P}_{cl} as a reference, that is

$$\begin{bmatrix} x \\ y \end{bmatrix} = \begin{bmatrix} x_{cl} \\ y_{cl} \end{bmatrix} + \begin{bmatrix} -ns\theta_{cl} \\ nc\theta_{cl} \end{bmatrix} \quad (3.115)$$

where the pair (x, y) represents the planar coordinates of \mathbf{P} , the pair (x_{cl}, y_{cl}) are the coordinates of \mathbf{P}_{cl} and θ_{cl} is the orientation of the track centre line with respect to the global x -axis. By differentiating Eq. 3.115 with respect to time, we get

$$\mathbf{S}_\psi \begin{bmatrix} u \\ v \end{bmatrix} = \mathbf{S}_{\theta_{cl}} \begin{bmatrix} \dot{s} - \dot{\theta}_{cl}n \\ \dot{n} \end{bmatrix} \quad (3.116)$$

where \mathbf{S}_ψ and $\mathbf{S}_{\theta_{cl}}$ are 2×2 rotation matrices associated to the vehicle frame and to the track centerline respectively. Then, by expanding these matrices and replacing $\dot{\theta}_{cl}$ by $\kappa\dot{s}$, we can write

$$\begin{bmatrix} c_\psi & -s_\psi \\ s_\psi & c_\psi \end{bmatrix} \begin{bmatrix} u \\ v \end{bmatrix} = \begin{bmatrix} c_{\theta_{cl}} & -s_{\theta_{cl}} \\ s_{\theta_{cl}} & c_{\theta_{cl}} \end{bmatrix} \begin{bmatrix} (1 - n\kappa)\dot{s} \\ \dot{n} \end{bmatrix} \quad (3.117)$$

which allows to derive the following explicit expression for the derivatives of the curvilinear coordinates s and n ,

$$\begin{aligned} \dot{s} &= \frac{uc_\chi - vs_\chi}{1 - n\kappa} \\ \dot{n} &= us_\chi + vc_\chi \end{aligned} \quad (3.118)$$

with

$$\chi = \psi - \theta_{cl} \quad (3.119)$$

i.e. the relative angle of the vehicle with respect to the track χ is equal to the difference between the yaw angle ψ and the angle of the track centre line θ_{cl} .

We need one more differential equation to fully determine the curvilinear coordinates from the vehicle states. This last equation can be obtained by differentiating Eq. 3.119 with respect to time, which yields:

$$\dot{\chi} = \dot{\psi} - \dot{\theta}_{cl} = \dot{\psi} - \kappa \dot{s} = \dot{\psi} - \kappa \frac{uc_{\chi} - vs_{\chi}}{1 - n\kappa} \quad (3.120)$$

The curvilinear coordinates constitute a set of three first order equations. As opposed to the tyre slips, the motorcycle equations do not depend on the curvilinear coordinates and therefore they can be considered mere kinematic outputs of the system, which means that they could be obtained offline in a postprocessing stage. However, in this thesis we need to integrate Eqs. 3.118 and 3.120 along with the motorcycle equations as the rider model will make use of the curvilinear coordinates during the simulation. We can collect them in the following vector equation,

$$\frac{d}{dt} \begin{bmatrix} s \\ n \\ \chi \end{bmatrix} = \begin{bmatrix} \frac{uc_{\chi} - vs_{\chi}}{1 - n\kappa} \\ us_{\chi} + vc_{\chi} \\ \dot{\psi} - \kappa \frac{uc_{\chi} - vs_{\chi}}{1 - n\kappa} \end{bmatrix} \quad (3.121)$$

which can be expressed in compact form as

$$\dot{\mathbf{p}}_t = \mathbf{f}_t(\mathbf{p}_t, \mathbf{q}_v, \mathbf{q}_p) \quad (3.122)$$

Global equations in state space form

The global equations of the motorcycle model, including tyre dynamics and track coordinates, are obtained in by coupling Eqs. 3.109, 3.114 and 3.122. This yields a system of first-order differential equations known as the nonlinear state-space representation of the model.

$$\frac{d}{dt} \begin{bmatrix} \mathbf{q}_v \\ \mathbf{q}_p \\ \mathbf{p}_{\lambda} \\ \mathbf{p}_t \end{bmatrix} = \begin{bmatrix} \mathcal{M}^{-1}(\mathbf{q}_p) \mathbf{Q}(\mathbf{q}_v, \mathbf{q}_p, \mathbf{p}_{\lambda}, \mathbf{u}) \\ \mathbf{A}_p \mathbf{q}_v \\ \mathbf{f}_{\lambda}(\mathbf{p}_{\lambda}, \mathbf{q}_v, \mathbf{q}_p) \\ \mathbf{f}_t(\mathbf{p}_t, \mathbf{q}_v, \mathbf{q}_p) \end{bmatrix} \quad (3.123)$$

In compact form, the model equations can be written as follows,

$$\begin{cases} \dot{\mathbf{x}} = \mathbf{f}(\mathbf{x}, \mathbf{u}) \\ \mathbf{y} = \mathbf{g}(\mathbf{x}, \mathbf{u}) \end{cases} \quad (3.124)$$

where \mathbf{f} represents the state equations, \mathbf{x} is the state vector and \mathbf{u} is the input vector.

$$\mathbf{x} = [\mathbf{q}_v \ \mathbf{q}_p \ \mathbf{p}_\lambda \ \mathbf{p}_t]^\top \quad \mathbf{u} = [M_{fw} \ M_{rw} \ \tau \ F_{ch}]^\top \quad (3.125)$$

The output function \mathbf{g} is needed to couple the motorcycle model with the virtual rider. The vector \mathbf{y} contains two elements, the transverse displacement of the motorcycle with respect to the track center line n and the curvilinear speed \dot{s} .

$$\mathbf{y} = [n \ \dot{s}]^\top \quad (3.126)$$

The target of the rider model developed in the successive chapters will be to minimize the error between the system outputs \mathbf{y} and a given reference imposed by the user \mathbf{y}_d .

The system presents a total of 22 states, 4 inputs and 2 outputs. In order to give an idea of its size, the number of operations required to evaluate one call to the state function \mathbf{f} is provided next.

Operation	Original Code	Optimized Code
Additions	4551	1342
Multiplications	8113	1465
Divisions	19	13
Function calls	1841	41
Assignments	785	174

Table 3.3: Number of operations needed to evaluate one call to \mathbf{f} .

The first column represents the original equations, while the second corresponds to the same system after performing a common subexpression optimization, i.e. an heuristic procedure that identifies, removes, and collects common subexpressions in the code. The Maple package `codegen[optimize]` [149] was used for this purpose. It is interesting to note how the code optimization greatly reduces the number of operations needed to evaluate the equations, thus improving the efficiency of the model. In particular, the most significant reduction is observed for the function calls. This is due to the fact that the optimization procedure replaces all the functions within the model (mainly trigonometric) by subexpressions which are evaluated just once per function call; e.g.

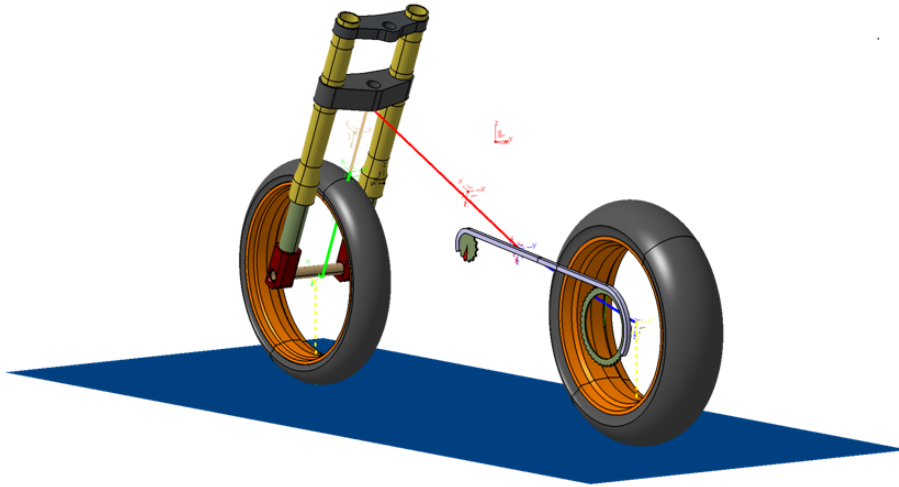


Figure 3.18: Reference multibody model developed in Virtual.Lab Motion.

all occurrences of $\sin(\phi)$ are replaced by $t1$, adding the statement $t1 = \sin(\phi)$ at the beginning of the code.

3.4 Model verification

A comparison between the symbolic motorcycle model defined in this chapter and an equivalent model developed within the commercial package Virtual.Lab Motion is presented in this section for verification purposes. The reference model, shown in Fig. 3.18, comprises 10 rigid bodies, including the chain and the linkage system, for a total of 60 dependent coordinates and 11 degrees of freedom. Both models possess exactly the same parameters. They correspond to a sports motorcycle; geometric and inertial properties come from [43] whereas the tyre model is parameterised according to [51].

Three different manoeuvres, designed to evaluate the longitudinal and lateral dynamics of the vehicle, are used to compare the models. Due to the intrinsic instability of motorcycles, all manoeuvres are performed in a closed-loop fashion by coupling the model to a virtual rider. The details of the rider algorithm are not relevant to understand the comparison and will be discussed in successive chapters.

3.4.1 Longitudinal dynamics

An acceleration test in straight line conditions is reported here with the purpose of comparing the in-plane behaviour of the models. The results are shown in Fig. 3.19, where the blue line represents the symbolic model and the red crosses correspond to the

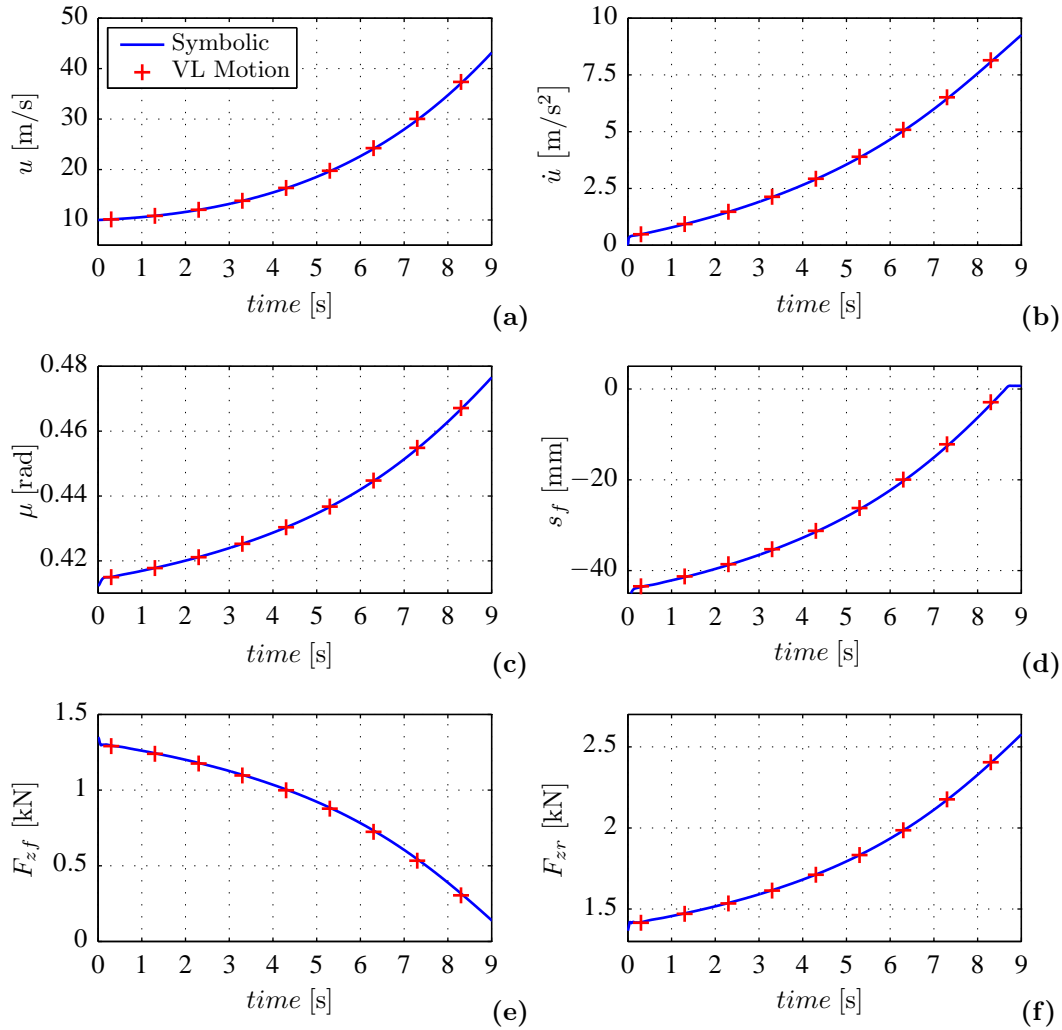


Figure 3.19: Comparison between the symbolic model and the reference model developed in Virtual.Lab Motion during an acceleration test in straight line. (a) Motorcycle speed. (b) Motorcycle acceleration. (c) Pitch angle of the main frame. (d) Front stroke. (e) Vertical load at the front tyre. (f) Vertical load at the rear tyre.

model developed in Virtual.Lab Motion. During the proposed manoeuvre, the motorcycle accelerates from 10 up to 44 m/s , reaching a maximum longitudinal acceleration of 9.3 m/s^2 .

The combined effect of the longitudinal acceleration of the vehicle, the aerodynamic drag and the chain force compresses the rear suspension and raises the front end. This is characterized by an increase in the pitch angle of the chassis μ and an extension of the fork s_f . It is worth pointing out that the fork stops extending at $t = 8.5s$ when the rebound limit is reached. This manoeuvre is also characterized by a big load transfer towards the rear tyre. In fact, at the end of the simulation the front wheel is nearly

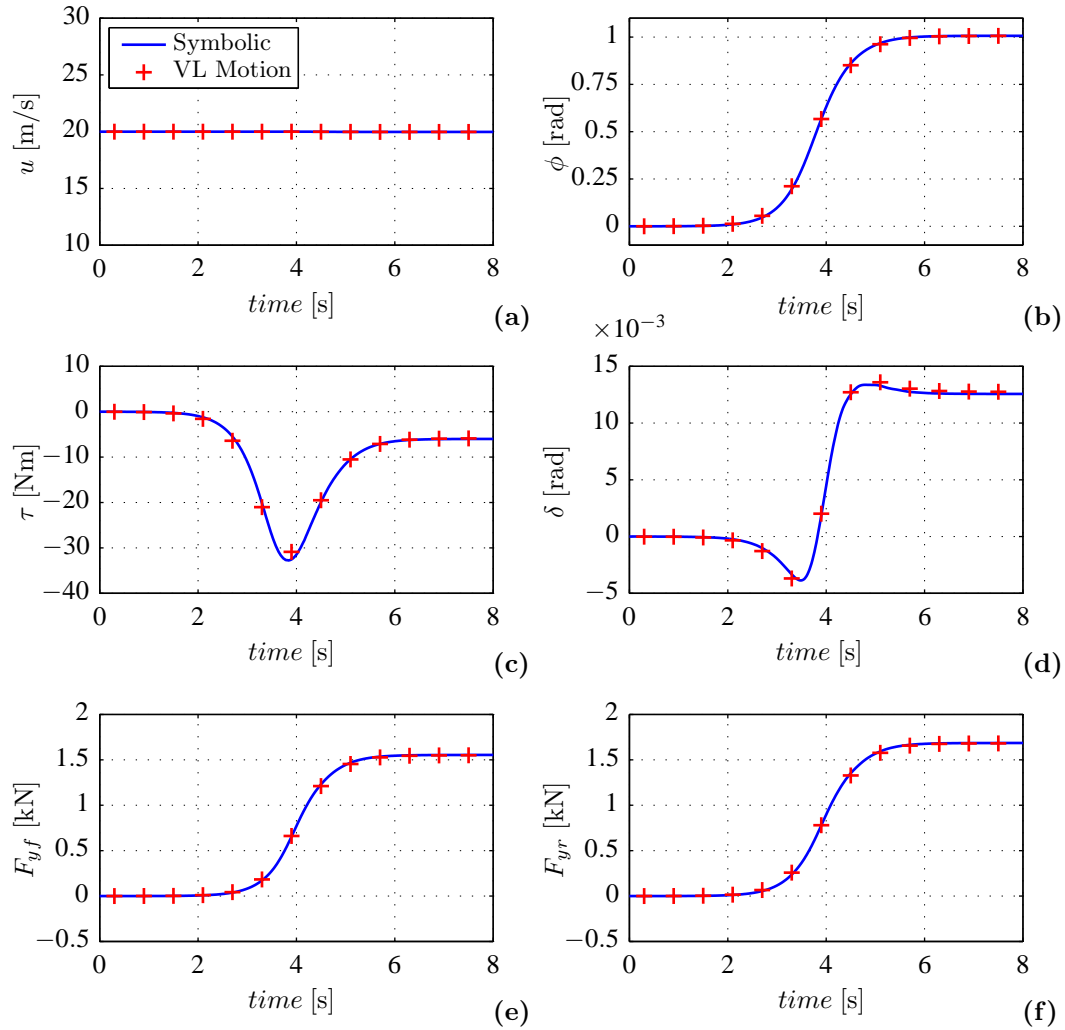


Figure 3.20: Comparison between the symbolic model and the reference model developed in Virtual.Lab Motion during a corner entry maneuver. (a) Motorcycle speed. (b) Roll angle. (c) Steering torque. (d) Steering angle. (e) Lateral force at the front tyre. (f) Lateral force at the rear tyre.

unloaded, $F_{zf} \approx 0$, while the rear load F_{zr} almost doubles its initial value.

A close agreement is observed between both models in terms of vehicle speed, longitudinal acceleration, chassis pitch angle, front stroke and tyre loads.

3.4.2 Lateral dynamics

Two maneuvers are reported next to compare the lateral response of the models. In particular, a corner entry and a slalom test, both performed at a constant speed of 20m/s .

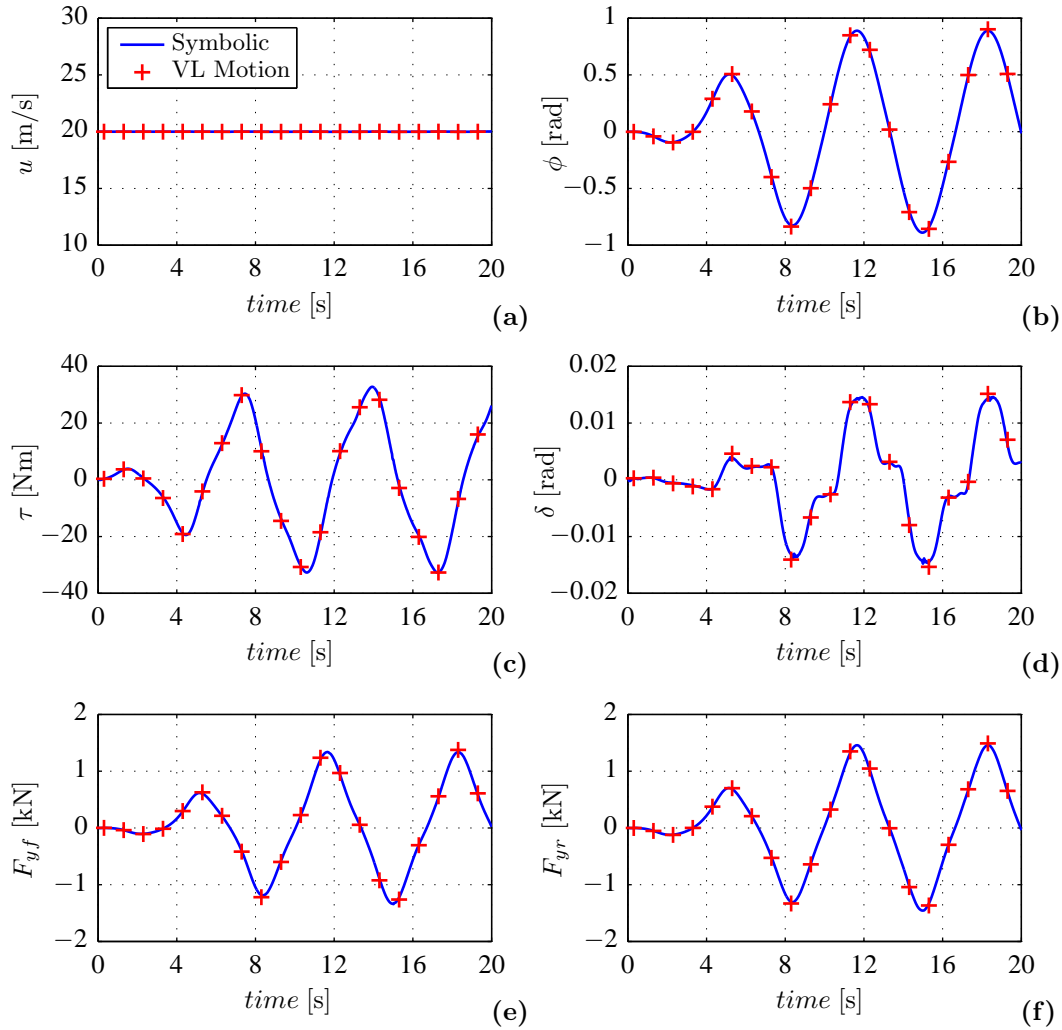


Figure 3.21: Comparison between the symbolic model and the reference model developed in Virtual.Lab Motion during a slalom test. (a) Motorcycle speed. (b) Roll angle. (c) Steering torque. (d) Steering angle. (e) Lateral force at the front tyre. (f) Lateral force at the rear tyre.

The corner entry is shown in Fig. 3.20; the motorcycle starts this maneuver running in straight line ($\phi = 0$) and then makes a right hand turn, reaching a stable steady state after a few seconds. The final state represents an aggressive corner, as shown by the extreme roll angle reached by the vehicle at the end of the simulation ($\phi > 55^\circ$) and by the large tyre forces. The roll motion initiates with a small rotation of the handlebar to the left side ($\delta < 0$); technique that is usually known as counter-steering since the rider steers in the opposite direction to the corner. This action generates a centrifugal force that leans the motorcycle to the right. Once the motorcycle is rolling, the rider turns the handlebar into the direction of the corner in order to make the vehicle follow

the desired line. Note that the steering torque is always negative during the maneuver, meaning that the rider prevents the handlebar from turning into the direction of the corner.

The results of the slalom test are depicted in Fig. 3.21. This maneuver is characterized by a series of cones that the rider must avoid alternately, i.e. leaving the first on the right, the second on the left and so on. The cones are usually positioned equidistantly, with the distance between cones being set to 62 m in this case. In order to execute the manoeuvre, the rider applies a periodic steering torque to the vehicle which in turn responds with a periodic motion. The roll angle reached by the vehicle during the slalom is also large, being the peak value over 50° .

As far as the lateral dynamics are concerned, a good match is observed between both models in terms of vehicle speed, roll angle, steering torque, steering angle and lateral tyre forces.

3.5 Concluding remarks

In this chapter we have introduced an eleven-degree-of-freedom vehicle model suitable for the simulation and control of motorcycle dynamics. The model includes the main bodies that compose any standard motorcycle, i.e.: the front and rear wheels, the main assembly (including the frame, the engine and the fuel tank), the rear assembly (including the swing arm and the rear brake calipers), the upper part of the fork assembly (including the sprung part of the fork, triple clamps, the steering column, and the handlebar), and the lower part of the fork assembly (including the unsprung part of the fork and the front brake calipers). Together with the multibody model, a series of subroutines and force elements have been developed in this chapter in order to calculate the suspension forces, the rear linkage kinematics, the chain effect, the aerodynamic map, and the tyre forces.

All the equations have been derived in a symbolic form, thus allowing a low-level control of the model throughout the development process: the model uses a combination of relative coordinates and track coordinates, which have been employed to describe the motion of the motorcycle along a given road; first order relaxation equations have been included to represent tyre dynamics; symbolic expressions have been derived for tyre kinematics, including the real cross-section of the carcass, etc. Furthermore, the equations of motion have been significantly simplified by exploiting algebraic manipulation, thus producing an efficient simulation code able to run in real-time. The resulting procedure has been subsequently exported to C and then compiled in Matlab, as an `S-function` and a `.mex` file, for the numerical evaluation of the equations. The

S-function implementation allows to fully exploit the capabilities of Matlab as the model can be coupled with any control algorithm developed in Simulink.

The equations of motion of the motorcycle model have been written as a system of first order ODEs, taking advantage that an analytical solution exists for the linkage of the rear suspension, which is the only closed-loop present in the system. As no constraint equations are included, this formulation provides a straightforward state space representation of the model, being perfectly suited for control system design and analysis. Another advantage offered by the chosen implementation is that a great variety of solvers are available to integrate the equations of motion.

In the final part of the chapter, a multibody model developed in the commercial software LMS Virtual.Lab Motion has been introduced. The model, which represents the same vehicle as the symbolic eleven-degrees-of-freedom motorcycle, has been employed as a validation tool. Both models have been simulated by means of in-plane and out-of-plane maneuvers, with the results showing a very good agreement.

The motorcycle model presented here will be used in the next chapters to build the virtual rider. It is in this process where the symbolic model will prove especially useful for research purposes as opposed to commercial programs such as ADAMS, Simpack, Virtual.Lab Motion, etc. In the next chapter, the model characteristics will be thoroughly exploited to solve the quasi-steady state motion of motorcycles in straight line and in cornering conditions.

*I'm not sure they understand
everything about racing cars.
I am not sure that this is wise.*

Jean Alesi

Chapter 4

A new methodology for the quasi-steady state analysis of motorcycles

The next two chapters introduce a new methodology for the quasi-steady state analysis of motorcycles in straight line and in cornering conditions. The approach presented here is based on the solution of the nonlinear algebraic equation system that arises from the dynamic model when the quasi-steady state conditions are imposed. The first part of the chapter describes the underlying assumptions of the proposed methodology and the details of its implementation. A continuation strategy to efficiently explore the quasi-steady state solutions of the motorcycle equations completes this section. The second part of the chapter includes an extensive analysis of the stationary equilibrium points as a function of the vehicle speed and the corner radius. Finally, a parametric study of the quasi-steady state motion of the motorcycle is performed and the results are discussed. The chapter is concluded with some remarks and conclusions regarding the application of the results to the development of the virtual rider.

4.1 Introduction

When a wheeled vehicle makes a turn, it normally goes through three phases. The first is the *transient corner entry*, for example after a straight section. In this phase the yaw

rate and the vehicle sideslip build up from zero in straight running until the stationary motion is reached in the mid section of the turn. The second phase is the *steady state corner*, where the vehicle moves along a circular path at constant speed. Most of the states that describe the motion of the vehicle, such as the yaw rate and the sideslip, remain constant in this part of the manoeuvre, and hence its name. The final phase of this process is the *transient corner exit*, where the yaw speed and the sideslip return to zero as the vehicle goes back to the straight running conditions.

The study of the steady state part of the cornering manoeuvre is widespread in the automotive literature, especially as far as four-wheeled vehicles are concerned [150, 151]. A simplified model with three degrees of freedom, known as the bicycle model, is usually employed for this purpose. This technique relies in the fact that the differential equations that characterize the response of the vehicle become algebraic if the radius of the corner and the speed of the vehicle are held constant. The resulting equations, which present an analytical solution for the linear bicycle model, allow to calculate all the states of the vehicle given its speed and the radius of the corner. The simplicity of this approach, which allows to investigate the directional stability of the vehicle without having to integrate the equations of motion, has led to the development of multiple metrics widely used to study vehicle handling such as the understeer coefficient and the handling diagram.

The study of more complex models requires, however, the use of multibody tools to represent the vehicle. A thorough analysis of the most popular multibody codes in the market, performed during the first stages of this thesis, revealed that none of them included the numerical tools needed to solve the steady state problem in a direct manner. Although most of the general-purpose packages currently available possess a built-in (static) equilibrium solver, this cannot be used to find the steady state configuration of the vehicle as it forces the system derivatives to be zero by definition. This means that the vehicle speed cannot be included in the solution and therefore only pure static problems can be solved.

The steady state equilibrium of multibody vehicle models is usually found by integrating the equations of motion until the desired condition is reached [40, 100]. This approach, which will be referred to as the indirect solution, has two significant drawbacks. Even though research in the field of numerical analysis has brought about efficient techniques for the numerical integration of multibody models, simulation times can be long. Moreover, if a dynamic solver is used to achieve a steady state solution, a controller is required to stabilize the vehicle around the desired condition. This process is slow and does not guarantee that all desired conditions (e.g. curvature and velocity) are accurately met at the same time. The above disadvantages are even more significant

when it comes down to motorcycles as they are intrinsically unstable, which makes it difficult to design a controller that is simultaneously fast, stable and steady state error free.

As an alternative to the indirect solution, Cossalter et al. presented in [39] an algebraic method to solve the steady state motion of a multibody motorcycle model. The scope of their work, based on a six degree-of-freedom model with no suspensions, was to study the steering torque in stationary conditions and its sensitivity to speed, curvature and several design parameters. The equations of the model were directly obtained in a steady state form and included only the stationary terms, i.e. those that do not vanish when the motorcycle runs along a circular path at constant speed. In addition, to further simplify the problem, they linearized the pitch equation and used the roll and the steering angles as the independent variables of the problem. Such selection of variables allowed them to precompute the kinematics of the motorcycle at position level, thus reducing the equilibrium problem to solving the curvature, the generalized velocities and the tyre reaction forces. The resulting system of non-linear algebraic equations was successfully solved by means of a fixed-point iteration method.

The approach proposed by Cossalter significantly reduces the complexity of finding the steady state equilibrium due to the fact that the position problem is not passed to the nonlinear solver. However, one of the major disadvantages of this method is that the speed of the vehicle and its trajectory cannot be directly set by the user; they are implicitly imposed through the steering and roll angles. In addition, it is not possible to extend the approach to more complex models including suspensions as the additional degrees of freedom would not allow to decouple the position problem.

The same authors proposed a different methodology for the steady state analysis of motorcycles in [152] where the speed and the curvature were considered the independent variables of the problem. This new method was specifically designed for the model presented in [43], which was built in dependent coordinates following the natural coordinates approach. The key idea behind this new method was to rewrite the Cartesian coordinates of all points in a reference frame moving and rotating along a circular path with the desired radius. Two additional constraints were introduced to fix the rear contact point to the origin of the moving frame. Finally, the solution was obtained by means of a nonlinear equation solver.

The author of the present thesis presented in [130] the first direct application of a general purpose multibody code, namely Virtual.Lab Motion, for the steady state analysis of motorcycles. In that work, the Newton-Euler approach was used to represent the equations of motion of the motorcycle according to the internal formulation of the Virtual.Lab Motion solver. Three translational coordinates and four Euler parameters

were employed to represent the position and orientation of each body respectively. Together with the standard constraints used to define the model joints, a set of velocity and acceleration constraints were added to the problem, thus allowing the application of the static solver to solve the steady state equilibrium. The influence of curvature and speed on the steering angle, the steering torque and the acceleration index were studied for a multibody motorcycle model with eleven degrees of freedom.

The approach introduced in this thesis extends the works described in the preceding paragraphs. As opposed to those works, we present here a quasi-steady state treatment of the motorcycle equations, with the solution not being limited to the constant speed case. By exploiting the minimal formulation of the multibody model introduced in the previous chapter, it is possible to easily include in the solution the effect of the longitudinal acceleration as well as the effect of the derivative of any other degree of freedom such as, for instance, the roll rate or the roll acceleration. The quasi-steady¹ state solution will be obtained by solving the nonlinear algebraic equation system that arises from the dynamic model when the quasi-steady state conditions are imposed. A nonlinear equation solver based on the Newton-Raphson's method will be used to that end.

4.2 The quasi-steady state method

In this section we describe the method developed to find the quasi-steady state solution of the motorcycle equations introduced in the previous chapter. We start by describing the reference frame where the velocity and the acceleration of the motorcycle are defined together with the constraint equations needed to impose them. Then, the underlying assumptions of the methodology and the details of its implementation are presented for the pure steady state case. Finally, the methodology is extended to the general quasi-steady state solution.

4.2.1 Reference frames and kinematic constraints

The main parameters that define the quasi-steady state equilibrium are the speed of the vehicle, its longitudinal acceleration and the local curvature of the trajectory at the point of interest. The lateral acceleration, on the other hand, is implicitly given by the vehicle speed and the track curvature. All the kinematic quantities involved in the

¹The prefix quasi is used in this case to emphasize that the solution does not represent a pure stationary condition as the equations may include general velocity/acceleration terms. The term quasi-steady state solution refers to a consistent set of states and derivatives that fulfill the dynamic equations of motion at a certain time instant.

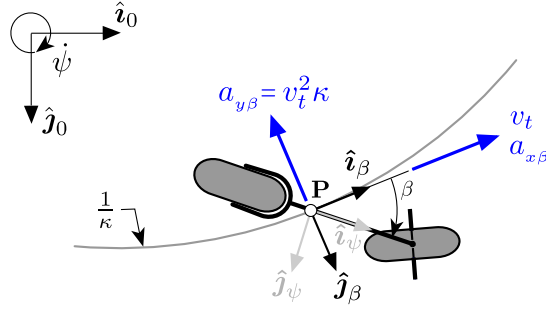


Figure 4.1: Kinematic quantities involved in the definition of the quasi-steady state problem. Two reference frames are shown in the figure: a frame attached to the vehicle \mathbf{T}_ψ , and a frame tangent to the trajectory \mathbf{T}_β . The speed and acceleration of the vehicle, shown in blue, are defined in the tangent frame.

definition of the problem are shown in Fig. 4.1. It is important to note that the vehicle speed and its acceleration, depicted in blue, are not defined in the vehicle frame \mathbf{T}_ψ but in a reference frame \mathbf{T}_β tangent to the trajectory. We will denote the unit vectors of these two frames as $\hat{\mathbf{i}}_\beta$, $\hat{\mathbf{j}}_\beta$ and $\hat{\mathbf{k}}_\beta$ for the tangent frame and $\hat{\mathbf{i}}_\psi$, $\hat{\mathbf{j}}_\psi$ and $\hat{\mathbf{k}}_\psi$ for the vehicle frame.

The angle between both frames, depicted as β in the figure, is generally known as the vehicle sideslip angle and represents the deviation of the longitudinal axis of the vehicle with respect to its direction of motion. It can be computed from the model states as follows,

$$\beta = -\arctan\left(\frac{v}{u}\right) \quad (4.1)$$

where u and v are respectively the longitudinal and lateral components of the vehicle velocity expressed in the body-fixed frame \mathbf{T}_ψ .

We can use the sideslip angle β to project the vehicle velocity along the axes of the tangent frame \mathbf{T}_β ,

$$\begin{bmatrix} v_t \\ 0 \end{bmatrix} = \begin{bmatrix} c_\beta & -s_\beta \\ s_\beta & c_\beta \end{bmatrix} \begin{bmatrix} u \\ v \end{bmatrix} \quad (4.2)$$

with v_t being the absolute velocity of the vehicle. The projections of u and v along the y -axis of the tangent frame cancel out due to the definition of β , which can be easily proven by comparing the second row of Eq. 4.2 to Eq. 4.1.

Similarly, the absolute acceleration of the vehicle can be projected on \mathbf{T}_β ,

$$\begin{bmatrix} a_{x\beta} \\ a_{y\beta} \end{bmatrix} = \begin{bmatrix} c_\beta & -s_\beta \\ s_\beta & c_\beta \end{bmatrix} \begin{bmatrix} a_{x\psi} \\ a_{y\psi} \end{bmatrix} \quad (4.3)$$

where $a_{x\beta}$ and $a_{y\beta}$ are the components of the vehicle acceleration in the tangent frame,

while $a_{x\psi}$ and $a_{y\psi}$ represent the same vector resolved in the vehicle frame.

The first row of Eq. 4.2 together with Eq. 4.3 constitute a set of three kinematic constraints that can be used to impose the desired speed and acceleration conditions for the quasi-steady state equilibrium. In order to make the constraint equations consistent with the motorcycle model, we need to rewrite them as functions of the model states, its derivatives and the imposed variables v_t , $a_{x\beta}$ and κ . This can be achieved by differentiating the velocity vector in the vehicle frame,

$$\begin{bmatrix} a_{x\psi} \\ a_{y\psi} \end{bmatrix} = \begin{bmatrix} \dot{u} - v\dot{\psi} \\ \dot{v} + u\dot{\psi} \end{bmatrix} \quad (4.4)$$

and by rewriting the lateral acceleration as the product of the speed and the track curvature,

$$a_{y\beta} = v_t^2 \kappa \quad (4.5)$$

which allows to define the following set of algebraic equations,

$$\Phi(\dot{\mathbf{q}}_v, \mathbf{q}_v) = \begin{bmatrix} uc_\beta - vs_\beta - v_t \\ (\dot{u} - v\dot{\psi})c_\beta - (\dot{v} + u\dot{\psi})s_\beta - a_{x\beta} \\ (\dot{u} - v\dot{\psi})s_\beta + (\dot{v} + u\dot{\psi})c_\beta - v_t^2 \kappa \end{bmatrix} = \mathbf{0} \quad (4.6)$$

where β is also a function of the model states as per Eq. 4.1. As far as the sign of the imposed variables is concerned, they are consistent with the tangent frame \mathbf{T}_β . Hence, the speed of the motorcycle v_t is always positive, the longitudinal acceleration $a_{x\beta}$ is positive in traction and negative in braking, whereas the lateral acceleration $a_{y\beta}$ is defined as positive when the motorcycle makes a right turn and negative when it turns in the opposite direction. Finally, the above equations can be further simplified if there is no longitudinal acceleration and $\dot{\psi} = v_t \kappa$ as it happens in the steady state case.

$$\Phi(\dot{\mathbf{q}}_v, \mathbf{q}_v) = \begin{bmatrix} uc_\beta - vs_\beta - v_t \\ \dot{u} \\ \dot{v} \end{bmatrix} = \mathbf{0} \quad (4.7)$$

It is worth highlighting two points here. Firstly, the path constraints introduced in Eq. 4.6 and Eq. 4.7 are used to specify the kinematics of the reference point \mathbf{P} , which means that the velocity and acceleration of the vehicle are imposed at the road level, see Fig. 4.2. Henceforth, we will refer to \mathbf{P} as the path point. Secondly, all constraints are defined so that the effect of the vehicle sideslip angle is properly taken into account, i.e. the imposed velocity v_t and the longitudinal acceleration $a_{x\beta}$ are both tangent to the trajectory, while the lateral acceleration $a_{y\beta}$ is perpendicular to it. This consideration

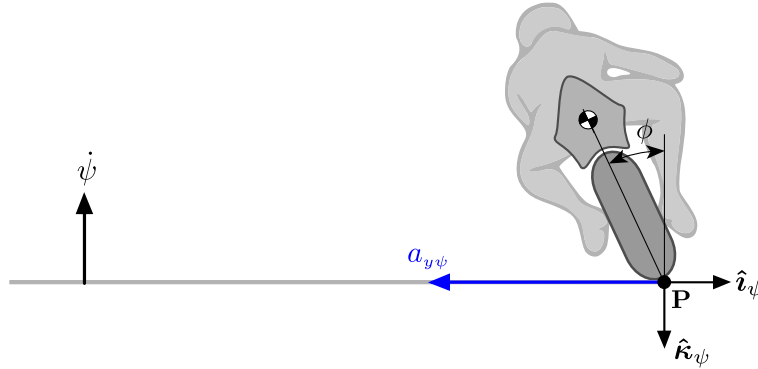


Figure 4.2: Rear view of the motorcycle during a left turn. The constraint vector Φ specifies the kinematics of the reference point \mathbf{P} . Hence, the velocity and acceleration of the vehicle are imposed at the road level. In the figure, the lateral acceleration of the reference point $a_{y\psi}$ is shown in blue while the longitudinal acceleration $a_{x\psi}$, not shown, points forward in traction and rearward in braking.

becomes especially important when it comes down to designing a rider model able to complete aggressive maneuvers such as those performed by racing riders, who often make use of significant vehicle slip. In other words, a rider model that neglects sideslip will fail to understand the response of the vehicle in the nonlinear regime.

4.2.2 Steady state equations

The starting point to solve the stationary equilibrium of the motorcycle are the differential equations of motion introduced in Eq. 3.123. Although there exist methods to find the steady state equilibrium by integrating the aforesaid equations [40, 100], they present important drawbacks that make them unsuitable for the scope of this thesis. Besides the simulation time, which can be relatively long until the desired conditions are met, a control algorithm is required to stabilize the vehicle around the desired condition. Furthermore, motorcycles are intrinsically unstable, which makes it difficult to design a controller that is simultaneously fast, stable and steady state error free.

The steady state equilibrium will be solved here by the transforming the differential equations of motion, which are partially reproduced below for ease of reference, into an algebraic system.

$$\frac{d}{dt} \begin{bmatrix} \mathbf{q}_v \\ \mathbf{p}_\lambda \end{bmatrix} = \begin{bmatrix} \mathcal{M}^{-1}(\mathbf{q}_p) \mathcal{Q}(\mathbf{q}_v, \mathbf{q}_p, \mathbf{p}_\lambda, \mathbf{u}) \\ \mathbf{f}_\lambda(\mathbf{p}_\lambda, \mathbf{q}_v, \mathbf{q}_p) \end{bmatrix} \quad (4.8)$$

Note that only the equations corresponding to the motorcycle and the tyre dynamics are included in Eq. 4.8. The remaining terms from Eq. 3.123 are not needed to solve the equilibrium as the track equations are mere kinematic outputs and the term $\mathbf{A}_p \mathbf{q}_v$

is only needed if the equations are to be solved by a first-order integrator.

Eq. 4.8 can be transformed into an algebraic system if we assume that the motorcycle performs a steady state motion along a circular path. Let's illustrate the method by using, for instance, the roll angle. In steady state conditions, the value of the roll angle is not known, however we can safely set its first and second derivatives to zero since the angle does not change with time. In this way the derivatives disappear from the problem and, in consequence, the roll angle becomes an algebraic variable. We can repeat the same procedure with all the degrees of freedom of the motorcycle, the tyre states and the control inputs.

The following table summarizes the values assigned to each degree of freedom and their first and second derivatives.

DOFs	\mathbf{q}_p	\mathbf{q}_v	$\dot{\mathbf{q}}_v$
u	-	z_1	0
v	-	z_2	0
z	z_3	0	0
ψ	-	$v_t \kappa$	0
ϕ	z_4	0	0
μ	z_5	0	0
δ	z_6	0	0
z_{frk}	z_7	0	0
μ_{swg}	z_8	0	0
θ_{fw}	-	z_9	0
θ_{rw}	-	z_{10}	0

Table 4.1: List of degrees of freedom.

All the unknown variables have been denoted by the letter z followed by a subscript indicating its position in the vector of unknowns \mathbf{z} .

$$\mathbf{z} = [z_1, z_2, \dots, z_{14}]^T \quad (4.9)$$

The remaining states have been set to zero with the exception of the yaw rate $\dot{\psi}$, which in stationary cornering conditions can be computed as the product of the speed v_t times the curvature κ .

During stationary cornering, the sideslip angles of the tyres do not change and the tyre forces stay constant. This condition can be included in the equilibrium solution by

setting the derivatives of the tyre states to zero. Their values, however, are not known and must be declared as unknown variables. Table 4.2 summarizes the values assigned to the tyres states and their derivatives.

Tyre states	\mathbf{p}_λ	$\dot{\mathbf{p}}_\lambda$
λ_f	z_{11}	0
λ_r	z_{12}	0

Table 4.2: List of tyre states.

The motorcycle model has four inputs but not all of them are used during stationary motion. Only the chain force, needed to overcome the effect of the aerodynamic drag, and the steering torque exerted by the rider are active. Obviously, the front and rear brakes are not needed when running at constant speed on a flat surface and thus they have been set to zero.

Inputs	\mathbf{u}
M_{fw}	0
M_{rw}	0
τ	z_{13}
F_{ch}	z_{14}

Table 4.3: List of model inputs.

By replacing the differential states of Eq. 4.8 by the algebraic variables introduced above, we obtain thirteen algebraic equations; eleven from the multibody equations and two from the tyre dynamics. If we also include the first constraint from Eq. 4.7, we get a fully determined system of fourteen equations and fourteen unknowns, the solution of which represents the vehicle motion in steady state conditions.

$$\mathbf{h}(\mathbf{z}, v_t, \kappa) = \begin{bmatrix} \mathbf{Q}(\mathbf{q}_v, \mathbf{q}_p, \mathbf{p}_\lambda, \mathbf{u}) \\ \mathbf{f}_\lambda(\mathbf{p}_\lambda, \mathbf{q}_v, \mathbf{q}_p) \\ \Phi_1(\mathbf{q}_v) \end{bmatrix} = \mathbf{0} \quad (4.10)$$

Note that the acceleration constraints, i.e. the second and third rows of Eq. 4.7, are not included in Eq. 4.10 since they have been explicitly applied to the state derivatives, see Table 4.1.

4.2.3 Quasi-steady state equations

The methodology presented in the previous pages is limited, by definition, to the analysis of the stationary motion of motorcycles. This implies that, as the vehicle travels at constant speed, no traction or braking forces are considered other than the thrust needed to overcome the aerodynamic drag and the rolling resistance. Furthermore, since all the state derivatives are forced to be zero, see Tables 4.1 and 4.2, the equilibrium solution cannot include, for instance, the load transfer originated by the longitudinal acceleration or the gyroscopic effect due to the roll rate. Hence, it is clear that the steady state solution covers only a reduced subset of the working range of the motorcycle. This limitation is even more relevant when it comes down to racing machines, which rarely travel at constant speed.

In order to avoid the limitations of the steady state solution, it is possible to extend the equilibrium equations to include the effect of the longitudinal acceleration together with the derivative of any other degree of freedom. For this purpose, we introduce the inertial terms from Eq. 4.8 and the full set of constraints from Eq. 4.6 into Eq. 4.10, which yields,

$$\begin{bmatrix} \mathcal{M}(\mathbf{q}_p)\dot{\mathbf{q}}_v - \mathcal{Q}(\mathbf{q}_v, \mathbf{q}_p, \mathbf{p}_\lambda, \mathbf{u}) \\ \dot{\mathbf{p}}_\lambda - \mathbf{f}_\lambda(\mathbf{p}_\lambda, \mathbf{q}_v, \mathbf{q}_p) \\ \Phi(\dot{\mathbf{q}}_v, \mathbf{q}_v) \end{bmatrix} = \mathbf{0} \quad (4.11)$$

where the vehicle equilibrium has been written in terms of forces to avoid the inversion of the mass matrix \mathcal{M} . It is worth noting that in this case the motion of the vehicle is no longer stationary. The scope here is to find a consistent set of states and derivatives that fulfill the dynamic equations of motion at a certain time instant given the motion conditions. For instance, imagine that we are interested in the torque needed to steer the motorcycle at a certain point of a corner entry maneuver. Then, if the velocity, deceleration and roll rate of the vehicle are known, the quasi-steady state problem can be easily formulated by introducing these values into the equilibrium equations. Additionally, we can estimate the yaw rate and the yaw acceleration from the reference trajectory if we assume that the vehicle progresses smoothly along it, i.e.

$$\dot{\psi} = v_t \kappa \quad (4.12)$$

$$\ddot{\psi} = v_t \dot{\kappa} + a_{x\beta} \kappa \quad (4.13)$$

The values assigned to each degree of freedom and their first and second derivatives are summarized in Table 4.4, where the vector \mathbf{z} ,

$$\mathbf{z} = [z_1, z_2, \dots, z_{18}]^T \quad (4.14)$$

includes the unknown variables and the vector ξ

$$\xi = [\xi_1, \xi_2, \dots, \xi_{14}]^T \quad (4.15)$$

contains all the imposed derivatives that replace the zeros present in Table 4.1.

DOFs	\mathbf{q}_p	\mathbf{q}_v	$\dot{\mathbf{q}}_v$
u	-	z_1	z_2
v	-	z_3	z_4
z	z_5	ξ_1	ξ_2
ψ	-	$v_t \kappa$	ξ_3
ϕ	z_6	ξ_4	ξ_5
μ	z_7	ξ_6	ξ_7
δ	z_8	ξ_8	ξ_9
z_{frk}	z_9	ξ_{10}	ξ_{11}
μ_{swg}	z_{10}	ξ_{12}	ξ_{13}
θ_{fw}	-	z_{11}	z_{12}
θ_{rw}	-	z_{13}	z_{14}

Table 4.4: List of degrees of freedom.

with $\xi_3 = v_t \dot{\kappa} + a_{x\beta} \kappa$ as per Eq. 4.13. In the same way, the values assigned to the tyre states and their derivatives are reported in Table 4.5.

Tyre states	\mathbf{p}_λ	$\dot{\mathbf{p}}_\lambda$
λ_f	z_{15}	ξ_{14}
λ_r	z_{16}	ξ_{15}

Table 4.5: List of tyre states.

The configuration of the control inputs in this case is slightly different than in the steady state case, and depends on whether the rider is accelerating (\mathbf{u}_+) or braking (\mathbf{u}_-), see Table 4.6. The parameter $\gamma \in [0, 1]$ represents the distribution of the braking torque between the front and rear wheels, e.g. $\gamma = 1$ means that only the front brake will be used to find the quasi-steady state equilibrium.

The quasi-steady state problem possesses a total of eighteen unknowns, four more than the stationary case. These new variables are all defined at acceleration level and

Inputs	\mathbf{u}_+	\mathbf{u}_-
M_{fw}	0	γz_{18}
M_{rw}	0	$(1 - \gamma)z_{18}$
τ	z_{17}	z_{17}
F_{ch}	z_{18}	0

Table 4.6: List of model inputs.

correspond to the derivatives of the vehicle speed (u, v) and to the wheel accelerations ($\ddot{\theta}_{fw}, \ddot{\theta}_{rw}$). The equation vector Eq. 4.11, on the other hand, has sixteen elements: eleven from the multibody equations, two from the tyre dynamics and three from the kinematic constraints. We therefore need two additional equations to complete the system, which have to link the acceleration of the wheels to the model states and their derivatives.

The acceleration of a wheel is related to the longitudinal dynamics of the vehicle through the slip ratio and its derivative. Indeed, we can obtain the wheel absolute acceleration from the slip ratio expression introduced in Eq. 3.69. By differentiating this equation, and after some manipulation, we get,

$$\dot{\Omega} = -(1 + \kappa) \frac{\dot{V}_x}{\rho} - \frac{V_x \dot{\kappa}}{\rho} - \frac{\Omega \dot{\rho}}{\rho} \quad (4.16)$$

where κ is the slip ratio, ρ is the effective rolling radius, V_x is the forward velocity of the contact point and Ω is the angular velocity of the wheel with respect to the ground frame as defined in Chapter 3. Three different effects contribute to the wheel acceleration in Eq. 4.16. The first is usually the most important since it represents the contribution of the longitudinal acceleration of the vehicle to the wheel acceleration. The second and the third, on the other hand, represent respectively the effect of the slip ratio derivative and the variation of the rolling radius.

Tyres typically show large values of slip stiffness in their working region, which causes the slip dynamics to be much faster than the longitudinal response of the vehicle. This means that, for smooth torque variations at the wheel, the slip evolves in a fast and stable way, with $\dot{\kappa}$ vanishing quickly. In this case, the contribution of the second term of Eq. 4.16 may be neglected, and hence we can write the following constraint,

$$(1 + \kappa) \left(\frac{\dot{V}_x}{\rho} + \frac{\dot{\rho} V_x}{\rho^2} \right) + \dot{\Omega} = 0 \quad (4.17)$$

where the derivatives of V_x and ρ can be obtained by symbolic differentiation, with the

resulting expression being a function of the model states and their derivatives. If we collect the constraint equations of the front and the rear wheels in the vector Υ , we can write the following system of eighteen nonlinear equations and eighteen unknowns,

$$\mathbf{h}(\mathbf{z}, v_t, \kappa, \boldsymbol{\xi}) = \begin{bmatrix} \mathcal{M}(\mathbf{q}_p)\dot{\mathbf{q}}_v - \mathcal{Q}(\mathbf{q}_v, \mathbf{q}_p, \mathbf{p}_\lambda, \mathbf{u}) \\ \dot{\mathbf{p}}_\lambda - \mathbf{f}_\lambda(\mathbf{p}_\lambda, \mathbf{q}_v, \mathbf{q}_p) \\ \Phi(\dot{\mathbf{q}}_v, \mathbf{q}_v) \\ \Upsilon(\dot{\mathbf{q}}_v, \mathbf{q}_v, \mathbf{q}_p) \end{bmatrix} = \mathbf{0} \quad (4.18)$$

the solution of which determines the vehicle configuration in quasi-steady state conditions. It is worth noting that the above system and the steady state solution presented in Eq. 4.10 are equivalent when no additional derivatives are imposed, ie. when $\boldsymbol{\xi}=\mathbf{0}$.

4.3 Solution of the equilibrium equations

The solution of the equilibrium equations constitutes the basis to design the virtual rider as it allows to explore the response of the vehicle in a great variety of conditions without the need of integrating the equations of motion. Basically, given the speed of the motorcycle v_t , the curvature of the trajectory κ and the vector of imposed derivatives $\boldsymbol{\xi}$, the problem consists in solving the resulting nonlinear system

$$\mathbf{h}(\mathbf{z}) = \mathbf{0} \quad (4.19)$$

in order to obtain the vector \mathbf{z} containing the unknown states, derivatives and inputs introduced in sections 4.2.2 and 4.2.3.

The Matlab nonlinear solver `fsolve`, based on the trust-region dogleg algorithm [153, 154], is used for that purpose. Generally, nonlinear solvers start from an initial guess \mathbf{z}_0 and improve the solution iteratively until convergence is reached. A proper choice of \mathbf{z}_0 is therefore essential. The closer the initial guess is to the solution, the fewer iterations the solver will need to converge. Conversely, the solver may not converge if the starting point is too far from the final solution. In particular, special attention must be taken when initializing the tyre elements due to their highly nonlinear behaviour. For example, if the longitudinal slip falls into the unstable region of the slip-force curve, i.e. beyond the grip peak, the solver will generally fail to find a solution.

So far we have described how to solve a single quasi-steady state problem. Next we define a continuation strategy to efficiently investigate how the solution \mathbf{z} evolves as we vary the equilibrium parameters v_t , κ and $\boldsymbol{\xi}$. The pseudo-code below illustrates the procedure, where, for the sake of readiness, only one the track curvature is swept.

Algorithm 1 Continuation strategy (curvature sweep)

given: initial curvature κ_0 and search step $\Delta\kappa$
 initialize model: \mathbf{z}_0
 set: $i = 1$
while $\kappa_i \leq \kappa_{\max}$ **and** $\Delta\kappa \geq \Delta\kappa_{\min}$ **do**
 update curvature: $\kappa_i = \kappa_{i-1} + \Delta\kappa$
 update equations: $\mathbf{h}_i(\mathbf{z}) \leftarrow \kappa_i$
 call nonlinear solver: $\mathbf{z}_i = \text{fsolve}(\mathbf{h}_i(\mathbf{z}), \mathbf{z}_{i-1})$
 if convergence **then**
 save current point: (κ_i, \mathbf{z}_i)
 move to next point: $i = i + 1$
 else
 reduce search step: $\Delta\kappa = \Delta\kappa/2$
 end if
end while

The methodology described above relies on the continuity of the solutions with respect to the equilibrium parameters. Note that the initial guess needed to solve the i^{th} problem is taken from the preceding solution, i.e. $\mathbf{z}_i = \text{fsolve}(\mathbf{h}_i(\mathbf{z}), \mathbf{z}_{i-1})$. This approach has several advantages over solving a set of single problems. Specifically, if the equilibrium parameters change smoothly, the use of the preceding solution as the initial guess reduces the number of solver iterations and improves the robustness of the solution against model nonlinearities. In addition to this, the procedure is easy to automate as we only need to provide the initial guess \mathbf{z}_0 to get it started.

Such guess is obtained during the initialization of the model, which takes place in two steps. First, the model is initialized in straight line conditions at constant speed v_{t0} by integrating the equations of motion until the vehicle settles down onto the suspensions. Subsequently a sequence of equilibrium problems is solved to gradually apply the remaining equilibrium parameters κ_0 and $\boldsymbol{\xi}_0$, thus bringing the system to the initial condition \mathbf{z}_0 .

There are several reasons for which the nonlinear solver could fail. In first place, the solution of the quasi-steady state equations might not exist for the given equilibrium parameters. This happens, for instance, when the tyres cannot generate enough lateral force to perform the desired manoeuvre. Therefore, it is always preferable to start by solving the less demanding conditions, e.g. low speed and acceleration, to then smoothly increase the requirements of the solution. However, convergence problems may arise as

we approach the physical limits of the vehicle. This usually happens when the preceding solution is not valid anymore as an initial guess. To avoid this problem, the search step is reduced iteratively until a solution is found or the minimum step is reached.

In the following section we use the strategy described above to explore the stationary solutions of the system, also known as equilibrium manifold in modern control literature [72, 155].

4.4 Steady state motion: sensitivity study

This section is structured in three different parts. We start by verifying that the model equations satisfy the power conservation law, which is a fundamental requirement for any physical system in stationary motion. Then we explore how the most relevant variables (e.g. steering angle, tyre forces, etc) vary in function of the vehicle speed and the curvature of its trajectory. Such study will allow us to improve our knowledge of the system and to identify its main nonlinearities. Finally, we briefly investigate the directional behaviour of the motorcycle by modifying the cornering stiffness of the tyres.

The steady state motion of the motorcycle is unequivocally determined by its speed v_t and by the curvature of its trajectory κ . These two variables provide a convenient and intuitive parametrization of the stationary solutions. The lateral acceleration, on the other hand, becomes a dependent quantity defined by the product $v_t^2 \kappa$. Only positive curvatures, i.e. right corners, are considered in the subsequent analysis as the behaviour of the vehicle is symmetric.

4.4.1 Power balance check

Basically, the power conservation law states that, under equilibrium conditions, the rate at which a system dissipates energy (output power) must equal the power supplied to it (input power), i.e.

$$P_{in} = P_{out} \quad (4.20)$$

This check not only constitutes a helpful tool to identify modelling problems but also gives an interesting insight into the power flow of the motorcycle.

Power supplied by the engine

Generally, the power of the motorcycle originates at the engine and is then transmitted to the rear wheel through the drivetrain. If we assume that no power is lost in the chain, the instantaneous power supplied to the engine sprocket P_e can be computed as the product of the angular speed of the wheel Ω_{rw} times the driving torque generated

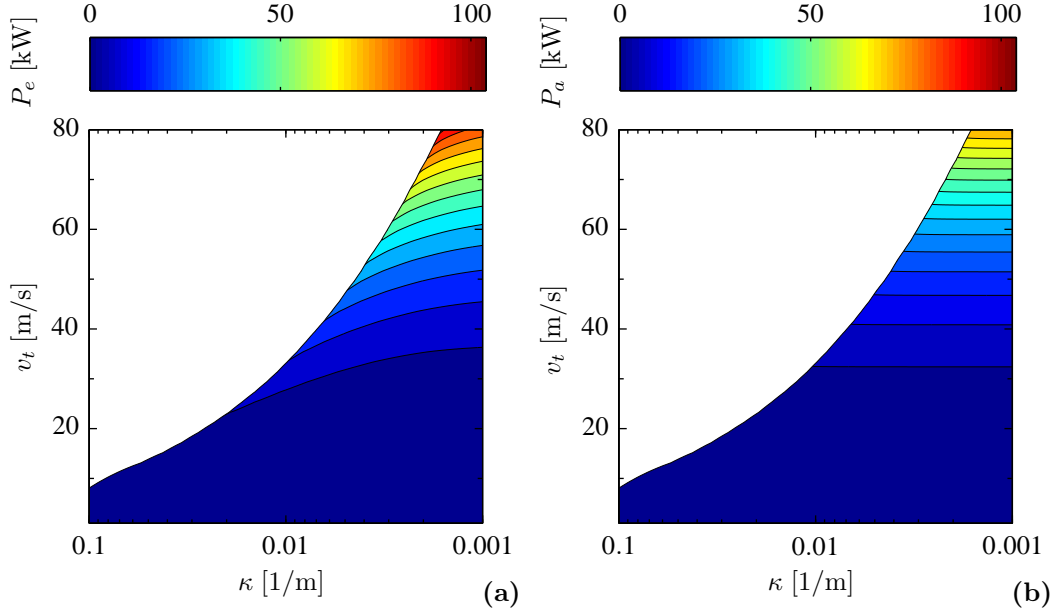


Figure 4.3: Power flow in stationary conditions: engine and aerodynamics. (a) Power supplied by the engine. (b) Power dissipated by the aerodynamic field. Each point of the graphs corresponds to a unique stationary condition characterized by the curvature of the trajectory k and by the tangential speed of the vehicle v_t .

by the chain M_{ch} , which in turn can be written as the product of the chain force F_{ch} times the radius of the rear sprocket R , yielding

$$P_e = M_{ch} \Omega_{rw} = F_{ch} R \Omega_{rw} \quad (4.21)$$

The power required to keep the motorcycle in stationary motion is shown in Fig. 4.3a as a two-dimensional contour plot. Each point of the graph corresponds to a unique condition characterized by the curvature of the trajectory k and by the speed of the vehicle v_t . The curvature is represented along the horizontal axis on a logarithmic scale, while the speed is linearly distributed along the vertical axis. The engine power, on the other hand, is depicted by means of a color scale, which ranges from 0 kW at rest up to more than 100 kW (136 hp) at high speeds. This last value is in line with the maximum power offered by commercial sport motorcycles.

It is important to observe that not all the combinations of speed and curvature lead to a feasible solution in stationary conditions. The white area on the top left part of the figure contains the non-feasible points, with its shape being mainly determined by the tyre properties. The boundary between this area and the contour plot constitutes an important characteristic of the motorcycle that will be referred to as the performance

limit.

Power dissipated by the aerodynamic field

The major cause of power dissipation at high speeds is the aerodynamic field. In Eq. 3.93 we introduced the three components of the aerodynamic map: two forces F_{ax} (drag) and F_{az} (lift) and one moment M_{ay} (pitch). As a general rule, all of them should be considered to compute the power dissipated by the aerodynamics. However, the lift force does not perform work in stationary conditions and can be omitted here, yielding

$$P_a = F_{ax}u + M_{ay}\dot{\psi}s_\phi \quad (4.22)$$

where u is the speed of the vehicle and the term $\dot{\psi}s_\phi$ is the projection of the yaw rate on the y -axis of the chassis. The power dissipated by the aerodynamic field, depicted in Fig. 4.3b, does not depend on the curvature and increases quadratically with the speed.

Power dissipated by the tyres

By comparing Figs. 4.3a and 4.3b, we can observe that the engine power required to keep the motorcycle in stationary motion is higher than the power dissipated by the aerodynamic forces. Moreover, for a given speed, the first increases with the curvature while the second remains constant. Such power difference is due to the tyres. In general, rubber tyres build up the contact forces by slipping on the road and, as a consequence, they dissipate energy. It is worth pointing out that, as opposed to the engine and the aerodynamic forces, the tyre forces are applied to a material point of the tread that changes continuously as the wheel rotates. For that reason, special attention must be taken in this case when computing the power dissipation.

The power loss due to the longitudinal F_x and lateral F_y forces can be computed as the product of each force times the slip velocity of the contact patch [51]. Such velocity, denoted by its components V_{sx} and V_{sy} , was introduced in Eqs. 3.71 and 3.74 to measure the velocity of the material point of the tread that is in contact with the road. The remaining dissipation effects result from the aligning/twisting moments of the tyres. They can be computed as the product of the vertical moment M_z times the angular velocity of the tyre around an axis perpendicular to the road ω_z .

$$P_t = F_xV_{sx} + F_yV_{sy} + M_z\omega_z \quad (4.23)$$

Fig. 4.4 depicts the power dissipated by the lateral forces and by the aligning/twisting moments. It is no surprise that the power dissipated by the lateral forces increases sig-

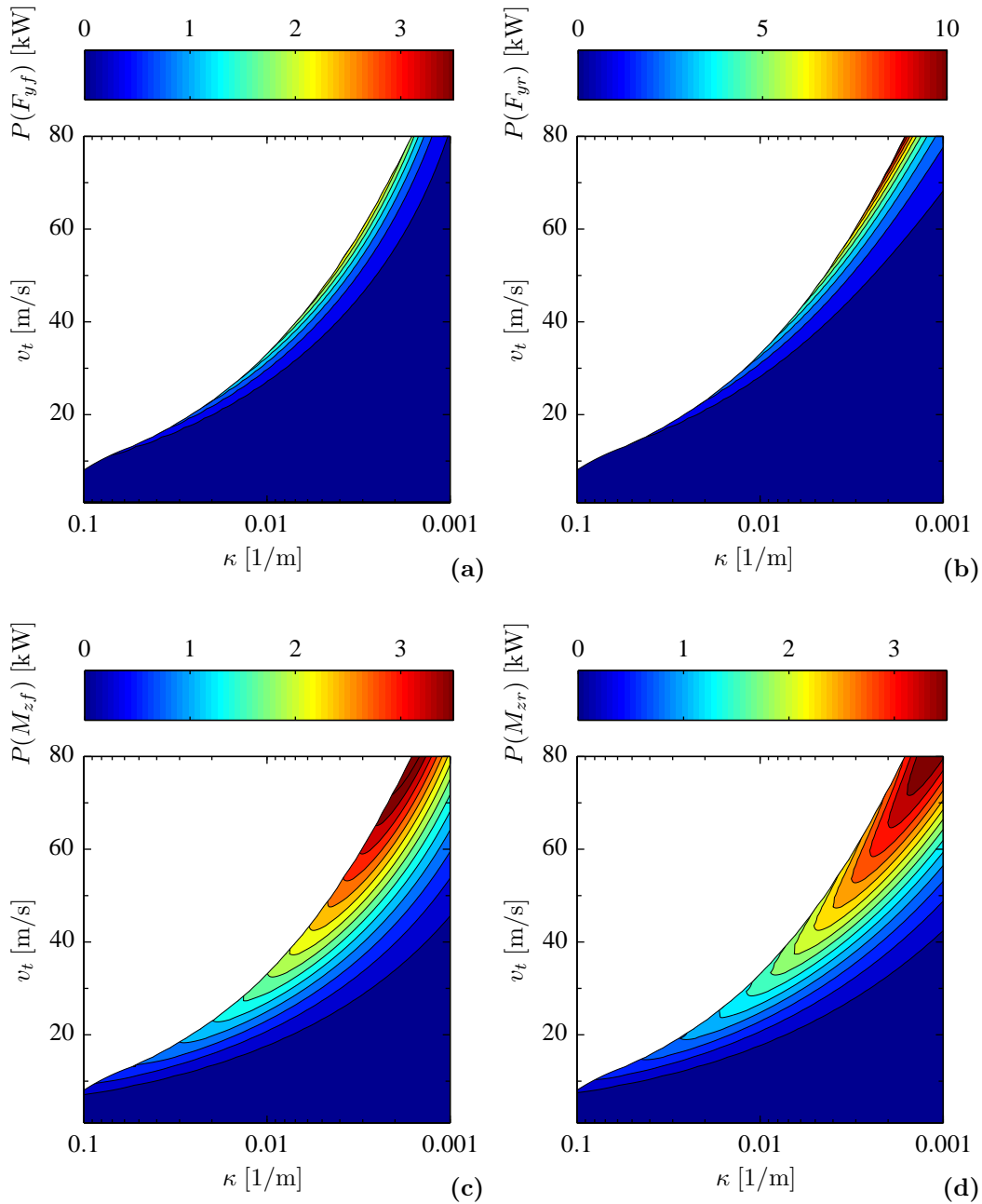


Figure 4.4: Power flow in stationary conditions: tyres. (a) Power dissipated by the front lateral force F_{yf} . (b) Power dissipated by the rear lateral force F_{yr} . (c) Power dissipated by the front aligning/twisting moment M_{zf} . (d) Power dissipated by the rear aligning/twisting moment M_{zr} . It is interesting to realize that the rear tyre dissipates more power, especially at high speeds. The reasons are threefold: first, this particular motorcycle is oversteering, second, the rear tyre works in combined conditions and, third, the rear camber angle is generally smaller than the front, which tends to increase the sideslip at the rear even further.

nificantly as we approach the performance limit of the vehicle. As a matter of fact, it is in these conditions that sideslip angles become considerably large. Furthermore, by comparing Figs. 4.4a and 4.4b with Fig. 4.6d (introduced in the next section) we can observe how the power dissipated by the lateral forces is only relevant at high camber angles above 35 degrees.

It is also interesting to realize that the power loss is larger at the rear tyre, especially at high speeds. The reasons are threefold. First of all, the motorcycle under analysis is oversteering, which essentially means that the rear end tends to slip laterally more than the front. Secondly, the rear tyre works in combined conditions as it generates both lateral and longitudinal forces. The combined use of the tyre reduces its lateral performance and increases the sideslip angle needed to generate a given lateral force. This effect becomes more important at high speeds as the driving force needed to keep the stationary motion increases notably due to the aerodynamic drag. Finally, due to the rotation of the steering system, and according to Fig.3.8c, the rear camber angle is in general smaller than the front, which in turn reduces the contribution of the camber thrust at the rear tyre and consequently increases its sideslip.

The power dissipated by the aligning/twisting torque is depicted in Figs. 4.4c and 4.4d for the front and rear tyres. Here, we can observe how the shape of the contour plot is different to that obtained for the lateral forces. First, the highest dissipation does not occur along the performance limit and, secondly, the peak is much wider in this case. It is also interesting to note that the aligning/twisting torque can dissipate more than 3 kilowatts per wheel at high speeds.

The power dissipated by the longitudinal force, not shown here, increases with the speed and with the curvature. However, its value has been found to be small with respect to the other effects described above except at very high speeds.

Conclusions

Finally, the power balance is depicted in Fig. 4.5. The first plot shows the percentage of the input power used to overcome all the tyre losses while the second shows the percentage needed to overcome the aerodynamic drag. Both plots are complementary of one another, i.e. their sum yields 100%, thus showing that the engine power accounts exactly for the aerodynamic and tyre losses. The maximum error has been found to be $\varepsilon < 1.3 \cdot 10^{-9} \%$, which confirms that the equations of motion on which the simulation model depends satisfy the power conservation law. In addition, we can draw an important conclusion here: the aerodynamic forces are dominant at high speeds and low curvatures, while the tyre forces become significant only at low speeds and high curvatures.

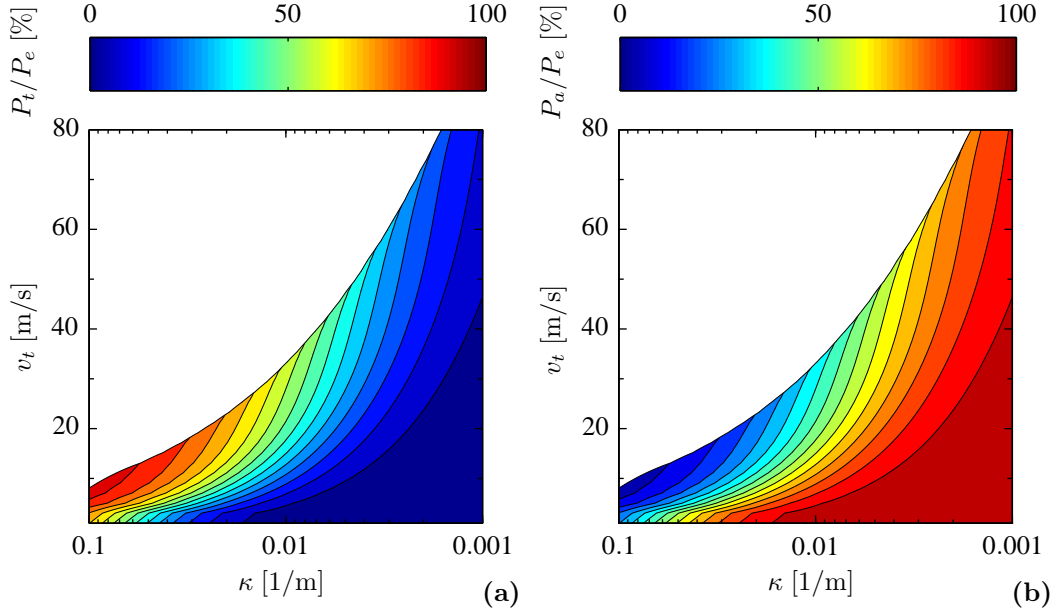


Figure 4.5: Power flow in stationary conditions: output/input ratio. (a) Ratio between the overall power dissipated by the tyres and the engine power. (b) Ratio between the power dissipated by the aerodynamic field and the engine power. Both plots are complementary of one another, i.e. their sum yields 100%. This proves that the engine power accounts exactly for the aerodynamic and tyre losses. The maximum error has been found to be very small, $\varepsilon < 1.3 \cdot 10^{-9} \%$.

4.4.2 Effect of speed and curvature

The purpose of this section is to explore the stationary solution of the motorcycle equations. For this end, we investigate next how the most relevant quantities (e.g. steering angle, roll angle, tyre slips, tyre forces, etc) vary in function of the imposed curvature κ and the motorcycle speed v_t .

Steering torque

Fig. 4.6a shows the steering torque applied by the rider to the handlebar in order to keep the desired trajectory. Let's remember that the graphs of this section include only positive curvatures, i.e. right corners. In this case, the steering torque is defined as positive if the rider tries to rotate the handlebar towards the inside of the corner and negative viceversa. We can therefore distinguish two areas in the figure according to the torque sign. They are divided by a bold black line that represents the equilibrium points where the rider exerts no torque on the handlebar. An interesting property of this line is that it determines the transition from stable to unstable capsizing dynamics. For example, imagine that the rider releases the handlebar in the middle of a corner.

If the steering torque is negative, the reaction torque will steer the handlebar into the corner as soon as it gets released, thus increasing the curvature of the trajectory and hence the centrifugal force. In consequence, the motorcycle will roll towards a stable upright position. However, if the steering torque is positive, the motorcycle will roll towards the ground as the handlebar is released.

Negative steering torques do not only provide better capsize stability but are also beneficial for cornering agility. Positive torques, on the other hand, generate an unpleasant sensation in the rider [13] as they make the motorcycle more difficult to control. Based on the above considerations, we can say that our reference motorcycle shows good overall steering characteristics. For a given curvature, the steering torque is mainly negative, being positive only at high speeds. In addition, the capsize mode is stable in most of the domain, which implies reduced rider effort.

Steering angle

Fig. 4.6b shows the kinematic steering angle. This angle is positive if the front wheel points towards the inside of the corner and negative viceversa. As with the steering torque, a black line is used to separate the positive and negative areas. According to the results, we can highlight two main points. First, the steering angle is strongly affected by the curvature at low speeds. Second, the steering angle becomes negative for speeds over 25 m/s (90 km/h), which means that at high speeds the rider steers towards the outside of the corner. Since we are simulating a right corner, one would intuitively expect the steering angle to be always positive. However, this is not the case due to the oversteering behaviour of the motorcycle under analysis.

Neutral or modest oversteering motorcycles generally show better handling, being easier for expert riders to push them to the limit [13]. Let's consider an understeering motorcycle to illustrate the above statement. Since understeering vehicles tend to expand their trajectory, the rider is generally forced to increase the roll angle in order to correct the cornering radius. This is achieved at the expense of increasing the steering angle. However, if the steering angle increases too much, the required lateral force at the front may overcome the maximum grip available, causing the tyre to slip and eventually leading to a fall. On the other hand, oversteering motorcycles tend to lose the rear end first. When this happens, expert riders can still control the vehicle by means of a countersteering action.

Motorcycle attitude

The sideslip angle of the vehicle β is depicted in Fig. 4.6c. This angle represents the deviation of the longitudinal axis of the vehicle with respect to its direction of motion.

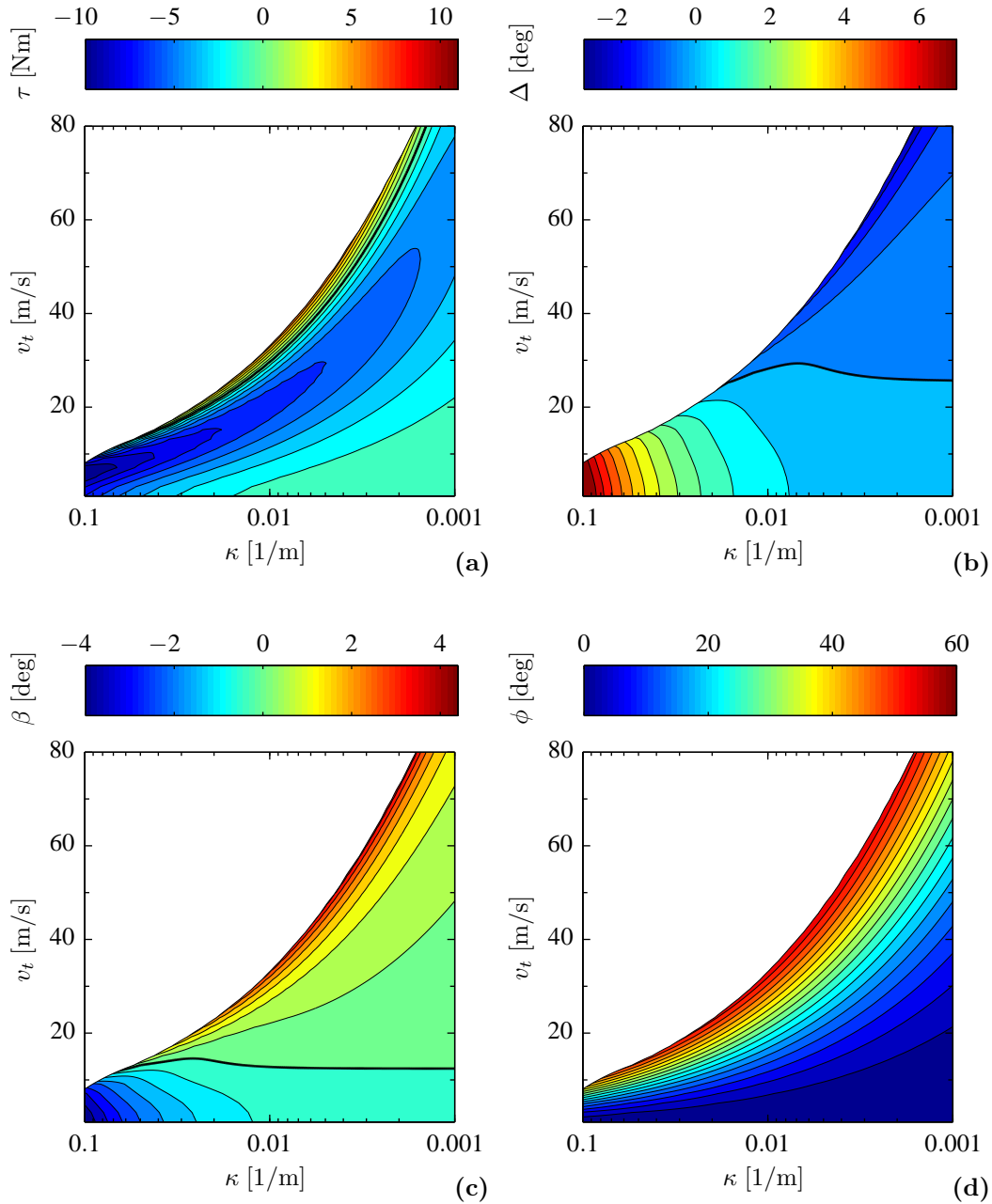


Figure 4.6: Steering torque and main kinematic variables. (a) Steering torque applied by the rider; positive if the rider tries to rotate the front wheel towards the inside of the corner. (b) Kinematic steering angle; positive if the front wheel points towards the inside of the corner. (c) Sideslip angle of the vehicle; positive if the vehicle points towards the inside of the corner. (d) Roll angle; positive if the motorcycle is inclined towards the inside of the corner.

At very low speeds the tyres do not slip significantly and hence the attitude of the vehicle is fully determined by its kinematic parameters, i.e. wheelbase, steering angle, etc. Under these conditions, the vehicle always points towards the outside of the corner and in consequence the sideslip angle is negative. As the lateral acceleration increases, tyre slips become progressively more important, which causes the sign of the sideslip angle to reverse. For speeds above 12 m/s, the vehicle points towards the inside of the corner, with the rear end following a path of greater radius than the front. This behaviour is characteristic of all wheeled vehicles, not only motorcycles, as described in [150, 156].

Roll angle

Finally, Fig. 4.6d shows the roll angle of the motorcycle, where we can observe how it increases with both the speed and the curvature. During steady turning the motorcycle is subject to two main moments, a restoring moment, generated by the centrifugal force that tends to return the vehicle to the upright position, and a tilting moment, generated by the weight force, that tends to increase the leaning angle. This means that, if the rider increases the lateral acceleration, either by increasing the speed, the curvature, or both, the roll angle must increase accordingly in order to counterbalance the additional restoring moment. However, the roll angle cannot be increased indefinitely. There exists an upper limit that depends on the lateral performance of the tyres and, in particular, on the maximum grip available. The maximum roll angle achieved by our reference motorcycle is slightly lower than 60 degrees.

It is also convenient to depict the roll angle as a function of the lateral acceleration in order to obtain a deeper insight into the lateral behaviour of the motorcycle. This is shown in Fig. 4.7a for multiple values of the longitudinal speed. The fact that all blue lines overlay on top of each other highlights the poor sensitivity of the roll angle to speed variations. Likewise, it is interesting to study the effect that the tyre thickness and the gyroscopic effect have on the lateral equilibrium. If we use infinitely thin tyres, and by neglecting wheel inertia, we obtain the family of black curves labeled as ϕ^* in the figure. Interestingly, the classical equation² from [13],

$$\phi^* \simeq \arctan\left(\frac{a_{y\beta}}{g}\right) = \arctan\left(\frac{v_t^2 \kappa}{g}\right) \quad (4.24)$$

²For further details, the derivation of the equation is available in Appendix A, where we introduce a reduced model that captures the fundamental motion of the motorcycle. Such model provides a simple set of equations that results very useful to understand simulation results, particularly in quasi-steady state conditions. We will use those equations throughout the rest of this chapter in order to qualitatively interpret the results of the full multibody model.

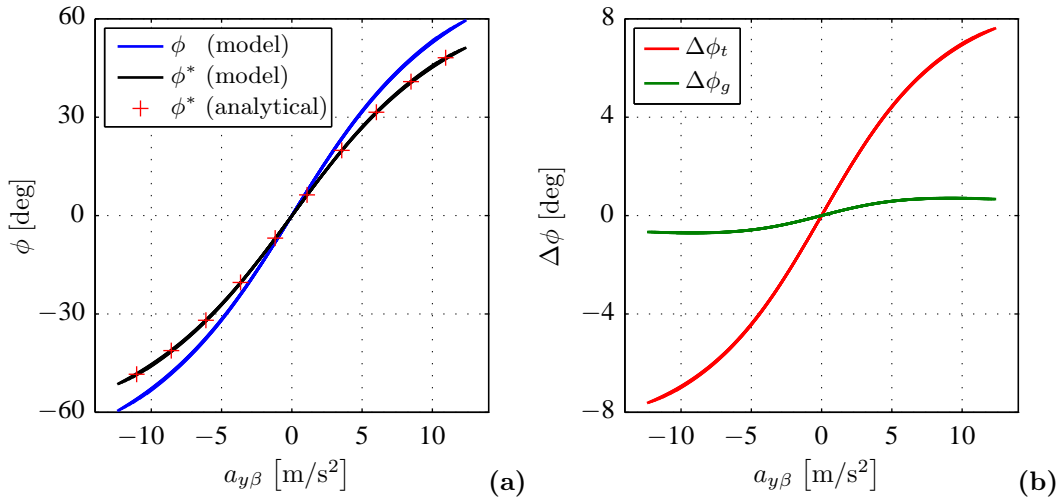


Figure 4.7: Roll angle decomposition. (a) The blue curves represent the roll angle of the full model. The fact that all lines overlay on top of each other highlights the poor sensitivity of the roll angle to speed variations. The the black curve, on the other hand, does not include the effect of tyre thickness and gyroscopic effects. The analytical solution is depicted with red crosses. (b) The contribution of the tyre thickness is shown in red, while the effect of the gyroscopic terms is depicted in green.

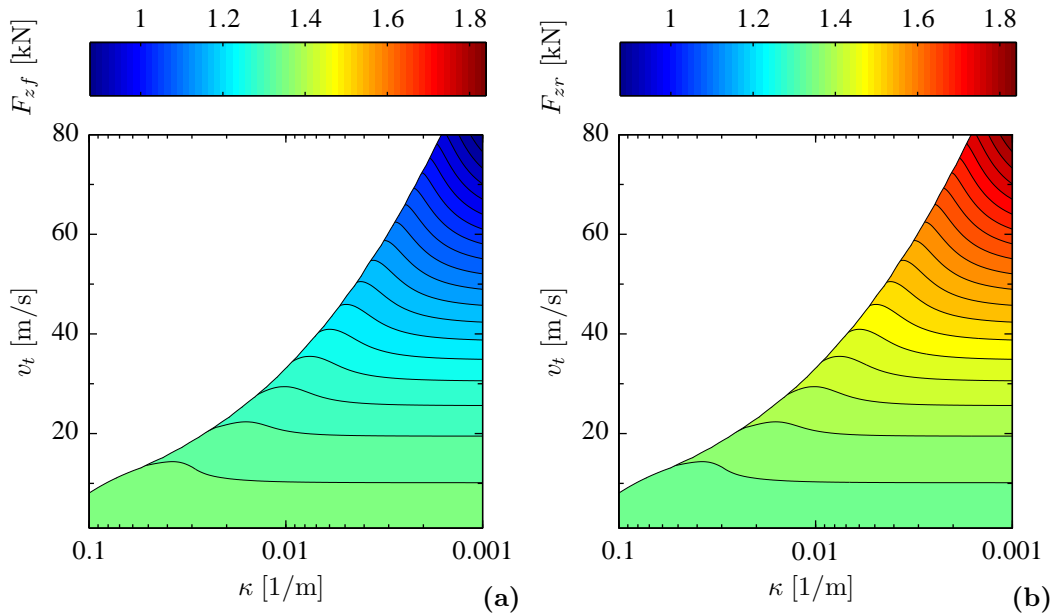


Figure 4.8: Tyre loads. (a) Front tyre vertical load. (b) Rear tyre vertical load. Note that the sum of the tyre loads is almost constant, independently of the equilibrium conditions, and equals the totals mass of the motorcycle and rider 276.9 kg.

provides a good approximation in this last case.

The contributions of the tyre thickness $\Delta\phi_t$ and the gyroscopic terms $\Delta\phi_g$ are shown in Fig. 4.7b. We can observe how both of them increase with the lateral acceleration, with the former being one order of magnitude higher than the latter. It is clear from the results that the tyre shape has a big impact on the lateral equilibrium of the motorcycle in stationary motion while the gyroscopic effect is of secondary importance.

Tyre loads

Next we study the tyre loads, i.e. the vertical reaction that the road exerts on the tyres. They are shown in Fig. 4.8 for the front and rear tyres. In stationary conditions, if we neglect the lift force, which is in general much smaller than the drag, the sum of the tyre loads matches the weight of the motorcycle, i.e.

$$F_{zf} + F_{zr} \simeq mg \quad (4.25)$$

which can be derived from Eq. A.7.

On the contrary, the load distribution is very sensitive to the speed of the motorcycle. As the rider increases the speed, the drag force reduces the load at the front tyre and increases it at the rear by the same amount. This effect increases quadratically with the speed due to the nature of the aerodynamic field. The roll angle plays also an important role in this load transfer. As the motorcycle leans, the centre of pressure lowers, thus reducing the lever arm of the drag force with respect to the ground and consequently decreasing the amount of transferred load. We can use Eq. A.20 to quantify this effect. If we simplify the aforesaid equation for the case of stationary motion, we get,

$$\Delta F_z \simeq \frac{F_{ax} h c_\phi}{a + b} \quad (4.26)$$

where F_{ax} is the drag force, the term $h c_\phi$ represents the lever arm of the force perpendicular to ground and the denominator $a+b$ is the wheelbase of the motorcycle. Note that a positive variation indicates, by definition, that the front load increases whereas the rear decreases.

We can observe the effect of the roll angle by comparing Figs. 4.8a and 4.8b. To do so it is convenient to keep the speed of the motorcycle constant so that the aerodynamic drag does not vary. Let's choose, for instance, a speed of 60 m/s for the comparison. If we now start from the rightmost point of the graph and increase the curvature progressively, the roll angle of the motorcycle increases as per Fig. 4.6d, which in turn modifies the load distribution, increasing the load at the front tyre and decreasing it at the rear.

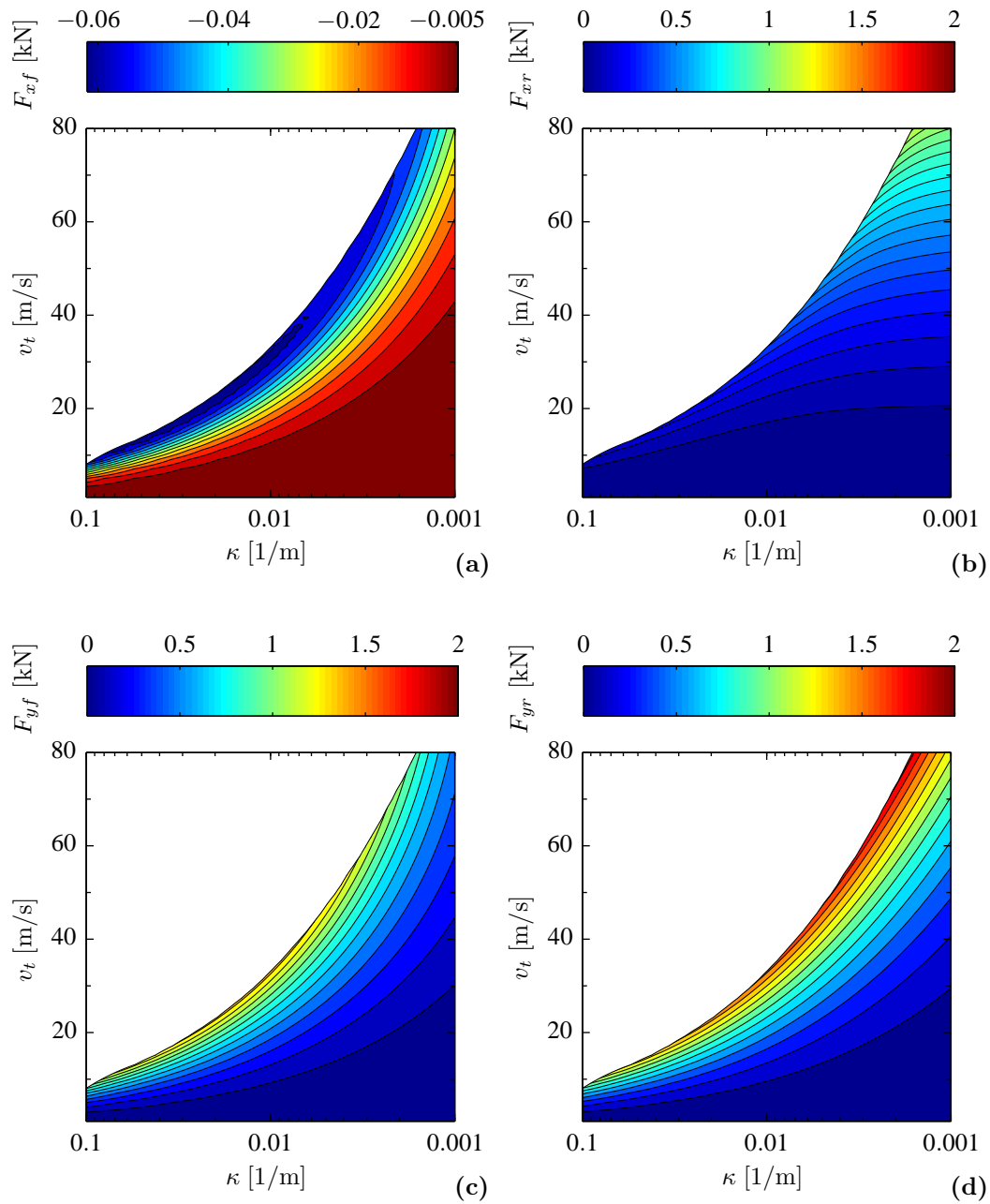


Figure 4.9: Tyre forces on the road plane. (a) Front longitudinal force. (b) Rear longitudinal force. (c) Front lateral force. (d) Rear lateral force. Note the different scale in the front longitudinal force.

The vertical loads have a big influence on the capability of tyres to generate longitudinal and lateral forces. As a matter of fact, in normal riding conditions, the maximum force that a tyre can generate is proportional to the normal load applied to it.

Forces and moments at the contact patch

Fig. 4.9 shows the forces generated by the tyres on the road plane. By definition, the longitudinal force is positive if it tends to accelerate the vehicle and negative if has a braking effect. The lateral force, on the other hand, is positive if it points towards the inside of a right corner and negative viceversa.

The longitudinal force generated by the front tyre is depicted in Fig. 4.9a. It is interesting to note that this tyre generates a small braking force despite no braking torque is applied to the wheel. The origin of this force lies in the twisting moment. Let's remember that this moment, introduced in the previous chapter, is always perpendicular to the road and tends to rotate the wheel into the corner. Hence, as the motorcycle leans, the twisting moment is progressively projected on the wheel axis. This projection tends to brake the wheel, thus generating negative force at the contact patch that increases with the roll angle.

The rear longitudinal force, also known as driving force, is very sensitive to the vehicle speed as shown in Fig. 4.9b. This trend is typically caused by the aerodynamic drag. What is not so intuitive, however, is why the driving force increases slightly with the curvature. We can use Eq. A.5 to identify the origin of such behaviour. In the particular case of stationary motion, this equation can be rearranged to yield,

$$F_{xr} \simeq F_{ax} + ma_{y\beta}s\beta - F_{xf}c\Delta + F_{yf}s\Delta \quad (4.27)$$

where the first term of the right hand side is the aerodynamic force whereas the last three represent the projections of the inertial force $ma_{y\beta}$ and the front tyre forces, F_{xf} and F_{yf} , on the longitudinal axis of the vehicle. According to the above equation, there are three different reasons why the driving force depends on the curvature:

- Firstly, the most important reason is related to the reference frame used to define the steady state problem. We can observe in Fig. 4.1 how the lateral acceleration is imposed in the tangent frame \mathbf{T}_β . Hence, as the sideslip angle β increases, so does the projection of the term $a_{y\beta} = v_t^2 \kappa$ along the longitudinal axis of the vehicle. According to Fig. 4.6c, the angle β is generally positive and increases with the curvature. Under these conditions, the second term in the right hand side of Eq. 4.27 increases the driving force as the curvature increases.

- Secondly, the longitudinal projection of the front force F_{xf} produces a braking effect that increases with the curvature according to Fig. 4.9a. As a result, the third term in the right hand side of Eq. 4.27 increases the driving force as the curvature increases, although its contribution is very small.
- Finally, the projection of the front lateral force F_{yf} on the longitudinal axis of the vehicle increases with the steering angle. This term can increase or decrease the driving force depending on the sign of the steering angle, which is shown in Fig. 4.6b.

The addition of these three terms results in an overall driving force that increases with the curvature.

The plots of the lateral forces are represented in Figs. 4.9c and 4.9d. Interestingly, the contour lines follow a pattern similar to that of the roll angle. We can explain this trend by means of two basic equations. In stationary conditions, the total lateral force exerted by the tyres can be approximated³ by rearranging Eq. A.6 as follows,

$$F_{yf}^* + F_{yr} \simeq ma_{y\beta} = mv_t^2 \kappa \quad (4.28)$$

where F_{yf}^* is the projection of the front tyre forces on the lateral axis of the vehicle, i.e. $F_{yf}^* = F_{xf} s_\Delta + F_{yf} c_\Delta$. The resulting expression relates the lateral forces to the speed of the motorcycle and to the curvature of its trajectory. By combining the above equation with Eq. A.23, we obtain the following expression,

$$F_{yf}^* + F_{yr} \simeq mg \tan \phi \quad (4.29)$$

which shows why the lateral forces are strongly related to the roll angle.

The geometry of the vehicle and the tyre characteristics ultimately determine how the lateral forces distribute between the front and rear axles, with the aerodynamic drag also playing an important role in this respect. As the speed goes up, the load transfer increases the capability of the rear tyre to generate contact forces, whereas the front tyre experiences the opposite effect. The lateral force transferred by the aerodynamic drag is described in Eq. A.17, which reduces to the following expression in stationary motion:

$$\Delta F_y \simeq \frac{F_{ax} h s_\phi}{a + b} \quad (4.30)$$

As with the vertical loads, a positive variation indicates a decrease of the front force and an increase of the rear.

³To simplify the result, we have made $c_\beta \simeq 1$ since the sideslip angle β is generally small as shown in Fig. 4.6c. Then, since $a_{x\beta} = 0$ in stationary motion, from Eq. 4.3 we can write $a_{y\psi} \simeq a_{y\beta}$.

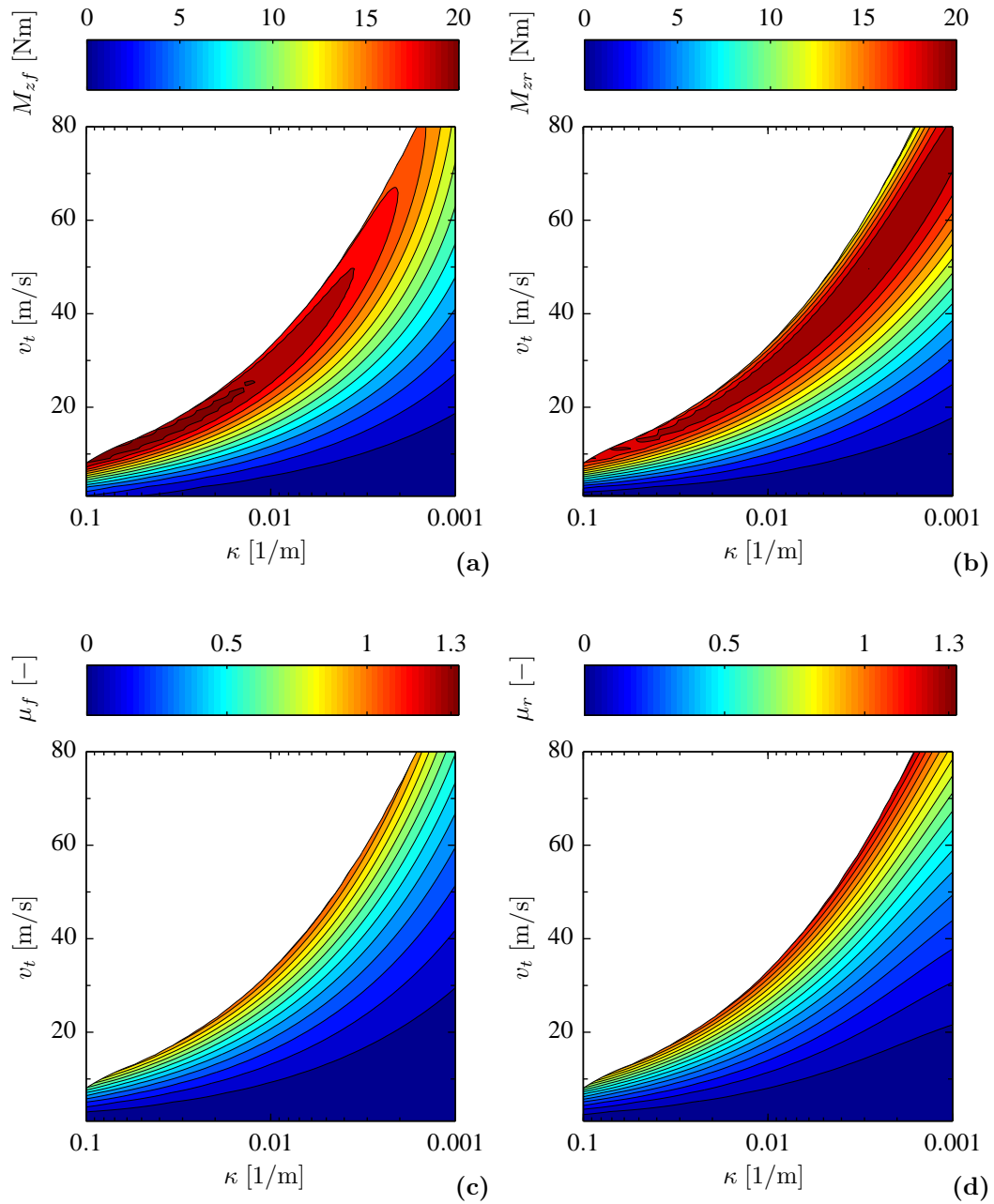


Figure 4.10: Tyre twisting moments and grip coefficients. (a) Front twisting moment. (b) Rear twisting moment. (c) Front grip coefficient. (d) Rear grip coefficient.

Figs. 4.10a and 4.10b show the twisting moments generated by the front and rear tyres. Both of them are always positive, which means that the tyres tend to rotate the motorcycle towards the inside of the corner. In addition to this, the front twisting moment has a big impact on the steering response. The projection of this moment on the steering axis significantly decreases (makes more negative) the torque that the rider must apply to steer the motorcycle. In particular, for the sports motorcycle considered in this thesis, the front twisting moment is responsible for the steering torque being negative in a wide range of speeds and curvatures as shown in Fig. 4.6a.

Grip coefficient

To conclude this section, we analyze the grip coefficients of both tyres. The grip coefficient μ is defined as the ratio of the contact force parallel to the road and the normal load, i.e.

$$\mu = \frac{\sqrt{F_x^2 + F_y^2}}{F_z} \quad (4.31)$$

Such metric is generally used to quantify the performance of tyres subject to combined longitudinal and lateral forces.

We can observe in Figs. 4.10c and 4.10d how for a given curvature the grip reaches its maximum value at the boundary of the contour plot. The same happens if we keep the speed constant and increase the curvature; we reach the maximum grip at the leftmost point of the graph, which also lies on the vehicle's performance limit. In stationary conditions, the front grip is mainly related to the lateral force as no braking forces are applied to the wheel. At the rear, however, we have to consider the driving force, which increases quadratically with the speed. This is the reason why the rear tyre shows higher grip values, especially at high speeds.

If we plot the lateral grip as a function of the lateral acceleration for several speeds ranging from 20 to 80 m/s, we obtain the curves shown in Fig. 4.11. The interesting point here is the slope of the curves, which is almost constant. By combining Eq. 4.25 and Eq. 4.28 we can approximate the overall lateral grip as,

$$\mu_y = \frac{F_{yf}^* + F_{yr}}{F_{zf} + F_{zr}} \simeq \frac{a_{y\beta}}{g} \quad (4.32)$$

Interestingly, despite of the simplifying assumptions, the slope predicted by the above equation, $1/g$, matches quite well the results obtained for both tyres with the full multibody model. The small speed sensitivity shown by the front grip is due to the steering angle, which reduces the effective lateral force perpendicular to the vehicle axis at high speeds. The rear grip, on the other hand, shows almost no speed sensitivity.

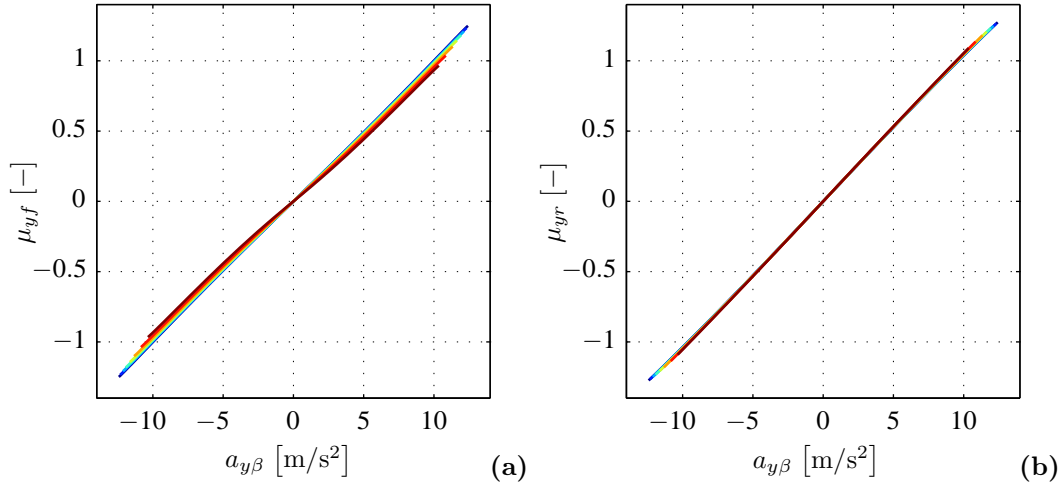


Figure 4.11: Grip analysis in function of the lateral acceleration. Each color corresponds to a different speed, which range from 20 to 80 m/s. The lowest speed is represented by a blue line, whereas the highest is represented by a red line. (a) Front grip coefficient. (b) Rear grip coefficient.

4.4.3 Directional behaviour: oversteering vs understeering

The steering behavior of the motorcycle depends on its geometry; parameters such as wheelbase, fork offset and caster angle have a big impact on the vehicle's response. However, it is usually the tyres that play the most important role in this respect. In the current section we briefly investigate the steering behavior of the model by comparing two setups with different tyre properties.

The first setup is the same used in the previous sections of this chapter. Let us remind the reader that our reference model was defined as having +15% more cornering stiffness than Sharp's reference data at the front tyre whereas the rear stiffness was scaled down by the same amount. These modifications were made to assure a marked oversteering behavior of the vehicle, which will be referred to as OS in this section. The second setup, introduced here for the first time, uses the opposite scaling, with the front tyre having greater cornering stiffness than the rear. The purpose of this change is to create a new model with increased understeering behaviour, which will be referred to as US.

The steering ratio ξ is commonly used in literature to study the steering response of double-track vehicles. Such metric is defined as the ratio between the kinematic curvature radius R_{c_0} and the actual cornering radius of the vehicle R_c . We can write it as a function of the sideslip angles, λ_f and λ_r , and the kinematic steering angle Δ as

per [13],

$$\xi = \frac{R_{c0}}{R_c} = \frac{\sin(\Delta - \lambda_f + \lambda_r)}{\cos(\Delta - \lambda_f) \tan \Delta} \simeq 1 - \frac{\lambda_f - \lambda_r}{\Delta} \quad (4.33)$$

where the last part of the equation applies only if the sideslip angles and the kinematic steering angle are small; an assumption that is perfectly valid in normal riding conditions. In view of the above definition, we can distinguish the following cases:

- $\xi < 1$ Understeering response. The sideslip of the rear tyre is smaller than the front, i.e. the actual cornering radius is greater than the kinematic one.
- $\xi = 1$ Neutral response. The sideslip angles of the front and rear tyres are equal, i.e. the actual cornering radius is equal to the kinematic one.
- $\xi > 1$ Oversteering response. The sideslip of the rear tyre is greater than the front, i.e. the actual cornering radius is smaller than the kinematic one.
- $\xi < 0$ Countersteering response. If the sideslip of the rear tyre is much greater than the front, the rider needs to apply a negative steering angle, i.e. towards the outside of the corner, which leads to a negative steering ratio.

Fig. 4.12a shows that the steering ratio of the first setup (OS) strongly depends on the cornering speed. In particular, for low and medium speeds the vehicle exhibits an oversteering behaviour that becomes more marked as the speed increases. At 26 m/s (94 km/h), however, the steering ratio presents a singularity and its sign changes from positive to negative. This particular speed, usually known as the critical speed, is characterized by the fact that the vehicle corners even though the steering angle is null. After that point, the vehicle exhibits a countersteering behaviour.

It is well known that the critical speed of any double-track vehicle must be well above its maximum speed [137]. This, however, does not apply to motorcycles as it is generally possible to control them over the critical point. The main reason of this difference lies in the method employed to control the vehicle. Double-track vehicles are controlled in position since their primary input is the angle of the steering wheel. This kind of control makes it difficult for the driver to stabilize the vehicle near the critical speed. On the contrary, motorcycles are controlled in force through the steering torque, with the steering angle being just an effect [157]. The control of the motorcycle in these circumstances is achieved by countersteering. Such behaviour can be easily observed in speedway and motard machines and, to a lower extent, also in road racing motorcycles.

The steering ratio of the second setup (US) is shown in Fig. 4.12b. This vehicle is slightly understeering in the whole speed range, except in the region around 60 m/s,

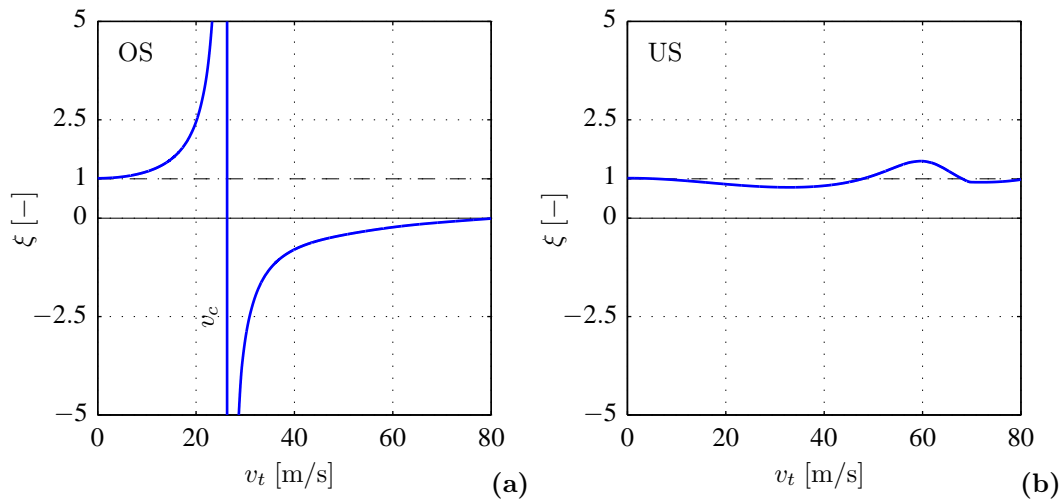


Figure 4.12: Steering ratio. $R_c = 1/\kappa = 500$ m. (a) Oversteering setup. (b) Understeering setup. It is important to note that, as opposed to double-track vehicles, the control of the motorcycle over the critical speed v_c is possible by performing countersteering maneuvers [13]. Such behaviour can be easily recognized, for instance, in speedway and motard machines.

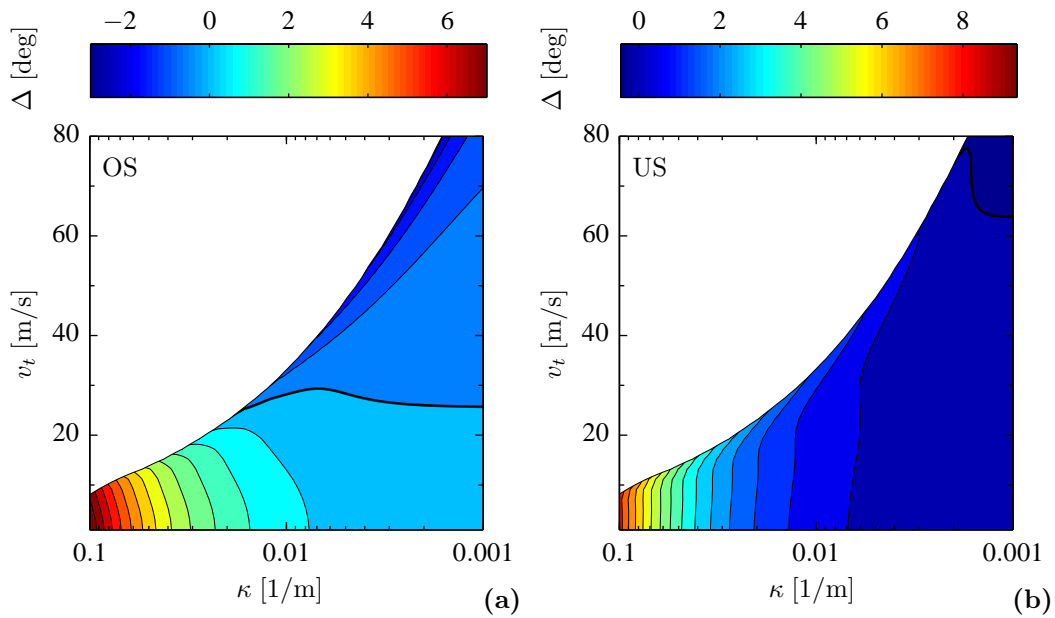


Figure 4.13: Kinematic steering angle comparison. (a) Oversteering setup. (b) Understeering setup. The locus of the points where the kinematic steering angle is null, depicted by a bold black line in the above plots, coincides, by definition, with the critical speed of the motorcycle. At that speed the vehicle corners even though the steering angle is null.

where it becomes slightly oversteering. Note that the steering ratio is always finite and therefore no critical speed can be defined in this case.

To conclude this section, we depict the kinematic steering angle as a function of the speed and curvature for both setups, see Fig. 4.13. The critical speed, which is represented by a bold black line, coincides, by definition, with the locus of the points where the kinematic steering angle is null. Above this line the motorcycle becomes countersteering, i.e. $\Delta < 0$. We can observe how both setups may exhibit a countersteering behaviour, although the speed that triggers it is different in both cases. The critical speed of the OS setup is relatively low and shows a poor sensitivity with respect to the path curvature, whereas the US setup shows a high critical speed that varies significantly with the curvature.

The directional behavior of the motorcycle is strongly affected by the presence of longitudinal forces between the tyres and the road. Any longitudinal force causes a reduction of the cornering stiffness. When applied to the rear tyre, as it is the case here, it makes the vehicle more oversteering. This explains why both setups become countersteering as the speed increases. It is also worth noting that the countersteering angles are small even for the OS setup, with Δ being lower than -2.5 degrees in Fig. 4.13a.

4.5 Quasi-steady state motion: sensitivity study

So far we have studied the steady state motion of the cornering motorcycle by solving Eq. 4.10. It is obvious, however, that the stationary motion represents only a reduced subspace of the working domain of the motorcycle. Therefore, in order to extend our knowledge of the system, we next use Eq. 4.18 to investigate the effect of the most relevant derivatives, namely the longitudinal acceleration, the roll rate and the roll acceleration.

4.5.1 Effect of longitudinal acceleration

The accelerated trim of the motorcycle is obtained by imposing the desired longitudinal acceleration in the quasi-steady state equations. The main difference with respect to the stationary solution, in addition to the supplementary constraints included in vectors Φ and Υ , is the configuration of the input vector \mathbf{u} . Two possible configurations exist, being the solution routine that, depending on the acceleration value, selects the most suitable inputs from Table 4.6.

The first configuration \mathbf{u}_+ is generally used when the imposed acceleration is positive (thrust), while the second \mathbf{u}_- is used for negative accelerations (braking). An exception occurs when imposing low deceleration levels at very high speeds. In these

circumstances, the deceleration generated by the drag force is generally higher (more negative) than the desired target. When this happens, we need to use the engine power to overcome the drag, meaning that the \mathbf{u}_+ configuration is required despite the target acceleration being negative.

As far as the braking distribution is concerned, and according to [158], experienced riders use mainly the front brake when the grip is good. We can easily reproduce this behaviour by setting the parameter γ to 1 in Table 4.6.

Next we carry out a sensitivity study to explore the effect that the longitudinal acceleration has on the behaviour of the motorcycle. In the subsequent figures, the horizontal axis represents the lateral acceleration while the vertical contains the parameter of interest, e.g. the braking force, the lateral force, etc. It is useful to recall that the lateral acceleration $a_{y\beta}$ is, by definition, positive for right corners. The longitudinal acceleration $a_{x\beta}$, on the other hand, is depicted by means of a chromatic scale that goes from blue for severe braking ($a_{x\beta} \ll 0$) to red for strong acceleration ($a_{x\beta} \gg 0$). The stationary motion ($a_{x\beta} = 0$) is represented by a green line.

Fig. 4.14 shows the effect of the acceleration on the longitudinal forces exerted by the tyres. To avoid oversaturating the graphs, we will use a single reference speed of 40 m/s (144 km/h) throughout this section. There are three points worth mentioning here:

- First of all, the change in the input configuration between braking \mathbf{u}_- and thrust \mathbf{u}_+ is evident in the results. When the imposed acceleration is negative, the front longitudinal force is active while the rear is almost negligible. On the other hand, when the imposed acceleration is positive we observe the opposite behavior, i.e. the front longitudinal force is negligible while the rear is active. Note that the front force is always negative whereas the rear is positive, i.e. we are using the front tyre to brake the motorcycle and the rear tyre to accelerate it.
- Secondly, the combined use of the tyres makes the range of feasible lateral accelerations narrower as the absolute value of the acceleration increases. For example, note in Fig. 4.14b the width difference between the green curve representing null acceleration and the red one corresponding to 10 m/s^2 . This is a common feature of all graphs shown in this section.
- Finally, we can observe how the lateral acceleration has an effect on the longitudinal forces needed to keep the quasi-steady state motion. As the lateral acceleration increases, the braking forces become less negative while the thrust forces become more positive. The reasons of this behaviour were discussed in section 4.4.2 when analyzing Eq. 4.27.

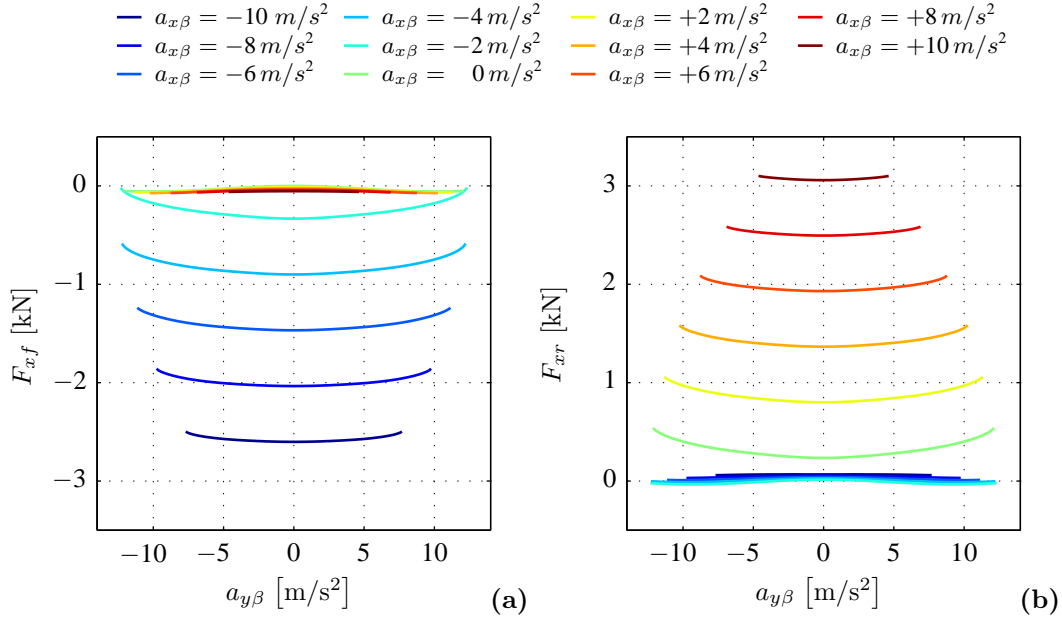


Figure 4.14: Effect of the longitudinal acceleration at 40 m/s : tyre forces in the longitudinal direction. (a) Front longitudinal force. (b) Rear longitudinal force. Note that the front tyre is used to brake the motorcycle while the rear is used to accelerate it.

The longitudinal acceleration has also a big impact on the lateral and vertical forces as shown in Fig. 4.15. Both sets of forces are closely connected: when the motorcycle accelerates, there is a transfer of vertical load from the front to the rear axle which, in turn, increases the lateral force generated by the rear tyre and decreases that of the front. The opposite happens during braking.

This behaviour can be easily noticed in the graphs by using the green line as a reference. Let's remember that this line represents a pure stationary motion. The forces generated by the front tyre in the lateral and vertical directions, shown in Figs. 4.15a and 4.15c, decrease with respect to the stationary case when the acceleration is positive (yellow/red lines) whereas they increase when the acceleration is negative (cyan/blue lines). We can observe the opposite trend in the forces generated by the rear tyre, see Figs. 4.15b and 4.15d. As a curiosity, it is interesting to realize that when $a_{x\beta}=10 \text{ m/s}^2$ it is the rear tyre that generates most of the lateral force needed for cornering since the front tyre is unloaded and generates almost no lateral force.

As in the previous sections, we can use the reduced model derived in Appendix A to better understand how the longitudinal acceleration affects the force distribution between the front and rear tyres. By rewriting Eqs. A.17 and A.20 for the current quasi-steady state conditions and extracting only the terms related to the longitudinal

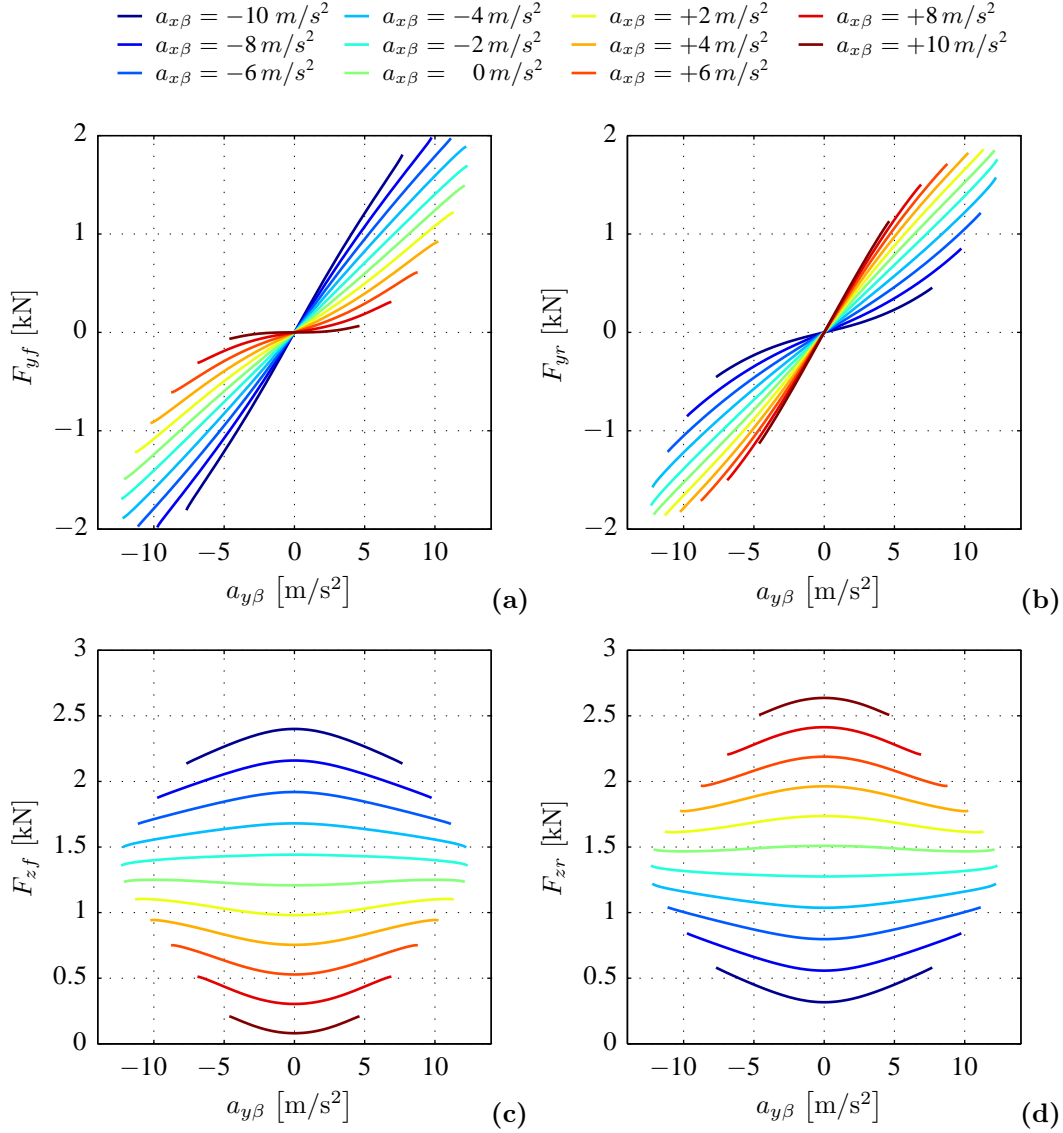


Figure 4.15: Effect of the longitudinal acceleration at 40 m/s : tyre forces in the lateral and vertical directions. (a) Front lateral force. (b) Rear lateral force. (c) Front vertical force. (d) Rear vertical force.

acceleration, we get⁴,

$$\Delta F_y \simeq \frac{ma_{x\beta}}{a+b}hs\phi$$

$$\Delta F_z \simeq \frac{ma_{x\beta}}{a+b}hc\phi$$
(4.34)

⁴We have omitted the contribution of the inertial torques described in Tables A.1 and A.2 since the effect of the wheel acceleration and the derivative of the yaw rate is generally small compared to that of the longitudinal acceleration. The above expressions have been derived assuming $c_\beta \simeq 1$ since the sideslip angle of the vehicle β is generally small as shown, for instance, in Fig. 4.6c.

where a positive variation indicates, by definition, a decrease of the front force with respect to the stationary motion and an increase of the rear. Interestingly, both equations are identical except for the trigonometric terms involving the roll angle ϕ , which allows us to conclude the following:

- The longitudinal acceleration modifies the lateral and vertical forces exerted by a given tyre in the same direction, i.e. if the vertical force increases so does the absolute value of the lateral force and viceversa.
- The roll angle, on the other hand, has opposite effects on the lateral and vertical forces due to the sine and cosine terms. Given that the roll angle is monotonically related to the lateral acceleration⁵, it follows from Eq.4.34 that the lateral load transfer is antisymmetric with respect to the lateral acceleration while the vertical load transfer is symmetric. This explains the trends observed in Fig. 4.15.

Fig. 4.16a shows the steering torque applied to the handlebar. It is useful to recall that this torque is defined as positive if the rider tries to rotate the handlebar towards the right. We observe from the results that the steering torque is very sensitive to the longitudinal acceleration during braking. The reason lies in the front braking force, which generates a moment around the steering axis that tends to rotate the wheel towards the inside of the corner. Moreover, this effect is amplified by the lateral acceleration, as the roll angle increases the distance between the front contact point and the steering axis. An accurate modeling of the cross section of the tyre is essential to capture this phenomenon.

Interestingly, the roll angle is unaffected by the longitudinal acceleration as shown in Fig. 4.16b. This angle is, by definition, positive when the motorcycle leans to the right.

The kinematic steering angle, on the other hand, shows a large sensitivity with respect to the longitudinal acceleration, see Fig. 4.16c. This angle follows the same sign convention as the steering torque, i.e. it is positive if the handlebar is rotated to the right. In order to simplify the analysis, and since the behaviour of the motorcycle is symmetric, let's focus on the right corners only, i.e. $a_{y\beta} > 0$. We can observe how the rider steers towards the inside of the corner $\Delta > 0$ when the longitudinal acceleration is highly negative. However, as the acceleration increases, this trend reverses rapidly and the rider steers towards the outside of the corner $\Delta < 0$ to keep the trajectory.

This behavior can be easily explained by means of the steering ratio, depicted in Fig. 4.16d. Based on the results, the motorcycle is understeering during hard braking,

⁵This is shown, for instance, in Fig.4.7a.

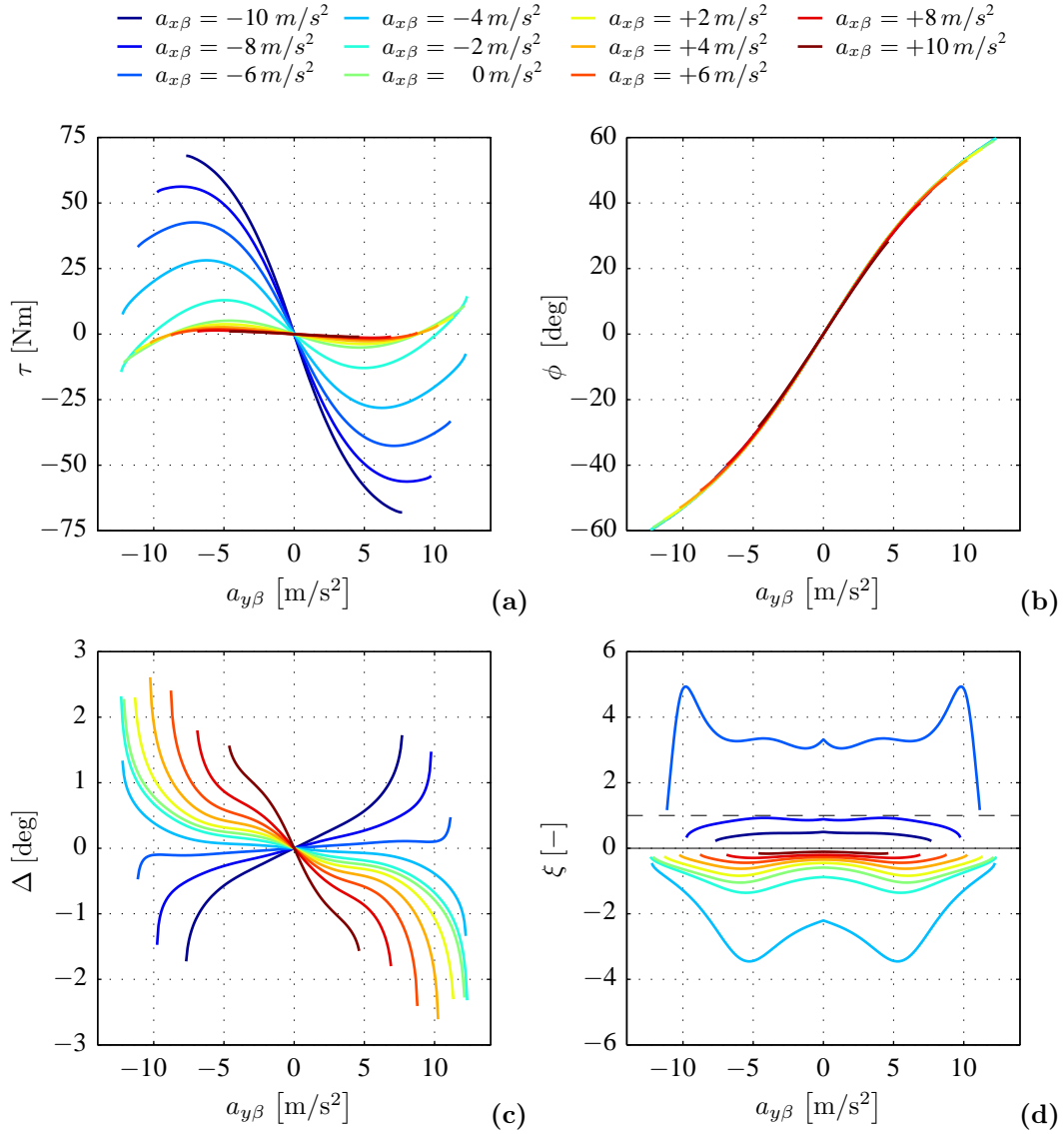


Figure 4.16: Effect of the longitudinal acceleration at 40 m/s: steering torque and main kinematic variables. (a) Steering torque. (b) Roll angle. (c) Kinematic steering angle. (d) Steering ratio.

becomes oversteering in a small range of decelerations and exhibits a countersteering behavior in the whole range of positive accelerations. Hence, it is clear that the longitudinal acceleration drastically changes the directional behavior of the motorcycle, making it understeer during braking and oversteer in acceleration. This strong sensitivity is due to the combined use of the tyres. The presence of longitudinal forces reduces the front cornering stiffness during braking, hence increasing the understeering character of the vehicle, whereas the opposite occurs in acceleration.

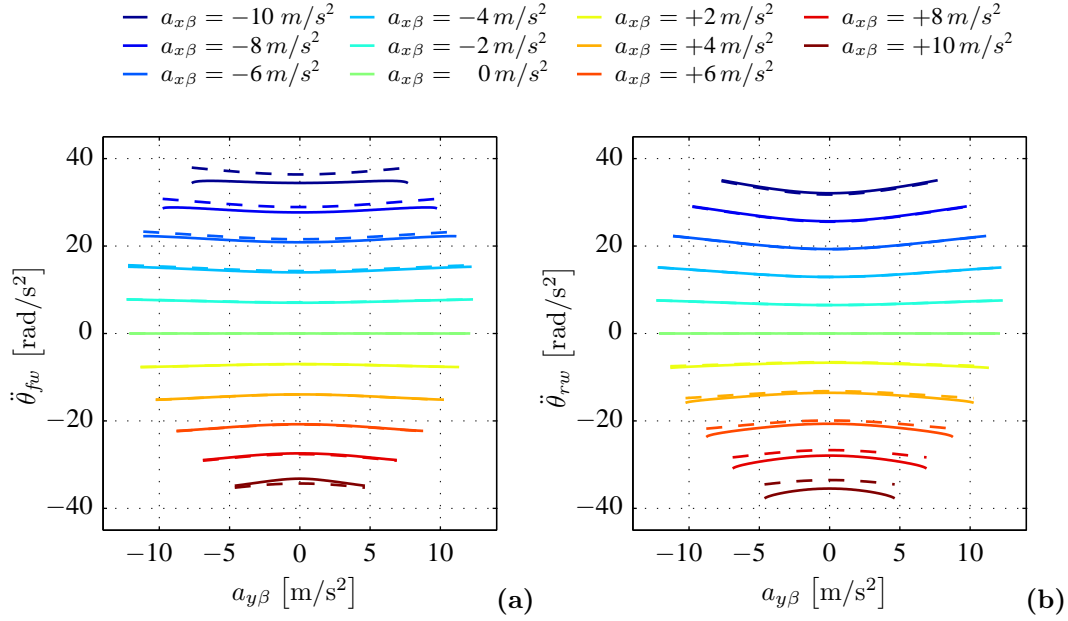


Figure 4.17: Effect of the longitudinal acceleration at 40 m/s: wheel acceleration. (a) Front wheel. (b) Rear wheel.

We finish this section by exploring the acceleration constraint defined in Eq. 4.17. This equation guarantees that the acceleration of the wheels is consistent with the longitudinal acceleration imposed to the motorcycle. Without it, both wheels would show no acceleration in the quasi-steady state solution. Essentially, we define the acceleration of each wheel according to the following expression⁶

$$\ddot{\theta} = -(1 + \kappa) \frac{\dot{V}_x}{\rho} \quad (4.35)$$

where κ is the slip ratio, ρ is the effective rolling radius, V_x is the forward velocity of the contact point and $\ddot{\theta}$ is the angular acceleration of the wheel with respect to the ground.

Fig. 4.17 shows the acceleration of the front and rear wheels for different values of the longitudinal acceleration. The solid lines are obtained by using the full constraint while the dashed lines are obtained by neglecting the longitudinal slip κ . Based on the results, we can conclude that the effect of the tyre slip is important at high accelerations and therefore must be considered. The change in the input configuration between braking and thrust causes the front tyre to slip during braking ($a_{x\beta} < 0$), whereas the rear tyre slips during thrust ($a_{x\beta} > 0$).

⁶We have adapted the constraint to the current quasi-steady state conditions by removing the term $\dot{\rho}V_x/\rho^2$ and replacing Ω by $\dot{\theta}$.

The small sensitivity with respect to the lateral acceleration is due to the shape of the tyre. As the lateral acceleration increases, so does the roll angle; this reduces the rolling radius and consequently increases the acceleration of the wheel as per Eq. 4.35.

4.5.2 Effect of roll motion

In this section we assess the effect of the roll rate $\dot{\phi}$ and its derivative, the roll acceleration $\ddot{\phi}$. It is clear that both represent a non-stationary condition as the vehicle cannot roll indefinitely. Therefore, as with the longitudinal acceleration, we need to solve a quasi-steady state problem. To do so, we only have to modify the vector of imposed derivatives ξ by setting ξ_4 and ξ_5 according to Table 4.4. It is convenient, however, to study each parameter independently in order not to combine their effects, which would unnecessarily complicate the interpretation of the results. For the same reason, we also set the longitudinal acceleration to zero in the subsequent analysis.

Roll rate

When the motorcycle leans, the roll angle goes through three successive phases: acceleration, constant speed and deceleration. Consequently, since the roll motion is continuous, the highest roll rate always occurs when its derivative vanishes. This condition is, in fact, a good choice for the present analysis since the roll rate is maximum and there is no roll acceleration.

Generally, the maximum roll rate is reached at low roll angles. For instance, in a direction change the motorcycle rolls from left to right or viceversa. In this type of maneuver the maximum rate is reached in the vicinity of the upright condition. During a corner entry, on the other hand, the motorcycle rolls from the upright position to a final inclination that can reach up to 60 deg. In this case, the maximum rate is usually observed halfway between the initial and final roll angles. After this point, and as the motorcycle approaches the desired inclination, the roll rate reduces progressively until it eventually vanishes. In view of this, and for the sake of simplicity, we can restrict our analysis to roll angles lower than 30 deg. It is also important to note that the effect of the roll rate is not symmetric with respect to the lateral acceleration, i.e. a positive roll rate has a different effect on right and left corners.

Next we perform a sensitivity study by increasing the roll rate from 0 to 120 deg/s as the motorcycle travels at a constant speed of 25 m/s. It is useful to recall that the roll rate is defined as positive when the motorcycle rolls from left to right.

Fig. 4.18 shows the effect that the roll rate has on the tyre forces. We can use the reduced equations derived in Appendix A to interpret the results. Unlike the longitudinal acceleration, the roll rate not only affects the load transfer but also the total force

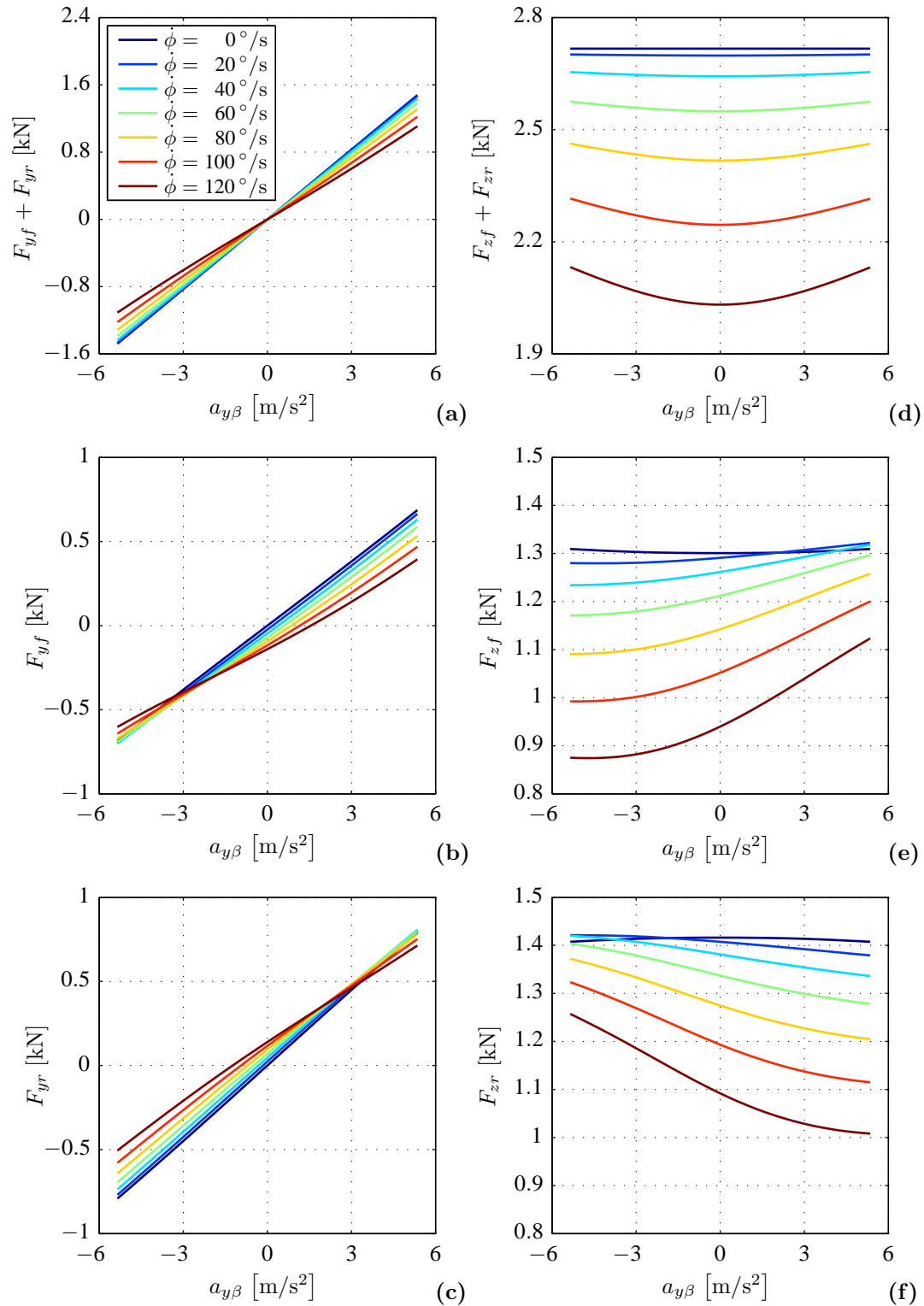


Figure 4.18: Effect of roll rate at 25 m/s: tyre forces. (a) Total lateral force applied by the tyres. (b) Front lateral force. (c) Rear lateral force. (d) Total vertical force applied by the tyres. (e) Front vertical force. (f) Rear vertical force.

exerted by the tyres. By removing the terms that are not significant for the current analysis from Eq. A.6, we get the following expression⁷,

$$F_{yf} + F_{yr} = ma_y^{cg} \simeq m(a_{y\beta} - \dot{\phi}^2 h s_\phi) \quad (4.36)$$

which states that the sum of the lateral forces generated by the front and rear tyres is equal to the mass of the vehicle times the lateral acceleration of its center of gravity.

Let's examine the right hand side in detail. The first term inside the parenthesis stands for the lateral acceleration of the path point \mathbf{P} , see Fig.4.2. The second term, on the other hand, represents the centripetal acceleration associated to the roll rate. These two terms allow us to explain Fig. 4.18a, where the sum of the lateral forces is depicted as a function of the lateral acceleration for different values of the roll rate. Firstly, it follows from the above expression that the slope of the stationary solution ($\dot{\phi}=0$) is equal to the mass of the vehicle. And secondly, we can also conclude that the roll rate reduces the total lateral force required to reach a given lateral acceleration.

The lateral force is distributed between the front and rear tyres according to the distance between the centre of gravity and the respective contact patches, which leads to a static force distribution close to 50% for our reference motorcycle. In addition to this, there exists a load transfer between the front and the rear axles that can be approximated by the following expression,

$$\Delta F_y \simeq \frac{F_{ax} h s_\phi}{a+b} - m \frac{2\dot{\psi}\dot{\phi}h^2 c_\phi s_\phi}{a+b} - \frac{(\mathcal{I}_{rw}\dot{\theta}_{rw} + \mathcal{I}_{fw}\dot{\theta}_{fw})\dot{\phi}c_\phi}{a+b} \quad (4.37)$$

which can be derived by simplifying Eq. A.17 to suit the current analysis conditions. Note that a positive variation indicates an increase in the rear force and a reduction of the front. The amount of force that is transferred depends on three different factors: the aerodynamic drag, that does not depend on the roll rate; the coriolis effect, which originates due to the combined rotation around the yaw and roll axis; and the gyroscopic moment induced by the rotation of the wheels. This last term is dominant, especially near the upright position, and tries to turn the motorcycle towards the right if the roll rate is positive and viceversa⁸.

The effect of the roll rate on the lateral forces depends therefore on whether the vehicle is entering or exiting a turn as observed in Figs. 4.18b and 4.18c. Note that the roll rate is always positive in the graphs. When the motorcycle rolls into the

⁷We have assumed that $c_\Delta \simeq 1$ and $c_\beta \simeq 1$ since the effective steering angle Δ and the sideslip angle of the vehicle β are generally small according to Figs. 4.6b and. 4.6c.

⁸Let's remember that the wheel speeds, $\dot{\theta}_{rw}$ and $\dot{\theta}_{fw}$, are always negative by definition. As a result the term $-(\mathcal{I}_{rw}\dot{\theta}_{rw} + \mathcal{I}_{fw}\dot{\theta}_{fw})\dot{\phi}c_\phi$ has the same sign as the roll rate.

corner ($a_{y\beta} > 0$) the gyroscopic moment decreases the front lateral force and increases the rear. This has an important implication on the directional behavior of the vehicle, which becomes more oversteering. The opposite effect is observed when the motorcycle rolls out of a corner ($a_{y\beta} < 0$). The steering ratio, shown in Fig. 4.19d, confirms this conclusion.

As far as the vertical forces are concerned, we can derive the following expression from Eq. A.7,

$$F_{zf} + F_{zr} = mg - ma_z^{cg} = mg - m\dot{\phi}^2 hc_\phi \quad (4.38)$$

that states that the sum of the vertical loads is equal to the difference between the weight of the vehicle and the centrifugal force generated by the roll rate. It is clear from the above that the roll rate reduces the tyre loads. This effect is symmetric with respect to the lateral acceleration and increases quadratically with the roll rate as shown in Fig. 4.18d, where the sum of the vertical forces is depicted as a function of the lateral acceleration for multiple values of the roll rate.

Similarly to the lateral forces, the distribution of the vertical loads depends mainly on three factors, namely the aerodynamic drag, the coriolis term associated to the motion around the yaw and roll axis, and the gyroscopic moment generated by the wheels.

$$\Delta F_z \simeq \frac{F_{ax} hc_\phi}{a+b} - m \frac{2\dot{\psi}\dot{\phi} h^2 c_\phi^2}{a+b} + \frac{(\mathcal{I}_{rw}\dot{\theta}_{rw} + \mathcal{I}_{fw}\dot{\theta}_{fw})\dot{\phi}s_\phi}{a+b} \quad (4.39)$$

As with the lateral forces, a positive value indicates an increase in the rear force and a reduction of the front. The last two terms of the above expression have the same sign and their effect depends on whether the vehicle is entering or exiting a turn. When the motorcycle rolls into the corner ($a_{y\beta} > 0$) the load transfer is negative, meaning that the front vertical force increases while the rear decreases. The opposite effect is observed when the motorcycle rolls out of a corner ($a_{y\beta} < 0$). This can be noticed in Figs. 4.18e and 4.18f, where the symmetry shown in Fig. 4.18d is broken due to the load transfer.

The roll rate has also a big impact on the steering torque applied by the rider. The gyroscopic effect of the front wheel generates a positive torque around the steering axis that tends to rotate the handlebar towards the right when the roll rate is positive, thus helping the motorcycle to change direction. As a consequence, the reaction torque exerted by the rider τ becomes more negative with respect to the steady state conditions as shown in Fig. 4.19a. The projection of the gyroscopic moment on the steering axis yields,

$$\Delta\tau \simeq -\mathcal{I}_{fw}\dot{\theta}_{fw}\dot{\phi}c_\epsilon \quad (4.40)$$

where ϵ is the caster angle of the motorcycle. We can observe how the torque variation increases linearly with the wheel speed and the roll rate; furthermore, its value is not

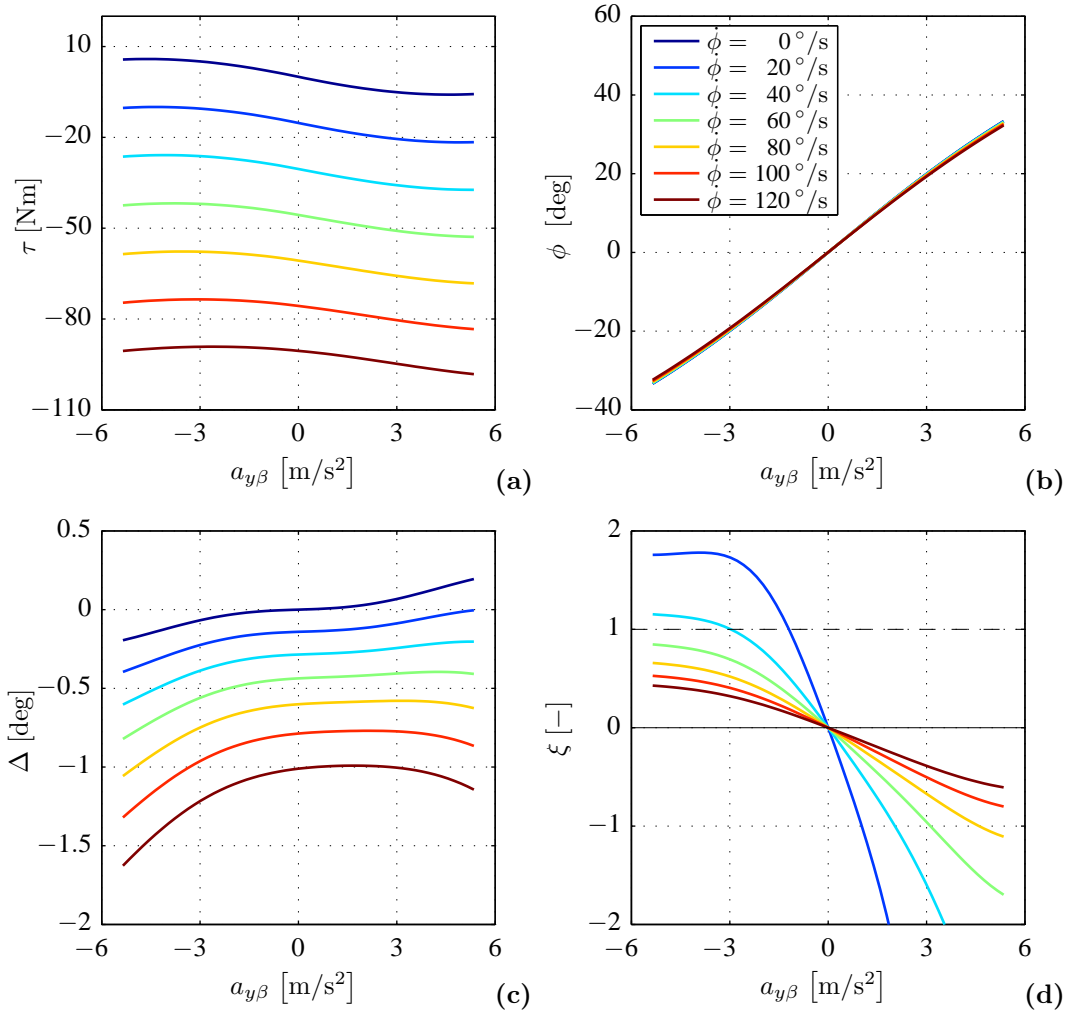


Figure 4.19: Effect of roll rate at 25 m/s: steering torque and main kinematic variables. (a) Steering torque. (b) Roll angle. (c) Kinematic steering angle. (d) Steering ratio.

affected by the roll angle. We can conclude that the effect of the roll rate is considerable even at moderate speeds as this example is carried out at 25 m/s (90 km/h). It is therefore essential to consider it in order to obtain an accurate prediction of the steering torque.

Fig. 4.19b shows that the roll angle ϕ is not very sensitive to the roll rate. The directional behaviour of the motorcycle, on the other hand, is strongly influenced by the roll rate as shown in Figs. 4.19c and. 4.19d. Reading each graph from left to right, we can interpret the results as a quasi-steady state direction change, i.e. a maneuver where the motorcycle goes from a left to a right corner at a constant roll rate. We observe how the steering angle Δ becomes more negative as the roll rate increases. This

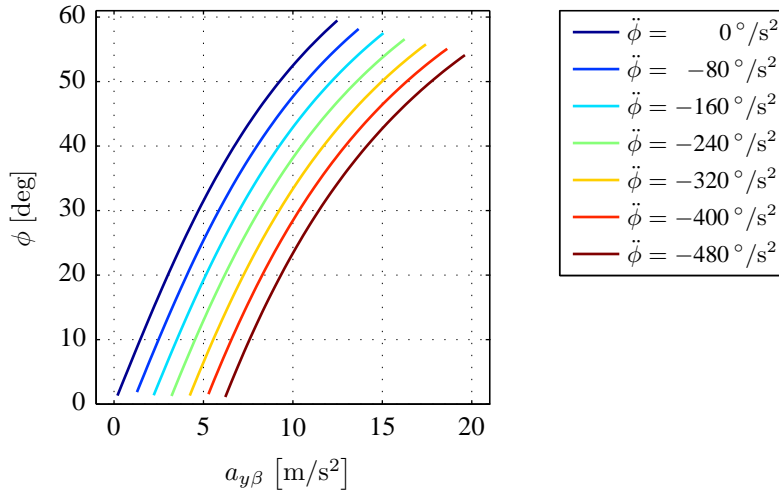


Figure 4.20: Effect of roll acceleration at 25 m/s: roll angle.

means that during the left corner (corner exit), the roll rate has an understeering effect as the rider has to increase the rotation of the handlebar towards the inside of the corner. The opposite happens during the right corner (corner entry). In this case, the roll rate has a countersteering effect, meaning that rider has to increase the rotation of the handlebar towards the outside of the corner. This behaviour is reflected in the steering ratio, which changes sign when the motorcycle goes through the vertical position.

Roll acceleration

In this case, unlike the roll rate, we cannot restrict the analysis to small roll angles. For instance, during a slalom maneuver the maximum roll deceleration takes place when the roll angle is maximum and the roll rate changes sign, e.g. when the motorcycle stops rolling towards the right and starts rolling in the opposite direction. We can use this condition, i.e. high roll acceleration and null roll rate, to investigate the effect that the roll acceleration has on the behaviour of the motorcycle.

Next we perform a sensitivity study by varying the roll acceleration from 0 to -480 deg/s^2 during a right corner. In other words, we study the effect of the roll acceleration when the motorcycle is inclined to the right and starts rolling to the left. In the subsequent analysis we use a speed of 25 m/s.

The main effect of the roll acceleration is a reduction in the roll angle needed to obtain a given lateral acceleration as observed in Fig. 4.20. Remember that the term $a_{y\beta}$ does not represent the lateral acceleration of the centre of mass but the acceleration of the path point \mathbf{P} , i.e. the point that follows the imposed trajectory as shown in Fig.4.2.

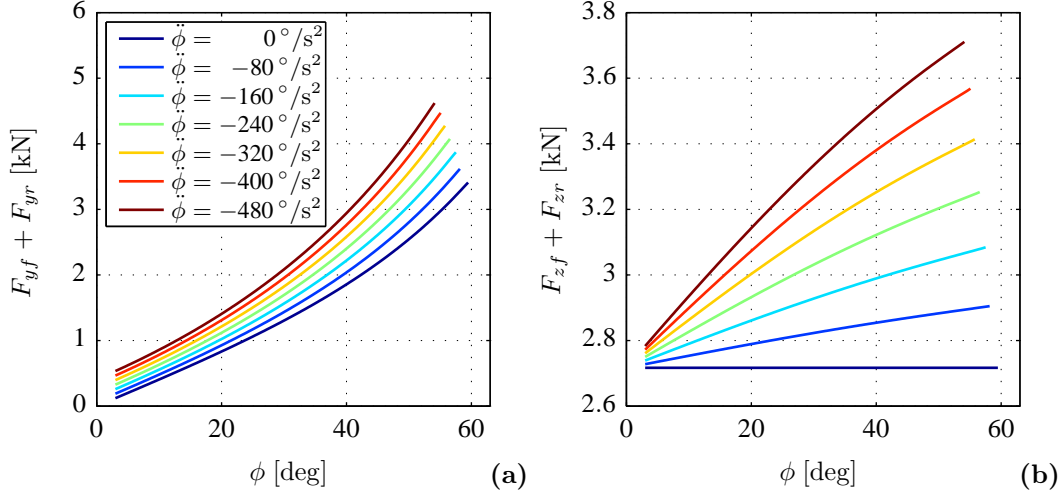


Figure 4.21: Effect of roll acceleration at 25 m/s: tyre forces. (a) Total lateral force applied by the tyres. (b) Total vertical force applied by the tyres.

Hence it follows from the results that, for the same roll angle, higher roll accelerations lead to tighter local trajectories as the lateral acceleration of point \mathbf{P} increases.

It is possible to explain this behaviour by means of the reduced equations derived in Appendix A, and, in particular, by making use of Eq. A.21. If we neglect the gyroscopic terms, which are of secondary importance in this case, and assuming that the sideslip angle of the vehicle β is small, i.e. $a_{x\psi}=0$ and $a_{y\psi}=a_{y\beta}$, we obtain the following expression,

$$a_{y\beta} \simeq - \left(1 + \frac{\mathcal{I}_x}{mh^2} \right) \frac{h}{c_\phi} \ddot{\phi} + g \tan \phi \quad (4.41)$$

where \mathcal{I}_x is the overall roll inertia of the motorcycle. It follows from the above that, for a given roll angle, the lateral acceleration of the path point $a_{y\beta}$ depends linearly on the roll acceleration $\ddot{\phi}$, which is consistent with the results obtained with the full model in Fig.4.20. As a matter of fact, note that all the lines in the graph are uniformly distributed along the x-axis.

As far as the tyre forces are concerned, the roll acceleration does not produce any load transfer. It simply modifies the overall force generated by the tyres along both lateral and vertical directions. Fig. 4.21 depicts the tyre forces as a function of the roll angle to allow for a more meaningful comparison. From the reduced model, Eq. A.17, we get the following expression for the overall lateral load

$$F_{yf} + F_{yr} = ma_y^{cg} \simeq m(a_{y\beta} + \ddot{\phi}hc_\phi) \quad (4.42)$$

which increases with the roll deceleration as the effect of the lateral acceleration $a_{y\beta}$,

defined in Eq. 4.41, is dominant. For the overall vertical load, on the other hand, we can write the following expression by simplifying Eq. A.17

$$F_{zf} + F_{zr} = mg - ma_z^{cg} \simeq mg - m\ddot{\phi}hs_\phi \quad (4.43)$$

which shows why the vertical loads also increase with the roll deceleration.

Due to the absence of load transfer, the effect of the roll acceleration on the directional behaviour of the motorcycle is very small. There exists, however, a small effect on the steering torque. As the front lateral force increases, so does the aligning moment, which becomes more negative, and forces the rider to slightly increase the torque on the handlebars in the opposite direction.

4.6 Concluding remarks

The quasi-steady state equilibrium of complex vehicle models may be computed in time domain by increasing the vehicle speed and the steering angle until the desired condition is reached [99, 100]. This approach, however, presents one significant drawback when it comes down to single track vehicles. Vehicles such as bicycles and motorcycles are intrinsically unstable and, consequently, a steering controller is required to stabilize the solution [51]. Furthermore, this process is slow and does not guarantee that all desired conditions (e.g. curvature, velocity, etc) are accurately met at the same time.

As an alternative to the time integration approach and other existing methods, in the first part of this chapter we introduced a methodology for the quasi-steady state analysis of motorcycles that avoids the drawbacks mentioned above. Basically, given a specific set of motion conditions, we solve the quasi-steady state equilibrium by transforming the differential equations that govern the motion of the motorcycle into an equivalent system of algebraic equations.

Depending on how the motion conditions are chosen, the solution may represent a pure steady state equilibrium, also known as stationary solution, or a generic quasi-steady state trim. The stationary solution is fully defined by the radius of the corner and by the speed of the motorcycle. In particular, it refers to the situation where the motorcycle travels along a circular path at constant speed. The quasi-steady state trim, on the other hand, represents a generic set of states and derivatives that fulfill the motion equations at a certain time instant. The prefix *quasi* is used to emphasize that the solution does not represent a pure stationary condition as the equations include general velocity and acceleration terms, e.g. roll rate, longitudinal acceleration, etc.

The steady state motion of the motorcycle model was thoroughly studied in the second part of the chapter. Results show how the most relevant variables (e.g. steering

angle, tyre forces, etc) vary as a function of the speed of the vehicle and of the curvature of the trajectory. Of particular interest is the high sensitivity of the lateral and longitudinal control variables with respect to the cornering conditions.

We have shown that the steering torque required to follow a given trajectory changes drastically with the vehicle speed and the corner radius, with the map that relates this three variables being highly nonlinear. In addition to this, a power balance analysis has allowed us to determine how the engine power is dissipated. Results show that the aerodynamic forces dissipate most of the power at high speeds, whereas the power dissipated by the tyres becomes only significant at low speeds and high curvatures. It is especially interesting that the tyre aligning/twisting moments of each tyre may dissipate more than 3 kW at high speeds.

The last part of the chapter focuses on the quasi-steady state motion of the motorcycle. In this section we assessed the effect of the most relevant derivatives, namely the longitudinal acceleration and the roll derivatives. The aim of this analysis was to determine to what extent these three terms modify the solution obtained in stationary conditions.

Results show that the longitudinal acceleration not only has a great impact on the longitudinal control of the motorcycle, as it is evident, but also on the steering torque. This happens especially during braking. The reason lies in the front braking force, which generates a moment around the steering axis that tends to rotate the wheel towards the inside of the corner. An accurate modeling of the cross section of the tyre has proven to be essential in order to capture this phenomenon.

Another important effect of the longitudinal acceleration is related to the combined use of the tyres, which tends to increase the understeering character of the motorcycle in braking and makes it more oversteering in acceleration. In addition to this, the longitudinal acceleration has a significant impact on the tyre loads. Motorcycles generally exhibit a significant load transfer due to their high center-of-gravity-to-wheelbase ratio. As the loads change, so do the driving and sideslip stiffness of the tyres, which in turn have a big effect on the dynamic response of the vehicle.

As far as the roll derivatives are concerned, they have a strong effect on the lateral control of the vehicle. In particular, the steering torque is highly sensitive to the roll rate. When the motorcycle approaches a corner, the gyroscopic effect of the front wheel tends to rotate the handlebar towards the inside of the corner, thus helping the vehicle to change direction. This effect increases with the roll rate. The roll acceleration, on the other hand, affects mainly the roll angle. It follows from the quasi-steady state analysis that, for the same roll angle, higher roll accelerations allow the motorcycle to follow tighter trajectories.

The sensitivity analysis performed in this chapter provides an insight on how challenging the control of the motorcycle is. Additionally, it permits us to anticipate some preliminary requirements of the virtual rider. It is essential that the controller adapts to the actual conditions of the motorcycle, hence accounting for the corner radius, the speed of the vehicle, its acceleration and the roll derivatives. Furthermore, given the variability of the control actions, it is expected that a feedforward term will be of great benefit to the control strategy. In the next chapter we extend the quasi-steady state approach to solve the motion of the motorcycle along continuous manoeuvres, thus providing a suitable feedforward term as well as a reference manoeuvre around which we will build the control strategy in Chapter 6.

*In automotive design, a straight line
is the most awkward path to follow
between two points.*

Maurice Olley

Chapter 5

Quasi-steady state analysis of continuous manoeuvres

Here we extend the methodology introduced in the previous chapter with the aim of solving the quasi-steady state motion of the motorcycle along continuous manoeuvres. Fundamentally, this means that, instead of finding the vehicle trim for a predefined set of conditions, in this chapter we find the control inputs needed to drive the vehicle along a given path in a quasi-steady state fashion. The curvature of the trajectory and the speed profile of the motorcycle constitute the main inputs of this new problem.

The chapter is structured in two parts. In the first part we use a dynamic inversion approach to estimate the roll dynamics of the motorcycle along the target trajectory. The results of the estimation problem are then used in the second part of the chapter to develop a solution procedure for the quasi-steady state analysis of continuous manoeuvres. The resulting strategy is demonstrated by solving two different manoeuvres, a slalom test and a chicane. Finally, some conclusions regarding the application of the proposed methodology to the development of the virtual rider are presented and discussed.

5.1 Roll dynamics estimation

According to the sensitivity study presented in Section 4.5.2, the effect of roll dynamics may become significant and cannot be generally neglected when studying the behaviour of the motorcycle. This is especially true for aggressive manoeuvres where the direction of travel changes quickly, e.g. slalom tests, lane change manoeuvres, etc.

Let's recall that such study was performed for a predefined set of roll rates and roll accelerations, which were selected to cover the working range of the motorcycle. In this chapter, in contrast, we consider the solution of continuous manoeuvres, i.e. the target is to solve the quasi-steady state equilibrium of a motorcycle that travels along a generic path. The most significant difference in this case is that the roll motion of the vehicle is not known a priori. Hence, as part of the novel solution procedure introduced in this chapter, it is necessary to estimate the roll dynamics of the motorcycle.

To that end, we can exploit the fact that the trajectory, the speed of the motorcycle and its roll motion are strongly related. Essentially, we are interested in the following question. Given an arbitrary path and a feasible speed profile, how would the roll angle evolve if the motorcycle perfectly follows the desired targets? In the following sections we consider that both the trajectory and the speed profile are known; they constitute the inputs of the extended quasi-steady state problem.

5.1.1 Problem formulation

We can pose the estimation of the roll rate and the roll acceleration as a dynamic inversion problem [47, 159]. The inversion consists in determining a set of feasible states and controls such that the system follows a preassigned reference trajectory. For that purpose, we use the simplified model shown in Fig. 5.1 as, despite its simplicity, it includes the most important terms that govern the roll dynamics of the motorcycle. The main advantage of such a simple model is that it leads to a fast and efficient implementation of the inversion problem while providing a good estimation of the roll angle and its derivatives.

NOTE: Sections 5.1.1, 5.1.2, 5.1.3 and 5.2 are protected by a confidentiality agreement, according to the decision of the Doctorate Commission of the University Miguel Hernández dated September 19, 2016.

5.2.1 Results: slalom test

Generally, a slalom test consists of multiple lined-up cones that must be avoided by the motorcycle. In our case, let's assume that such cones are equally distributed along a straight line at a distance of 12.5 m from one another. In order to complete the manoeuvre, the vehicle is driven along the trajectory depicted in Fig. 5.6a at a constant speed of 23.5 m/s as shown Fig. 5.6b.

The acceleration of the motorcycle is depicted in Fig. 5.6c, where $a_{x\beta}$ and $a_{y\beta}$ are the longitudinal and lateral acceleration of the vehicle as defined in Fig. 4.1. There are two points to be noted here. First, the lateral acceleration reaches significant values

during the manoeuvre, exceeding 14 m/s^2 at the points of maximum curvature. And second, its value varies quickly, changing sign every 12.5m. These two points make the slalom test an aggressive manoeuvre as far as the lateral behaviour of the vehicle is concerned.

Under these circumstances, it is essential to consider the roll rate and the roll acceleration in the quasi-steady state solution of the motion equations. To prove this, we compare two different sets of results. The first is the legitimate solution obtained by including the roll derivatives as per Table 5.1. The second solution, on the other hand, is obtained by neglecting their effect. The imposed values of the roll rate and roll acceleration are shown in Figs. 5.6d and 5.6e for both cases. Note that the legitimate solution is depicted in blue, whereas the solution obtained by neglecting the roll derivatives is depicted in red. Let's first focus on the legitimate solution, ignoring for a moment the fact that the red curves are not complete.

The response of the vehicle to this particular manoeuvre is clearly periodic, with a fundamental period equal to two times the distance between cones. In Fig. 5.6f we can observe that the motorcycle rolls to the right ($\phi > 0$) in order to avoid the first cone, then it rolls to the left ($\phi < 0$) at the second, and so on. As a consequence, the sign of the roll angle alternates during the manoeuvre, with the maximum roll angle matching the position of the cones. These are placed at 62.5 m, 75 m, 87.5 m, 100 m, etc. Similarly, the lateral displacement of the motorcycle is also maximum at these points. However, its phase is shifted 180 degrees with respect to the roll angle, i.e. the vehicle moves to the right at the same time it rolls to the left and viceversa.

The torque applied by the rider during the manoeuvre is shown in Fig. 5.6g. Let's remember that the steering torque is defined as positive if the rider tries to steer towards the right. Due to the high roll rate, the steering torque is dominated by the gyroscopic effect of the front wheel and therefore, in agreement with Eq. 4.40, its magnitude is proportional to the wheel speed and to the roll rate, while its phase is shifted 180 degrees with respect to the latter.

Figs. 5.7a and 5.7b show the control torques needed to follow the desired speed profile. By definition, negative torques tend to accelerate the vehicle while positive torques have the opposite effect. Interestingly, we can observe that such torques are not constant despite the fact that the imposed longitudinal acceleration $a_{x\beta}$ is null. In order to understand this behaviour, we must recall that $a_{x\beta}$ represents the acceleration of the path point \mathbf{P} , which is located at the road level as per Fig. 4.2. However, it is not the acceleration of this point what decides the control torques but that of the centre of gravity. In essence, the control torques are calculated so that the resulting longitudinal forces at the tyres balance the product of the vehicle mass times the longitudinal

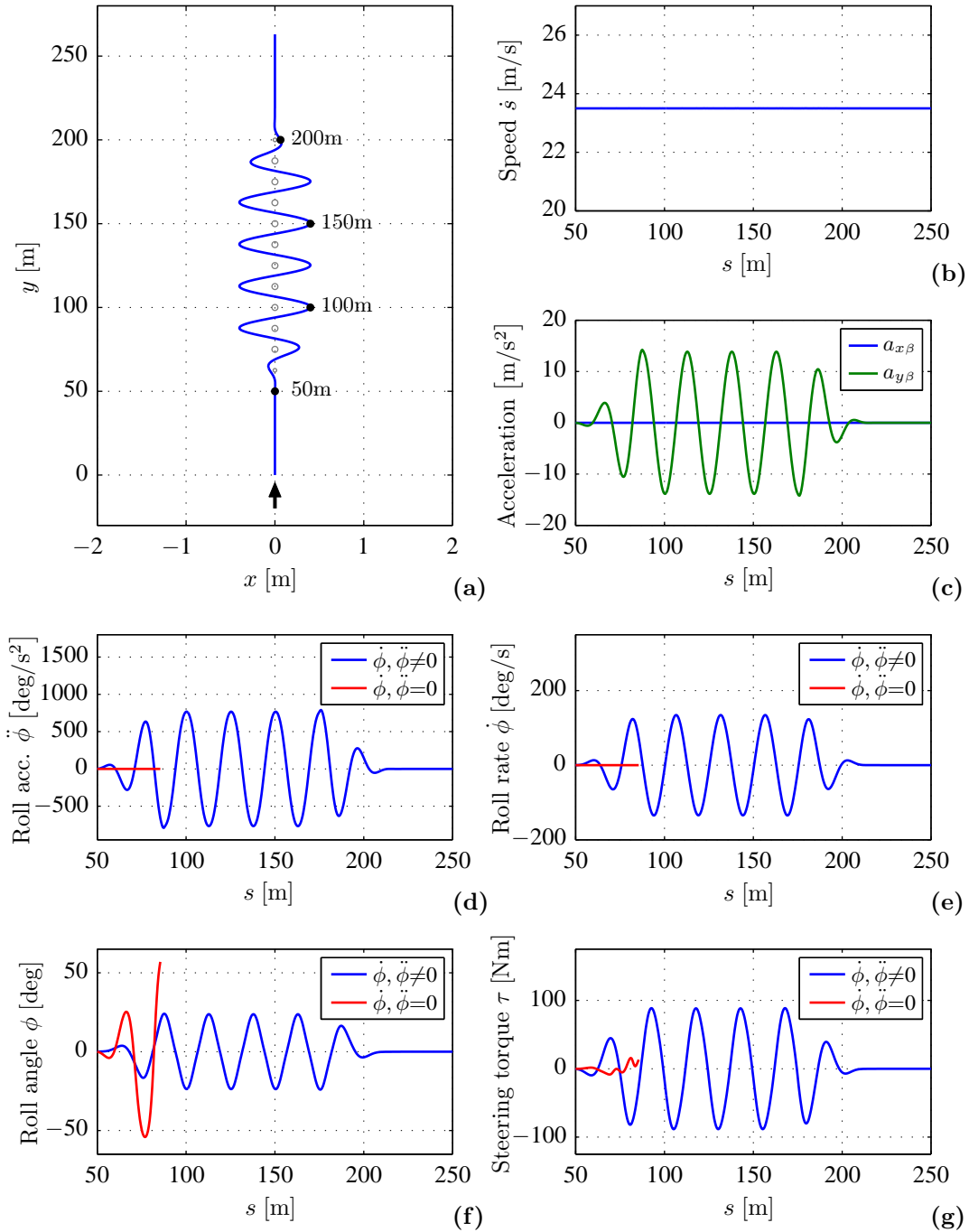


Figure 5.6: Quasi-steady state results: slalom test. a) Trajectory. b) Curvilinear speed. c) Acceleration on the tangent frame \mathbf{T}_β . d) Roll acceleration. e) Roll rate. f) Roll angle. g) Steering torque.

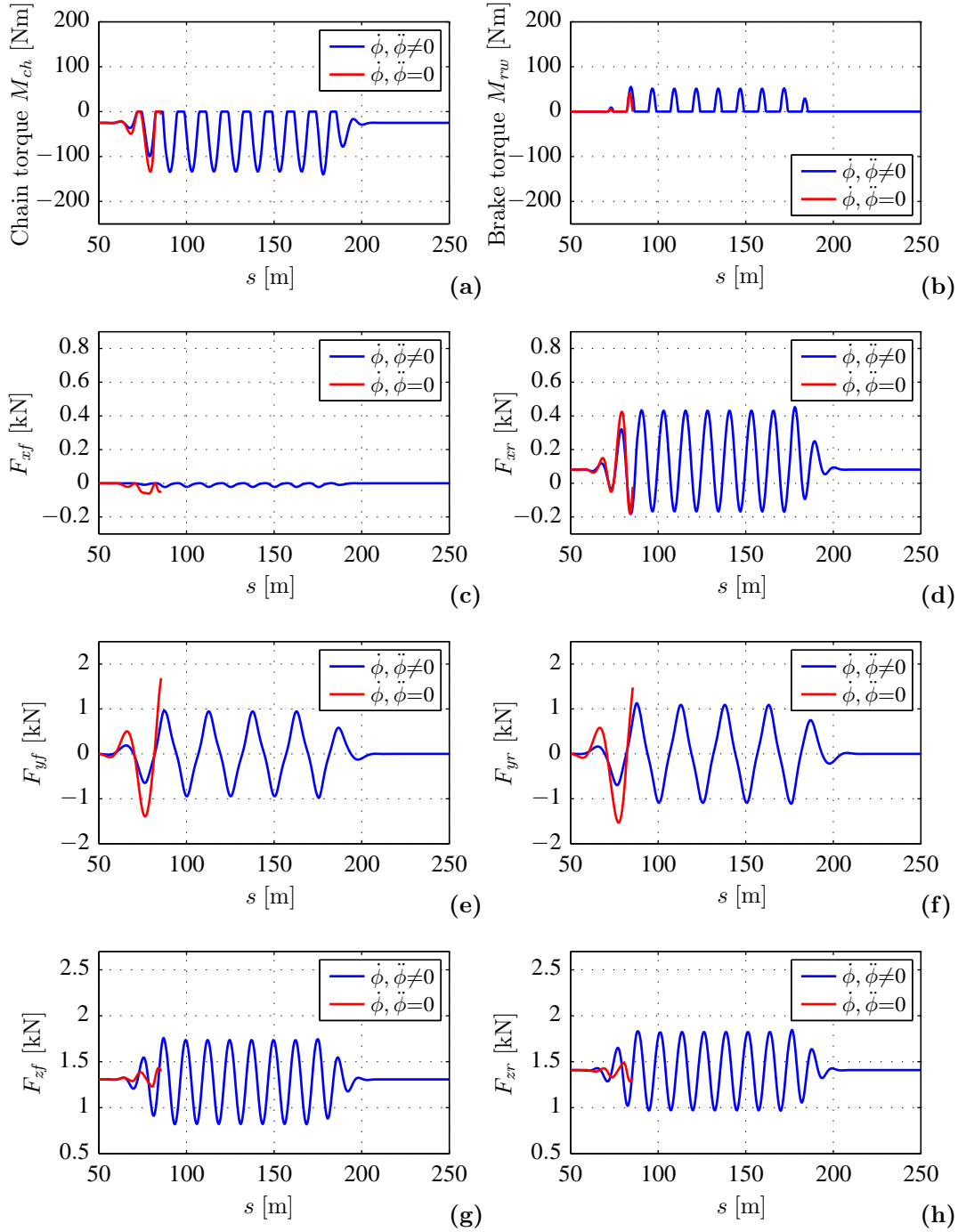


Figure 5.7: Quasi-steady state results: slalom test. a) Chain torque. b) Brake torques. c) Front tyre longitudinal force. d) Rear tyre longitudinal force. e) Front tyre lateral force. f) Rear tyre lateral force. g) Front tyre vertical force. h) Rear tyre vertical force.

acceleration of its centre of gravity.

We can use the reduced model developed in Appendix A to explain why the control torques fluctuate during the slalom manoeuvre. By using Eq. A.1, and since $a_{x,\beta}$ is null, we can write the acceleration of the centre of gravity of the vehicle along its longitudinal axis as the sum of three different terms.

$$a_x^{cg} = a_{y\beta} s_\beta - \ddot{\psi} h s_\phi - 2\dot{\psi}\dot{\phi} h c_\phi \quad (5.19)$$

The first is simply the projection of $a_{y\beta}$ on the longitudinal axis of the motorcycle, the second represents the contribution of the yaw acceleration $\ddot{\psi}$ and the last is the Coriolis effect generated by the combined motion of the motorcycle around the yaw and roll axes. Although all terms contribute to the fluctuation of the control torques, the Coriolis effect is dominant over the other two.

Before each apex⁴ the yaw rate and the roll rate have the same sign, thus causing the Coriolis term to be negative. After the apex, the sign of the roll rate changes and the Coriolis term becomes positive. This change in the acceleration is the main cause of the torque fluctuation. The rider, in order to keep constant the tangential speed, applies a braking torque before each apex and a thrust torque afterwards. As far as the brake distribution is concerned, and given that the required breaking force is small, it is convenient to brake only with the rear tyre as it helps to turn in the vehicle. This is achieved by setting $\gamma=0$ in Table 5.3.

The last six figures depict the forces applied to the tyres in the longitudinal, lateral and vertical directions. The following sign convention is used: longitudinal forces are defined as positive if they tend to accelerate the motorcycle and negative if they have a braking effect; lateral forces are positive if they push the vehicle to the right and negative if they point in the opposite direction; vertical forces are always positive. The longitudinal forces are depicted in Fig. 5.7c and 5.7d. The lateral forces are shown in Figs. 5.7e and 5.7f for the front and rear tyres respectively. Note that both of them are in phase with the roll angle, i.e. large roll angles require large lateral forces and viceversa. Lastly, the vertical forces are depicted in Figs. 5.7g and 5.7h.

If we now focus on the red curves, obtained by neglecting the roll rate and the roll acceleration, the first thing we notice is that the quasi-steady state solution does not exist for the whole manoeuvre. This is due to several factors. In first place, the lateral forces exerted by the tyres increase notably when the roll rate and the roll acceleration are not considered. Such increase in the lateral forces, together with the fact that the

⁴The word apex denotes those points of the trajectory where the curvature presents a local maxima/minima. In the slalom test the trajectory presents an apex at every cone.

vertical loads follow the opposite trend, make it impossible to solve the quasi-steady state problem as the tyres are not able to generate the required tyre forces. Furthermore, we can observe clear differences in the steering torque and in the roll angle.

It is worth noting that the roll acceleration $\ddot{\phi}$ is shifted 180 degrees with respect to the lateral acceleration of the path point $a_{y\beta}$, i.e. the lateral acceleration always points towards the inside of the corner while the roll acceleration goes in the opposite direction. This generates an additional tilting torque around the roll axis that tends to reduce the roll angle. Consequently, when the roll acceleration is neglected, the resulting roll angle increases drastically as shown in Fig. 5.6f. The steering torque, on the other hand, is dominated by the roll rate and therefore, when we neglect it, the torque required to perform the manoeuvre drops significantly as shown in Fig. 5.6g.

The slalom manoeuvre is a clear example of the big effect that the roll rate and the roll acceleration may have on the quasi-steady state analysis of the motorcycle.

5.2.2 Results: chicane

The second set of results presented here represents a racing manoeuvre along a chicane. As opposed to the slalom test, which is characterized by an aggressive lateral acceleration profile, this manoeuvre is introduced to assess the behaviour of the vehicle during combined conditions, including also an abrupt transition from acceleration to braking. In order to complete the manoeuvre, the motorcycle is driven along the trajectory shown in Fig. 5.8a at the speed specified by Fig. 5.8b.

Basically, the manoeuvre is composed of two successive corners, one to the right and one to the left. Likewise, each of these corners can be divided in two parts, which we will refer to as corner entry and corner exit. During the entry phase the longitudinal acceleration is negative and the (absolute) lateral acceleration increases. On the other hand, during the exit phase the longitudinal acceleration is positive and the (absolute) lateral acceleration decreases. These four phases are clearly shown in Fig. 5.8c. The most critical point of this manoeuvre is the transition between corners, where the motorcycle stops accelerating and starts braking. Note the discontinuity in the longitudinal acceleration at $s=250$ m.

The imposed values of the roll rate and the roll acceleration are shown in Figs. 5.8d and 5.8e, while the resulting roll angle is shown in Fig. 5.8f. We can observe that the motorcycle rolls to the right in the first corner and to the left in the second. Unlike the slalom test, the differences between the legitimate solution (blue curves) and that obtained by neglecting the roll rate and the roll acceleration (red curves) are not so obvious in most of the graphs of Figs. 5.8 and 5.9.

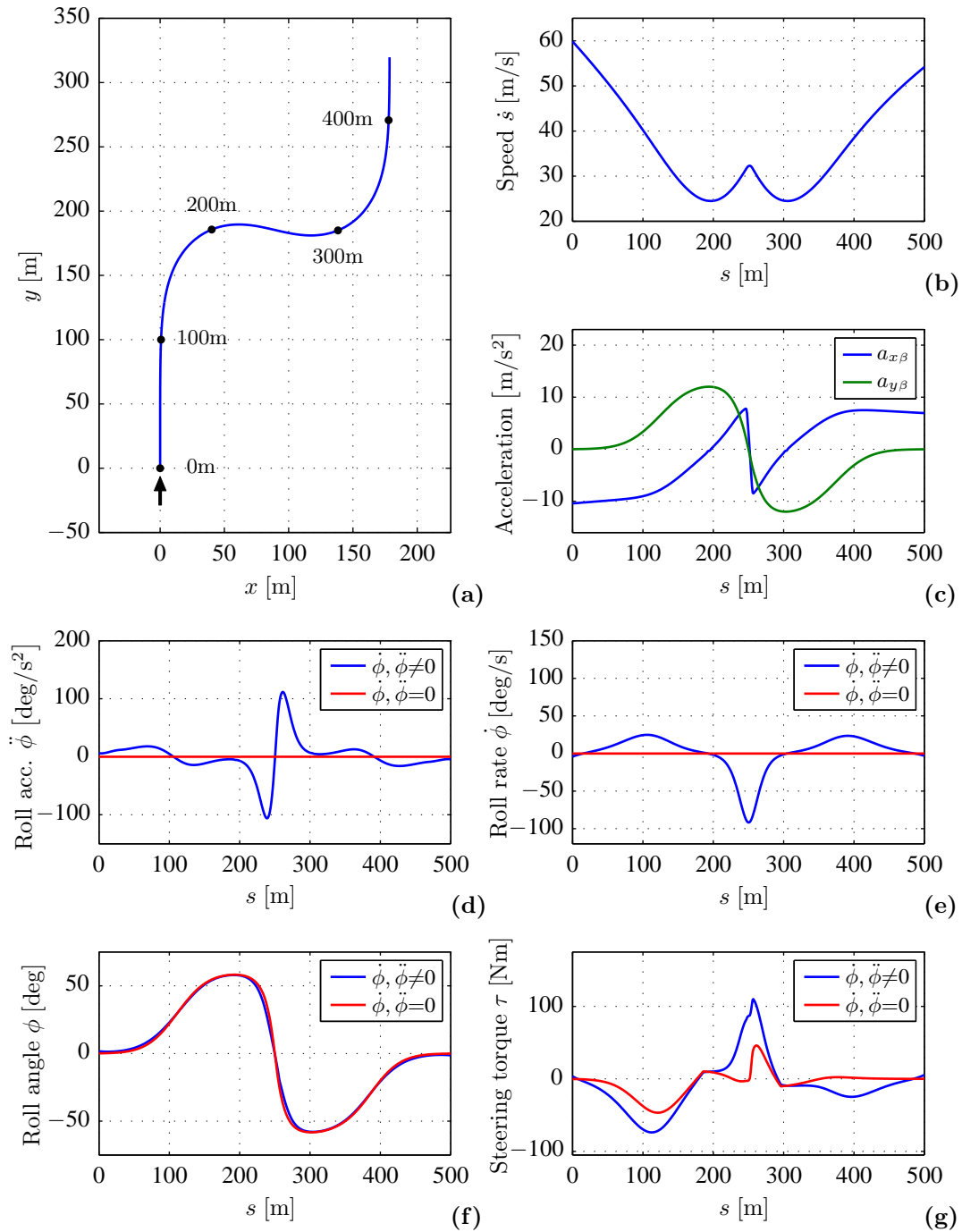


Figure 5.8: Quasi-steady state results: chicane. a) Trajectory. b) Curvilinear speed. c) Acceleration on the tangent frame \mathbf{T}_β . d) Roll acceleration. e) Roll rate. f) Roll angle. g) Steering torque.

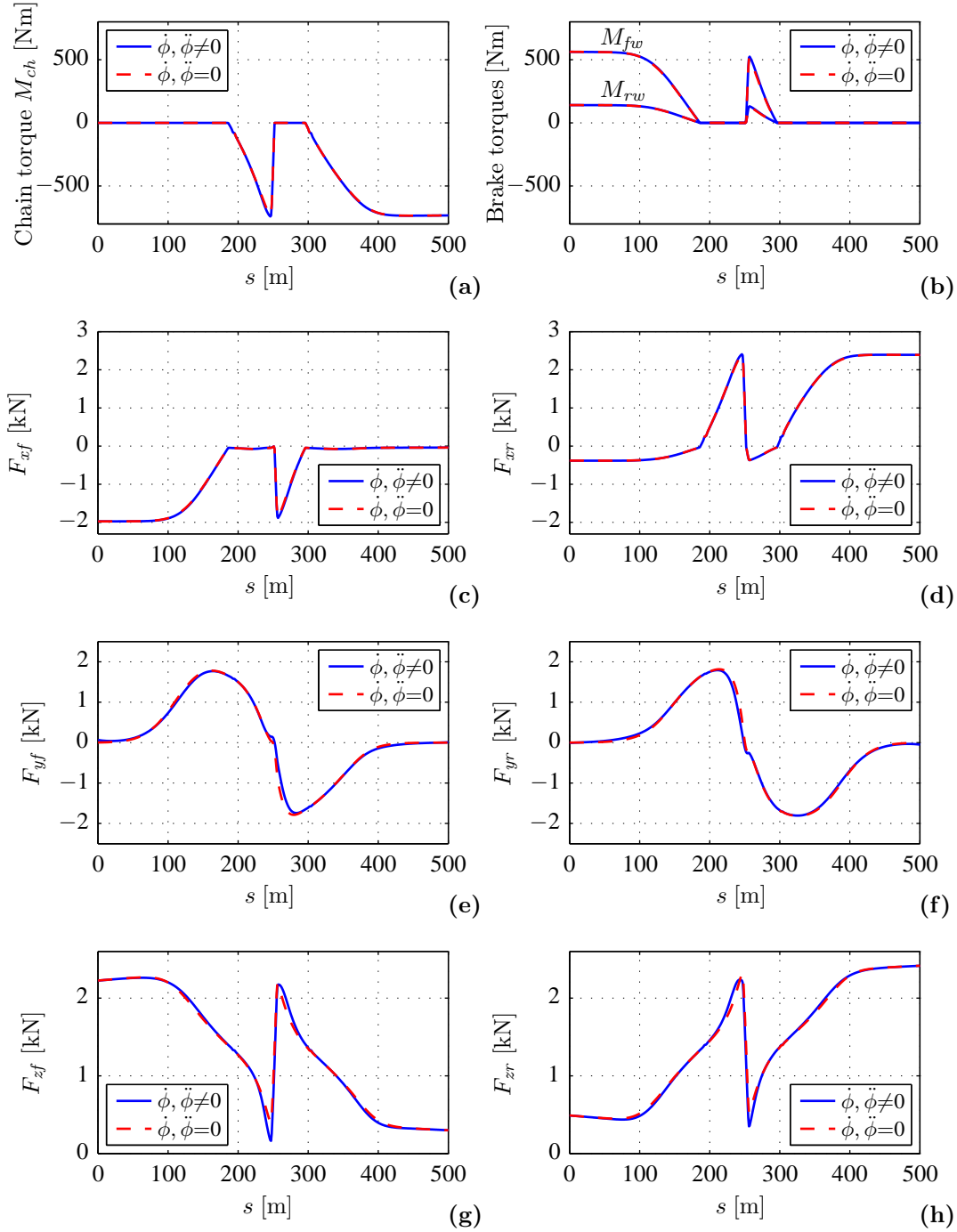


Figure 5.9: Quasi-steady state results: chicane. a) Chain torque. b) Brake torques. c) Front tyre longitudinal force. d) Rear tyre longitudinal force. e) Front tyre lateral force. f) Rear tyre lateral force. g) Front tyre vertical force. h) Rear tyre vertical force.

There are however important differences, especially during the transition between corners ($s \in [200, 300]$ m) as the roll derivatives reach their highest values in this region. We can observe in Fig. 5.8f that the roll angle computed by neglecting the roll derivatives is up to 8 degrees larger than that of the quasi-steady state solution. Such difference is mainly caused by the roll acceleration. The roll rate, on the other hand, has a significant effect on the steering torque as shown in Fig. 5.8g. It is interesting to notice that the difference between both solutions is proportional to the roll rate.

The steering torque is also very sensitive to the front braking force during the entry phase. Such force generates a twisting torque that tends to steer the vehicle towards the inside of the corner. The rider, in order to keep the trajectory, has to counteract this effect by applying a torque in the opposite direction. Hence, this leads to a negative steering torque in the first corner and a positive torque in the second. When the roll derivatives are not considered, the steering torque is dominated by this effect.

The control torques needed to follow the desired speed profile are depicted in Figs. 5.9a and 5.9b. As shown in the graphs, the engine (chain force) is used during the exit phase to accelerate the motorcycle, while the brakes are used to decelerate it in the entry phase. The braking distribution is kept constant during the whole manoeuvre, with the front tyre generating the 80% of the total braking torque.

The last six figures represent the tyre forces along the longitudinal, lateral and vertical directions. The longitudinal forces exerted by the tyres, depicted in Figs. 5.9c and 5.9d, are directly related to the control torques. The lateral forces, on the other hand, are dominated by the lateral acceleration as shown in Figs. 5.9e and 5.9f. Finally, the vertical forces from Figs. 5.9g and 5.9h show the load transfer that takes place when the motorcycle stops accelerating and starts braking. Note that at that point more than 2 kN are transferred from the rear to the front tyre, which highlights the severity of the manoeuvre.

The effect of the roll derivatives is also noticeable in the lateral and vertical forces. The quasi-steady state solution requires up to 400 N less lateral force, whereas the difference in terms of vertical load ranges between -250 N and $+200$ N. Such differences are not negligible, especially if they occur in the transition between corners, which is the most critical part of the manoeuvre.

NOTE: Section 5.2.3 is protected by a confidentiality agreement, according to the decision of the Doctorate Commission of the University Miguel Hernández dated September 19, 2016.

5.3 Concluding remarks

We have shown in this chapter that the quasi-steady state solution of the motion equations represents an efficient way to study the behaviour of the motorcycle along continuous manoeuvres.

In the first part of the chapter we set the basis to estimate the roll motion of the motorcycle along any target manoeuvre. In essence, the problem comes down to the following question: given an arbitrary path and a feasible speed profile, how would the roll angle evolve if the motorcycle perfectly follows the desired targets? To answer it, we applied a dynamic inversion approach to a simplified motorcycle model, created by synthesizing the most important terms that govern the roll dynamics of the vehicle. The main advantage of such model is that it leads to a fast and efficient implementation of the inversion problem while providing a good estimation of the roll angle and its derivatives.

In the second part of the chapter we combined the results of the inversion problem with the methodology introduced in Chapter 4 to solve the quasi-steady state motion of the motorcycle along continuous manoeuvres. This new approach was successfully tested on two different manoeuvres, a slalom test and a chicane. Interestingly, the roll derivatives proved to be essential for the feasibility of the solution. In particular, it was shown that the slalom maneuver becomes unfeasible when the roll rate and the roll acceleration are neglected, which highlights the importance of these two terms.

Despite the successful results obtained with the quasi-steady state method, it is worth noting that such solution only considers the gross motion of the vehicle. Specifically, the current solution does not capture, by definition, any transient effect associated to the vibration modes of the motorcycle.

In order to study the dynamic response of the vehicle, we need to integrate the differential equations that govern its behaviour. However, this is not straightforward as we have to overcome two major drawbacks. In first place, the motorcycle is unstable and tends to fall sideways during the dynamic solution. In second place, the speed of the vehicle and its trajectory cannot be directly imposed as in the quasi-steady state solution.

Therefore, it is indispensable to stabilize the motorcycle during the integration process and, in addition to that, we also need to apply the appropriate actions so that the vehicle follows the predefined path at the desired speed. In the real world, these tasks are performed by the rider, while in the simulation world we may mimic the rider actions by using an appropriate control algorithm. Such controller, which will be referred to as the virtual rider, is introduced in the next chapter, where the quasi-steady

state solution will prove to be an excellent reference to derive the internal model of the controller.

The vehicle and driver constitute a complex feedback system. The behavior of the vehicle results in certain reactions by the driver. Inversely, the behavior of the driver affects the behavior of the vehicle. This man-machine system cannot, in many instances, be separated into the purely mechanical and the purely human components. The system must be treated as a whole.

N. Rashevsky, Neglected Factors in Highway Safety (1966)

Chapter 6

A rider model for the dynamic simulation of motorcycles

This chapter introduces a new methodology for the dynamic simulation of motorcycles based on Model Predictive Control (MPC). In particular, we develop an algorithm to drive a nonlinear motorcycle model along a control target, defined by a reference path and a given speed profile. The first part of this chapter deals with the linearization of the motion equations along the quasi-steady state solution of the problem. The outcome is a family of state space models that represent the rider's mental model of the vehicle at every point of the reference path. The second part of the chapter describes the underlying equations of the rider model and the details of its implementation. In the third part, a series of maneuvers are simulated and their results are thoroughly discussed. Finally, the robustness of the developed methodology is shown by including the road unevenness in the simulations. To finish, some remarks and conclusions on the performance of the rider model are presented.

6.1 Introduction

The introduction of computer-controlled chassis components during the last decades of the twentieth century initiated a technological revolution that is completely changing the

motorcycle market nowadays. Recently, terms such as ABS (Antilock Braking System), TCS (Traction Control System), CBS (combined braking system) are becoming more and more known among motorcycle riders. These acronyms designate mechatronic devices aimed at improving the stability, manoeuvrability and comfort of motorcycles, helping thus the rider and ultimately enhancing safety.

It is well known that motorcycle manufacturers are continuously investigating how to improve road safety and vehicle comfort. However, despite the huge effort they have put forward in this respect, their current technology still lags behind that of the automotive industry. In general, the knowhow related to cars cannot be directly reused in motorcycles as both vehicles differ in many aspects: motorcycles are intrinsically unstable; they reach large roll angles; there is less space for sensors/actuators and less power available; and what is most important, motorcyclists are less prone than car drivers to accept a system that interferes with the dynamics of the motorcycle and their personal riding style.

Furthermore, most of the present devices involve the enhancement of one single feature at a time, not considering the vehicle as a whole. Current technology has reached the point where, to further improve the performance of the motorcycle, a global and multidisciplinary understanding of the vehicle is essential; it is indispensable to consider the interaction of such diverse elements as road, suspensions, chassis, engine, driver, sensors and electronics in the design process of new devices.

It is in this challenging framework where simulation takes a crucial role in the evolution and development of new ideas and concepts. The use of virtual models allows to reduce costs, decreases the development time and limits the number of prototypes needed to validate a new design. Additionally, computer simulations permit conducting experiments in conditions that would not be feasible in the real world. A fundamental element of this complex process is the mathematical algorithm employed to mimic the behaviour of the human rider within the simulation environment, also known as rider model or virtual rider. Existing rider models have not reached their maturity yet as discussed in Chapter 2, which motivated the development of the current PhD thesis.

In this chapter we extend the work presented by Cole in [101] to propose a novel rider model for motorcycles. His work is considered one of the first applications of Model Predictive Control (MPC) to driver modelling. Based on the control theory introduced by Maciejowski in [125], he derived a virtual driver to steer a linear car model along a target path at constant speed. Cole's model was based on the standard bicycle model, which comprises four states and one control input. Several methods to transform the controller gains from global to vehicle-fixed axes were comprehensively discussed following [112], where it was stated that the driver views the road relative to the longitudinal

axis of the vehicle instead of relative to the ground-fixed axes. Despite the simplicity of Cole's model and the limitation imposed by the constant speed assumption, the results obtained were very promising and showed a great potential for developing more advanced vehicle controllers based on MPC.

The approach presented here features three new contributions with respect to Cole's work. In first place, the new control strategy is able to successfully drive the motorcycle in a wide range of speeds. For this purpose, the internal model of the controller is constantly updated as the vehicle travels along the reference path. Thus, the controller gains are always optimized for the current dynamics of the motorcycle. Secondly, in this case the controlled vehicle is a nonlinear multibody model composed by twenty two states and four control inputs. The internal model of the controller is obtained by linearizing the system along the quasi-steady state solution of the problem. Finally, the use of curvilinear coordinates makes unnecessary any transformation from ground-fixed axes to vehicle-fixed axes as the gains are directly derived with respect to the reference path.

6.2 The rider model as a control problem

In this section, which is structured in five parts, we pose the task of modeling the human rider as an unconstrained predictive control problem. We start by providing an overview of the control scheme and by introducing some important definitions. Then, we derive the internal model of the controller by linearizing the system equations along a nominal manoeuvre, defined as the quasi-steady state solution of the problem. After that, we use the resulting set of linear models to study the stability of the system and to formulate a prediction model, which constitutes the core of the controller. Finally, we obtain the control gains by solving a series of quadratic optimization problems.

6.2.1 General structure of the controller

The structure of the simulation environment employed in this chapter is shown in Fig. 6.1 including both the motorcycle and the rider models. The former is the nonlinear multibody model of the vehicle introduced in Chapter 3 and needs no further discussion here, whereas the latter represents the control strategy that mimics the human rider.

Essentially, the task of the rider model is to compute the necessary control actions \mathbf{u} to guide the motorcycle model along a target path at the desired speed. These two elements, i.e. the path and the speed profile, constitute the control target, denoted by the capital letter \mathbf{Y}_d . The control strategy is divided in three main blocks as we

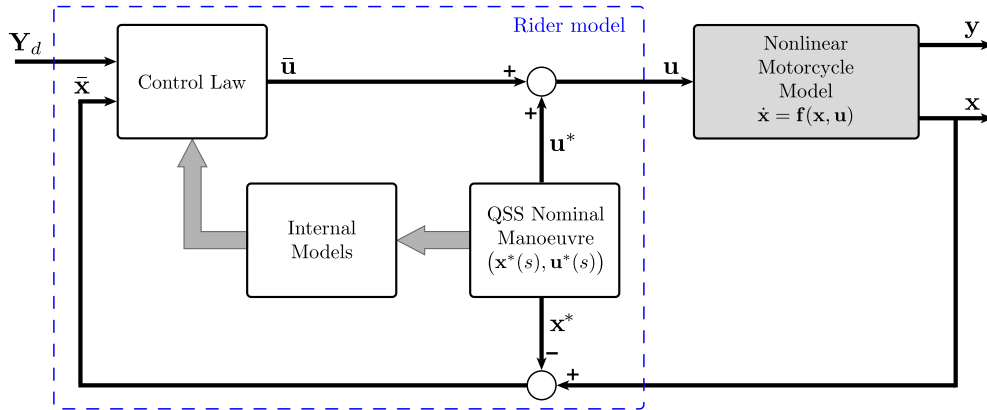


Figure 6.1: Rider model control scheme. The control strategy is divided in three main blocks, depicted in white: the quasi-steady state nominal manoeuvre, the family of internal models and the control law. The block depicted in grey represents the nonlinear plant, i.e. the multibody model of the motorcycle.

can notice in the figure: solution of the nominal manoeuvre, definition of the family of internal models and computation of the control law.

We define the nominal manoeuvre as the quasi-steady state solution of the problem, i.e. as the state vector \mathbf{x}^* and the input vector \mathbf{u}^* obtained according to the methodology introduced in Chapter 5. An asterisk is employed to differentiate the nominal values from the actual states \mathbf{x} and inputs \mathbf{u} .

The concept of internal model is used here to denote the rider's mental model of the motorcycle, i.e. a representation of the inverse dynamics of the vehicle that the human mind constantly tunes based on experience. Humans use this stored knowledge while riding to estimate the future behaviour of the vehicle and then act accordingly to achieve the desired goal, e.g. to follow a predefined path. The controller works in a similar way. It uses the internal model to formulate a prediction model, which is subsequently optimized in order to minimize the error between the system's output and the control target. Such optimization procedure is carried out by the last block, the control law, according to the MPC theory.

It is essential that the controller takes into account that the dynamic response of the motorcycle changes along the reference path. For that purpose, we obtain the internal model as the linearization of the system equations along the nominal manoeuvre. We use the bar symbol on the input $\bar{\mathbf{u}}$ and state vectors $\bar{\mathbf{x}}$ to denote variations with respect to the nominal values \mathbf{x}^* and \mathbf{u}^* . Hence, this approach remains valid as long as the motorcycle tracks the nominal manoeuvre and the variations remain small. Although the control law is based on a family of linear models, the overall control action provided

by the rider is nonlinear due to the feedforward action \mathbf{u}^* and due to the fact that the gains vary during the simulation.

6.2.2 The internal model

We derive the internal model starting from the state-space equations defined in Eq. 3.124, which are reproduced below for convenience,

$$\begin{aligned}\dot{\mathbf{x}} &= \mathbf{f}(\mathbf{x}, \mathbf{u}) \\ \mathbf{y} &= \mathbf{g}(\mathbf{x}, \mathbf{u})\end{aligned}\tag{6.1}$$

where \mathbf{x} , \mathbf{u} and \mathbf{y} are the state, input and output vectors respectively. Since we want the motorcycle to remain in the neighborhood of the nominal manoeuvre, we can approximate its dynamics by linearizing the above equations around the nominal solution defined by \mathbf{x}^* and \mathbf{u}^* . Provided that \mathbf{f} is differentiable in its two arguments, we obtain

$$\dot{\mathbf{x}} = \mathbf{f}(\mathbf{x}^*, \mathbf{u}^*) + \left. \frac{\partial \mathbf{f}}{\partial \mathbf{x}} \right|_{(\mathbf{x}^*, \mathbf{u}^*)} (\mathbf{x} - \mathbf{x}^*) + \left. \frac{\partial \mathbf{f}}{\partial \mathbf{u}} \right|_{(\mathbf{x}^*, \mathbf{u}^*)} (\mathbf{u} - \mathbf{u}^*)\tag{6.2}$$

where quadratic and higher order terms in \mathbf{x} and \mathbf{u} have been neglected. The same applies to the output equation \mathbf{g} , which yields

$$\mathbf{y} = \mathbf{g}(\mathbf{x}^*, \mathbf{u}^*) + \left. \frac{\partial \mathbf{g}}{\partial \mathbf{x}} \right|_{(\mathbf{x}^*, \mathbf{u}^*)} (\mathbf{x} - \mathbf{x}^*) + \left. \frac{\partial \mathbf{g}}{\partial \mathbf{u}} \right|_{(\mathbf{x}^*, \mathbf{u}^*)} (\mathbf{u} - \mathbf{u}^*)\tag{6.3}$$

In order to simplify the notation, we denote the Jacobian matrices as follows,

$$\begin{aligned}\mathbf{A}_c(s) &= \left. \frac{\partial \mathbf{f}}{\partial \mathbf{x}} \right|_{(\mathbf{x}^*, \mathbf{u}^*)} & \mathbf{B}_c(s) &= \left. \frac{\partial \mathbf{f}}{\partial \mathbf{u}} \right|_{(\mathbf{x}^*, \mathbf{u}^*)} \\ \mathbf{C}_c(s) &= \left. \frac{\partial \mathbf{g}}{\partial \mathbf{x}} \right|_{(\mathbf{x}^*, \mathbf{u}^*)} & \mathbf{D}_c(s) &= \left. \frac{\partial \mathbf{g}}{\partial \mathbf{u}} \right|_{(\mathbf{x}^*, \mathbf{u}^*)}\end{aligned}\tag{6.4}$$

where $\mathbf{A}_c \in \mathbb{R}^{n_x \times n_x}$, $\mathbf{B}_c \in \mathbb{R}^{n_x \times n_u}$, $\mathbf{C}_c \in \mathbb{R}^{n_y \times n_x}$ and $\mathbf{D}_c \in \mathbb{R}^{n_y \times n_u}$. The subindex c stands for continuous system. All four matrices can be written as functions of the curvilinear coordinate s as the nominal manoeuvre is parameterized according to this variable, i.e. $\mathbf{x}^* = \mathbf{x}^*(s)$ and $\mathbf{u}^* = \mathbf{u}^*(s)$.

The structure of the state matrix \mathbf{A}_c and the input matrix \mathbf{B}_c depends on the subsystems that compose the motorcycle model and how they are related. Essentially, the model comprises three different sets of equations, namely the multibody model, the tyre model and the track model. They were assembled in Eq. 3.123, which is reproduced

below for ease of reference.

$$\mathbf{f}(\mathbf{x}, \mathbf{u}) = \begin{bmatrix} \mathcal{M}^{-1}(\mathbf{q}_p)\mathcal{Q}(\mathbf{q}_v, \mathbf{q}_p, \mathbf{p}_\lambda, \mathbf{u}) \\ \mathbf{A}_p\mathbf{q}_v \\ \mathbf{f}_\lambda(\mathbf{p}_\lambda, \mathbf{q}_v, \mathbf{q}_p) \\ \mathbf{f}_t(\mathbf{p}_t, \mathbf{q}_v) \end{bmatrix} \quad \text{with} \quad \mathbf{x} = \begin{bmatrix} \mathbf{q}_v \\ \mathbf{q}_p \\ \mathbf{p}_\lambda \\ \mathbf{p}_t \end{bmatrix} \quad (6.5)$$

The first two lines of the above expression represent the multibody equations, the third corresponds to the tyre dynamics and the fourth contains the track equations. Note also that the state vector \mathbf{x} comprises the local states of all subsystems, whereas the input vector \mathbf{u} appears only in the multibody equations. In consequence, the Jacobians of \mathbf{f} with respect to the states \mathbf{x} and the inputs \mathbf{u} present the following structure,

$$\mathbf{A}_c(\mathbf{x}, \mathbf{u}) = \begin{bmatrix} \frac{\partial(\mathcal{M}^{-1}\mathcal{Q})}{\partial\mathbf{q}_v} & \frac{\partial(\mathcal{M}^{-1}\mathcal{Q})}{\partial\mathbf{q}_p} & \frac{\partial(\mathcal{M}^{-1}\mathcal{Q})}{\partial\mathbf{p}_\lambda} & \mathbf{0} \\ \mathbf{A}_p & \mathbf{0} & \mathbf{0} & \mathbf{0} \\ \frac{\partial\mathbf{f}_\lambda}{\partial\mathbf{q}_v} & \frac{\partial\mathbf{f}_\lambda}{\partial\mathbf{q}_p} & \frac{\partial\mathbf{f}_\lambda}{\partial\mathbf{p}_\lambda} & \mathbf{0} \\ \frac{\partial\mathbf{f}_t}{\partial\mathbf{q}_v} & \mathbf{0} & \mathbf{0} & \frac{\partial\mathbf{f}_t}{\partial\mathbf{p}_t} \end{bmatrix} \quad \mathbf{B}_c(\mathbf{x}, \mathbf{u}) = \begin{bmatrix} \frac{\partial(\mathcal{M}^{-1}\mathcal{Q})}{\partial\mathbf{u}} \\ \mathbf{0} \\ \mathbf{0} \\ \mathbf{0} \end{bmatrix} \quad (6.6)$$

where $\mathbf{0}$ denotes a null matrix of appropriate dimensions.

The output vector \mathbf{y} , on the other hand, is defined in terms of the track coordinates. It contains two elements. The first is the lateral position of the motorcycle with respect to the reference path n , while the second is the curvilinear speed \dot{s} . These variables, which will be used in a later section to define the cost function of the controller, depend on the vehicle states \mathbf{q}_v and on the track coordinates \mathbf{p}_t , i.e.

$$\mathbf{g}(\mathbf{x}, \mathbf{u}) = \begin{bmatrix} n(\mathbf{p}_t) \\ \dot{s}(\mathbf{p}_t, \mathbf{q}_v) \end{bmatrix} \quad (6.7)$$

Hence, the output matrix \mathbf{C}_c becomes,

$$\mathbf{C}_c(\mathbf{x}, \mathbf{u}) = \begin{bmatrix} \frac{\partial\mathbf{g}}{\partial\mathbf{q}_v} & \mathbf{0} & \mathbf{0} & \frac{\partial\mathbf{g}}{\partial\mathbf{p}_t} \end{bmatrix} \quad (6.8)$$

while the feedthrough matrix \mathbf{D}_c vanishes as the output vector \mathbf{y} does not depend directly on the input \mathbf{u} .

The resulting linear time-varying system can be expressed as a perturbation with

respect to the nominal trajectory. By using the bar symbol to represent variations with respect to the nominal values, we obtain the standard state-space representation,

$$\begin{aligned}\dot{\bar{\mathbf{x}}} &= \mathbf{A}_c(s)\bar{\mathbf{x}} + \mathbf{B}_c(s)\bar{\mathbf{u}} \\ \bar{\mathbf{y}} &= \mathbf{C}_c(s)\bar{\mathbf{x}}\end{aligned}\tag{6.9}$$

where

$$\begin{aligned}\bar{\mathbf{x}} &= \mathbf{x} - \mathbf{x}^* \\ \bar{\mathbf{u}} &= \mathbf{u} - \mathbf{u}^* \\ \dot{\bar{\mathbf{x}}} &= \dot{\mathbf{x}} - \mathbf{f}(\mathbf{x}^*, \mathbf{u}^*) \\ \bar{\mathbf{y}} &= \mathbf{y} - \mathbf{g}(\mathbf{x}^*, \mathbf{u}^*)\end{aligned}\tag{6.10}$$

Eq. 6.9 will be referred to as the internal model of the controller in continuous time.

6.2.3 Stability analysis

If the motorcycle performs a stationary motion, either in straight line or in cornering conditions, the system matrices remain constant over time and the internal model becomes time-invariant. Consequently, we can simplify Eq. 6.9 to the following set of linear differential equations with constant coefficients,

$$\begin{aligned}\dot{\bar{\mathbf{x}}} &= \mathbf{A}_c\bar{\mathbf{x}} + \mathbf{B}_c\bar{\mathbf{u}} \\ \bar{\mathbf{y}} &= \mathbf{C}_c\bar{\mathbf{x}}\end{aligned}\tag{6.11}$$

which represents the motion of the vehicle around a stationary equilibrium point.

It is well known from modern control theory [79] that the eigenvalues of the state matrix \mathbf{A}_c characterize the stability of time-invariant systems against external perturbations. In general, the eigenvalues may be represented by complex numbers of the form,

$$s = \sigma \pm j\omega_d\tag{6.12}$$

where the real part σ and the imaginary part ω_d are respectively the attenuation and the damped natural frequency of the associated eigenvectors, also known as modal shapes or vibration modes.

The attenuation σ gives information about the stability of the modes, which are said to be stable if the attenuation is negative and unstable if the attenuation is zero or positive. The damped frequency ω_d , on the other hand, is the frequency at which each mode would oscillate in free vibration conditions. The damping ratio ξ is commonly used to characterize how fast the oscillations decay after the system is perturbed. It

can be defined as a function of the attenuation and the damped frequency as follows,

$$\xi = -\frac{\sigma}{\sqrt{\sigma^2 + \omega_d^2}} \quad (6.13)$$

with its value ranging from 0 to 1. Vibration modes with a ratio close to 1 attenuate the effects of external perturbations very quickly, whereas modes with ratios close to 0 show little attenuation.

Since the eigenvalues of the motorcycle are very sensitive to the equilibrium conditions, namely the travelling speed and the lateral acceleration, we split the stability analysis into straight running and cornering conditions. The first provides a good insight into the effect of speed while the second allows us to understand the effect of lateral acceleration.

Straight running

Fig. 6.2 shows the nonlinear¹ root locus of the motorcycle in straight line conditions as the speed increases from 5 m/s up to 70 m/s. The horizontal axis of the graph represents the attenuation σ in rad/s whereas the vertical axis represents the damped natural frequency $f_d = \omega_d / 2\pi$ in Hz.

Note that the graph is divided in two different regions. The eigenvalues associated to stable modes fall in the left-half plane, which is in turn divided in function of the damping ratio ξ . The right-half plane, on the other hand, is depicted in grey to emphasize the fact that the system becomes unstable in the case any eigenvalue falls in this region.

Each trace of the root locus represents one vibration mode of the motorcycle. Their names have been assigned according to existing literature [11,13,18]. We can distinguish two groups of modes in Fig. 6.2. All the vibration modes that do not involve lateral motion, i.e. bounce, pitch and wheel hops, are usually classified as in-plane modes. On the contrary, the remaining modes, i.e. capsizes, weave, wobble and rear wobble, are classified as out-of-plane modes. The in-plane modes are generally related to the ride and comfort performance of the motorcycle, whereas the out-of-plane modes are linked to its stability.

The vibration modes of the motorcycle are depicted in Fig. 6.3 by means of polar graphs. Each set of arrows represents the amplitude and phase of the multiple degrees of freedom that compose the specified vibration mode. The longitudinal motion of the

¹The root locus is nonlinear since each point of the graph is obtained by linearizing the equations of motion around a different equilibrium point. In particular, the steady state solution is first computed for all the speeds and the equations of motion are then linearized around the resulting equilibrium points.

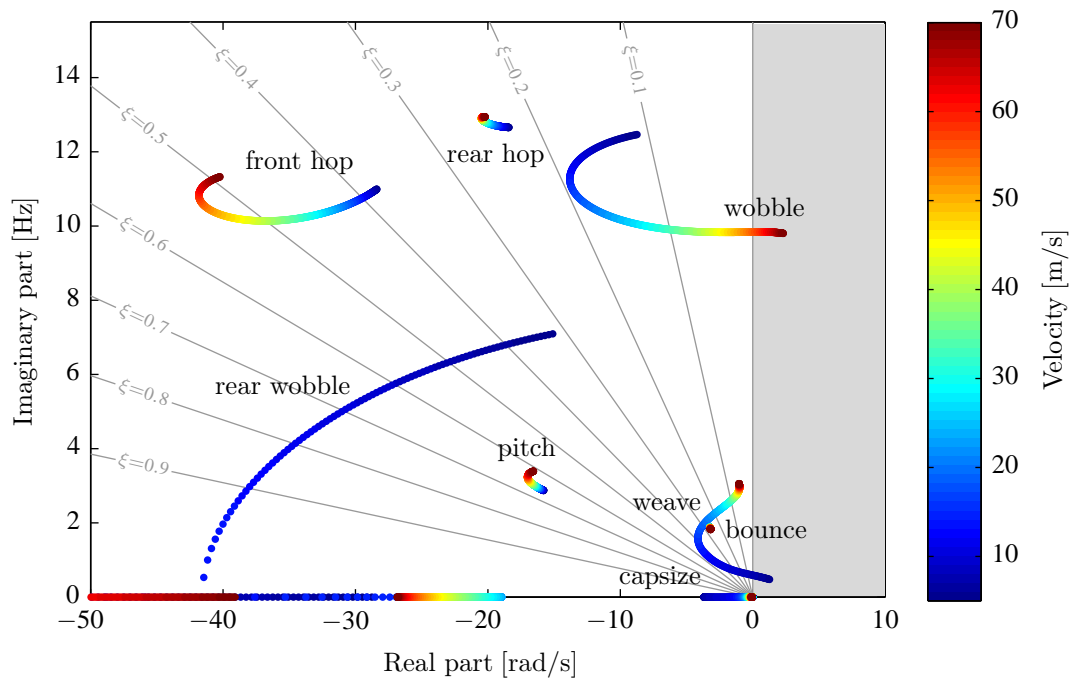


Figure 6.2: Root locus in straight line conditions. The horizontal axis of the graph represents the attenuation σ in rad/s whereas the vertical axis represents the damped natural frequency $f_d = \omega_d / 2\pi$ in Hz. The speed is represented by the color scale, which goes from 5 m/s (blue) up to 70 m/s (red).

vehicle and the wheel rotations are not included as their contribution to the displayed modes is insignificant. Hence, we define the mode shapes in function of eight degrees of freedom, five rotational ($\chi, \phi, \mu, \delta, \mu_r$) and three translational (n, z, d_f).

In order to visualize all the degrees of freedom in one graph, we have transformed the translational degrees of freedom into fictitious angular quantities. In particular, we have divided the lateral displacement n , the fork deformation d_f and the vertical displacement z by the length of the swingarm. This adimensionalization leads to three new angles (n^*, z^*, d_f^*) that can be directly compared to the other rotational degrees of freedom. Finally, it is to be noted that the eigenvectors are normalized so that the magnitude of their maximum component is equal to one. A brief description of each mode is provided below:

- **Weave** (out-of-plane). The weave mode is characterized by low frequency oscillations of the following degrees of freedom: lateral displacement of the sprung mass n^* , trajectory angle χ , roll angle ϕ and steering angle δ . We can observe that the roll angle is 90 degrees out of phase with respect to the track angle and almost 180 with respect to the lateral displacement. For the motorcycle under analysis,

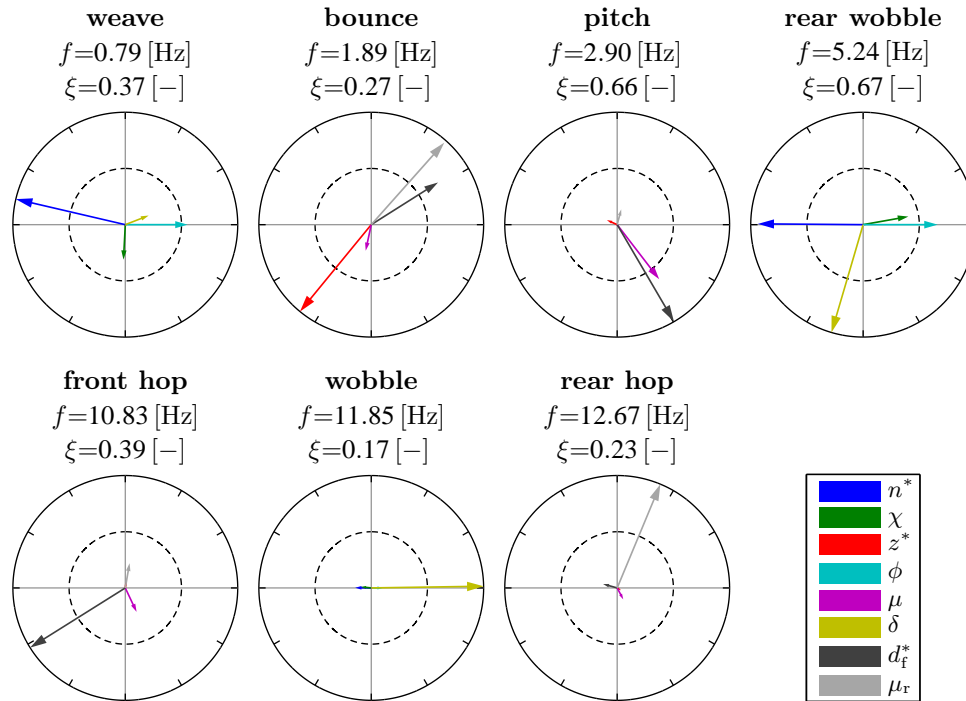


Figure 6.3: Vibration modes of the motorcycle at 10 m/s. Two things are to be noted in the above graph: first, the eigenvectors are normalized so that the magnitude of their maximum component is equal to one; second, the phase of the roll angle is used as the phase reference in all cases.

this mode is unstable at low speeds, gets slightly stabilized at medium speeds and becomes progressively less damped at very high speeds.

- **Bounce** (in-plane). The bounce mode shows a large vertical movement of the sprung mass z^* that is in phase opposition with respect to both the pitch angle of the rear suspension μ_r and the fork deformation d_f . Basically, when the sprung mass moves up and down the unsprung masses move in the opposite direction to keep the contact with the ground. There is also a small rotation of the sprung mass μ that indicates that pitch and bounce are not fully decoupled.
- **Pitch** (in-plane). The pitch mode is characterized by a large rotation of the sprung mass μ . Such rotation is in phase with the fork deformation d_f and in phase opposition with respect to the pitch angle of the rear suspension μ_r . This means that when the sprung mass pitches forward, the fork compresses and the swingarm extends. Similarly to the bounce mode, there is also a small displacement of the sprung mass in the vertical direction z that indicates that pitch and bounce are

not decoupled.

- **Rear wobble** (out-of-plane). The rear wobble is characterized by oscillations of the trajectory angle χ and the roll angle ϕ that are in phase with one another, and in phase opposition with respect to the lateral displacement n^* . The steering angle δ is almost 90 degrees out of phase with respect to the lateral displacement. This mode is not particularly interesting as far as the lateral stability is concerned since it is highly damped.
- **Front and rear hops** (in-plane). The front hop shows mainly fork deformation d_f with small rotations of the sprung mass μ and the swingarm μ_r around the y -axis. The rear hop, on the other hand, shows a large rotation of the swingarm μ_r together with small motions of the sprung mass μ and the fork d_f .
- **Wobble** (out-of-plane). The wobble mode is characterized by large oscillations of the steering angle δ . This mode is qualitatively similar to the well-known wheel shimmy on aircrafts and cars [12] and tends to become unstable at high speeds.

There is an additional out-of-plane mode that is non-oscillatory, the capsize. It consists mainly in a roll motion combined with a lateral displacement where the whole vehicle behaves as an inverted pendulum that falls laterally. This mode evolves very slowly, on the order of seconds, being easy for the rider to control it. For the motorcycle under analysis, the stability of the capsize mode decreases with the speed and the real part becomes almost null over the speed of 30 m/s.

Cornering conditions

The most important difference between cornering and straight running conditions is the coupling between the in-plane and out-of-plane modes. The roll angle of the motorcycle plays an important role in this phenomenon.

When the motorcycle is upright all tyre forces are either contained in the mid-plane of the vehicle or orthogonal to it. Thus, the vertical loads can only excite the in-plane modes whereas the out-of-plane modes are only affected by the lateral forces. This causes the in-plane and the out-of-plane modes to be fully decoupled, i.e. capsize, weave and wobble do not involve suspension motion whereas pitch and bounce do not involve lateral motion.

This situation changes drastically in cornering conditions as both lateral and vertical forces possess in-plane and out-of-plane components. Hence, when the motorcycle is inclined all modes involve both suspension and lateral motions at different extents. The effect of such coupling is shown in Fig. 6.4, which depicts the root locus of the motorcycle

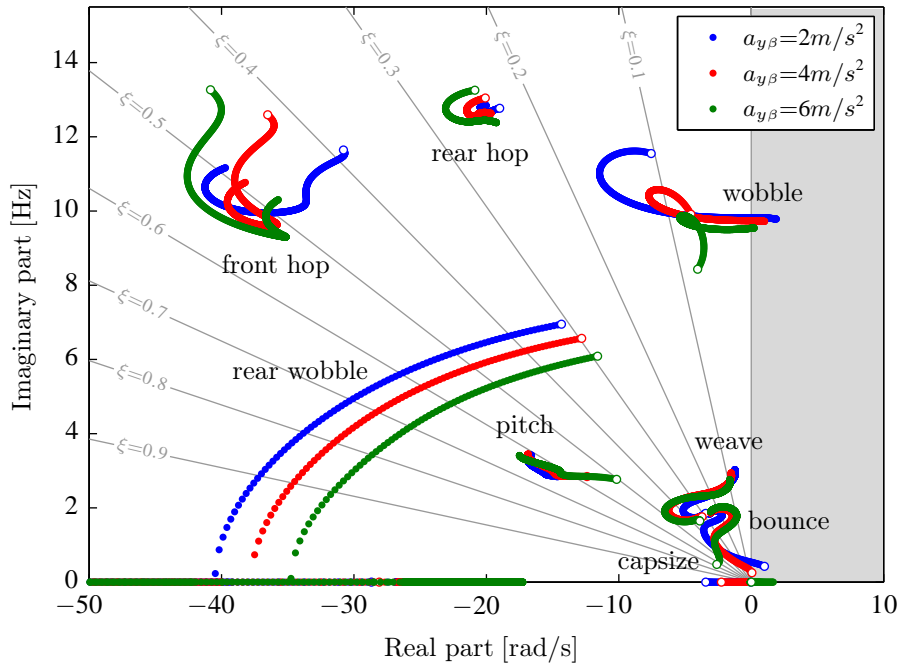


Figure 6.4: Root locus in cornering conditions. The horizontal axis of the graph represents the attenuation σ in rad/s whereas the vertical axis represents the damped natural frequency $f_d = \omega_d/2\pi$ in Hz. The speed range goes from 5 m/s up to 70 m/s. Note that each color represents a different acceleration and that the initial speed is indicated by a circle (\circ).

at three different levels of lateral acceleration. Note that each color represents a different acceleration and that the initial speed is indicated by a circle (\circ).

The most coupled modes are generally the weave and the bounce since their frequencies are not far off. As a matter of fact, we can observe how the traces associated to these modes change significantly with respect to the straight running case. In particular, the bounce frequency now depends on the speed and the weave frequency increases. As far as the damping is concerned, the damping of the weave mode increases with the lateral acceleration, especially at low speeds, while that of the bounce increases at low speeds and shows the opposite behaviour at high speeds.

It is worth noting that the frequency of the wobble decreases with the lateral acceleration. This trend is maximum at low speeds and becomes less pronounced as the speed increases. Interestingly, the lateral acceleration has a destabilizing effect on the wobble mode, causing its eigenvalues to move towards the instability region. As a consequence, this mode becomes clearly unstable at high speeds.

The stability of the capsizes mode is also greatly influenced by the lateral acceleration. It is stable in straight running for all speeds, but becomes progressively more unstable

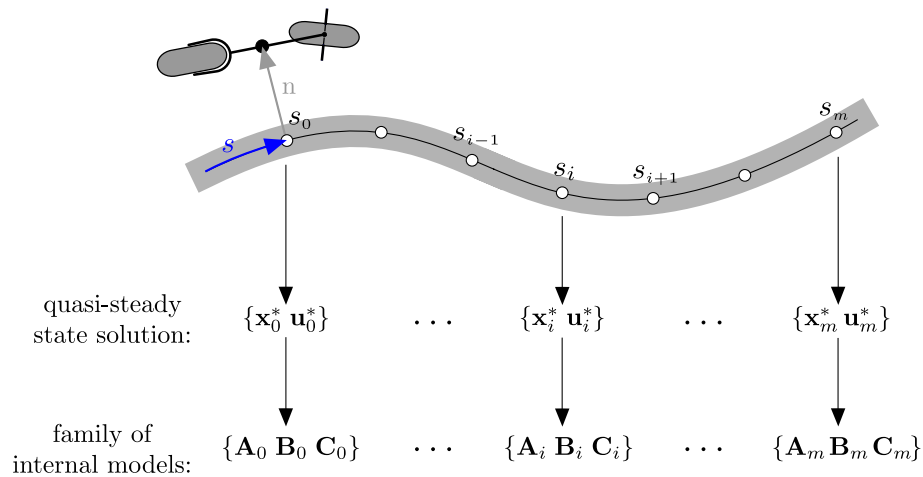


Figure 6.5: Family of internal models. Each internal model represents the dynamics of the motorcycle at one point of the reference path. The family internal models comprises $m+1$ discrete models, which are obtained by linearizing the system equations around the nominal manoeuvre $(\mathbf{x}^*, \mathbf{u}^*)$ followed by a subsequent discretization.

as the lateral acceleration increases.

The lateral acceleration does not have a big effect on the frequency of the wheel hop modes but it does increase their damping ratio slightly. In effect, when the motorcycle is inclined and any of the wheel hop modes gets excited, the contact patch of the corresponding tyre slides on the road surface. Such motion dissipates energy and increases the effective damping.

The effect of the lateral acceleration on the two remaining modes is small. It slightly decreases the damping ratio of the pitch mode and tends to reduce the frequency of the rear wobble.

In this section we have shown that the dynamic response of the motorcycle varies significantly with the speed and the lateral acceleration. In particular, there are two lightly-damped vibration modes, namely wobble and weave, that may become unstable. Furthermore, such modes involve both in-plane and out-of-plane dynamics in cornering conditions. This highlights the importance of designing the rider model so that it takes into account the actual dynamics of the motorcycle.

NOTE: Sections 6.2.4, 6.2.5, 6.3, 6.3.1, 6.3.2 and 6.3.3 are protected by a confidentiality agreement, according to the decision of the Doctorate Commission of the University Miguel Hernández dated September 19, 2016.

6.3.4 Results: slalom test

Let's recall that the slalom test consists of multiple line-up cones that must be avoided by the rider, leaving the first at the right, the second at the left and so on. Such cones are equally distributed along a straight line at a distance of 12.5 m from one another. To complete the manoeuvre, the motorcycle is driven along the trajectory depicted in Fig. 6.15a at a constant speed of 23.5 m/s.

The tracking performance of the controller can be assessed by looking at the path error and by comparing the actual and target speeds. These two metrics are depicted in Figs. 6.15b and 6.15c respectively, where we can observe that the performance of the controller is remarkable: the maximum path deviation is lower than 2.5 cm whereas the speed difference is almost insignificant, of the order of 0.1 m/s.

The slalom test is very demanding as far as the lateral control of the motorcycle is concerned. In particular, the lateral acceleration of the vehicle measured at the path point \mathbf{P} reaches peaks of 17.5 m/s^2 at the cones according to Fig. 6.15d. The complexity of this manoeuvre is also observable from the lateral forces exerted by the tyres, see Fig. 6.15f. Note that not only they reach values over 1.3 kN but their rate of change is also significant. As a matter of fact, the rear force goes from -1.3 kN to $+1.3 \text{ kN}$ as the vehicle travels between to consecutive cones.

The most interesting point of this simulation, however, is that the combination of cone spacing and travelling speed is selected so as to excite the bounce mode. Such excitation occurs at the following frequency

$$f_c = \frac{\dot{s}}{d_c} = \frac{23.5 \text{ m/s}}{12.5 \text{ m}} = 1.88 \text{ Hz} \quad (6.52)$$

where \dot{s} is the constant travelling speed whereas d_c represents the distance between cones. The resulting frequency f_c matches the bounce frequency of the motorcycle as per the root locus of Fig.6.2. This leads to severe in-plane oscillations of the motorcycle that were not captured by the quasi-steady state solution of the problem. We can observe in Fig. 6.15g that the load variation surpasses 2.2 kN peak to peak, with a minimum value of 250 N. Interestingly, the rider model is able to successfully deal with such a big load variation.

In general, the longitudinal control of the motorcycle tends to be less challenging than the lateral. Nevertheless, in this case the coupling between the lateral and longitudinal dynamics leads to interesting results. We can observe in Fig. 6.15e that the longitudinal forces oscillate, becoming even negative, despite the velocity of the vehicle

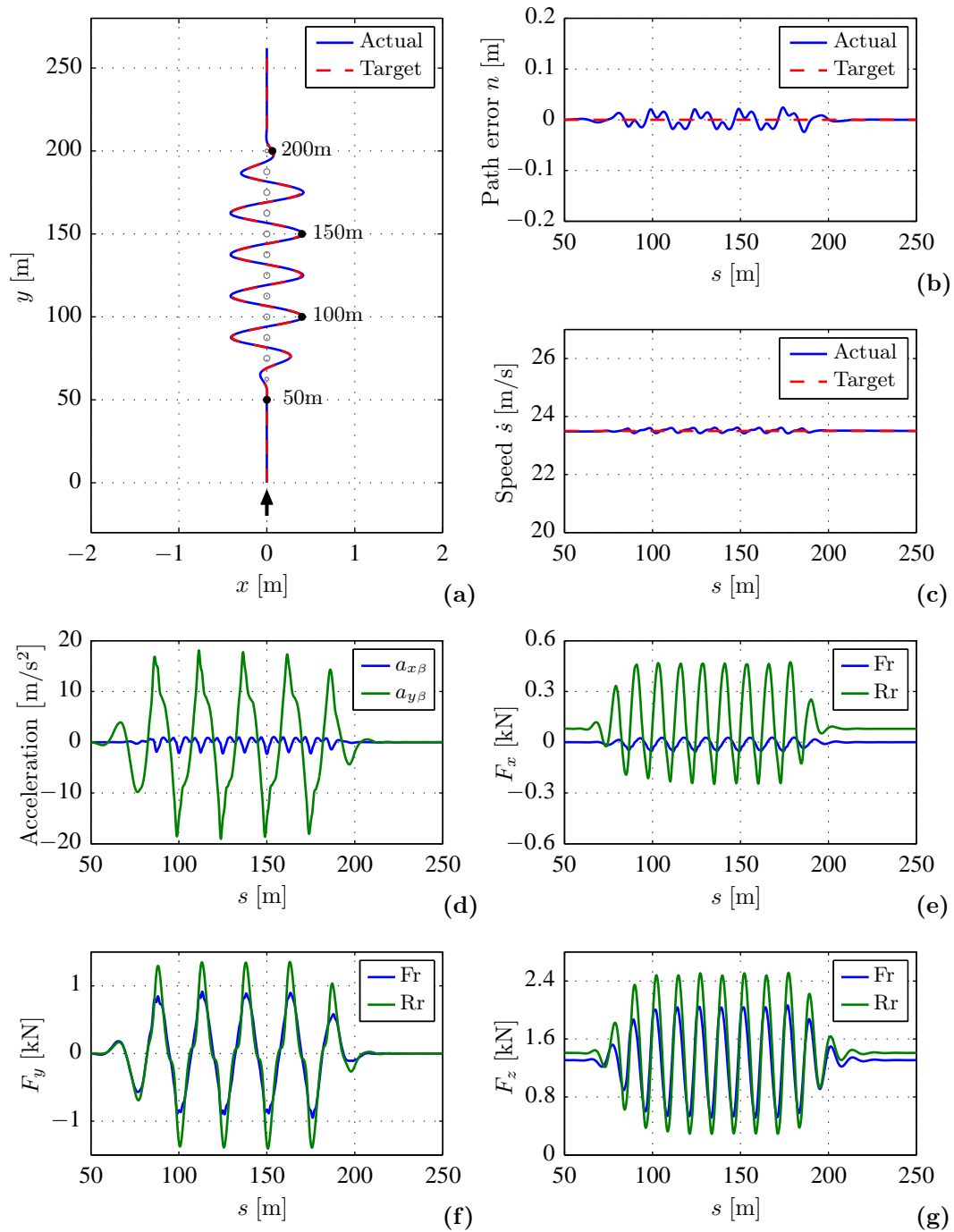


Figure 6.15: Slalom results. a) Trajectory. b) Path error. c) Curvilinear speed. d) Acceleration on the tangent frame \mathbf{T}_β . e) Tyre longitudinal forces. f) Tyre lateral forces. g) Tyre loads.

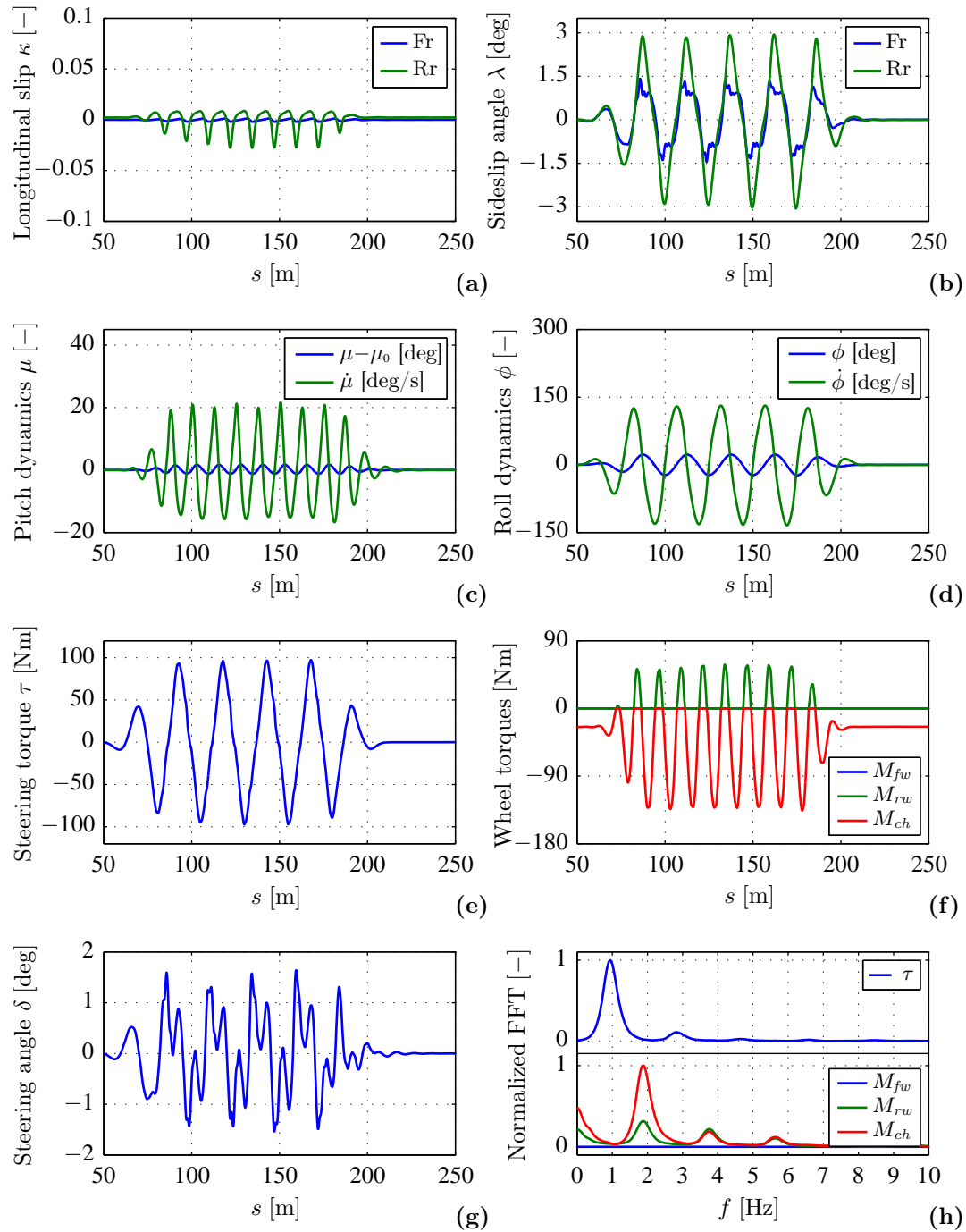


Figure 6.16: Slalom results. a) Longitudinal slips. b) Sideslip angles. c) Pitch angle and pitch rate. d) Roll angle and roll rate. e) Steering torque. f) Wheel torques. g) Steering angle. h) Normalized FFT (peak hold spectrum).

being constant throughout the manoeuver. The same behaviour is observed if we look at the slip ratios, Fig. 6.16a, especially as far as the rear tyre is concerned.

According to Fig. 6.16d, the slalom manoeuver is characterized by an extreme roll rate that oscillates between ± 130 deg/s. Under these conditions, the combined motion of the vehicle around the yaw and roll axes tends to accelerate the vehicle before the apex, i.e. when the roll angle increases, and has the opposite effect after it⁴. Thus, in order to keep the speed constant, the rider has to brake before each apex and open the throttle afterwards. This behaviour is confirmed by Fig. 6.16f, where the longitudinal controls are depicted. Note that the brake distribution is fully biased towards the rear in order to help the motorcycle rotation into the corner.

The lateral dynamics are mainly controlled by the steering torque, depicted in Fig. 6.16e. It is important to note that the steering angle, which is shown in Fig. 6.16g is not directly determined by the rider. In fact, the steering dynamics depend not only on the steering torque exerted by the rider but also on all the external forces applied to the steering system, e.g. tyre forces, gyroscopic effects, etc.

The frequency content of the control actions is summarized in Fig. 6.16h, where we can observe that the frequency of the steering torque is $f_c/2$, i.e. half of the cone frequency, whereas the longitudinal controls oscillate at f_c . Both frequencies are feasible for human riders.

The sideslip angle of the tyres, Fig. 6.16b, and the pitch response of the motorcycle, Fig. 6.16c, are also included for completeness. The first is directly related to the lateral forces while the second shows that the pitch dynamics are significantly excited during the manoeuvre.

6.3.5 Results: chicane

As opposed to the slalom test, which is characterized by an aggressive lateral acceleration, a chicane is used here to assess the behaviour of the rider model under severe combined conditions. In this case the motorcycle is ridden along the s-shaped trajectory depicted in Fig. 6.17a, which is a typical feature of racing courses. The combination of high longitudinal and lateral accelerations, together with the abrupt transition from acceleration to braking, make this manoeuver a challenging test for the rider model.

According to Figs. 6.17b and 6.17c, which show the path error and the vehicle speed respectively, the tracking performance of the virtual rider is also remarkable along the chicane. We can observe that the maximum path error is 4.5 cm whereas the speed error lies below 0.05 m/s.

⁴The coupling between the lateral and longitudinal dynamics was detailed during the quasi-steady state solution of the slalom manoeuver in section 5.2.1.

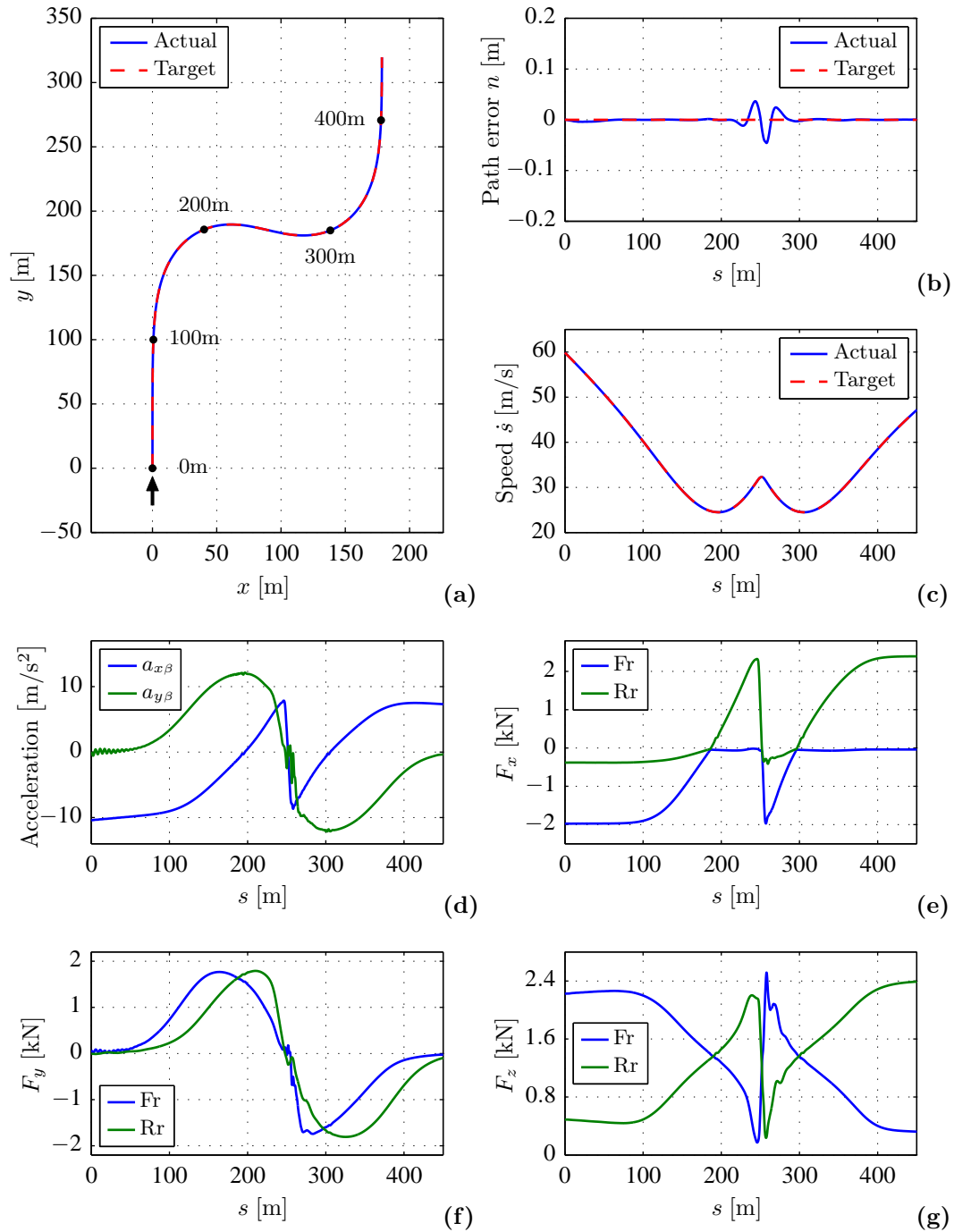


Figure 6.17: Chicane results. a) Trajectory. b) Path error. c) Curvilinear speed. d) Acceleration on the tangent frame \mathbf{T}_β . e) Tyre longitudinal forces. f) Tyre lateral forces. g) Tyre loads.

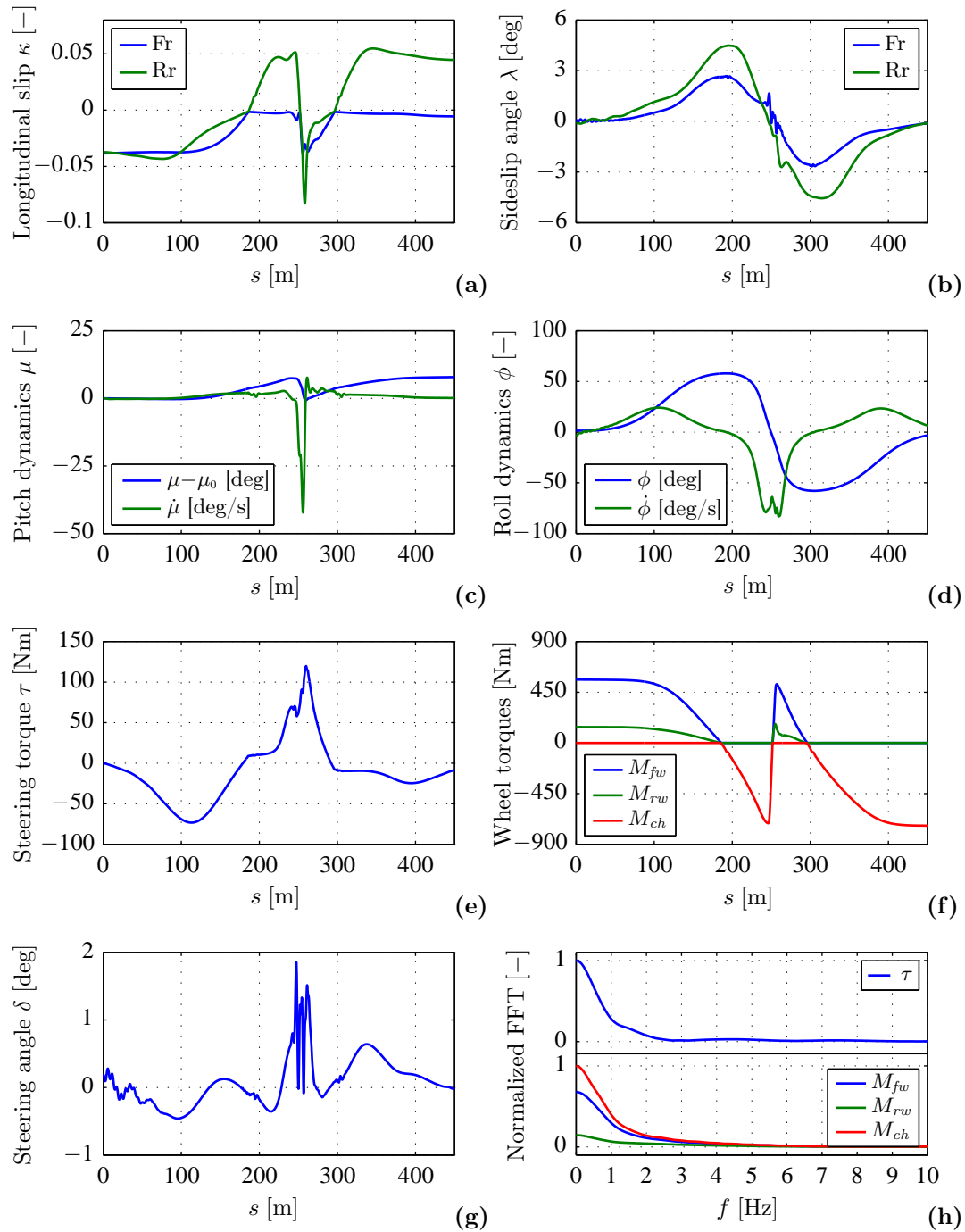


Figure 6.18: Chicane results. a) Longitudinal slips. b) Sideslip angles. c) Pitch angle and pitch rate. d) Roll angle and roll rate. e) Steering torque. f) Wheel torques. g) Steering angle. h) Normalized FFT (peak hold spectrum).

Due to the fact that the lateral acceleration changes slowly, the quasi-steady state solution obtained in section 5.2.2 and the results presented here show no significant differences. This is true for the whole manoeuvre except for the oscillations caused by the aggressive braking at $s=250\text{m}$. This point corresponds to the center of the chicane, where the rider stops accelerating and brakes before entering the second corner. Note the discontinuity exhibited by the longitudinal acceleration in Fig. 6.17d and also by the longitudinal tyre forces in Fig. 6.17e.

We will therefore focus on this part of the manoeuvre. We can observe from Fig. 6.17d that the aggressive braking causes small out-of-plane oscillations of the vehicle. These oscillations are also noticeable from the lateral forces in Fig. 6.17f, from the sideslip angles in Fig. 6.18b and, to a lower extent, from the roll rate in Fig. 6.18d. It is clear from this last figure that the braking occurs at the point where the roll rate is maximum. This favours the coupling between the braking forces and the out-of-plane motion of the motorcycle.

The largest oscillations, however, are related to the in-plane dynamics of the vehicle. When the rider brakes, the rear tyre unloads and more than 2.3 kN are quickly transferred to the front tyre, see Fig. 6.17g. This load transfer triggers the pitch dynamics of the vehicle, which in turn cause the tyre loads to oscillate. The pitch angle and its derivative are shown in Fig. 6.18c, where we can observe how the pitch rate reaches its maximum value at the beginning of the braking phase and then damps out quickly.

The oscillations described above, both in-plane and out-of-plane, together with the fact that the motorcycle is not perfectly upright during load transfer cause the fast steering oscillations shown in Fig. 6.18g. However, they do not represent a major problem for the rider model, which successfully manages to stabilize the vehicle along the desired trajectory. The steering torque applied by the rider for this purpose is shown in Fig. 6.18e. Its spectrum, depicted in Fig. 6.18h, additionally shows that the control of the motorcycle along this manoeuvre requires a limited bandwidth that is perfectly feasible for human riders.

6.3.6 Results: corner exit

The third example represents an aggressive corner exit manoeuvre, similar to those performed by racing riders. We can observe the target trajectory in Fig. 6.19a. The manoeuvre starts with the motorcycle cornering in steady state conditions, i.e. travelling at constant speed along a circular trajectory. As the end of the circular section approaches, the rider progressively opens the throttle and the motorcycle accelerates. Consequently, the load at the front tyre decreases and the motorcycle eventually wheelies⁵. If the tyre

⁵The term wheelie is usually employed to denote the loss of contact between the front wheel and the track

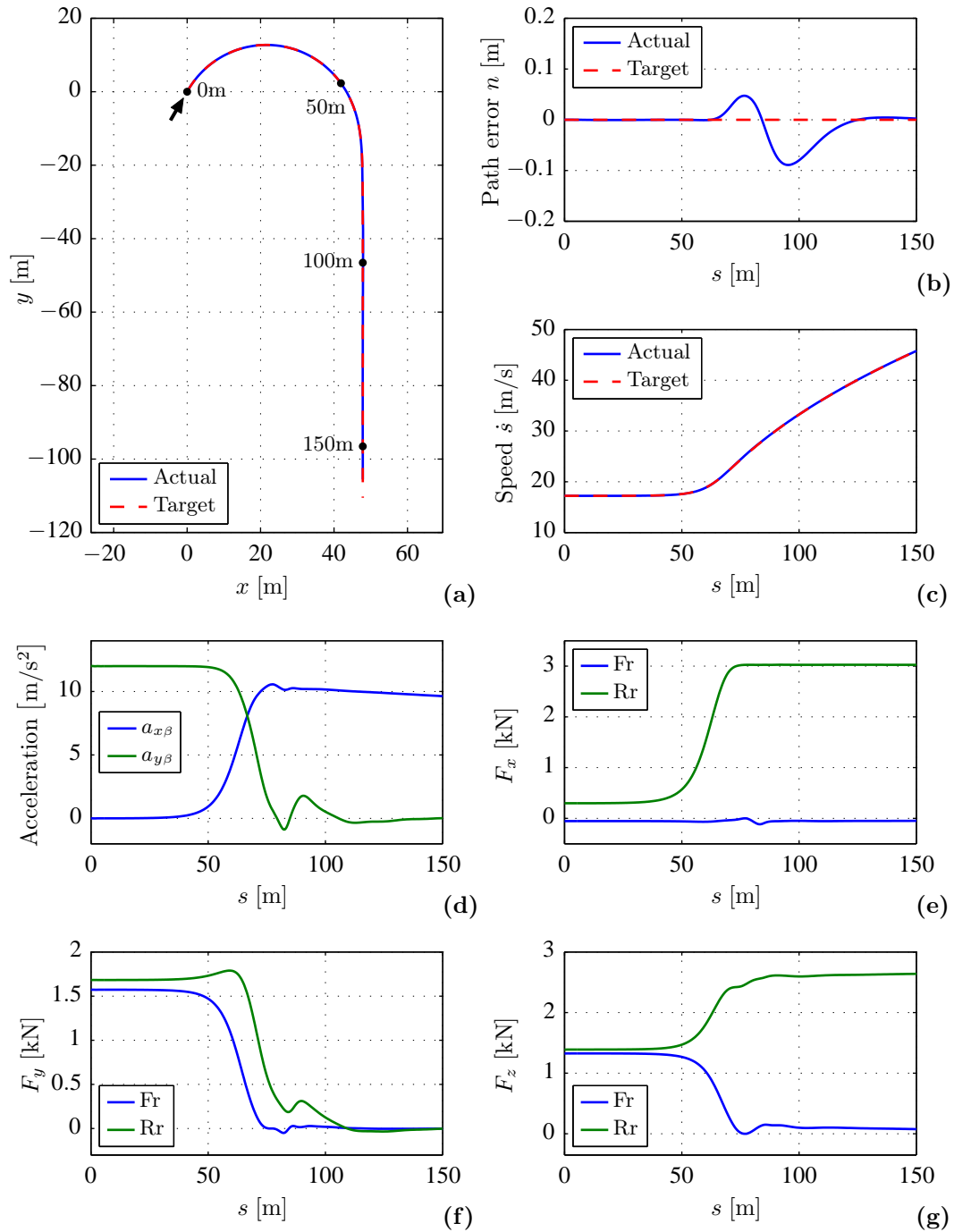


Figure 6.19: Corner exit results. a) Trajectory. b) Path error. c) Curvilinear speed. d) Acceleration on the tangent frame \mathbf{T}_β . e) Tyre longitudinal forces. f) Tyre lateral forces. g) Tyre loads.

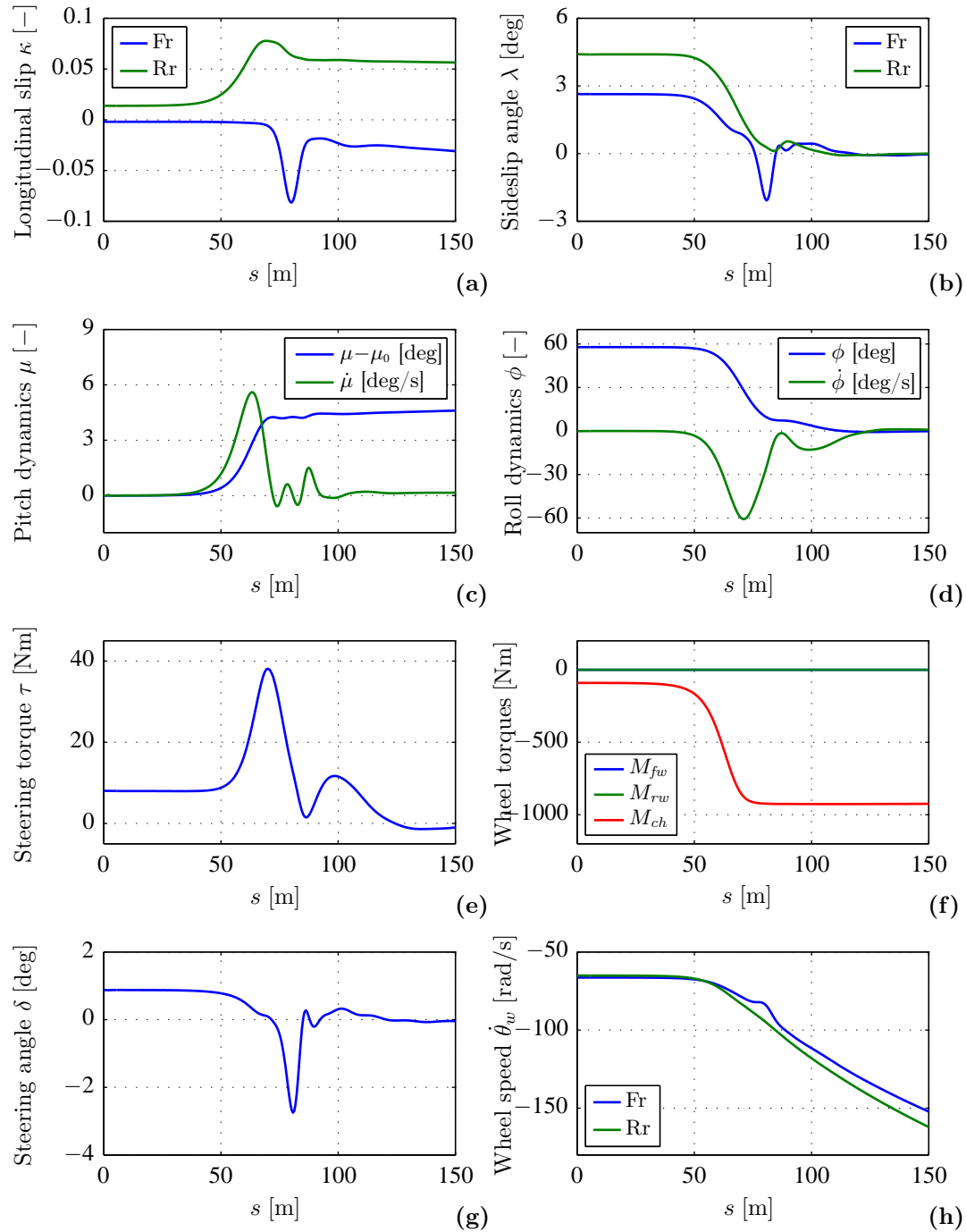


Figure 6.20: Corner exit results. a) Longitudinal slips. b) Sideslip angles. c) Pitch angle and pitch rate. d) Roll angle and roll rate. e) Steering torque. f) Wheel torques. g) Steering angle. h) Wheel rotational speeds.

grip is high enough, this condition determines the maximum longitudinal acceleration of the vehicle as any further increase would cause it to flip backwards. Such manoeuvre is especially challenging for the rider model due to the high acceleration reached both in the longitudinal and lateral directions and, in particular, due to the low load available at the front tyre.

We can observe from Fig. 6.19b how the maximum path error is around 9 cm, slightly larger than those obtained in the previous simulations. Errors of that order of magnitude can be considered very small, especially if we compare them with the width of the track. The speed comparison shows also excellent results according to Fig. 6.19c, with the biggest difference between the actual and target speeds being lower than 0.05 m/s.

The acceleration of the motorcycle clearly reflects the severity of the manoeuvre. The longitudinal and lateral components are depicted in Fig. 6.19d, where we can observe how the maximum longitudinal acceleration exceeds 10.5 m/s^2 while the lateral reaches 12 m/s^2 . It is important to notice that longitudinal component builds up progressively as the lateral decreases. The same trend can be observed in the longitudinal and lateral components of the tyre forces from Figs. 6.19e and 6.19f. Since we are simulating a rear-powered motorcycle, only the rear tyre generates thrust force whereas both tyres generate lateral forces.

One of the most interesting plots in this case is that of the tyre loads, depicted in Fig. 6.19g, as it shows how the load is transferred from the front to the rear tyre. Furthermore, the wheelie can be easily identified from this graph as the point where the front load vanishes. This occurs at $s=75 \text{ m}$. Note that the front load shows a value of about 75 N after that point. This small load is required so that the motorcycle can follow the target trajectory⁶. For this reason, the target speed profile has been designed so as to keep a small residual load at the front wheel during the last part of the manoeuvre.

The slip of the front tyre reaches significant values during the acceleration phase. The longitudinal slip, shown in Fig. 6.20a, is automatically generated as the front wheel is dragged by the rest of the vehicle. In fact, we can note from Fig. 6.20f that the rider does not apply any torque to the front wheel. It is also interesting to observe from Fig. 6.20h that the rotational speed of the front wheel stays constant for a short period of time, which corresponds to the point where the front load vanishes. The sideslip angle, on the other hand, is deliberately increased by the rider in order to build up the lateral force required to keep the trajectory, see Fig. 6.20b. This is achieved by significantly increasing the steering angle as shown in Fig. 6.20g.

⁶The load available at the front tyre is related to the controllability of the vehicle. As a matter of fact, null load implies that the rider cannot correct eventual errors in the motorcycle trajectory by applying realistic steering inputs. The control of the motorcycle with the front wheel in the air requires further investigation, including additional control inputs such as the motion of the rider's torso, which are outside the scope of the present thesis.

The torque applied by the rider to steer the motorcycle is shown in Fig. 6.20e. Due to the high roll rate achieved during the manoeuvre, the steering torque is dominated by the gyroscopic effect of the front wheel, i.e. its magnitude is proportional to the product of the wheel speed and the roll rate whereas its phase is shifted 180 degrees with respect to the latter. Note indeed that the steering torque and the roll rate, shown in Fig. 6.20d, have the same shape with opposite sign.

The evolution of the pitch angle during the manoeuvre is also included for completeness. We can observe in Fig. 6.20c that the pitch angle increases with the longitudinal acceleration and then stabilizes, exhibiting some oscillations around the point where the front wheel loses contact with the ground.

6.3.7 Results: corner entry on uneven road

The fourth and last example represents a corner entry simulation where the rider decelerates aggressively as the vehicle rolls into a right corner. As opposed to the previous simulations, where the road was assumed to be perfectly flat, in this case we use an extended tyre model that allows us to consider road irregularities.

Wheeled vehicles are generally subject to two types of road perturbations: a uniformly distributed excitation, usually referred to as road unevenness, and a series of single features, such as bumps and potholes, which can be considered road anomalies. The former represents a permanent source of excitation whereas the latter result in short-lived vehicle vibrations. In the following analysis the road unevenness will allow us to assess the robustness of the rider model in presence of external noise.

A widespread method to model the road profile is by using a stochastic approach [137, 150]. This technique is based on the fact that the road unevenness can be statistically characterized in spatial domain by its power spectral density. The following equation is frequently used in literature to represent the road,

$$\Phi(\Omega) = \Phi_0 \left(\frac{\Omega_0}{\Omega} \right)^\omega \quad (6.53)$$

where Φ is the power spectral density in $\text{m}^2/(\text{rad}/\text{m})$ and Ω is the spatial angular frequency (wave number) given in rad/m . The terms Φ_0 , Ω_0 and ω are just constants that represent the degree of unevenness of a given road. The wave number can be also expressed as a function of the wave length λ as $\Omega = 2\pi/\lambda$.

In this thesis we use an extension of the previous model from [164],

$$\Phi(\Omega) = \frac{b_0}{a_0 + a_2\Omega^2 + a_4\Omega^4} \quad (6.54)$$

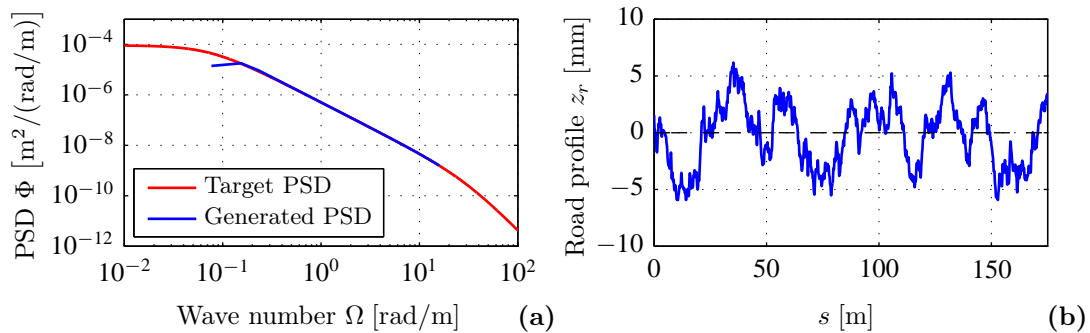


Figure 6.21: Road profile and statistical properties. a) Power spectral density. b) road profile.

where the power spectral density is specified as a rational function of two polynomials. Their coefficients have been selected so that the resulting road represents a smooth surface similar to that found on racing tracks⁷.

The resulting power spectral density is represented by the red curve of Fig. 6.21a, which shows a drop in magnitude as the wave number increases. Such characteristic shape reflects the fact that the amplitude of road irregularities are larger at long wavelengths (e.g. they may reach several meters over the length of hundreds of meters) whereas they reduce significantly at short wavelengths (e.g. the amplitude only reaches some millimeters over the length of one meter).

We can use a superposition of N sine waves to build the desired road profile,

$$z_r = \sum_{i=1}^N A_i \sin(\Omega_i s - \Psi_i) \quad (6.55)$$

where each sine is determined by its amplitude A_i , its wave number Ω_i and its phase offset Ψ_i . According to [165], the amplitude for each wave number can be determined from the power spectral density as follows,

$$A_i = \sqrt{2\Phi(\Omega_i)\Delta\Omega} \quad (6.56)$$

with $\Delta\Omega$ being the interval used to discretize the frequency range of interest. By restricting the wave lengths to lie between 0.4 and 80 m and using randomly distributed phase angles, we obtain the profile shown in Fig. 6.21b. Its associated power spectral density, depicted in blue in Fig. 6.21a, confirms the results. Note that the road profile

⁷The selected coefficients belong to the category *good asphalt concrete*. The power spectral density has been multiplied by an additional scaling factor of 0.1 in order to reach the desired level of unevenness.

has a maximum amplitude of 1.2 cm peak to peak.

The results of the simulation are summarized in Figs. 6.22 and 6.23. In order to facilitate their interpretation, the results corresponding to the uneven road (blue) are shown together with those corresponding to the flat road (red). By comparing both sets of results it is possible to assess the effect of the road unevenness on the motorcycle response and on the rider controls.

The present manoeuvre is characterized by the J-shaped trajectory shown in Fig. 6.22a and by the speed profile depicted in Fig. 6.22c. From these two figures it is evident that the road noise does not have a significant impact on the tracking capabilities of the rider model. In particular, if we look at the maximum path error in Fig. 6.22c, we can observe that its value only increases from 4 cm on the flat road to 7 cm on the uneven road. Such a small error constitutes an excellent tracking performance, especially if we consider the high acceleration levels to which the motorcycle is subject.

The main difference between both sets of results is that the road irregularities do not allow the motorcycle to reach a perfect steady state condition. This can be noticed by looking at the last part of the manoeuvre, where the target speed and the corner radius remain constant. In principle, the path error should vanish as the motorcycle travels along the corner but this only happens if we use the flat road. On the other hand, if we consider the road unevenness, the motorcycle exhibits small oscillations around the target trajectory. This is due to the combination of two factors, the road excitation that tends to perturb the vehicle motion and the high camber angle of the motorcycle, slightly lower than 60 deg, that couples the lateral and vertical dynamics. As a consequence, the rider has to constantly correct the path in order to follow the desired trajectory. In any case, the path error remains lower than 7 cm.

The motorcycle reaches very high acceleration levels during the simulated manoeuvre as shown in Figs. 6.23d and 6.23e. As a matter of fact, the average longitudinal acceleration of the vehicle during the braking phase is -11.5 m/s^2 whereas the lateral acceleration in the corner reaches more than 12 m/s^2 . Both acceleration profiles are smooth when the vehicle travels on the flat road and show high frequency oscillations if the road irregularities are considered. It is interesting to observe that the lateral acceleration starts oscillating as the vehicle progresses into the corner. This is due to the coupling effect of the roll angle, which remains small during the initial phase of the manoeuvre and increases as the motorcycle enters the turn.

One of the most interesting results of the corner entry manoeuvre are the tyre loads, shown in Figs. 6.23f and 6.23g for the front and rear tyres respectively. The load available at the rear tyre is of particular importance as it allows to measure the severity of the braking. We can observe that the rear load reaches a minimum value of 60 N

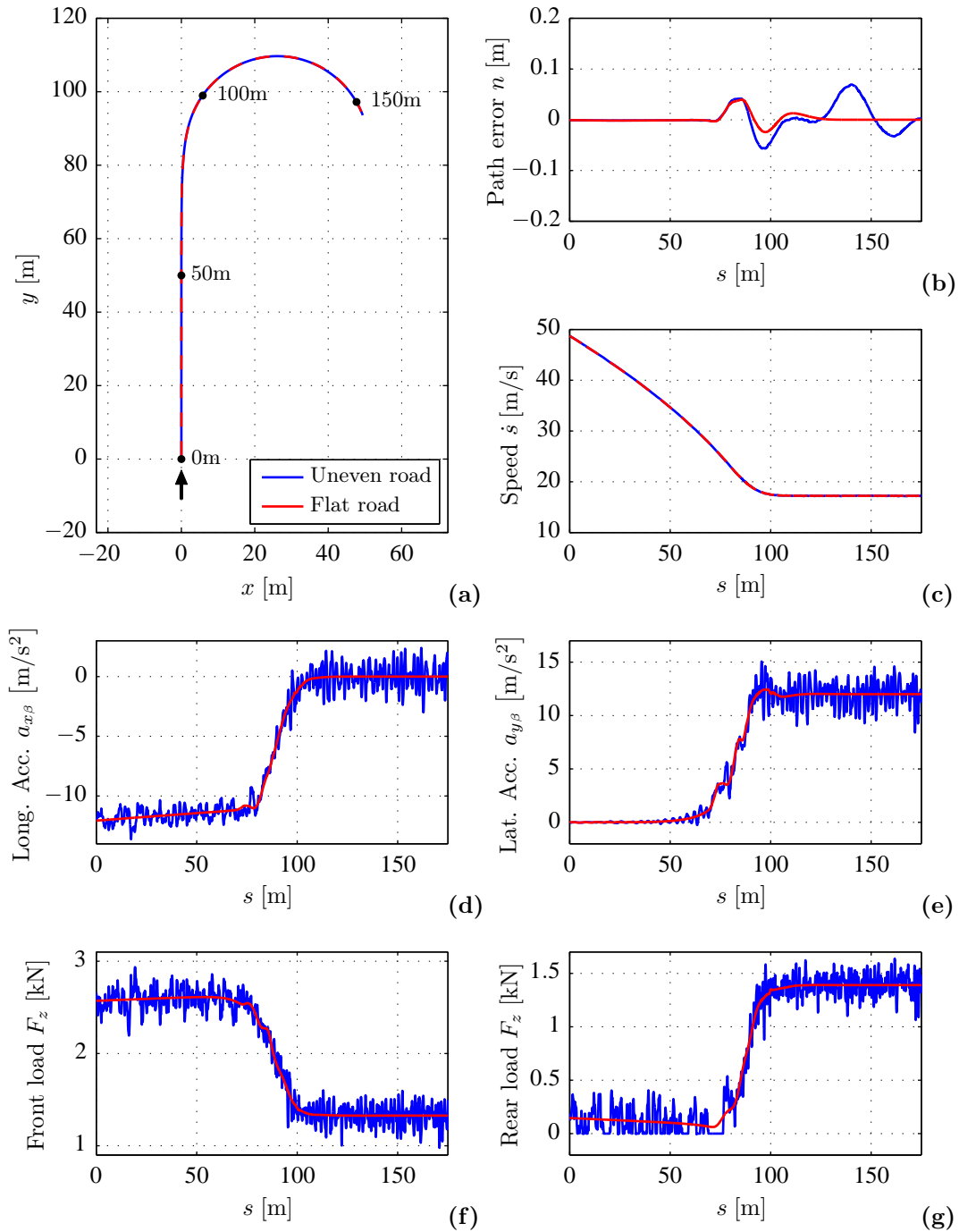


Figure 6.22: Corner entry results. a) Trajectory. b) Path error. c) Curvilinear speed. d) Longitudinal acceleration. e) Lateral acceleration. f) Front tyre load. g) Rear tyre load.

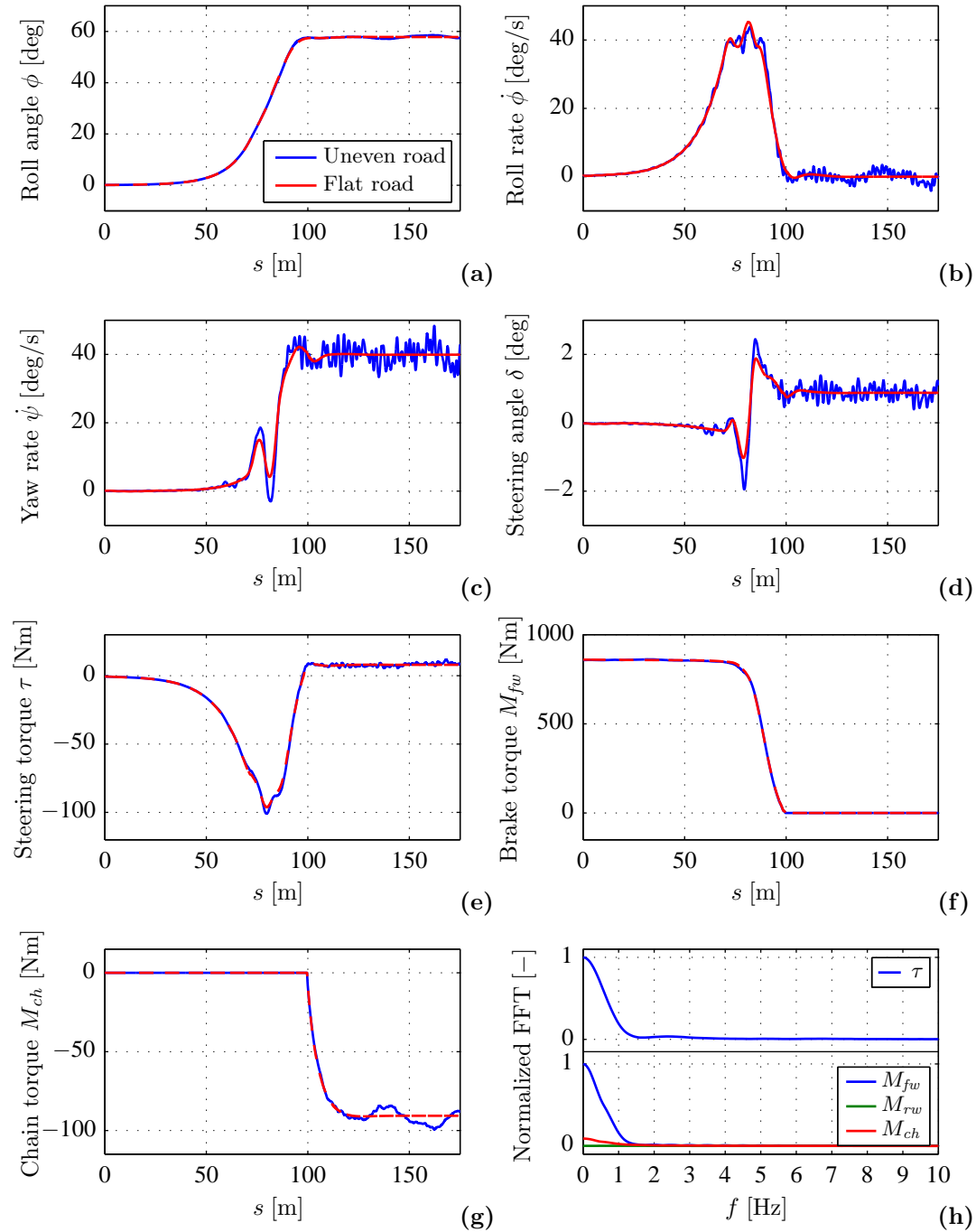


Figure 6.23: Corner entry results. a) Roll angle. b) Roll rate. c) Absolute yaw rate. d) Steering angle. e) Steering torque. f) Front brake torque. g) Chain torque. h) Normalized FFT for the uneven road case (peak hold spectrum).

when the road is flat and vanishes repeatedly on the uneven road. Basically, this implies that the rider cannot brake any harder as the rear wheel is virtually floating over the road and any additional deceleration could cause the motorcycle to flip over.

The most significant loss of contact happens between $s=69$ m and $s=76.3$ m, meaning that the wheel is in the air for more than 7 m. This interval also coincides with the point of minimum load in the flat road case. It is worth noting from Figs. 6.23a and 6.23b that at that point the motorcycle is moderately inclined (20 deg) and that the roll rate is close to its maximum (40 deg/s). As a consequence, the rear end of the motorcycle tends to move towards the outside of the corner, thus leading to a high yaw rate that can be clearly observed in Fig. 6.23c. As a countermeasure, and in order not to lose the control of the vehicle, the rider applies a negative steering angle, i.e. steers towards the left, see Fig. 6.23d, which brings the rear end back onto the trajectory. Note also that the steering angle is larger when the road excitation is considered.

After this stabilization manoeuvre, the rider steers to the right in order to stop the roll motion and to progressively reach a steady state motion. As discussed earlier, the road unevenness generates oscillations around the stationary conditions. This can be observed in both the yaw rate and the steering angle.

The next three figures show the control actions exerted by the rider, namely the steering torque, the front braking torque and the chain torque. The rear braking torque is not used in this case due to the low load available at the rear tyre. We can observe that the blue curves are slightly more oscillatory than the red ones but in general there are no significant differences between the flat and uneven roads. To conclude, the last figure shows the frequency content of the rider control actions for the uneven road case. Interestingly, the frequency content is quite limited despite the high frequency excitation introduced by the road.

6.4 Concluding remarks

In this chapter we have introduced a novel methodology for the dynamic simulation of motorcycles. In particular, we have developed a control strategy capable of riding a nonlinear motorcycle model in a wide range of conditions, including extremely demanding manoeuvres such as those performed by racing riders.

As a dynamic system, motorcycles can be regarded as nonlinear, non-minimum phase, unstable and underactuated. This makes the design of a virtual rider a rather challenging task. In this context, the application of Model Predictive Control (MPC) has proven to be successful, leading to a virtual rider that is at the same time versatile, efficient and robust.

The simulation methodology introduced in this chapter combines the main tools developed throughout the present PhD thesis with a model predictive controller. These tools comprise a symbolic multibody model, a novel procedure to estimate the roll dynamics of the vehicle and an extended methodology for the quasi-steady state analysis of motorcycles.

The multibody model of the motorcycle is employed at two different levels in this chapter. In first place, it is used as the *nonlinear plant* to be controlled, i.e. it represents the real vehicle within the simulation environment. In second place, and most importantly, it is used to build the *internal model* on which the controller is based. Such model symbolizes the rider's mental image of the motorcycle, i.e. a representation of the inverse dynamics of the vehicle that the human mind constantly tunes based on experience. Humans use this stored knowledge while riding to estimate the future behavior of the vehicle and then act accordingly to achieve the desired goal, e.g. to follow a predefined path. The proposed controller works in a similar way. It uses the internal model to formulate a prediction model, which is subsequently optimized in order to minimize the error between the system's output and the control target.

The highly nonlinear character of the motorcycle makes the design of the internal model a complex task. Variables such as the travelling speed, the curvature of the trajectory or the longitudinal acceleration have a strong impact on the system dynamics. It is here that the quasi-steady analysis becomes essential. Let's recall that this approach allows us to estimate all system states and control inputs along the target manoeuvre. Based on that, we have built a family of internal models by linearizing the motorcycle equations around the quasi-steady state solution of the problem. As a result, the response of the proposed controller changes along the track in order to adapt to the varying dynamics of the vehicle.

The control actions of the rider model are the result of three different contributions: feedforward, state feedback and predictive. The feedforward contribution simply contains the quasi-steady state estimation of the control variables. This term, which is applied in open loop, might be seen as the rider's idea on how to negotiate the desired manoeuvre before it actually takes place. The other two terms, on the other hand, are included to compensate the differences between the quasi-steady state solution and the actual dynamics of the vehicle. Additionally, a learning strategy has been introduced to iteratively improve the internal model and the feedforward action of the controller, leading to a significant enhancement in the tracking performance of the rider model.

The tracking capabilities of the rider model have been tested on four aggressive manoeuvres: a slalom test, a chicane, a corner exit and a corner entry. Excellent results have been observed in all cases. The speed error has been found to be negligible in all

manoeuvres whereas the maximum path error varies between 2.5 cm in the slalom test to 9 cm in the corner exit manoeuvre. Errors of that order of magnitude are considered small, especially if we take into account the dimensions of the motorcycle and the extreme conditions to which it is subject.

The slalom maneuver is characterized by an extreme roll rate that oscillates between ± 130 deg/s. Under these conditions, both tyres undergo a severe load variation, with the rear changing more than 2.2 kN at 1.88 Hz. The chicane, on the other hand, is characterized by a high combined use of the tyres as the motorcycle corners and accelerates at the same time. In addition to this, the abrupt transition from acceleration to braking makes this manoeuvre a challenging test for the rider model.

The last two manoeuvres are particularly demanding, not only due to the high acceleration levels but also due to the low tyre loads reached during the simulation. The most interesting feature of the corner exit manoeuvre is that the vertical load at the front wheel vanishes due to the high acceleration. Similarly, the load at the rear wheel vanishes during the corner entry manoeuvre. Furthermore, in this last simulation, the road unevenness has been considered, which makes the rider control task highly demanding due to the presence of external noise.

The rider model has shown an excellent tracking performance in all four manoeuvres, being able to successfully deal with short-lived discontinuities in the tyre forces such as wheelie and stoppie events. In addition to that, it has shown to be robust against external disturbances like, for instance, those introduced by the road profile. The capability to simulate aggressive motorcycle manoeuvres along uneven roads had, to the best of the author's knowledge, never been presented in literature before.

Success can only be achieved with a kind of pioneer spirit and the repeated use of three tools: failure, introspection and courage.

Soichiro Honda

Chapter 7

Conclusions and future work

In this final chapter we summarize the main findings of the present work and their practical applications. To conclude, we present a series of recommendations for future research lines.

7.1 Conclusions

The existing literature on motorcycle dynamics and rider modelling was reviewed in the first part of this thesis. A thorough analysis revealed that current motorcycle models have reached a high level of applicability. As a matter of fact, simulation is applied nowadays within the motorcycle industry for a wide range of purposes that go, for example, from comfort analysis to the design of advanced riding assistance systems. However, most of these simulations are limited to basic manoeuvres, mainly straight line and slow cornering. It emerges from the literature that, although significant progress has been made in the last decade in the field of rider modelling, a satisfactory solution for the dynamic simulation of motorcycles is yet to be found.

As a dynamic system, motorcycles are highly nonlinear, non-minimum phase, unstable and underactuated. This makes motorcycle control a rather challenging task. Existing rider models work well only under certain conditions, being generally limited to smooth speed profiles, moderate longitudinal accelerations and low roll angles. Most

of them also require a great deal of interaction from the user to adjust the controller parameters. Finally, many of these rider models are based on highly simplified motorcycle models that do not take into account the main vibration modes of the vehicle (wobble, weave, etc), which in turn compromises their accuracy.

The lack of tools for the dynamic simulation of motorcycles inspired the development of the present thesis, which introduces a novel approach for the simulation of complex manoeuvres based on Model Predictive Control (MPC). The main contribution of this work is a control strategy capable of riding a nonlinear motorcycle model in a wide range of conditions, including extremely demanding manoeuvres such as those performed by racing riders.

Thanks to the literature review, it became clear from the early stages of this thesis that the development of an advanced rider model would require the implementation of specific simulation tools not available in any commercial code. Such limitation motivated the in-house development of all necessary tools for the realization of this project. These include, in addition to the virtual rider, a detailed multibody model of the motorcycle and a new methodology for the quasi-steady state analysis of motorcycles.

The multibody model of the motorcycle

The multibody model, which describes the nonlinear dynamics of a generic road motorcycle, comprises several characteristics that make it especially suitable for the purposes of this thesis. In first place, it is formulated in minimal coordinates as a system of Ordinary Differential Equations (ODE). This approach makes the state space representation of the system straightforward and facilitates the design of control systems like the virtual rider. In second place, the equations of motion have been significantly simplified by exploiting algebraic manipulation, thus producing an efficient simulation code able to run in real-time. Finally, the model equations have been augmented by including three curvilinear coordinates that allow the user to parameterize the target manoeuvre in a direct and intuitive way.

This last feature represents an improvement with respect to Sharp's work [100], who defines the target trajectory in terms of Cartesian coordinates. The shape of the road, slender along its longitudinal dimension and narrow across it, makes curvilinear coordinates a more appropriate choice for the simulation of road vehicles. One of the main benefits of this approach is that the computation of the tracking error becomes straightforward. As a matter of fact, the lateral and angular deviations of the motorcycle with respect to the target trajectory are included, by definition, in the vector of curvilinear coordinates.

However, the most important difference, and what makes curvilinear coordinates more convenient in this case, is that they significantly simplify the design of the control

strategy. Basically, Cartesian coordinates require the control gains to be transformed from the inertial frame on which they were derived to the vehicle frame [119]. This process, which must be repeated at each time step, is not required when using curvilinear coordinates.

The multibody model of the motorcycle has been employed at two different levels throughout the thesis. In first place, it is used as the *nonlinear plant* to be controlled, i.e. it represents the real vehicle within the simulation environment. In second place, and more importantly, the motorcycle model is used to build the *internal model* on which the virtual rider is based. Such model symbolizes the rider's mental image of the motorcycle, i.e. a representation of the inverse dynamics of the vehicle that the human mind constantly tunes based on experience. Humans use this stored knowledge while riding to estimate the future behavior of the vehicle and then act accordingly to achieve the desired goal, e.g. to follow a predefined path. The proposed controller works in a similar way. It uses the internal model to formulate a prediction model, which is subsequently optimized in order to minimize the error between the system's output and the desired control targets.

In contrast to other authors, such as Frezza [73–75] and Saccon [76], who use highly simplified models in their control strategies, the internal model developed in this thesis possesses a higher level of detail. In particular, it includes a detailed description of the steering kinematics, nonlinear thick tyres, suspensions, etc. Those features are essential to implement control strategies based on the steering torque (force control).

Conversely, Saccon's model possesses only four degrees of freedom and features a simplified steering geometry. As far as the tyre model is concerned, this author uses thin linear tyres and neglects the aligning/twisting moments. Due to these simplifications, models like Saccon's are only suitable to design control strategies based on the steering angle (position control). Although such approach has been widely accepted to model car drivers, it leads to unrealistic vibration modes when applied to motorcycles as it cancels the steering dynamics [11]. In order to avoid the drawbacks of position control, a force approach has been used in this thesis at the expense of a higher complexity of the internal model.

The internal model of the virtual rider

Motorcycle dynamics are known to be notably influenced by the travelling speed, the curvature of the trajectory and the longitudinal acceleration among other factors. To deal with such a nonlinear system, the control strategy introduced in this work uses a varying internal model that continuously adapts to the vehicle conditions. The quasi-steady state solution of the motion equations has played a fundamental role in the development of the internal model.

The study of the stationary motion of vehicles is widespread in the automotive literature, especially as far as four-wheeled vehicles are concerned. In this thesis we have extended the method to solve the quasi-steady state motion of motorcycles along continuous manoeuvres. The proposed approach is based on the reduction of the dynamic model to a set of nonlinear algebraic equations. Unlike other existing techniques in literature, the method presented here is not limited to the constant speed analysis of motorcycles. In addition to the longitudinal acceleration, we also account for the roll rate and its derivative, the roll acceleration. The inclusion of these two terms has been found to be essential when the direction of the motorcycle changes rapidly.

Given the manoeuvre specifications, defined in terms of the target trajectory and the desired speed profile, the solution of the extended problem yields an approximation of all vehicle states and control inputs along the target path. Such solution provides an appropriate framework on which to develop the rider control strategy. Based on it, we have built a family of internal models by linearizing the motorcycle equations around the quasi-steady state solution of the manoeuvre. This procedure constitutes the core of the MPC controller and ensures that the rider's response is always aligned with the current dynamics of the vehicle.

Another advantage of the quasi-steady state solution is that the estimated control inputs can be used as a feedforward action during the dynamic simulation. We have shown that such strategy significantly improves the performance of the rider model. The reason lies in the fact that the feedforward action takes up most of the control effort whereas the MPC controller only needs to apply small corrections to compensate the differences between the quasi-steady state estimation and the actual dynamic behaviour of the vehicle.

In addition to the above, we have introduced an iterative algorithm that improves the tracking performance of the controller after each simulation. We can see this iterative loop as a learning algorithm where the rider, based on the results of previous simulations, progressively updates its internal model and its feedforward term until the desired behaviour is reached. This procedure has allowed to significantly reduce the trajectory errors down to a few centimeters even during extreme manoeuvres.

In 2010, during the development of the present PhD thesis, Massaro introduced his rider model based on MPC [166–168]¹. The main improvements of this thesis with respect to Massaro's work are the procedure employed to obtain the internal model and the learning algorithm.

¹It is important to mention here that the research to be defended in this thesis was developed previously to the publication of Massaro's results and has no relation whatsoever with his work. Massaro's work was first published in October 2010 [166], whereas the methodology introduced in this thesis was first presented in February 2010 [128].

Specifically, Massaro obtains his internal model by linearizing the equations of motion around a pure steady state condition, whereas in this thesis we use an extended quasi-steady state approach. The main difference between both approaches lies in the longitudinal acceleration and the roll derivatives, which are not considered by the aforesaid author. As we have seen throughout this dissertation, these terms are essential to simulate aggressive manoeuvres. In fact, we proved that neglecting the effect of roll dynamics leads to an unfeasible solution in some cases like, for example, the slalom manoeuvre of Chapter 5. This implies that it would not be possible to solve this particular manoeuvre by using a pure stationary approach like Massaro's. Additionally, the learning algorithm presented in this thesis together with a more accurate estimation of the feedforward term allow us to reach lower tracking errors with respect to Massaro's model.

Sensitivity study in quasi-steady state conditions

In addition to the development of the control strategy, the quasi-steady state analysis has been used as a standalone tool in order to gain insight into the behaviour of the motorcycle. An extensive sensitivity study in steady state and quasi-steady state conditions was conducted in the initial chapters of this thesis, thus allowing us to anticipate some of the design requirements of the virtual rider.

The steady state motion of the motorcycle permitted us to explore how the most relevant variables (e.g. steering angle, tyre forces, etc) vary as a function of the corner radius and the vehicle speed. Of particular interest is the high sensitivity of the lateral and longitudinal control variables with respect to the cornering conditions. We have shown that the steering torque required to follow a given trajectory changes drastically with the vehicle speed and the corner radius, with the map that relates these three variables being highly nonlinear.

On the other hand, the quasi-steady state motion of the motorcycle allowed us to assess the effect of the most relevant derivatives, namely the longitudinal acceleration and the roll derivatives. The aim of this analysis was to determine to what extent these three terms modify the solutions obtained assuming pure stationary conditions.

The study of the longitudinal acceleration confirmed well known evidences, i.e. that the longitudinal acceleration has a great impact on the steering torque during braking and that the combined use of the tyres tends to increase the understeering character of the motorcycle in braking and makes it more oversteering in acceleration. As far as the roll derivatives are concerned, it has been shown that they have a strong effect on the lateral control of the vehicle and cannot be neglected in the quasi-steady state solution.

This is especially true in those manoeuvres where the direction of travel changes quickly, e.g. slalom tests and lane change manoeuvres.

In particular, the steering torque is highly sensitive to the roll rate. When the motorcycle approaches a corner, the gyroscopic effect of the front wheel tends to rotate the handlebar towards the inside of the corner, thus helping the vehicle to change direction. At high roll rates, this effect generally dominates the steering torque. The roll acceleration, on the other hand, affects mainly the roll angle required to perform a given manoeuvre. Interestingly, higher roll accelerations allow the motorcycle to follow tighter (local) trajectories.

Performance of the rider model

The performance of the rider model has been tested on four aggressive manoeuvres: a slalom test, a chicane, a corner exit and a corner entry. Excellent results have been observed in all cases. The speed error has been found to be negligible in all manoeuvres whereas the maximum path error varies between 2.5 cm in the slalom test to 9 cm in the corner exit manoeuvre. Errors of that order of magnitude can be considered small, especially if we consider the extreme conditions to which the motorcycle is subject.

The slalom maneuver is characterized by a high roll rate that oscillates between ± 130 deg/s. Under these conditions, both tyres undergo a severe load variation, with the rear changing more than 2.2 kN peak to peak at 1.88 Hz. The chicane, on the other hand, is characterized by a high combined use of the tyres as the motorcycle corners and accelerates at the same time. In addition to this, the abrupt transition from acceleration to braking makes this manoeuvre a challenging test for the rider model.

The corner exit and corner entry manoeuvres are particularly demanding, not only due to the high acceleration levels but also due to the low tyre loads reached during the simulation. The most interesting feature of the corner exit manoeuvre is that the vertical load at the front wheel vanishes due to the high acceleration. Similarly, the load at the rear wheel vanishes during the corner entry manoeuvre. These phenomena, usually called *wheelie* and *stoppie* in the racing jargon, only happen when the vehicle approaches its acceleration limit, which gives us an idea of the severity of the manoeuvre. Furthermore, the road unevenness has been considered in the last simulation, which makes the rider control task even more challenging due to the presence of road noise.

To conclude, we can say that the rider model has shown an unprecedented tracking performance even in the presence of road noise. To the best of the author's knowledge there is no rider model in the literature that shows a similar performance.

7.2 Summary of the main contributions

We can summarize the main contributions of this dissertation in the following four points, with the first three being intermediate steps needed to reach the fourth.

- A symbolic multibody model of the motorcycle. This model provides a suitable framework for the development of simulation tools aimed at the study of motorcycle dynamics. Some of these applications are exploited in the research, others are only suggested. The model comprises several characteristics that make it unique. In first place, it is formulated in minimal coordinates as a system of Ordinary Differential Equations (ODE), which simplifies the design of rider's control strategy. In second place, the model equations have been augmented with three curvilinear coordinates that allow to parameterize the desired manoeuvre in a direct and intuitive way. In addition to that, the equations of motion have been significantly simplified by exploiting algebraic manipulation, thus producing an efficient simulation code.
- An extended methodology for the quasi-steady state analysis of motorcycles. Given target trajectory and the desired speed profile, the solution of the extended quasi-steady state problem allows us to obtain a suitable estimation of the model states and control inputs along the target manoeuvre. Unlike other existing techniques in literature, the methodology presented in this thesis is not limited to the stationary analysis of motorcycles. In addition to the longitudinal acceleration, we account for the roll rate and its derivative, the roll acceleration. These two terms have been shown to be fundamental when simulating quick direction changes.
- An extensive sensitivity study of the motorcycle behaviour in steady state and quasi-steady state conditions. The steady state analysis has shown how the most relevant variables (e.g. steering angle, tyre forces, etc) vary as a function of the speed of the vehicle and the corner radius. The quasi-steady state analysis, on the other hand, has shown the effect of the longitudinal acceleration and the roll derivatives. Despite the simplifying assumptions, this analysis is capable of predicting important aspects of vehicle behaviour; limitations have been discussed and analysed.
- A novel rider model for motorcycles based on Model Predictive Control. As the major contribution of the present thesis, we present a nonlinear controller capable of driving a multibody motorcycle model along extremely demanding manoeuvres. Such controller is assisted by a learning strategy that builds a feedforward action

based on previous results, thus iteratively improving its performance. The proposed rider model shows an unprecedented tracking performance, with the maximum path deviation being of the order of a few centimeters during aggressive manoeuvring. Excellent results have also been obtained when the road unevenness is considered in the simulations.

7.3 Practical application of the results

Motorcycle performance has reached a point where, to make further improvements, a global and multidisciplinary understanding of the vehicle is essential. The interaction of such diverse elements as road, suspensions, chassis, engine, driver, sensors and electronics cannot be neglected in the design process of new devices. It is in this challenging framework where the rider model introduced in this thesis can contribute to the evolution and development of new concepts.

One potential application of the virtual rider is the development and validation of active safety devices for motorcycles such as antilock braking systems (ABS), combined braking systems (CBS), electronic steering dampers, slipper clutches, traction control systems (TCS) and wheelie protection systems. In this case, computer simulations not only decrease the development time and limit the number of prototypes needed to validate a new design, but they also permit conducting experiments in dangerous conditions with no risk for the human rider.

For example, ABS enhances motorcycle safety by reducing the likelihood of the brakes locking in an emergency situation. The concept is basically the same as for passenger cars; when a wheel is about to lock during hard braking, the caliper pressure is automatically decreased through a modulator. However, the large roll angles achieved during cornering make the application of ABS to motorcycles a more challenging task. Some manufacturers also combine ABS and CBS, which introduces additional complexity to the problem.

The virtual rider enables us to simulate emergency braking situations in both straight line and cornering conditions. By integrating the ABS/CBS strategy into the simulation loop, the rider model can provide valuable information to assess new strategies. Simulations can also highlight undesired interactions between the braking strategy, the steering system and lightly damped modes such as wobble and weave. In addition to this, we can use the rider model to investigate the response of these devices on bumpy roads. The robustness of the rider model becomes essential in this last case.

Most of the systems listed above are also used at the racing track for different purposes. In particular, slipper clutches, traction control systems and anti-wheelie

systems are broadly used in modern racing machines to enhance their performance. The development and tuning of these devices is a complex task that is usually based on the subjective opinion of the rider.

In this context, the virtual rider allows racing engineers to assess the performance of new devices from an objective point of view. A typical application would be the assessment of anti-wheelie systems, which are designed to prevent the front wheel from lifting-off during acceleration. To do so, one simply has to request the rider model to accelerate over the wheelie limit and investigate the response of the wheelie controller when it kicks in. As with the ABS, the road profile plays an important role in the performance of the controller as bumps tend to push the front wheel up. A similar approach could be used to assess the performance of traction control systems.

Too much engine brake during corner entry can lead to instability problems, e.g. wheel hop, chatter, traction loss, etc. In order to prevent them, racing motorcycles are fitted with slipper clutches. Such devices disengage the clutch when the engine brake overcomes a predefined threshold. Hence, the setting of the clutch is usually a compromise between maximizing the deceleration and improving braking stability. By adding a powertrain model to the existing simulation framework, it is possible to evaluate the effect of clutch settings on both vehicle performance and stability.

In addition to the development of the control strategies described above, the rider model can also be used to study the impact of standard setup changes in the response of the vehicle, e.g. suspension tuning, mass distribution, etc. In conclusion, the versatility and robustness shown by the rider model presented in this thesis opens the door to a wide range of applications.

7.4 Future research lines

It is worth noting that we have not considered the neuromuscular limits of human beings in the development of the virtual rider. More specifically, the controller includes no delays and its bandwidth is only bounded by the model dynamics. Although the frequency content of the rider controls seems realistic in the time domain simulations of Chapter 6, an accurate representation of the rider's neuromuscular behavior is desirable. This is especially important for the simulation of those active safety devices that interact with the steering system. An extensive work on the neuromuscular behavior of car drivers has been carried at the University of Cambridge [169–171] and could be used as a reference point for future research lines.

Experimental evidence [172] suggests that the rider rolls and moves laterally on the saddle during weave oscillations. In addition to this, the assumption that the rider is

rigidly connected to the chassis is no longer valid at high frequencies. This is especially important for the ride analysis of two wheeled vehicles, where the effect of the rider's mass can be significant. It is considered that a detailed model of the human body could be highly beneficial in this case. Further research in this direction is strongly recommended.

The application of the virtual rider to assess the effect of chassis flexibility is also suggested. As a matter of fact, the consequences of structural modifications on motorcycle performance are yet to be fully understood. This is one of the most challenging topics in modern motorcycle racing. Several tests performed by the author outside the scope of this thesis have shown very promising results. It should be emphasized that most of the effort to go from rigid to flexible simulations concerns the nonlinear plant. The internal model, on the other hand, requires only minor modifications as we are not interested in controlling the high frequency dynamics related to body flexibility.

Also related to motorsports, it could be interesting to investigate the applicability of the rider model to laptime optimization. The current model requires the target path and the desired speed profile to be provided. Ideally, only the track boundaries should be needed to optimize the travelling time around any given track. To that end, a constrained MPC formulation is recommended. Constraints are necessary to model the different factors that limit the performance of the vehicle, e.g. track boundaries, engine power, tyre grip, etc. The work presented in [173] on the laptime optimization of Formula 1 cars could be a good starting point for this research. Following the same research line, it would be of great interest for motor racing teams to quantify the effect of the road profile on both rider effort and vehicle performance.

As far as the quasi-steady state analysis is concerned, it would be straightforward to extend it for optimization purposes. In particular, acceleration envelopes and optimal speed profiles could be computed with minor modifications of the methodology introduced in Chapters 4 and 5. An example of the acceleration envelope is shown in Fig. 7.1a. These kind of figures, also known as g-g diagrams, are obtained by maximizing the combined acceleration of the vehicle at a given speed. They are especially helpful to understand the performance limits of the vehicle and how they vary as the speed changes. For example, the concave regions at the top and bottom parts of the diagram reveal that at 20 m/s this specific motorcycle is slightly limited in acceleration by the lifting of the front wheel (wheelie) and strongly limited in braking by the lifting of the rear end (stoppie). Likewise, the quasi-steady state optimization of the speed profile would require a limited effort. As an example, Fig. 7.1b shows the optimal speed profile along Mugello track, where the braking and acceleration traces can be clearly identified.

Some other topics of interest are the following: a comprehensive study about the

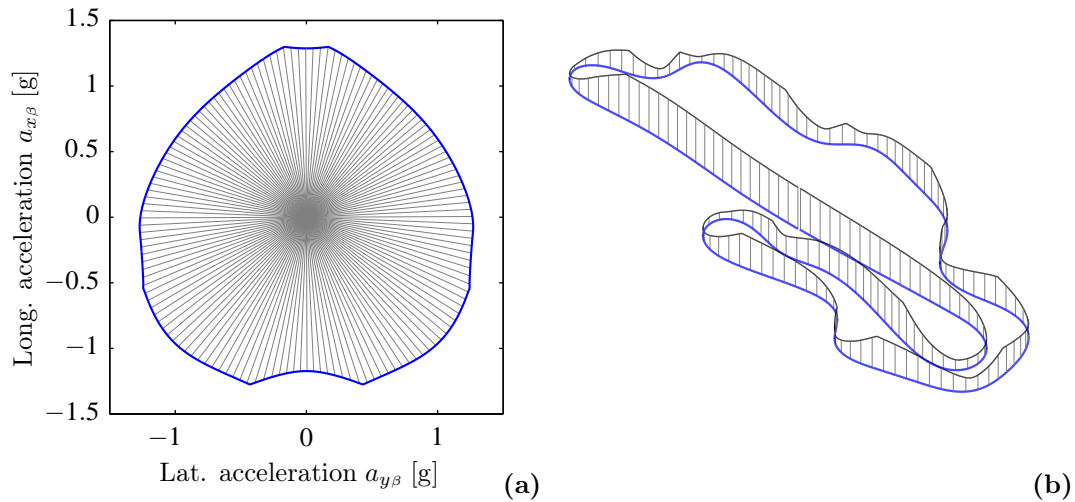


Figure 7.1: Future research lines: applications of the symbolic motorcycle model to performance analysis and optimization. a) Example of g-g diagram at 20 m/s . b) Optimal speed profile for Mugello track.

learning algorithm introduced in Chapter 6 and how to improve its convergence rate; the development of more efficient continuation strategies for the quasi-steady state analysis of Chapter 5; the introduction of new constraints to enhance the definition of the roll axis in the quasi-steady state formulation of Chapter 4; and the use of more appropriate tyre models for the simulation of uneven roads, e.g. MF-SWIFT [12].

Finally, it could also be interesting to verify the capabilities of the virtual rider within a hardware-in-the-loop system and to validate it against experimental data. This would permit us to evaluate the response of embedded systems (e.g. safety systems, ECUs, control systems, etc.) prior to track testing. Additional work on the model efficiency would be beneficial in this context. This should try to exploit the latest advances in the field of parallelization and GPU computing.

Appendix A

Reduced model

In Chapter 3 we introduced the multibody model of the motorcycle used throughout this thesis for quasi-steady state and dynamic simulations. Such model is composed of 6 rigid bodies, possesses 11 degrees of freedom and includes a relaxation model for the lateral dynamics of the tyres. Its complexity is perfectly suited for the purposes of this thesis. However, it is usually difficult to interpret simulation results by looking at the symbolic equations due to their large size, e.g. to investigate how the roll rate and the tyre loads are linked. In order to overcome this limitation, we introduce in this appendix a reduced model that captures the fundamental motion of the motorcycle. This new model is not intended for simulation purposes but to provide a simple set of equations, useful to interpret simulation results, particularly in quasi-steady state conditions.

A.1 Newton-Euler equations

The reduced model, shown in Fig. A.1, is composed of one main body plus the rotational effect of the wheels. Next we describe the main assumptions used to derive its equations of motion.

The equations are derived by lumping the inertial properties of the vehicle at its centre of gravity \mathbf{G} with the exception of the rotational inertia of the tyres. The distance between the centre of gravity of the vehicle \mathbf{G} and the ground point \mathbf{P} is assumed constant and equal to h . The motorcycle is directly controlled by the kinematic steering angle Δ . Due to the simplified steering geometry and the absence of suspensions, the pitch motion is not considered. The tyre forces are applied at the contact points, \mathbf{C}_f and \mathbf{C}_r , which are located at a constant distance from the centre of gravity. We denote with the letter a the distance from the front contact point to point \mathbf{P} and with b the distance from the rear contact point to point \mathbf{P} . Lastly, the tyres are modelled as thin discs, i.e. we do not consider the shape of their cross section in the reduced model.

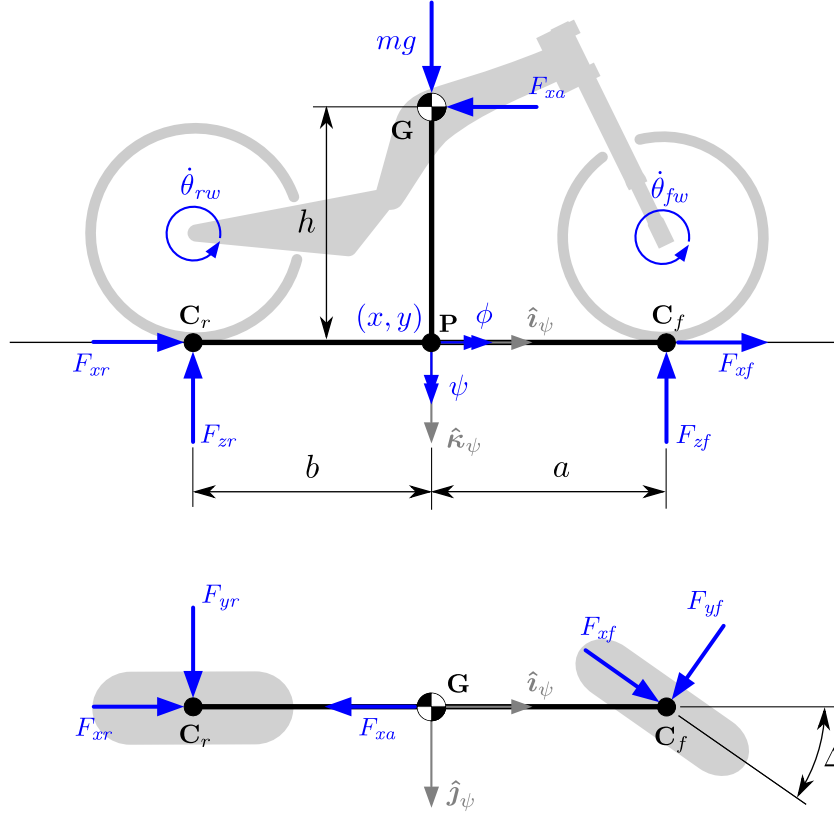


Figure A.1: Reduced model. The model is composed of one main body plus the rotational effect of the wheels. The distance between the centre of gravity of the vehicle \mathbf{G} and the ground point \mathbf{P} is constant and equal to h . We denote with the letter a the distance from the front contact point to point \mathbf{P} and with b the distance from the rear contact point to point \mathbf{P} .

We use here the same reference frame employed to derive the equations of the full model, i.e. the vehicle frame \mathbf{T}_ψ has its origin at the reference point \mathbf{P} , $\hat{\mathbf{i}}_\psi$ is aligned with the longitudinal direction of the vehicle, $\hat{\mathbf{j}}_\psi$ points to the right side and $\hat{\mathbf{k}}_\psi$ points downwards. The motion of the main body is parameterized by the Cartesian position of the reference point \mathbf{P} with respect to the inertial frame (x, y) and by the rotations associated to the roll ϕ and yaw ψ degrees of freedom. Based on the above, we can write the acceleration of the centre of gravity as

$$a_x^{cg} = a_{x\psi} - \ddot{\psi}hs_\phi - 2\dot{\psi}\dot{\phi}hc_\phi \quad (\text{A.1})$$

$$a_y^{cg} = a_{y\psi} + \ddot{\phi}hc_\phi - \dot{\psi}^2hs_\phi - \dot{\phi}^2hs_\phi \quad (\text{A.2})$$

$$a_z^{cg} = \ddot{\phi}hs_\phi + \dot{\phi}^2hc_\phi \quad (\text{A.3})$$

where $a_{x\psi}$ and $a_{y\psi}$ are the longitudinal and lateral acceleration of the reference point \mathbf{P}

expressed in the vehicle frame, i.e.

$$\begin{bmatrix} a_{x\psi} \\ a_{y\psi} \end{bmatrix} = \begin{bmatrix} c_\psi & s_\psi \\ -s_\psi & c_\psi \end{bmatrix} \begin{bmatrix} \ddot{x} \\ \ddot{y} \end{bmatrix} = \begin{bmatrix} \dot{u} - v\dot{\psi} \\ \dot{v} + u\dot{\psi} \end{bmatrix} \quad (\text{A.4})$$

The Newton equations in the vehicle frame \mathbf{T}_ψ are straightforward,

$$ma_x^{cg} = F_{xr} - F_{yf}s_\Delta + F_{xf}c_\Delta - F_{ax} \quad (\text{A.5})$$

$$ma_y^{cg} = F_{yr} + F_{xf}s_\Delta + F_{yf}c_\Delta \quad (\text{A.6})$$

$$ma_z^{cg} = mg - F_{zr} - F_{zf} \quad (\text{A.7})$$

whereas the Euler equations are computed as the equilibrium of moments about the three axes of \mathbf{T}_ψ , which yields:

$$m(-\ddot{\phi}h + \dot{\psi}^2hc_\phi s_\phi - a_{y\psi}c_\phi + gs_\phi)h + M_x^{\mathcal{I}} = 0 \quad (\text{A.8})$$

$$ma_x^{cg}hc_\phi + F_{ax}hc_\phi - bF_{zr} + aF_{zf} + M_y^{\mathcal{I}} = 0 \quad (\text{A.9})$$

$$ma_x^{cg}hs_\phi + F_{ax}hs_\phi - bF_{yr} + aF_{xf}s_\Delta + aF_{yf}c_\Delta + M_z^{\mathcal{I}} = 0 \quad (\text{A.10})$$

They are expressed in implicit form for convenience. The terms $M_x^{\mathcal{I}}$, $M_y^{\mathcal{I}}$ and $M_z^{\mathcal{I}}$ comprise the moments related to the inertia matrix of the main body ($\mathcal{I}_x, \mathcal{I}_y, \mathcal{I}_z$) and to the axial inertia of the wheels ($\mathcal{I}_{fw}, \mathcal{I}_{rw}$). They are summarized in Tables A.1 and A.2.

axis	gyroscopic	inertial
$M_x^{\mathcal{I}}$	$-(\mathcal{I}_z - \mathcal{I}_y)\dot{\psi}^2c_\phi s_\phi$	$-\mathcal{I}_x\ddot{\phi}$
$M_y^{\mathcal{I}}$	$+ \left(2(\mathcal{I}_z - \mathcal{I}_y)c_\phi^2 - \mathcal{I}_z + \mathcal{I}_y - \mathcal{I}_x \right) \dot{\psi}\dot{\phi}$	$(\mathcal{I}_z - \mathcal{I}_y)\ddot{\psi}c_\phi s_\phi$
$M_z^{\mathcal{I}}$	$+ 2(\mathcal{I}_z - \mathcal{I}_y)\dot{\psi}\dot{\phi}c_\phi s_\phi$	$- \left((\mathcal{I}_z - \mathcal{I}_y)c_\phi^2 + \mathcal{I}_y \right) \ddot{\psi}$

Table A.1: Gyroscopic and inertial torques generated by the main body.

axis	gyroscopic	inertial
$M_x^{\mathcal{I}}$	$+(\mathcal{I}_{rw}\dot{\theta}_{rw} + \mathcal{I}_{fw}\dot{\theta}_{fw})\dot{\psi}c_\phi$	-
$M_y^{\mathcal{I}}$	$+(\mathcal{I}_{rw}\dot{\theta}_{rw} + \mathcal{I}_{fw}\dot{\theta}_{fw})\dot{\phi}s_\phi$	$-(\mathcal{I}_{rw}\ddot{\theta}_{rw} + \mathcal{I}_{fw}\ddot{\theta}_{fw})c_\phi$
$M_z^{\mathcal{I}}$	$-(\mathcal{I}_{rw}\dot{\theta}_{rw} + \mathcal{I}_{fw}\dot{\theta}_{fw})\dot{\phi}c_\phi$	$-(\mathcal{I}_{rw}\ddot{\theta}_{rw} + \mathcal{I}_{fw}\ddot{\theta}_{fw})s_\phi$

Table A.2: Gyroscopic and inertial torques generated by the wheels.

Note that, in order to be consistent with the full model, the wheel speeds of the reduced model, θ_{rw} and θ_{fw} , are defined as negative. Therefore, it is important to consider their sign when evaluating the gyroscopic and inertial effects described in Table A.2.

A.2 Tyre longitudinal forces

From Eq. A.5 we can determine the total force needed to drive the vehicle as,

$$F_{xf}^* + F_{xr} = ma_x^{cg} + F_{ax} \quad (\text{A.11})$$

where

$$F_{xf}^* = F_{xf}c_\Delta - F_{yf}s_\Delta \quad (\text{A.12})$$

is the force exerted by the front tyre along the longitudinal axis of the motorcycle $\hat{\mathbf{i}}_\psi$ and F_{ax} represents the aerodynamic drag. It is interesting to observe how the front lateral force F_{yf} generates a braking effect. In addition to the above terms, the effect of the rotating inertias such as the wheels or the engine may be accounted for by using an augmented mass \bar{m} , defined as

$$\bar{m} = \sum_i \mathcal{I}_i \eta_i^2 \quad (\text{A.13})$$

where \mathcal{I}_i is the i^{th} rotating inertia and η_i is the motion ratio between its angular speed and the forward velocity of the vehicle. Hence, based on the modelling assumptions of the reduced model, we can say that the overall longitudinal force exerted by the tyres is used to brake/accelerate the vehicle and to overcome the aerodynamic drag and the braking effect induced by the front wheel.

A.3 Tyre lateral forces

We can solve the lateral forces from the equation system formed by Eqs. A.6 and A.10. If we define the total force exerted by the front tyre along the lateral axis of the vehicle $\hat{\mathbf{j}}_\psi$ as

$$F_{yf}^* = F_{xf}s_\Delta + F_{yf}c_\Delta \quad (\text{A.14})$$

we can express the front and rear lateral forces as follows

$$F_{yf}^* = \frac{b}{a+b} ma_y^{cg} - \Delta F_y \quad (\text{A.15})$$

$$F_{yr} = \frac{a}{a+b} ma_y^{cg} + \Delta F_y \quad (\text{A.16})$$

where ma_y^{cg} represents the total lateral force applied by the tyres, i.e. $ma_y^{cg} = F_{yf}^* + F_{yr}$, and ΔF_y is the force transferred between tyres due to the aerodynamic drag F_{ax} and to the inertial moment $M_z^{\mathcal{I}}$ about $\hat{\mathbf{k}}_\psi$.

$$\Delta F_y = \frac{(ma_x^{cg} + F_{ax})hs_\phi + M_z^{\mathcal{I}}}{a + b} \quad (\text{A.17})$$

A.4 Tyre vertical forces

Similarly, starting from Eqs. A.7 and A.9 we can solve for the vertical forces,

$$F_{zf} = \frac{b}{a + b} (mg - ma_z^{cg}) - \Delta F_z \quad (\text{A.18})$$

$$F_{zr} = \frac{a}{a + b} (mg - ma_z^{cg}) + \Delta F_z \quad (\text{A.19})$$

where $mg - ma_z^{cg}$ represents the total vertical load, i.e. $mg - ma_z^{cg} = F_{zf} + F_{zr}$,

$$\Delta F_z = \frac{(ma_x^{cg} + F_{ax})hc_\phi + M_y^{\mathcal{I}}}{a + b} \quad (\text{A.20})$$

and ΔF_z is the load transfer originated by the aerodynamic drag F_{ax} and by the inertial moment $M_y^{\mathcal{I}}$ about $\hat{\mathbf{j}}_\psi$.

A.5 Roll dynamics

We have not used Eq. A.8 yet. Such equation, which represents the equilibrium of moments about the longitudinal axis of the motorcycle $\hat{\mathbf{i}}_\psi$, gives a good insight into the roll dynamics of the motorcycle.

The term $\dot{\psi}^2 hs_\phi$ represents the lateral acceleration of the centre of gravity \mathbf{G} with respect to the reference point \mathbf{P} due to the yaw rate $\dot{\psi}$. Its value is small compared to the absolute lateral acceleration of \mathbf{P} , denoted by $a_{y\psi}$, and hence it can be safely neglected. Such term would become relevant only for very small curvature radius of the same order of magnitude of h . Similarly, the moment $-(\mathcal{I}_z - \mathcal{I}_y)\dot{\psi}^2 c_\phi s_\phi$ can be neglected since its value is small compared to the other components of the equation.

Consequently, we can rewrite Eq. A.8 as:

$$(mh^2 + \mathcal{I}_x)\ddot{\phi} = -ma_{y\psi}hc_\phi + mghs_\phi + (\mathcal{I}_{rw}\dot{\theta}_{rw} + \mathcal{I}_{fw}\dot{\theta}_{fw})\dot{\psi}c_\phi \quad (\text{A.21})$$

Each term in the right hand side represents a moment about $\hat{\mathbf{i}}_\psi$: the first term is the restoring moment originated by the inertial force $ma_{y\psi}$ that tends to return the vehicle

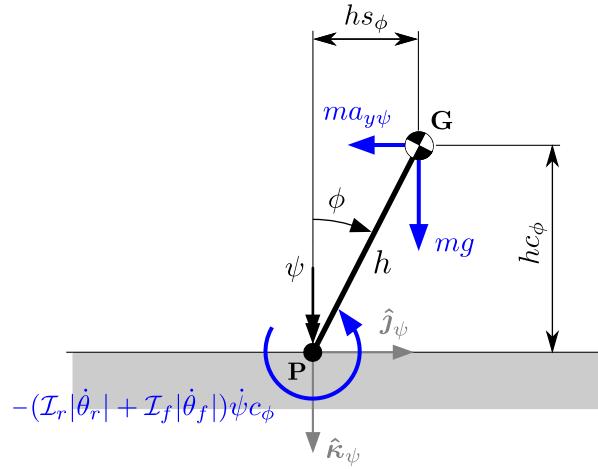


Figure A.2: Reduced model: equilibrium of moments about the longitudinal axis of the vehicle \hat{i}_ψ .

to the upright position, the second is the tilting moment originated by the weight of the motorcycle mg and the last represents the gyroscopic effect of the wheels. The effect of the last term depends on the sign of the roll rate. All contributions are depicted in Fig. A.2.

The classical equation from [13] that approximates the roll angle of the motorcycle in steady state cornering may be obtained by simply neglecting the gyroscopic effect in Eq. A.21, which yields

$$\phi = \arctan\left(\frac{a_{y\psi}}{g}\right) \quad (\text{A.22})$$

since in stationary motion $\ddot{\phi}=0$. If, as in [13], we assume that the vehicle axis \hat{i}_ψ is aligned with the trajectory, i.e. if we neglect the vehicle sideslip angle β , we can write the roll angle as a function of the longitudinal speed of the vehicle v_t and the curvature of the trajectory κ :

$$\phi = \arctan\left(\frac{v_t^2 \kappa}{g}\right) \quad (\text{A.23})$$

Appendix B

Model parameters

In the present appendix we summarize the parameters of the multibody motorcycle model employed throughout this thesis. In particular, the vehicle represents a modern sports motorcycle composed of six bodies: the front and rear wheels, the main assembly (including the frame, the engine and the fuel tank), the rear assembly (including the swingarm and the rear brake calipers), the upper part of the front assembly (including the sprung part of the forks, both triple clamps, the steering column, and the handlebar), and the lower part of the front assembly (including the unsprung part of the forks and the front brake calipers).

The geometric and inertial properties of the vehicle have been extracted from two papers [43, 51] together with the non-linear elastic and damping characteristics of the suspensions. As far as the tyre model is concerned, Pacejka’s Magic Formula has been employed. The equations used in this thesis as well as the full parameter set come from [40, 51]. The most relevant parameters of the model are reproduced below for the sake of completeness.

Body	Frame	m_i [kg]	\mathbf{r}_i [m]	I_{ii} [kgm ²]
Front wheel	\mathbf{T}_{fw}	12.0	(0, 0, 0)	(0.22, 0.47, 0.22)
Rear wheel	\mathbf{T}_{rw}	16.2	(0, 0, 0)	(0.33, 0.66, 0.33)
Main assembly	\mathbf{T}_m	223.0	(0.255, 0, -0.020)	(24.4, 26.2, 30.3)
Rear assembly	\mathbf{T}_r	10.0	(0.275, 0, -0.052)	(0.20, 0.80, 0.80)
Front assembly (uf)	\mathbf{T}_{uf}	8.8	(0.023, 0, -0.098)	(0.29, 0.14, 0.21)
Front assembly (lf)	\mathbf{T}_{lf}	7.0	(-0.029, 0, -0.189)	(0.22, 0.18, 0.07)

Table B.1: Inertial properties of the motorcycle. For each body the following properties are specified: mass (m_i), centre of gravity position (\mathbf{r}_i) and inertia matrix (I_{ii}).

Description	Name	Value	Units
Swingarm length	l_r	0.535	[m]
Frame length	l_m	0.730	[m]
Fork offset	l_f	0.034	[m]
Front sprocket radius	r	0.041	[m]
Rear sprocket radius	R	0.104	[m]
Front sprocket x-coordinate	x_{sp}	0.080	[m]
Front sprocket z-coordinate	z_{sp}	-0.030	[m]
Castor angle	ε	24.6	[deg]
Fork length (fully extended)	l_{frk}	0.517	[m]
Shock length (fully extended)	l_{shk}	0.300	[m]
Maximum fork stroke	$s_{max,f}$	0.130	[m]
Maximum shock stroke	$s_{max,r}$	0.055	[m]
Fork main stiffness	k_f	25	[N/mm]
Shock main stiffness	k_r	140	[N/mm]
Steering damper coefficient	b_δ	10	[Nms]
Drag force coefficient	c_x	0.47	[-]
Lift force coefficient	c_z	0.08	[-]
Pitch moment coefficient	c_μ	0.19	[-]
Reference frontal area	A	0.6	[m ²]
Air density	ρ	1.225	[Kg/m ³]
Front tyre lateral stiffness	K_{yf}	84.4	[N/mm]
Front tyre vertical stiffness	K_{zf}	130.0	[N/mm]
Front tyre vertical damping	C_{zf}	50	[Ns/m]
Rear tyre lateral stiffness	K_{yr}	92.0	[N/mm]
Rear tyre vertical stiffness	K_{zr}	141.0	[N/mm]
Rear tyre vertical damping	C_{zr}	50	[Ns/m]

Table B.2: Motorcycle model parameters.

Par.	Front tyre	Rear Tyre	Par.	Front tyre	Rear Tyre
C_x	1.6064	1.6064	q_{Bz1}	10.486	10.041
p_{Dx1}	1.3806	1.3548	q_{Bz2}	-0.00115	-1.61e-8
p_{Dx2}	-0.0414	-0.0603	q_{Bz5}	-0.68973	-0.76784
p_{Ex1}	0.0263	0.0263	q_{Bz6}	1.0411	0.73422
p_{Ex2}	0.2706	0.2706	q_{Bz9}	27.445	16.39
p_{Ex3}	-0.0769	-0.0769	q_{Bz10}	-1.0792	-0.35549
p_{Ex4}	1.1268	1.1268	q_{Dz1}	0.19796	0.26331
p_{Kx1}	25.939	25.940	q_{Dz2}	0.06563	0.030987
p_{Kx2}	-4.2327	-4.2330	q_{Dz3}	0.2199	-0.62013
p_{Kx3}	0.3369	0.3369	q_{Dz4}	0.21866	0.98524
C_y	0.8327	0.9	q_{Dz8}	0.3682	0.50453
p_{Dy1}	1.3	1.3	q_{Dz9}	0.1218	0.36312
p_{Dy2}	0	0	q_{Dz10}	0.25439	-0.19168
p_{Dy3}	0	0	q_{Dz11}	-0.17873	-0.40709
p_{Ey1}	-1.2556	-2.2227	q_{Ez1}	-0.91586	-0.19924
p_{Ey2}	-3.2068	-1.669	q_{Ez2}	0.11625	-0.017638
p_{Ey4}	-3.9980	-4.288	q_{Ez3}	1.4387	3.6511
p_{Ky1}	22.841	15.791	q_{Hz3}	-0.00379	-0.028448
p_{Ky2}	2.1578	1.6935	q_{Hz4}	-0.01557	-0.009862
p_{Ky3}	2.5058	1.4604	r_{Bx1}	13.476	13.476
p_{Ky4}	-0.08088	0.669	r_{Bx2}	11.354	11.354
p_{Ky5}	-0.22882	0.18708	r_{Bx3}	0	0
C_γ	0.86765	0.61397	$C_{x\alpha}$	1.1231	1.1231
p_{Ky6}	0.69677	0.45512	r_{By1}	7.7856	7.7856
p_{Ky7}	-0.03077	0.01329	r_{By2}	8.1697	8.1697
E_γ	-15.815	-19.99	r_{By3}	-0.05914	-0.05914
C_t	1.0917	1.3153	$C_{y\kappa}$	1.0533	1.0533

Table B.3: Tyre model parameters.

Appendix C

Extended literature

The current PhD thesis has been developed throughout a long period of time, starting from 2006 until 2016. The original literature review presented in Chapter 2 was carried out during the initial stages of the thesis and contains bibliographic references up to 2010. Therefore, an update is deemed necessary prior to the release of this manuscript. This is the aim of the current Appendix, where we summarize the most important publications not included in the original analysis of the state of the art.

One of the most relevant works in the field of rider control was presented between 2010 and 2012 by Massaro, who also developed a rider model based on MPC. Taking the work of Cole [101] as a starting point, two different approaches were introduced by the above-mentioned author. In [168] the rider target was defined in terms of the vehicle path whereas in [174] the controller was rearranged in order to follow a given roll profile, thus making it easier to reproduce experimental measurements. Path tracking simulations showed good results for roll angles up to 50 deg and moderate longitudinal accelerations slightly lower than 8 m/s^2 . However, the resulting roll rate was small in all cases, of the order of 25 deg/s. Differences between the present PhD thesis and Massaro's work have already been discussed in Chapter 7. They are repeated below for completeness.

The main improvements of this thesis with respect to [168] are the procedure employed to obtain the internal model and the learning algorithm. Specifically, Massaro obtained his internal model by linearizing the equations of motion around a pure steady state condition, whereas in this thesis we used an extended quasi-steady state approach. The main difference between both approaches lies in the longitudinal acceleration and the roll derivatives, which were not considered by the aforesaid author. As we have seen throughout this dissertation, these terms are essential to simulate aggressive manoeuvres. In fact, we proved that neglecting the effect of roll dynamics leads to an unfeasible solution in some cases like, for example, the slalom manoeuvre of Chapter 5.

This implies that it would not be possible to solve this particular manoeuvre by using a pure stationary approach like Massaro's. Additionally, the learning algorithm presented in this thesis together with a more accurate estimation of the feedforward term allow us to reach smaller tracking errors.

Another relevant work in the field of rider modelling was presented in 2012 by Sharp [175]. In this publication the controller first introduced in [99, 100] was applied to the simulation of a racing motorcycle near to its cornering limits. Essentially, Sharp used a linear quadratic controller with multiple preview points to develop both longitudinal and lateral control strategies for a two-wheeled machine. In order to ensure the alignment between the controller gains and the current conditions of the vehicle, Sharp proposed a scheduling strategy based on the vehicle speed and its lateral acceleration. As opposed to this thesis, the longitudinal acceleration of the vehicle and its roll derivatives were not considered when computing the trim states of the controller. Good tracking results were obtained for two slow-varying manoeuvres, with the maximum roll rate being around 15 deg/s and the maximum longitudinal acceleration being lower than 4 m/s². Optimal gains and closed-loop system frequency responses were also illustrated. As part of the conclusions, Sharp stated that further work was needed to provide good tracking performance during aggressive braking, referring to the need to improve the trim conditions used to develop the controller.

In 2013 Saccon published an update of his previous works [176] regarding manoeuvre regulation. In this publication there were no significant changes as far as the internal model and the control approach are concerned, which were already introduced in Chapter 2. However, new results were presented, where a multibody model of a modern sport motorcycle was driven through a portion of a racing track. Results were limited to roll angles below 50 deg and moderate longitudinal accelerations, with their maximum absolute value being lower than 6 m/s². An excellent tracking performance was observed for the vehicle speed whereas the path error reached values up to 0.6 m in the neighbourhood of the corner apexes, where the lateral acceleration is maximum. It is worth noting that the simplified internal model used in this approach limits its application as far as the simulation of weave and wobble phenomena is concerned, which are of special interest in the racing world.

In addition to the above works, there have not been any other major contributions to the field of rider control in the last years. Next we review several publications about the topological modelling of the rider's body and its influence on motorcycle stability.

In 2012 Massaro presented a detailed study of the passive effect of the rider's body on the weave mode [172]. The compliance of the human body influences the vibration modes of the motorcycle, being difficult for the rider to control his/her own oscillations.

In order to simulate this phenomenon, a (passive) anthropometric rider model was built, which included torso and steering impedances based on the rider's height, weight and posture. A method for the quantitative evaluation of on-road stability was discussed and then used to compare simulation results against experimental measurements for two riders in hands-on and hands-off configurations. Results showed differences in weave stability in function of the rider stature and also in function of the hands configuration, with smaller stature and hands-on condition leading to worse weave stability. This work was later expanded by Doria in 2013 [177].

Following a completely different approach, Sequenzia proposed in 2014 an elaborated multibody model of the rider's body [178]. The model was composed of 15 bodies, according to the proportions established in AMVO (Anthropometric Specification for Mid-Sized Male Dummy) [179], with a total of 5 degrees of freedom. The main scope of this research project was to study the effect of the rider movements in racing conditions. For this purpose, the rider body was coupled to a racing motorcycle model in ADAMS. A PID controller with constant look-ahead distance was used to control the steering torque whereas no details were given about the stabilization of the rider's body. As it could be expected, results indicated that both the roll angle and the steering torque decrease when the rider model is allowed to move laterally. Sequenzia did not present any conclusions regarding the effect of the rider motion on vehicle stability.

This work was later continued in 2015 by the same research group at the University of Catania [180]. In this new publication, the model complexity was increased, including the steering impedance of the rider's arms and a variable drag map in function of the rider's position (up/down). Results were presented for a full lap around Monza track. However, the vehicle speed and its roll angle, which reached a maximum value of 40 deg, indicate that the vehicle was far from its performance limit during the simulation.

Another topic that has been gaining interest in the recent years is the study of component flexibility on motorcycle dynamics. An example of this research was presented by Cossalter in 2015 [181], where an experimental/numerical study was performed to investigate the effect of fork compliance on vehicle stability. Several forks, from both enduro and sport motorcycles, were characterized with the aim of developing a lumped element model of this component. Their modal analysis showed one main mode of vibration in the frequency of interest, referred to as the lateral mode. In order to simplify the simulation of the flexible fork, the concept of wheel twisting axis was proposed. A lumped rotational stiffness was placed around the static twist axis whereas a pure moment of inertia was added to the front assembly in order to obtain the same natural frequency of the identified lateral mode. Simulations confirmed the effect of the front assembly deformability on the weave and wobble vibration modes.

This line of research is of special interest within the motorsport industry since it is yet to be understood how the chassis flexibility affects motorcycle performance. Several tests performed by the author of this thesis revealed that the rider here presented successfully works with FE flexible models, thus allowing the user to perform detailed investigations on the effect of component flexibility (chassis, arm, etc) on motorcycle dynamics.

References

- [1] König, J., Pérez-Magallón, B., Pieve, M., Galliano, F., and Ducci, I. Report on analyses of motorcycles accidents databases. Technical report, Safety In Motion (SIM), European Union Framework Programme FP6, 2007.
- [2] <http://www.mymosa.eu>, 2006.
- [3] Haug, E. J. *Computer aided kinematics and dynamics of mechanical systems*, volume 1. Allyn and Bacon Boston, 1989.
- [4] Smith, R. and Haug, E. DADS - Dynamic analysis and design system. In *Multibody systems handbook*, pages 161–179. Springer, 1990.
- [5] Rankine, W. J. M. On the dynamical principles of the motion of velocipedes. *The Engineer*, 28 (79), pp. 129, 1869.
- [6] Whipple, F. J. W. The stability of the motion of a bicycle. *Quarterly Journal of Pure and Applied Mathematics*, 30 (120), pp. 312–321, 1899.
- [7] Carvallo, E. Théorie du mouvement du monocycle et de la bicyclette. *Paris: Gauthier-Villars*, 2 (5), pp. 119–188, 1899.
- [8] Sharp, R. S. The lateral dynamics of motorcycles and bicycles. *Vehicle System Dynamics*, 14 (4-6), pp. 265–283, 1985.
- [9] Limebeer, D. J. N. and Sharp, R. S. Bicycles, motorcycles, and models. *Control Systems, IEEE*, 26 (5), pp. 34–61, 2006.
- [10] Meijaard, J. P., Papadopoulos, J. M., Ruina, A., and Schwab, A. L. Linearized dynamics equations for the balance and steer of a bicycle: a benchmark and review. *Proceedings of the Royal Society A: Mathematical, Physical and Engineering Science*, 463 (2084), pp. 1955–1982, 2007.
- [11] Sharp, R. S. The stability and control of motorcycles. *Journal of mechanical engineering science*, 13 (5), pp. 316–329, 1971.

- [12] Pacejka, H. B. *Tyre and vehicle dynamics*. Butterworth-Heinemann, 2006.
- [13] Cossalter, V. *Motorcycle dynamics*. Race Dynamics, 2002.
- [14] Fajans, J. Steering in bicycles and motorcycles. *American Journal of Physics*, 68 (7), pp. 654–659, 1999.
- [15] Sharp, R. S. The influence of frame flexibility on the lateral stability of motorcycles. *Journal of Mechanical Engineering Science*, 16 (2), pp. 117–120, 1974.
- [16] Kane, T. R. The effect of frame flexibility on high speed weave of motorcycles. *SAE*, Technical Paper 780306, 1978.
- [17] Jennings, G. A study of motorcycle suspension damping characteristics. *SAE*, Technical Paper No. 740628, 1974.
- [18] Sharp, R. The influence of the suspension system on motorcycle weave-mode oscillations. *Vehicle System Dynamics*, 5 (3), pp. 147–154, 1976.
- [19] Koenen, C. *The dynamic behaviour of a motorcycle when running straight ahead and when cornering*. PhD thesis, Delft University, 1983.
- [20] Koenen, K. and Pacejka, H. Vibrational modes of motorcycles in curves. 1980. HS-029 684.
- [21] Koenen, C. and Pacejka, H. The influence of frame elasticity, simple rider body dynamics and tyre moments on free vibrations of motorcycles in curves. In *Proceedings of the 7th IAVSD Symposium on the Dynamics of Vehicles on Roads and Tracks, held in Cambridge, September 7-11, 1982*.
- [22] Eaton, D. J. *Man-machine dynamics in the stabilization of single-track vehicles*. PhD thesis, University of Michigan, 1973.
- [23] Weir, D. H. and Zellner, J. W. Experimental investigation of the transient behavior of motorcycles. *SAE*, Technical Paper No. 790266, 1979.
- [24] Sharp, R. Variable geometry active rear suspension for motorcycles. In *Proc. AVEC*, volume 5, pages 22–24, 2000.
- [25] Limebeer, D. J., Sharp, R., and Evangelou, S. The stability of motorcycles under acceleration and braking. *Proceedings of the Institution of Mechanical Engineers, Part C: Journal of Mechanical Engineering Science*, 215 (9), pp. 1095–1109, 2001.
- [26] Weir, D. H. and Zellner, J. W. Lateral-directional motorcycle dynamics and rider control. *SAE*, Technical Paper No. SP-428, 1978.

-
- [27] Nishimi, T., Aoki, A., and Katayama, T. Analysis of straight running stability of motorcycles. In *10th International Technical Conference on Experimental Safety Vehicles*, pages 1080–1094, 1985.
- [28] Katayama, T., Aoki, A., and Nishimi, T. Control behaviour of motorcycle riders. *Vehicle System Dynamics*, 17 (4), pp. 211–229, 1988.
- [29] Sharp, R. Vibrational modes of motorcycles and their design parameter sensitivities. In *Institution of Mechanical Engineers Conference Publications*, volume 3, pages 107–107, 1994.
- [30] Sharp, R. and Alstead, C. The influence of structural flexibilities on the straight-running stability of motorcycles. *Vehicle system dynamics*, 9 (6), pp. 327–357, 1980.
- [31] Bayer, B. Flattern und pendeln bei krafträdern. *Automobil Industrie*, 2, pp. 193–197, 1988.
- [32] Sharp, R. The application of multi-body computer codes to road vehicle dynamics modelling problems. *Proceedings of the Institution of Mechanical Engineers, Part D: Journal of Automobile Engineering*, 208 (1), pp. 55–61, 1994.
- [33] Gani, M., Sharp, R., and Limebeer, D. Multi-body simulation software in the study of two-wheeled road vehicles. In *Decision and Control, 1996., Proceedings of the 35th IEEE*, volume 3, pages 2804–2805. IEEE, 1996.
- [34] Mechanical Simulation Corporation, 709 West Huron, Ann Arbor MI. *Autosim Reference Manual*, 1998. <http://www.carsim.com>.
- [35] Imaizumi, H., Fujioka, T., and Omae, M. Rider model by use of multibody dynamics analysis. *JSAE Review*, 17 (1), pp. 75–77, 1996.
- [36] Imaizumi, H. and Fujioka, T. Motorcycle-rider system dynamics by multibody dynamics analysis: Effects of frame stiffness and tire characteristic on weave mode. *JSAE*, 28, pp. 131–136, 1997.
- [37] Imaizumi, H. and Fujioka, T. Motorcycle-rider system dynamics by multibody dynamics analysis: Effects of the rear load on wobble motions and the control assembly. *JSAE*, 19 (1), pp. 54–57, 1998.
- [38] Imaizumi, H. and Fujioka, T. Motorcycle-rider system dynamics by multibody dynamics analysis. the 4th report: Analysis of rider control behavior and motorcycle dynamics. In *Proceedings. JSAE Annual Congress*, number 54-99, pages 9–12, 1999.

- [39] Cossalter, V., Doria, A., and Lot, R. Steady turning of two-wheeled vehicles. *Vehicle system dynamics*, 31 (3), pp. 157–181, 1999.
- [40] Evangelou, S. *Control and Stability Analysis of Two-wheeled Road Vehicles*. PhD thesis, Imperial College London, 2003.
- [41] Sharp, R. S. and Limebeer, D. J. A motorcycle model for stability and control analysis. *Multibody System Dynamics*, 6 (2), pp. 123–142, 2001.
- [42] Mechanical Simulation Corporation, 709 West Huron, Ann Arbor MI. *Bikesim Reference Manual*, 2006. <http://www.bikesim.com>.
- [43] Cossalter, V. and Lot, R. A motorcycle multi-body model for real time simulations based on the natural coordinates approach. *Vehicle System Dynamics*, 37 (6), pp. 423–447, 2002.
- [44] Lot, R. A motorcycle tire model for dynamic simulations: theoretical and experimental aspects. *Meccanica*, 39 (3), pp. 207–220, 2004.
- [45] Waterloo Maple Inc, Waterloo, ON. *Maple 14 Reference Manual*, 2010. <http://www.maplesoft.com>.
- [46] Lot, R. and Da Lio, M. A symbolic approach for automatic generation of the equations of motion of multibody systems. *Multibody System Dynamics*, 12 (2), pp. 147–172, 2004.
- [47] De Jalon, J. G. and Bayo, E. *Kinematic and dynamic simulation of multibody systems*. Springer-Verlag New York, USA, 1994.
- [48] Cossalter, V., Da Lio, M., and Berritta, R. Studio e realizzazione di una macchina per la determinazione delle caratteristiche di rigidità e smorzamento di un pneumatico motociclistico. *V Convegno di Tribologia*, 1998.
- [49] Da Lio, M., Doria, A., and Lot, R. A spatial mechanism for the measurement of the inertia tensor: Theory and experimental results. *Journal of dynamic systems, measurement, and control*, 121 (1), pp. 111–116, 1999.
- [50] Bortoluzzi, D., Doria, A., Lot, R., and Fabbri, L. Experimental investigation and simulation of motorcycle turning performance. In *3rd International Motorcycle Conference*, pages 175–191, 2000.
- [51] Sharp, R., Evangelou, S., and Limebeer, D. J. Advances in the modelling of motorcycle dynamics. *Multibody system dynamics*, 12 (3), pp. 251–283, 2004.

-
- [52] De Vries, E. d. and Pacejka, H. Motorcycle tyre measurements and models. *Vehicle System Dynamics*, 29 (S1), pp. 280–298, 1998.
- [53] De Vries, E. and Pacejka, H. The effect of tyre modeling on the stability analysis of a motorcycle. *Proc. AVEC'98*, pages 355–360, 1998.
- [54] Tezuka, Y., Ishii, H., and Kiyota, S. Application of the magic formula tire model to motorcycle maneuverability analysis. *JSAE review*, 22 (3), pp. 305–310, 2001.
- [55] Evangelou, S., Limebeer, D. J., Sharp, R. S., and Smith, M. C. Steering compensation for high-performance motorcycles. In *Decision and Control, 2004. CDC. 43rd IEEE Conference on*, volume 1, pages 749–754. IEEE, 2004.
- [56] Evangelou, S., Limebeer, D. J., Sharp, R. S., and Smith, M. C. Control of motorcycle steering instabilities. *Control Systems, IEEE*, 26 (5), pp. 78–88, 2006.
- [57] Donida, F., Ferreti, G., Savaresi, S. M., Tanelli, M., and Schiavo, F. Motorcycle dynamics library in modelica. In *Proceedings of the Fifth International Modelica Conference*, volume 5, pages 157–166, 2006.
- [58] Tanelli, M., Schiavo, F., Savaresi, S. M., and Ferretti, G. Object-oriented multi-body motorcycle modelling for control systems prototyping. In *Computer Aided Control System Design, 2006 IEEE International Conference on Control Applications, 2006 IEEE International Symposium on Intelligent Control, 2006 IEEE*, pages 2695–2700. IEEE, 2006.
- [59] Donida, F., Ferretti, G., Savaresi, S., and Tanelli, M. Object-oriented modelling and simulation of a motorcycle. *Mathematical and Computer Modelling of Dynamical Systems*, 14 (2), pp. 79–100, 2008.
- [60] Mavroudakis, B. and Eberhard, P. Analysis of alternative front suspension systems for motorcycles. *Vehicle System Dynamics*, 44 (sup1), pp. 679–689, 2006.
- [61] Cossalter, V., Lot, R., and Massaro, M. The influence of frame compliance and rider mobility on the scooter stability. *Vehicle System Dynamics*, 45 (4), pp. 313–326, 2007.
- [62] Cossalter, V., Lot, R., Sartori, R., and Massaro, R. A motorcycle riding simulator for the improvement of the rider safety. *Proceedings of the FISITA 2008 World Automotive Congress*, pages 11–015, 2008.
- [63] Sharp, R. and El-Nashar, M. A generally applicable digital computer based mathematical model for the generation of shear forces by pneumatic tyres. *Vehicle System Dynamics*, 15 (4), pp. 187–209, 1986.

- [64] Fujioka, T. and Goda, K. Discrete brush tire model for calculating tire forces with large camber angle. *Vehicle system dynamics*, 25 (S1), pp. 200–216, 1996.
- [65] Fujioka, T. and Goda, K. Tire cornering properties at large camber angles: mechanism of the moment around the vertical axis. *JSAE Review*, 16 (3), pp. 257–261, 1995.
- [66] Bakker, E. and Nyborg, L. Tyre modelling for use in vehicle dynamics studies. *SAE paper*, 870421, 1987.
- [67] Verstedden, W. Improving a tyre model for motorcycle simulations. Master's thesis, Eindhoven University of Technology, 2005.
- [68] Cossalter, V., Doria, A., and Ruffo, N. Testing of motorcycle tires by means of a rotating disc machine. In *Tyre Technology EXPO 2002 Conference, Hamburg*, pages 20–22, 2002.
- [69] Cossalter, V., Lot, R., and Maggio, F. The influence of tire properties on the stability of a motorcycle in straight running and curves. In *SAE Conference Proceedings*, pages 87–94. SAE, 2002.
- [70] Rashevsky, N. Neglected factors in highway safety. Technical report, University of Michigan Mental Health Research Institute, 1966. Grant GM-12032-01.
- [71] Guo, K. and Guan, H. Modelling of driver/vehicle directional control system. *Vehicle System Dynamics*, 22 (3-4), pp. 141–184, 1993.
- [72] Getz, N. H. *Dynamic inversion of nonlinear maps with applications to nonlinear control and robotics*. PhD thesis, University of California, Berkeley, 1995.
- [73] Frezza, R. and Beghi, A. Simulating a motorcycle driver. In *New trends in Nonlinear Dynamics and Control and their Applications*, pages 175–186. Springer, 2003.
- [74] Frezza, R., Beghi, A., and Saccon, A. Model predictive for path following with motorcycles: application to the development of the pilot model for virtual prototyping. In *Decision and Control, 2004. CDC. 43rd IEEE Conference on*, volume 1, pages 767–772. IEEE, 2004.
- [75] Frezza, R. and Beghi, A. A virtual motorcycle driver for closed-loop simulation. *Control Systems, IEEE*, 26 (5), pp. 62–77, 2006.
- [76] Saccon, A. *Maneuver regulation of nonlinear systems: The challenge of motorcycle control*. PhD thesis, University of Padova, 2006.

-
- [77] Cofelice, N., Locatelli, D., Zanni, R., Toso, A., Moreno, D., Kang, J., and Donders, S. A multibody virtual dummy for vibrational analysis in car and motorcycle environments. In *Proceedings, ISMA conference on Noise and Vibration Engineering*. Katholieke Universiteit Leuven, 2010.
- [78] Bennett, S. *A History of Control Engineering*, volume 47. IET, 1993.
- [79] Ogata, K. *Modern control systems*. Prentice Hall, 1998.
- [80] McRuer, D. T. and Jex, H. R. A review of quasi-linear pilot models. *Human Factors in Electronics, IEEE Transactions on*, (3), pp. 231–249, 1967.
- [81] McRuer, D. and Weir, D. H. Theory of manual vehicular control. *Ergonomics*, 12 (4), pp. 599–633, 1969.
- [82] Iguchi, M. A study of manual control. *Journal of mechanic Society of Japan*, 62 (481), 1959.
- [83] Iguchi, M. and others,. A fundamental study of driver behaviour for automobile simulation. Symposium of SAE-Japan, 1960.
- [84] Ashkenas, I. L. and McRuer, D. T. *A theory of handling qualities derived from pilot-vehicle system considerations*. Institute of the Aerospace Sciences, 1962.
- [85] McRuer, D. T. and Klein, R. H. Comparison of human driver dynamics in simulators with complex and simple visual displays and in an automobile on the road. In *Proceedings of the 11th Annual Conference on Manual Control*, 1975.
- [86] McRuer, D. and Klein, R. Effects of automobile steering characteristics on driver/vehicle performance for regulation tasks. In *Proceedings of the 11th Annual Conference on Manual Control*, 1975.
- [87] Kondo, M. and Ajimine, A. Driver's sight point and dynamics of the driver-vehicle-system related to it. *SAE*, Technical Paper No. 680104, 1968.
- [88] Yoshimoto, K. Simulation of driver/vehicle system including preview control. *Journal of Mechanics Society Japan*, 7, 1968.
- [89] Weir, D. *Motorcycle Handling Dynamics and Rider Control and the Effect of Design Configuration on Response and Performance*. PhD thesis, University of California at Los Angeles, 1972.

- [90] Weir, D. A manual control view of motorcycle handling. in second international congress on automotive safety. In *Proceedings of the Second International Congress on Automotive Safety, Dept. of Transportation. July 16 - 18, San Francisco*, number 73018, 1973.
- [91] Zellner, J. W. and Weir, D. H. Development of handling test procedures for motorcycles. *SAE*, Technical Paper No. 780313, 1978.
- [92] Prem, H. and Good, M. A rider-lean steering mechanism for motorcycle control. *Vehicle System Dynamics*, 12 (1-3), pp. 29–32, 1983.
- [93] Berritta, R., Biral, F., and Garbin, S. Evaluation of motorcycle handling with multibody modelling and simulation. In *Proc. 6th Int. Conf. on High Tech. Engines and Cars, Modena*, 2000.
- [94] Lot, R. and Cossalter, V. A non linear rider model for motorcycles. In *Proceedings of the FISITA 2006 World Automotive Congress*, pages 22–27, 2006.
- [95] Massaro, M. and Lot, R. Application of laplace transform techniques to non-linear control optimization. *Proc of the multibody dynamics*, pages 25–28, 2007.
- [96] Lot, R., Massaro, M., and Sartori, R. Advanced motorcycle virtual rider. *Vehicle System Dynamics*, 46 (S1), pp. 215–224, 2008.
- [97] Cossalter, V., Da Lio, M., Lot, R., and Fabbri, L. A general method for the evaluation of vehicle manoeuvrability with special emphasis on motorcycles. *Vehicle system dynamics*, 31 (2), pp. 113–135, 1999.
- [98] Cossalter, V., Da Lio, M., Biral, F., and Fabbri, L. Evaluation of motorcycle maneuverability with the optimal maneuver method. *SAE transactions*, 107 (6), pp. 2512–2518, 1998.
- [99] Sharp, R. S. Optimal linear time-invariant preview steering control for motorcycles. *Vehicle system dynamics*, 44 (sup1), pp. 329–340, 2006.
- [100] Sharp, R. S. Motorcycle steering control by road preview. *Transaction American Society of Mechanical Engineers. Journal of Dynamic Systems, Measurement, and Control*, 129 (4), pp. 373, 2007.
- [101] Cole, D., Pick, A., and Odhams, A. Predictive and linear quadratic methods for potential application to modelling driver steering control. *Vehicle System Dynamics*, 44 (3), pp. 259–284, 2006.

-
- [102] Naidu, D. S. *Optimal control systems*. CRC Press, 2003.
- [103] Bryson, A. E. and Ho, Y.-C. *Applied optimal control: optimization, estimation, and control*. Taylor & Francis, 1975.
- [104] Baron, S., Kleinman, D., and Levison, W. An optimal control model of human response part ii: prediction of human performance in a complex task. *Automatica*, 6 (3), pp. 371–383, 1970.
- [105] Kleinman, D., Baron, S., and Levison, W. An optimal control model of human response part i: Theory and validation. *Automatica*, 6 (3), pp. 357–369, 1970.
- [106] MacAdam, C. C. An optimal preview control for linear systems. 1980.
- [107] MacAdam, C. C. Application of an optimal preview control for simulation of closed-loop automobile driving. *Systems, Man and Cybernetics, IEEE Transactions on*, 11 (6), pp. 393–399, 1981.
- [108] Peng, H. Evaluation of driver assistance systems—a human centered approach. *AVEC proceedings*, 2002.
- [109] Bertolazzi, E., Biral, F., and Da Lio, M. Symbolic–numeric indirect method for solving optimal control problems for large multibody systems. *Multibody System Dynamics*, 13 (2), pp. 233–252, 2005.
- [110] Bertolazzi, E., Biral, F., and Da Lio, M. Symbolic-numeric efficient solution of optimal control problems for multibody systems. *Journal of computational and applied mathematics*, 185 (2), pp. 404–421, 2006.
- [111] Bertolazzi, E., Biral, F., and Da Lio, M. Motion planning algorithms based on optimal control for motorcycle-rider system. FISITA, 2006.
- [112] Sharp, R. and Valtetsiotis, V. Optimal preview car steering control. *Vehicle System Dynamics*, 35, pp. 101–117, 2001.
- [113] Sharp, R., Casanova, D., and Symonds, P. A mathematical model for driver steering control, with design, tuning and performance results. *Vehicle System Dynamics*, 33 (5), pp. 289–326, 2000.
- [114] Sharp, R. S. Driver steering control and a new perspective on car handling qualities. *Proceedings of the Institution of Mechanical Engineers, Part C: Journal of Mechanical Engineering Science*, 219 (10), pp. 1041–1051, 2005.

- [115] Antos, P. and Ambrósio, J. A. A control strategy for vehicle trajectory tracking using multibody models. *Multibody System Dynamics*, 11 (4), pp. 365–394, 2004.
- [116] Huyge, K., Ambrósio, J., and Pereira, M. A control strategy for the dynamics of a motorcycle, including rider. In *Proceedings of EUROMECH Nonlinear Dynamics Conference (ENOC 2005), Eindhoven, The Netherlands, 2005*.
- [117] Sharp, R. S. Optimal preview speed-tracking control for motorcycles. *Multibody System Dynamics*, 18 (3), pp. 397–411, 2007.
- [118] Thommypillai, M., Evangelou, S., and Sharp, R. Car driving at the limit by adaptive linear optimal preview control. *Vehicle system dynamics*, 47 (12), pp. 1535–1550, 2009.
- [119] Thommypillai, M., Evangelou, S., and Sharp, R. Advances in the development of a virtual car driver. *Multibody System Dynamics*, 22 (3), pp. 245–267, 2009.
- [120] Banaszuk, A. and Hauser, J. Feedback linearization of transverse dynamics for periodic orbits. *Systems & control letters*, 26 (2), pp. 95–105, 1995.
- [121] Hauser, J. and Hindman, R. Maneuver regulation from trajectory tracking: Feedback linearizable systems. In *Proc. IFAC Symp. Nonlinear Control Systems Design*, pages 595–600, 1995.
- [122] Hauser, J. and Meyer, D. G. The trajectory manifold of a nonlinear control system. In *Decision and Control, 1998. Proceedings of the 37th IEEE Conference on*, volume 1, pages 1034–1039. IEEE, 1998.
- [123] Hauser, J. A projection operator approach to the optimization of trajectory functionals. In *IFAC world congress*, 2002.
- [124] Abate, A. Nonlinear predictive control for a nonholonomic nonminimum phase system. Master’s thesis, University of Padova, 2002.
- [125] Maciejowski, J. Predictive control with constraints. *Harlow, England: Pearson Education*, 2002.
- [126] Moreno, D. and Manka, M. Motorcycle dynamic models for virtual rider design and cornering analysis. In *Proceedings of the ASME 2009 International Design Engineering Technical Conferences & Computers and Information in Engineering Conference IDETC/CIE 2009, August 30 - September 2, San Diego, California, USA*. ASME, 2009.

-
- [127] Moreno, D., Kang, J., and Manka, M. A “corner solver” for motorcycles as a tool for the development of a virtual rider. In *Vehicle Power and Propulsion Conference, VPPC'09, September 7-11, 2009, Dearborn, MI, USA*, pages 1110–1117. IEEE, 2009.
- [128] Moreno, D. Latest advances on the virtual rider. In *MYMOSA open workshop, Eindhoven, February*, 2010. <http://www.mymosa.eu>.
- [129] Moreno, D., Toso, A., Cofelice, N., and Kang, J. Motorcycle dynamics in virtual lab motion. In *Proceedings of the ASME 2010 International Design Engineering Technical Conferences & Computers and Information in Engineering Conference, IDETC/CIE 2010, August 15-18, 2010, Montreal, Quebec, Canada*. ASME, 2010.
- [130] Moreno, D., Cofelice, N., Toso, A., and Kang, J. Steady turning analysis of motorcycles in lms virtual.lab motion. In *The 1st Joint International Conference on Multibody System Dynamics, May 25-27, Lappeenranta, Finland*, 2010.
- [131] Blundell, M., Harty, D., and others,. *The multibody systems approach to vehicle dynamics*. Elsevier, 2004.
- [132] Milliken, W. F., Whitcomb, D. W., and others,. General introduction to a programme of dynamic research. *Proceedings of the Institution of Mechanical Engineers: Automobile Division*, 10 (1), pp. 287–309, 1956.
- [133] Nikravesh, P. E. *Computer-aided analysis of mechanical systems*. Prentice-Hall, Inc., 1988.
- [134] Jain, A. *Robot and Multibody Dynamics: Analysis and Algorithms*. Springer, 2011.
- [135] Schwerin, R. V., Schlick, T., Keyes, D., Nieminen, R., Griebel, M., and Roose, D. *Multibody system simulation: numerical methods, algorithms, and software*. Springer-Verlag New York, Inc., 2000.
- [136] Jalón, J. G. Twenty-five years of natural coordinates. *Multibody System Dynamics*, 18 (1), pp. 15–33, 2007.
- [137] Popp, K. and Schiehlen, W. O. *Ground Vehicle Dynamics*. Springer, 2010.
- [138] Wanner, G. and Hairer, E. *Solving Ordinary Differential Equations II: stiff and differential-algebraic problems*. Springer-Verlag, Berlin, 1996.
- [139] Laulusa, A. and Bauchau, O. A. Review of classical approaches for constraint enforcement in multibody systems. *Journal of computational and nonlinear dynamics*, 3 (1), pp. 011004, 2008.

- [140] Bauchau, O. A. and Laulusa, A. Review of contemporary approaches for constraint enforcement in multibody systems. *Journal of Computational and Nonlinear Dynamics*, 3 (1), pp. 011005, 2008.
- [141] Baumgarte, J. Stabilization of constraints and integrals of motion in dynamical systems. *Computer methods in applied mechanics and engineering*, 1 (1), pp. 1–16, 1972.
- [142] Eich-Soellner, E. and Führer, C. *Numerical methods in multibody dynamics*, volume 45. Teubner Stuttgart, 1998.
- [143] Samin, J.-C. and Fiset, P. *Symbolic modeling of multibody systems*, volume 112. Springer, 2003.
- [144] Shabana, A. A. *Computational dynamics*. Wiley, 2001.
- [145] Wolfram, S. The mathematica book 4th edition (champaign, il: Wolfram media; cambridge, uk, 1999).
- [146] Kreuzer, E. and Schiehlen, W. NEWEUL - software for the generation of symbolic equations of motion. In *Multibody systems handbook*, pages 181–202. Springer, 1990.
- [147] Fiset, P. and Samin, J. Robotran: Symbolic generation of multi-body system dynamic equations. In *Advanced Multibody System Dynamics*, pages 373–378. Springer, 1993.
- [148] Cossalter, V., Lot, R., and Massaro, M. The chatter of racing motorcycles. *Vehicle System Dynamics*, 46 (4), pp. 339–353, 2008.
- [149] Wittkopf, A. Automatic code generation and optimization in maple. *JNAIAM J. Numer. Anal. Indust. Appl. Math*, 3, pp. 167–180, 2008.
- [150] Genta, G. *Motor vehicle dynamics: modeling and simulation*, volume 43. World Scientific, 1997.
- [151] Wong, J. Y. *Theory of ground vehicles*. Wiley, 2001.
- [152] Cossalter, V., Lot, R., and Maggio, F. The modal analysis of a motorcycle in straight running and on a curve. *Meccanica*, 39 (1), pp. 1–16, 2004.
- [153] Powell, M. J. A FORTRAN subroutine for solving systems of nonlinear algebraic equations. *Numerical Methods for Nonlinear Algebraic Equations*, 1970.

-
- [154] More, J. J., Garbow, B. S., and Hillstom, K. E. User guide for MINPACK-1. *Argonne National Laboratory, Rept. ANL-80-74*, 1980.
- [155] Jarzebowska, E. *Model-based tracking control of nonlinear systems*. CRC Press, 2012.
- [156] Dixon, J. *Suspension Analysis and Computational Geometry*. John Wiley & Sons, 2009.
- [157] Cossalter, V., Lot, R., and Peretto, M. Steady turning of motorcycles. *Proceedings of the Institution of Mechanical Engineers, Part D: Journal of Automobile Engineering*, 221 (11), pp. 1343–1356, 2007.
- [158] Cossalter, V., Doria, A., and Lot, R. Optimum suspension design for motorcycle braking. *Vehicle system dynamics*, 34 (3), pp. 175–198, 2000.
- [159] Bastos Jr, G., Seifried, R., and Bröls, O. Inverse dynamics of serial and parallel underactuated multibody systems using a dae optimal control approach. *Multibody System Dynamics*, 30 (3), pp. 359–376, 2013.
- [160] Betts, J. T. *Practical methods for optimal control and estimation using nonlinear programming*, volume 19. Siam, 2010.
- [161] Bazaraa, M. S., Sherali, H. D., and Shetty, C. M. *Nonlinear programming: theory and algorithms*. John Wiley & Sons, 2013.
- [162] Chengxian, X. and de Jong, J. Sequential quadratic programming methods for optimal control problems with state constraints. *Applied Mathematics-A Journal of Chinese Universities*, 8 (2), pp. 163–174, 1993.
- [163] Fritsch, F. N. and Carlson, R. E. Monotone piecewise cubic interpolation. *SIAM Journal on Numerical Analysis*, 17 (2), pp. 238–246, 1980.
- [164] Mitschke, M. and Wallentowitz, H. *Dynamik der kraftfahrzeuge*. Springer, 1990.
- [165] Rill, G. *Vehicle dynamics*. Hochschule Regensburg, University of Applied Sciences, 2006.
- [166] Massaro, M., Cossalter, V., and Lot, R. A virtual rider for reproducing experimental manoeuvres. In *Proceedings, Bicycle and Motorcycle Dynamics 2010, Symposium on the Dynamics and Control of Single Track Vehicles, 20 - 22 October, Delft, The Netherlands*. Delft University, 2010.

- [167] Massaro, M. and Lot, R. A virtual rider for two wheeled vehicles. In *Decision and Control (CDC), 2010 49th IEEE Conference*, pages 5586–5591. IEEE, 2010.
- [168] Massaro, M. A nonlinear virtual rider for motorcycles. *Vehicle System Dynamics*, 49 (9), pp. 1477–1496, 2011.
- [169] Cole, D. J. Influence of steering torque feedback and neuromuscular dynamics on driver and vehicle response to lateral force disturbance. *Driver-Vehicle Dynamics Group, University of Cambridge*, 2011.
- [170] Cole, D. J. A path-following driver–vehicle model with neuromuscular dynamics, including measured and simulated responses to a step in steering angle overlay. *Vehicle System Dynamics*, 50 (4), pp. 573–596, 2012.
- [171] Na, X. and Cole, D. J. Linear quadratic game and non-cooperative predictive methods for potential application to modelling driver–afs interactive steering control. *Vehicle System Dynamics*, 51 (2), pp. 165–198, 2013.
- [172] Massaro, M., Lot, R., Cossalter, V., Brendelson, J., and Sadauckas, J. Numerical and experimental investigation of passive rider effects on motorcycle weave. *Vehicle System Dynamics*, 50 (sup1), pp. 215–227, 2012.
- [173] Timings, J. and Cole, D. Robust lap-time simulation. *Proceedings of the Institution of Mechanical Engineers, Part D: Journal of Automobile Engineering*, 228 (10), pp. 1200–1216, 2014.
- [174] Massaro, M., Lot, R., and Cossalter, V. A virtual motorcycle driver to simulate real manoeuvres from experimental data. *Proceedings of the Institution of Mechanical Engineers, Part D: Journal of automobile engineering*, pages 1211–1219, 2012.
- [175] Sharp, R. Rider control of a motorcycle near to its cornering limits. *Vehicle System Dynamics*, 50 (8), pp. 1193–1208, 2012.
- [176] Saccon, A., Hauser, J., and Beghi, A. A virtual rider for motorcycles: Maneuver regulation of a multi-body vehicle model. *Control Systems Technology, IEEE Transactions on*, 21 (2), pp. 332–346, 2013.
- [177] Doria, A., Tognazzo, M., and Cossalter, V. The response of the rider’s body to roll oscillations of two wheeled vehicles; experimental tests and biomechanical models. *Proceedings of the Institution of Mechanical Engineers, Part D: Journal of Automobile Engineering*, 227 (4), pp. 561–576, 2013.

- [178] Sequenzia, G., Oliveri, S., Fatuzzo, G., and Cali, M. An advanced multibody model for evaluating rider's influence on motorcycle dynamics. *Proceedings of the Institution of Mechanical Engineers, Part K: Journal of Multi-body Dynamics*, 2014.
- [179] Robbins, D. Anthropometric specifications for mid sized male dummy, volume 2. Technical report, 1983.
- [180] Barbagallo, R., Sequenzia, G., Oliveri, S., and Cammarata, A. Dynamics of a high-performance motorcycle by an advanced multibody/control co-simulation. *Proceedings of the Institution of Mechanical Engineers, Part K: Journal of Multi-body Dynamics*, 230 (2), pp. 207–221, 2015.
- [181] Cossalter, V., Doria, A., Massaro, M., and Taraborrelli, L. Experimental and numerical investigation on the motorcycle front frame flexibility and its effect on stability. *Mechanical Systems and Signal Processing*, 60, pp. 452–471, 2015.

Curriculum Vitae

PERSONAL DATA

Name	David Moreno-Giner
Birth	18 th of March 1980, Alicante (Spain)
Contact	david.morenoginer@gmail.com
Interests	Multibody Dynamics, Control Theory, Optimization, Vehicle Dynamics.

PROFESSIONAL EXPERIENCE

Jun 2012 to present	Simulation Engineer at Yamaha Motor Racing, Lesmo (Italy). Research and development of tools for the dynamic simulation of racing motorcycles. Rider modelling for aggressive manoeuvring.
Jun 2010 Jun 2012	Simulation and Analysis Engineer at Red Bull Racing F1, Milton Keynes (UK). Research, development and implementation of mathematical models, simulation tools and analysis algorithms to determine the optimum performance of F1 cars. Inboard suspension tuning (i.e. spring, dampers and k-dampers) for ride optimization. Track data analysis. 7-poster tests pre/post processing.
Jul 2007 Jun 2010	R&D Engineer at the Simulation Division of LMS international (Siemens PLM), Leuven (Belgium). Development and optimization of efficient motorcycle multibody models based on the symbolic approach. Development of a novel rider model based on on Model Predictive Control. Rider behaviour investigation.
Aug 2006 Jul 2007	R&D Engineer at the Department of Mechanical Engineering of the University of Ferrara (Italy) in collaboration with Ducati Corse. Kineto-Elastodynamic modelling and simulation of the desmodromic valve train of the Ducati MotoGP engine. In particular, the research

Dec 2004 Aug 2006	<p>focused on the development of a flexible multibody model of the desmodromic valve train to study the effect of rocker compliance at high speeds.</p> <p>Associate Lecturer (part-time) at the Polytechnic School of Engineering, Miguel Hernández University (Elche, Spain).</p> <p>Lectures on mechanics, vibration theory and technical drawing.</p>
----------------------	--

ACADEMIC BACKGROUND

2007	<p><i>Diploma de Estudios Avanzados (DEA)</i>. Polytechnic School of Engineering, Miguel Hernández University (Spain).</p> <p>Dissertation title: Multobody simulation of the desmodromic valve train (MotoGP engine GP06).</p>
2004 - 2006	<p>Master in Theory and Practical Application of Finite Element Method and Mechanical Simulation. UNED University, Madrid (Spain).</p> <p>Thesis Title: Study and optimization of the external geometry of a car by means of computer fluid dynamics.</p>
1998 - 2004	<p>MSc. in Industrial Engineering (specialization in mechanical and control engineering). Polytechnic School of Engineering, Miguel Hernández University (Spain).</p> <p>Award: <i>Premio Extraordinario de Fin de Carrera</i> for the best academic record in the Industrial Engineering degree.</p> <p>Thesis Title: Design and simulation of an innovative suspension system for downhill bicycles.</p>

SELECTED PUBLICATIONS

May 2010	<p>Steady Turning Analysis of Motorcycles in LMS Virtual.Lab Motion. Proceedings of the 1st Joint International Conference on Multibody System Dynamics May 25 – 27, 2010, Lappeenranta, Finland. D. Moreno, N. Cofelice, A. Toso and J. Kang.</p>
Sep 2009	<p>A "corner solver" for motorcycles as a tool for the development of a virtual rider. Proceedings of IEEE Vehicle Power and Propulsion Conference (IEEE VPPC, Dearborn, MI, USA, Sept. 7 – 10, 2009. D. Moreno, M. Manka and J. Kang.</p>
Sep 2009	<p>Motorcycle dynamic models for virtual rider design and cornering analysis. J.Proc. ASME 2009. International Design Engineering</p>

- Technical Conferences & Computers and Information in Engineering Conference IDETC/CIE 2009, San Diego, CA, USA. Aug. 30 – Sept. 2, 2009. D. Moreno and M. Manka.
- Jun 2007 **Multibody analysis of the desmodromic valve train of the Ducati MotoGP engine.** ECCOMAS Thematic Conference on Multibody Dynamics (ECCOMAS), Milano (Italy). June 2007. D. Moreno, E. Mucchi, G. Dalpiaz and A. Rivola.
- Dec 2004 **Analysis of the influence of pedalling on the performance of suspension systems for mountain bikes.** Journal of the Spanish Association of Mechanical Engineering. Vol. 3, No. 15, December 2004. pp. 1679-1684. ISSN - 0212-5072. D. Moreno, M. Sánchez and M.A. Oliva.